National Library
of Canada

Acquisitions and
Bibliographic Services Branch

395 Wellington Street
Ottawa, Ontario
K1A 0N4

Bibliothèque nationale
du Canada

Direction des acquisitions et
des services bibliographiques

395, rue Wellington
Ottawa (Ontario)
K1A 0N4

Your file Votre référence

Our file Notre référence

NOTICE

The quality of this microform is heavily dependent upon the quality of the original thesis submitted for microfilming. Every effort has been made to ensure the highest quality of reproduction possible.

If pages are missing, contact the university which granted the degree.

Some pages may have indistinct print especially if the original pages were typed with a poor typewriter ribbon or if the university sent us an inferior photocopy.

Reproduction in full or in part of this microform is governed by the Canadian Copyright Act, R.S.C. 1970, c. C-30, and subsequent amendments.

AVIS

La qualité de cette microforme dépend grandement de la qualité de la thèse soumise au microfilmage. Nous avons tout fait pour assurer une qualité supérieure de reproduction.

S'il manque des pages, veuillez communiquer avec l'université qui a conféré le grade.

La qualité d'impression de certaines pages peut laisser à désirer, surtout si les pages originales ont été dactylographiées à l'aide d'un ruban usé ou si l'université nous a fait parvenir une photocopie de qualité inférieure.

La reproduction, même partielle, de cette microforme est soumise à la Loi canadienne sur le droit d'auteur, SRC 1970, c. C-30, et ses amendements subséquents.

Canada

Analytical and Experimental Investigation of the Existence of Simultaneous Forward and Backward Whirling Motion of Jeffcot Rotor Supported on Hydrodynamic Bearings

Chandrashekar Rao

A Thesis
in
The Department
of
Mechanical Engineering

Presented in Partial Fulfillment of the Requirements
for the
Degree of Master of Applied Science
at
Concordia University
Montreal, Quebec, Canada

August 1993

National Library
of Canada

Acquisitions and
Bibliographic Services Branch

395 Wellington Street
Ottawa, Ontario
K1A 0N4

Bibliothèque nationale
du Canada

Direction des acquisitions et
des services bibliographiques

395, rue Wellington
Ottawa (Ontario)
K1A 0N4

Your file Votre référence

Our file Notre référence

ISBN 0-315-87328-0

Canada

Abstract

Analytical and Experimental Investigation of the Existence of Simultaneous Forward and Backward Whirling Motion of Jeffcot Rotor Supported on Hydrodynamic Bearings

Chandrashekar Rao

Whirling of rotating shafts is defined as the rotation of the plane made by the bent shaft and the line of centers of the bearings. The phenomenon results from such causes as mass unbalance, gyroscopic forces and fluid forces in bearings. The whirling of the shaft may take place in the same or opposite sense as that of the rotation of the shaft, depending upon which it is referred to as *forward or backward whirl.* Rotor systems in industrial machinery are commonly supported on hydrodynamic bearings and the dynamic behaviour of such rotors is significantly influenced by the bearing properties. The stiffness anisotropy of bearings, in the absence of damping, can cause backward whirling in a Jeffcot rotor, in between the critical speeds. The stiffness asymmetry of the supporting bearing has a destabilizing influence, and when it is sufficiently small, the backward whirling is still bound to occur in between the critical speeds.

Whirling motion of *Jeffcot Rotor* supported on two identical hydrodynamic bearing is taken as a basis for this study. Effect of flexibility and load parameter on the occurrence of backward whirl between critical speeds is studied. As the disk whirls in the backward sense in between the critical speeds, the journal continues to whirl in the forward sense. The present investigation reveals that the backward whirl commences at the disk and as the speed increases, it extends over a certain central portion of the shaft and then shrinks back towards the disk before disappearing.

Although the assumption of identical bearings at the two ends of the rotor renders the analysis simple, this may not be the case in reality. In actual practice the manufacturing precision difficulties and wear does introduce dissimilarity in the supportive bearings. The response analysis of the rotor supported on the dissimilar bearings is analyzed analytically. Effect of dissimilarity of the bearings on the pattern and occurrence of forward and backward whirling motion is studied.

Experimental verification of the simultaneous forward and backward whirl motion is carried out on a laboratory model of a simple Jeffcot rotor mounted on identical journal bearings. Instrumentation involving proximity pickups, oscillator, amplifiers, demodulator are used to provide an output voltage signal proportional to the displacement. A differentiator - multiplier - filter circuits is designed and built to identify the sense of the whirling motion with the input voltage signal from the demodulator. The phenomenon of the existence of forward and backward whirling motions at the bearing and at the rotor disk is established through experimental measurements.

Dedicated to Amma, Anna, Rama and my Teachers

Acknowledgement

The author wishes to express his deep sense of gratitude and appreciation to his supervisors, Dr. R. B. Bhat and Dr. G. D. Xistris for their continued support, encouragement, and guidance during the course of this work.

Special thanks are due to Dr. C. Rajalingam for his continued help in various stages of this work.

The author is also grateful for the help and suggestions of Mr. Danny Juras, Mr. Bob Suresh, Mr. John Elliott and Mr. Joseph Sarruf in the development of the experimental setup and instrumentation.

The financial support by the Mechanical Engineering Department at Concordia University, is further acknowledged.

Sincerest thanks are due to Mrs. Joan Shaw, Mr. George Shaw and Mr. Donald Jue for their valuable help and emotional support.

Contents

List of Figures

List of Tables

Nomenclature

$\overline{A}$	non-dimensional area of the whirl orbit
a_{jx}, a_{jy}	coefficients of cosine terms defined in Eqns. (3.9, 3.10)
a_{rx}, a_{ry}	coefficients of cosine terms defined in Eqns. (3.1, 3.12)
$a_{xc}, a_{yc}, c_{xc}, c_{yc}$	coefficients of cosine terms defined in Eqn.(4.35) for rotor
a_{xl}, a_{yl}	coefficients of cosine terms defined in Eqn.(4.35) for left bearing
a_{xr}, a_{yr}	coefficients of cosine terms defined in Eqn.(4.35) for right bearing
b	bearing width
b_{jx}, b_{jy}	coefficients of sine terms defined in Eqns. (3.9, 3.10)
b_{rx}, b_{ry}	coefficients of sine terms defined in Eqns. (3.11, 3.12)
$b_{xc}, b_{yc}, d_{xc}, d_{yc}$	coefficients of sine terms defined in Eqn. (4.35) for rotor
b_{xl}, b_{yl}	coefficients of sine terms defined in Eqn.(4.35) for left bearing
b_{xr}, b_{yr}	coefficients of sine terms defined in Eqn.(4.35) for right bearing
c	radial clearance
$[C]$	damping coefficient matrix
$[\overline{C}]$	$[C](2c\omega/W)$ = dimensionless damping coefficient matrix
c_l	radial clearance at left bearing
$\overline{c}_l$	non-dimensional clearance ratio, $\overline{c}_l = c_l/c$
$[\overline{C}_p]$	dimensionless damping coefficient matrix with respect to the radial-transverse frame
c_r	radial clearance at right bearing
$\overline{c}_r$	non-dimensional clearance ratio, $\overline{c}_r = c_r/c$
$C_{xx}, \ldots$	damping coefficients
$\overline{C}_{xx}, \ldots$	$\overline{C}_{xx} = C_{xx} c\omega/(W/2)$
$C_{xx,l}, \ldots$	damping coefficients for left journal bearing
$\overline{C}_{xx,l}, \ldots$	non-dimensional damping coefficients, $\overline{C}_{xx,l} = C_{xx,l} c_l \omega/(W/2)$
$C_{xx,r}, \ldots$	damping coefficients for right journal bearing

$\overline{C}_{xx,r},\ldots$	non-dimensional damping coefficients, $\overline{C}_{xx,r} = C_{xx,r}c_r\omega/(W/2)$
d	diameter of journal
D_c, D_s	dimensionless damping force coefficients
D_c^*	$D_c = /(1-2\beta')$, modified damping force coefficients
D_s^*	$D_s = /(1-2\beta')$, modified damping force coefficients
e	eccentricity of journal
g	acceleration due to gravity
G	$G = G_1 + \nu\mu_s G_2 + \nu^2\mu_s^2 G_3$
G_1, G_2, G_3	defined in Eqn. (3.44 to 3.46)
G_x, G_y	gyroscopic couple
h	film thickness
$\overline{h}$	h/c, dimensionless film thickness
J	polar moment of inertia
$\overline{J}$	$\overline{J} = J/ml^2$, non-dimensional polar moment of inertia
J_1	$J_1 = \overline{K}_{xx} + \overline{K}_{yy}$
J_2	$J_2 = \overline{C}_{xx} + \overline{C}_{yy}$
J_3	$J_3 = \overline{K}_{xx}\overline{K}_{yy} - \overline{K}_{xy}\overline{K}_{yx}$
J_4	$J_4 = \overline{C}_{xx}\overline{C}_{yy} - \overline{C}_{xy}\overline{C}_{yx}$
J_5	$J_5 = \overline{K}_{xx}\overline{C}_{yy} + \overline{K}_{yy}\overline{C}_{xx} - \overline{K}_{xy}\overline{C}_{yx} - \overline{K}_{yx}\overline{C}_{xy}$
J_6	$J_6 = \overline{K}_{xy} - \overline{K}_{yx}$
J_7	$J_7 = \overline{C}_{xy} + \overline{C}_{yx}$
J_8	$J_8 = \overline{K}_{xx}\overline{C}_{yx} + \overline{K}_{xy}\overline{C}_{yy} - \overline{K}_{yx}\overline{C}_{xx} - \overline{K}_{yy}\overline{C}_{xy}$
J_9	$J_9 = (\overline{K}_{xx} + \overline{K}_{yy})(\overline{C}_{xy} + \overline{C}_{yx}) - (\overline{C}_{xx} + \overline{C}_{yy})(\overline{K}_{xy} - \overline{K}_{yx})$ $+ (\overline{K}_{xx}\overline{C}_{yx} + \overline{K}_{xy}\overline{C}_{yy} - \overline{K}_{yx}\overline{C}_{xx} - \overline{K}_{yy}\overline{C}_{xy})$
$[K]$	stiffness coefficient matrix
$[\overline{K}]$	$[K](2c/W)$ = dimensionless stiffness coefficient matrix
$[\overline{K}_p]$	dimensionless stiffness coefficient matrix with respect to the radial-transverse frame

K_s	stiffness of shaft
$K_{xx}, \ldots$	stiffness coefficients
$\overline{K}_{xx}, \ldots$	$\overline{K}_{xx} = (C_{xx}c/W)$
$K_{xx,l}, \ldots$	stiffness coefficients for left journal
$\overline{K}_{xx,l}, \ldots$	$\overline{K}_{xx,l} = (K_{xx,l}c_l/W/2)$ non-dimensional stiffness coefficients
$K_{xx,r}, \ldots$	stiffness coefficients for right journal
$\overline{K}_{xx,r}, \ldots$	$\overline{K}_{xx,r} = (K_{xx,r}c_r/W/2)$ non-dimensional stiffness coefficients
L	length of shaft
M	mass of shaft
$\overline{p}$	$pc^2/\eta\omega$, dimensionless pressure
p	pressure
p^*	$\overline{p}/(1-2\beta')$, modified pressure
P_c, P_s	hydrodynamic force components
$\overline{P}_c$	$[(P_c/bd)c^2/\eta\omega]$, dimensionless force components
P_c^*	$P_c/(1-2\beta')$, modified force components
$\overline{P}_s$	$[(P_s/bd)c'^2/\eta\omega]$, dimensionless force components
P_s^*	$P_s/(1-2\beta')$, modified force components
P_x, P_y	force components that are being used in Chapter 4
$\overline{Q}$	non-dimensional flow rate
r	$d/2$, journal radius
$\overline{R}$	non-dimensional unbalance response
S_c^*, S_s^*	steady state hydrodynamic force components
S_0	$(p_{av}c'^2)/\eta\omega$, non-dimensional Sommerfeld number
So	Sommerfeld number, $So = \{(W/bd)c'^2/(\eta\omega)\}$
So_o	non-dimensional load parameter, $So_o = \{(W/bd)c'^2/(\eta\omega_o)\}$
t	time
T	transformation matrix given by Eqn. (2.41)
W	load, $W = Mg$

x, y, z	co-ordinates
$\bar{x}, \bar{y}, \bar{z}$	$\bar{x} = (x/r)$, $\bar{y} = (y/h)$, $\bar{z} = (z/r)$
(x_j, y_j)	co-ordinates of journal
$(\bar{x}_j, \bar{y}_j)$	$\bar{x}_j = (x_j/c)$, $\bar{y}_j = (y_j/c)$
(X_0, Y_0)	co-ordinates of mean position of journal center
$(\bar{X}_0, \bar{Y}_0)$	$\bar{X}_0 = (X_0/c)$, $\bar{Y}_0 = (Y_0/c)$
$(\bar{x}_p, \bar{y}_p)$	radial-transverse displacements shown in Fig. (2.4)
(x_r, y_r)	co-ordinates of disk
$(\bar{x}_r, \bar{y}_r)$	$\bar{x}_r = \{(x_r/c) - \mu_s\}$. $\bar{y}_r = (y_r/c)$
z	axial co-ordinate from the left end
β	attitude angle
δ_s	static deflection, $\delta_s = (ml^3)/48EI$
ϵ	eccentricity ratio, $\epsilon = (\epsilon/c)$
ϵ^*	$2\epsilon'/\epsilon(1 - 2\beta')$
η	coefficient of viscosity
θ	angular coordinate shown in Fig. (2.4)
θ_1	inlet boundary
θ_2	outlet boundary
ω	angular velocity
ω_o	$\omega_o = (g/c)^{1/2}$
ω_s	$\omega_s = (K_s/M)^{1/2}$
Λ	speed parameter, $\Lambda = \{(\omega_o^2/\omega^2) - (\omega_o^2/\omega_s^2)\}$
μ_s	non-dimensional flexibility parameter, $\mu_s = (\omega_o^2/\omega_s^2)$; $= \delta_s/c$
ψ	clearance ratio, $\psi = (2c/d)$
δ_o	unbalance eccentricity of disk
(ξ_{xl}, ξ_{yl})	co-ordinates of left bearing
(ξ_{xr}, ξ_{yr})	co-ordinates of right bearing
(ξ_{xc}, ξ_{yc})	co-ordinates of disk

$(\bar{\xi}_{xl}, \bar{\xi}_{yl}); (\bar{\xi}_{xr}, \bar{\xi}_{yr})$	non-dimensional co-ordinates of journal
$\bar{\xi}_{xl}$··	$\bar{\xi}_{xl} = \left(\frac{\xi_{xl} - \xi_{xlo}}{c}\right)$
$\dot{\bar{\xi}}_{xl}$	$\dot{\bar{\xi}}_{xl} = \omega\bar{\xi}_{xl}{}'$
$\dot{\bar{\xi}}_{yl}$	$\dot{\bar{\xi}}_{yl} = \omega\bar{\xi}_{yl}{}'$
$\bar{\xi}_{xr}$··	$\bar{\xi}_{xr} = \left(\frac{\xi_{xr} - \xi_{xro}}{c}\right)$
$(\bar{\xi}_{xc}, \bar{\xi}_{yc}); (\bar{\theta}_{xc}, \bar{\theta}_{yc})$	non-dimensional co-ordinates of disk
$\bar{\xi}_{xc}$··	$\bar{\xi}_{xc} = \left(\frac{\xi_{xc} - \xi_{xco}}{c}\right)$
$\bar{\theta}_{xc}$··	$\bar{\theta}_{xc} = \frac{1}{c}(\theta_{xc} - \theta_{xco})$
$\dot{\bar{\xi}}_{xc}$··	$\dot{\bar{\xi}}_{xc} = \omega\bar{\xi}_{xc}{}''$
$\ddot{\bar{\xi}}_{xc}$	$\ddot{\bar{\xi}}_{xc} = \frac{\xi_{xc}}{c}$
$\ddot{\bar{\xi}}_{xc}$	$\ddot{\bar{\xi}}_{xc} = \omega^2\bar{\xi}_{xc}{}''$
$'$	differentiation with respect to ωt
$\cdot$	differentiation with respect to t

Chapter 1

Introduction and Literature Review

1.1 Introduction

Rotating shafts are employed in industrial machines such as steam and gas turbines, turbogenerators, internal combustion engines, electric motors, reciprocating and centrifugal compressors for power transmission. Because of the ever increasing demand for power and high speed transportation, the rotors of these machines are made extremely flexible, which makes the study of vibratory motion and the resulting dynamic stresses an essential part of their design. The shafting of these machine installations is subjected to torsional and bending vibrations and in some cases may encounter unstable conditions of operation.

The dynamics of rotor bearing systems has become extremely important due to the increased speed and power level requirements in advanced design of the rotating equipment. The aircraft jet engine industry has as their ultimate goal a lighter, more powerful, more efficient, and more dependable power plant. Industrial Compressor and gas turbine manufacturers are concerned with reduced development costs, high reliability, and low maintenance costs over extended useful service life. These factors are responsible for the interest in and the growth of the study on the stability and forced response of rotor bearing systems. Power plants for ground installation and outer space are relying on fluid-film bearings to provide long, maintenance free service. To avoid the classical instability associated with plain cylindrical bearings the designers have employed multi-lobe, tilting pad, pressure dam, and other designs such as herringbone groove to increase the stable speed range of their equipment.

Modern turbo-machines produce or absorb an amazing amount of power in a relatively small package. Undoubtedly, the most impressive example is NASA's Space Shuttle main engine turbo-pumps, which produce 70,000 hp in two turbine stages, about the size of a frisbee. In more common applications, turbo-jet engines provide propulsion for supersonic airplanes, turbine-compressor trains accomplish astounding flow rates for petrochemical industries, and steam turbines produce mega-watts of electrical power for utilities. The property of turbo-machinery which allows these high energy densities and flow rates to be achieved is the high shaft speed relative to other types of machines of the same physical size. Along with high speeds, comes high inertial loads and potential problems with shaft whirl, vibration, dynamic stresses, and rotor-dynamic instability.

In general, rotors are used in machinery whenever power is transmitted from one point to another. Rotors are rotating shafts with concentrated masses such as disks, impellers etc., supported on stationary structures called bearings. These bearings can be either rolling element type such as ball or roller bearings or journal bearings with a fluid film separating the annular area between the journal and the bearing surfaces. The rotor systems are mainly classified as (i) light rotors or (ii) heavy rotors depending upon the applied loads and the type of operation they are subjected to. Again, on the basis of the geometrical configurations, they are further classified as simple systems and large rotor systems. Heavy rotor systems such as generator rotors are generally supported on fluid film bearings. Rotors can also be classified into rigid rotors and flexible rotors. A rigid rotor is one in which motions are completely described by what occurs at the mass center.

With the increasing trend towards the concept of lighter weight components in structures, the weight of the rotor can be reduced either by resorting to different geometrical configurations or by adopting different materials. When all other geometrical parameters of a rotor remain the same, reduction in weight of a rotor will make it flexible and thereby, bring down the critical speeds of the system.

In designing, operating and troubleshooting rotor systems, rotor analysis can help accomplish the following objectives:

1. Predict critical speeds.
2. Determine design modifications to change critical speeds.
3. Predict vibration natural frequencies in torsion.
4. Calculate balance correction masses and locations from measured vibration data.
5. Predict amplitudes of synchronous vibration caused by rotor imbalance.
6. Predict threshold speeds and vibration frequencies for dynamic instability.
7. Determine design modifications to suppress dynamic instabilities.
8. Determine the regions of change of whirl directions and instability.

The phenomenon of bending vibrations and critical speeds of rotating shafts is perhaps the most common problem of rotor design. Rotors always have some amount of residual unbalance however well they may be balanced, and will go into resonance when they rotate at speeds equal or approaching the bending natural frequency. These speeds are called as critical speeds and far as possible, they should be avoided.

The operating speed of a machine can be kept away from the critical speeds, either by changing the operational shaft speed or by changing the critical speed itself. In practice the latter is usually accomplished by modifying the rotor support stiffness. This parameter is not included in *Jeffcot* model, but it has the same effect on critical speeds as the shaft stiffness k. In general, changing the critical speed is most useful in the case of constant speed machines with a narrow range of operational speeds.

If the machine must be driven through a critical speed slowly or repeatedly, or if machine operation near a critical speed cannot be avoided, then the most effective way to reduce the amplitude of synchronous whirl is to add damping. This would be difficult in a Jeffcot rotor, since the only source of damping is aerodynamic drag. However usually most turbo-machines have flexible bearing supports in which damping can be added or oil-film bearings in which damping is inherent and can be changed conveniently by the design modifications.

Rotors supported on hydrodynamic bearings, exhibit asymmetric cross-coupled stiffness and damping properties which vary with the speed of operation. Such properties influence the dynamic behaviour of rotors significantly. Even though, other aspects of rotors such as rotating inertia, shear deformation and hysteresis damping etc., influence the dynamic behaviour of high speed rotors, the major design parameters of the bearings in fact, control the design of rotor systems irrespective of their classifications. Because the fluid film bearings influence the dynamic behaviour of the rotor system, it is highly essential to have a realistic rotor bearing support model for analysis. Fluid film bearings, in fact are nonlinear in nature and the resulting nonlinear model is most involved. However, the nonlinear model is essential only if the dynamic behaviour of the rotor system is required at or near critical regions. Most of the practical rotors operate well away from these critical regions and the response behaviour in these regions can be predicted using a linear model. Hence, it is reasonable to proceed with the linear model of the bearing support to analyze the rotor system behaviour.

Different models were adopted to explain the rotor system behaviour. The two-degrees-of-freedom model was used by Rankine in 1869 for the first published analysis of machinery rotor [1] was an attempt to explain the "critical speed" behaviour of rotor-bearing systems. The system model consisted of a rigid mass whirling in a circular orbit, with an elastic spring acting in the radial direction. Rankine used Newton's second law incorrectly in a rotating coordinate system, and predicted that rotating machines would never be able to exceed their first critical speed.

Although the two-degrees-of-freedom spring-mass model can execute the orbital motions of a rotor-bearing system, it does not contain a realistic representation of the rotating unbalance in the rotor. Since a perfectly balanced rotor never occurs in real machines, and since it is the rotating unbalance which excites the most commonly observed type of vibration (synchronous) in turbo-machines, it follows that the rotating imbalance is an essential ingredient for rotor-dynamic analysis. *Jeffcot rotor* named after the English dynamicist who first used the model in 1919 to analyze the response of high speed rotating machines to rotor unbalance [2], is a very useful model to analyze rotors. It consists of a massive unbalanced disk mounted midway between the bearing supports on a flexible shaft of negligible mass. The bearings are rigidly supported, and viscous damping acts to oppose absolute motion of the disk. Jeffcot's analysis explained how the rotor whirl amplitude has a maximum value at the critical speed but diminishes as the critical speed is exceeded due to the "critical speed inversion" of the unbalance. In the present analysis, the *Jeffcot* model is used to analyze the whirling motion of the rotor system.

The response analysis by most of the researchers was carried out assuming the linear bearing model with fluid film translational stiffness and damping coefficients. When the rotor is flexible or when the support span is large, the tilted or inclined journal provides rotational stiffness and damping effects in the fluid film about the rotor transverse axes. Hence, it is important to include the rotational springs and dampers along with translational stiffness and dampers in order to represent an accurate bearing support model. The fluid film bearings which support the rotor, are in turn mounted on support structures such as pedestals which possess definite stiffness and damping properties.

A phenomenon which is of utmost importance in rotor dynamics is *whirling of rotating shafts*. Rotating shafts tend to bow out at certain speeds and whirl in a complicated manner. *Whirling* is defined as the rotation of the plane made by the bent shaft and the line of centers of the bearings. This results from such causes as mass unbalance, hysteresis damping in the shaft, gyroscopic forces, fluid friction in the bearings, etc. The whirling of a shaft may take place in the same or opposite direction as that of the rotation of the shaft, and the whirling frequency may or may not be equal to the rotation frequency. When the whirling speed is equal to the rotation speed, the whirl is known as *synchronous whirl.*

The subject of shaft whirl is an interesting topic, and its general motion comes under the classification of self excited motion in which the exciting forces inducing the motion are controlled by the motion itself. In practice however, all rotating shafts are flexible. If a flexible shaft carries an unbalanced rotating mass, the unbalance produces bending in the shaft, which in turn alters the effect of unbalance.

Experience has taught that most shaft whirls are forward i.e, the shaft center moves in the same direction as the shaft rotation. For instance, mechanical unbalance causes a closed-loop motion of the shaft center in a forward direction as does oil whip, internal friction, shrink-fit friction, and many other disturbing phenomena. When the shaft center whirls in a direction opposite to that of shaft rotation it is called a backward whirl. Occurrences of backward shaft whirl are less common; a journal rolling around in a dry bearing constitutes the most familiar example.

It is analytically predicted that the journal always whirls in the forward direction, whereas, the shaft can go into backward whirl motion in between two critical speeds in the fundamental mode region. The objective of the present investigation is to derive a comprehensive model for the response analysis of a *Jeffcot* rotor supported on two identical hydrodynamic bearings, to show the existence of simultaneous backward and forward whirling in between critical speeds, and to verify this concept experimentally. The analysis is extended to a Jeffcot rotor supported on dissimilar hydrodynamic bearings.

1.2 Literature Review

With the increasing demand for power accompanied by a decrease in the weight of rotating machines, the study of rotor dynamics has become very important to a power systems design engineer. Jeffcot [2] analyzed the dynamic response of a single mass unbalanced rotor on two identical rigid bearings. Tondl [3], studied a rotor in bearings having stiffness asymmetry. He showed that there are two distinct critical speeds in the fundamental mode region due to stiffness asymmetry which splits the critical speed. He also showed that the rotor whirls in backward direction when the shaft speed is in between the two criticals, even though the unbalance excitation is in the forward direction. Lund [4] gave design charts to determine the two critical speeds corresponding to the fundamental mode of the rotor in bearing supports.

It is generally recognised that the flexibility of support bearings significantly influences the rotor response. There are two areas of primary but separate concern, instability and dynamic response. Whirl instability is a self-excited phenomenon and can occur in lightly loaded, high speed bearings or in high pressure environments and derives from the forces generated orthogonal to the direction of journal displacements. In any rotor, where whirl may be a problem, it becomes the primary concern which must be investigated and eliminated. This is usually accomplished by a suitable change in bearing geometry. Irrespective of the self-excited stability characteristics of the bearings, dynamic response of the bearing rotor system to unbalance forces are important and must be analyzed, so as to estimate the stresses in the rotor shaft.

The instability associated with the plain cylindrical journal bearing has received considerable attention in the literature. Pinkus [5] reported that flexible mountings gave greater stability to rotor bearing systems while Poritsky [6] and Hagg and Warner [7] found that support flexibility lowered the stability threshold speed. Gunter [8] explained the discrepancy by showing that a symmetrical undamped support lowered the threshold speed whereas damped and/or asymmetric supports can greatly increase the stability of a rotor system. Hori [9] presented an analysis of a long bearing by neglecting the negative fluid film pressures (to model cavitation) which indicated that the journal was not inherently unstable at all speeds.

An investigation by Badgley [10] reported on a time transient analysis method of obtaining the stability threshold speed of short, long and finite bearings. The orbits of a balanced horizontal rotor on rigid supports were examined for various levels of perturbation to determine the influence on the stability boundary. He indicated that the threshold speed at high eccentricities is reduced by large initial velocities. Lund [11] examined the stability of a flexible rotor with damped supports and concluded that damped flexible supports can considerably increase the threshold speed. Gunter [12] presented a linear analysis of the influence of damped supports on the response characteristics of a rigid rotor including gyroscopic effects. The analysis of a rotor system indicated significant reduction of forces transmitted to damped bearing supports. Kirk, Choudhury and Gunter [13] presented the effect of support flexibility on stability of rotors mounted on plain cylindrical journal bearing and investigated the influence of unbalance on the stability of vertical rotors.

In actual practice, the rotors are complicated in shape. To determine the out of balance response of a general rotor with properties defined at several conditions, numerical methods can be used. Lund [14] used the Prohl-Myklestad method for this purpose. Transfer matrices have been used by Pestel and Leckie [15] and Pilkey and Chang [16]. Kramer [17] and Rao [18] used transfer matrix analysis for a system of rotors, while Nelson and McVaugh [19] used finite element methods.

To study the effect of supports on the dynamic behaviour of a rotor, Morton [20] and Kirk and Gunter [21] used the Jeffcot model. A model similar to that was used to study the effect of cross-coupled spring coefficients of a hydrodynamic bearing on the critical speeds and out of balance synchronous whirl response of a rotor in the fundamental rigid support mode region. Particular attention was given to determine the conditions under which backward whirl response can be present in a rotor and as a limiting case, the damping in the bearings is ignored.

Fluid film bearings commonly used in heavy machines, play a significant role in the dynamic behaviour of the rotor. Because the thin film that separates the moving surfaces supports the rotor load, it acts like a spring and provides damping due to squeeze film effect. The stiffness and damping properties of the film significantly alter the critical speeds and out of balance of a rotor. In addition, the rotor instability occurs, which is a self excited vibration arising out of the bearing fluid film effects, and this is an important factor to be considered in the rotor design.

The subject of fluid film lubrication is very broad concerning hydrodynamic, hydrostatic or hybrid bearings, with a compressible fluid medium such as gas or an incompressible medium such as a liquid operating in laminar or turbulent regimes. Moreover, the geometry of the bearing, eg., plain cylindrical, elliptical, multi-lobe and tilting pad type, is also considered while evaluating the steady state or dynamic characteristics of the bearing.

Rao [24] studied the effect of cross-coupled spring coefficients of a hydrodynamic bearing of a flexible rotor in synchronous whirl. Depending on the values of cross-coupled spring coefficients of the bearing he showed that:

1. There is a possibility of two distinct critical speeds in the fundamental mode region of the rotor, when the two cross-coupled spring coefficients are positive or one of them is negative. Under these circumstances, there is a backward whirl of the rotor, for speeds in between the two critical speeds, and
2. There is no distinct critical speed as it is conventionally known when one of the cross coupled spring coefficients of the bearing is negative. Under these circumstances the rotor has only forward whirl for all the speeds.

In the initial stages, one of the difficulties was that the only available solution of Reynold's equation was that of Sommerfeld for the infinitely long bearing, sometimes modified by a suitable end leakage factor, and that the only calculations of rotor dynamics was that of the first critical speed, using the methods of either Rayleigh or Stodola. In the late forties, more advanced rotor dynamic calculation methods were developed, and with the advent of the digital computers in the fifties, it soon became feasible at little cost to obtain numerical solutions of Reynold's equation and to perform elaborate rotor calculations.

Even so, the concept of bearing coefficients was not immediately accepted, probably because the load-displacement characteristic of a journal bearing is so evidently non-linear. Experience, however, has demonstrated the practical usefulness of the coefficients, and modern rotor dynamics calculations are firmly based on this concept. The concept of stiffness and damping coefficients for journal bearings has proven very useful, and modern rotor dynamics calculations for unbalance response, critical speeds, and stability use this concept. The theoretical limitation of small amplitudes is of little importance in practice.

In order to study the effect of support stiffness and damping on the dynamic behaviour of a rotor, the Jeffcot model is used. This simplifies the analysis and gives fairly good results for symmetrical rotors in the fundamental mode region. There has always been some confusion as to what the term *critical speed* means. In the early work by Rankine, Dunkerly, and others, it was observed that a rotating shaft had certain speed ranges in which deflection of large amplitudes were developed. The shaft, rotating in a non-oscillatory or simultaneously rotating and oscillating - deflected position, initiated vibrations of the whole supporting structure and often caused catastrophic failure of some part of the system. Hence, those particularly dangerous operating speeds became known as critical speeds.

The dynamic response of rotors to residual unbalance is of vital interest to industry. In the vicinity of a critical speeds of the rotor, the response is quite large and hence, the normal steady state operating speeds of the rotor must be away from the criticals. When the rotors are mounted on hydrodynamic bearings, the evaluation of the damped critical speeds and the unbalance response is quite complicated due to the asymmetry in the direct and cross-coupled stiffness and damping coefficients in the horizontal and vertical directions. Also, these coefficients are dependent on the operating speed of the rotor [22, 23].

The response of rotors in the fundamental rigid support mode region has been investigated by Rao [24], Rao, Bhat and Sankar [25] employing a Jeffcot rotor model. In their investigations, the rotor disk was at the center of the shaft and two identical fluid-film bearings supported the rotor at the two extreme ends. Their study was limited to response evaluation for synchronous whirl conditions only. However, in practice, the rotor may not be mounted exactly at the shaft center and the bearings supporting the rotor ends may not be identical due to practical limitations imposed in the design stage or due to tolerances in production. When the disk is not at the center or when the bearings are not identical, the rotor is likely to exhibit a coupled type of behaviour with the two ends of the rotor having different orbital motions. Unstable vibrations of an unsymmetric rotor system were studied by Yamamoto, Ota and Kono [26]. Also, an asymmetrically mounted rotor on dissimilar bearings was investigated by Ardayfio and Frohrib [27] using energy methods. But, their investigations did not include the cross-coupled stiffness and damping of the fluid-film bearings.

A study of the journal response at the bearing locations is important since this response must be small compared to the bearing clearance for the satisfactory operation. Hence, the bearings have to be designed considering the rotor response at the bearing locations. Subbiah, Bhat and Sankar [28] studied the critical speeds and unbalance response of a single mass rotor, mounted on dissimilar fluid-film bearings at the ends. The direct and cross-coupled coefficients of stiffness and damping at the bearings were included in the analysis. An energy method was used to develop the system model and Lagrange's equations were utilized to derive the equations of motion. The dissimilarity in bearings was achieved by having different bearing clearances at the two ends and by varying the disk position. They also studied the damped critical speeds and unbalance response of a laboratory model of a single mass rotor for different combinations of clearances for the two bearings and for different disk positions. However, the rotor response at the two bearing locations will have different magnitudes and phase. The dissimilarity in the two bearings influences the unbalance response significantly, and the peak response to some extent. Also, the rotor may change its behaviour either showing a single peak in its response or a double peak.

The term *forward whirl* is used in literature to describe the classical orbital motion of the shaft where the shaft center has zero apparent rotation in the rotating system of coordinates. Another often-mentioned rotating shaft motion is that of reverse precession or *backward whirl*. This term is used to describe a situation where the shaft center viewed in the fixed system follows a path whose direction of rotation is opposite to that of the true shaft rotation and at the same frequency as the rotational speed but in the opposite direction. It is generally much more difficult to excite the reverse whirl or backward whirl than the forward whirl. Eubanks and Eshleman mentioned that Lowell was able to excite backward whirl (reverse precession) with pulsating torques. Dimintberg [32] showed that mass unbalance may cause a shaft center line to precess in a direction opposite to that of the shaft rotation, but with the same speed, provided that support elasticity is different in two directions perpendicular to the shaft. This occurs at operating speeds between two classical, forward-whirl critical speeds and is not a resonance phenomenon. However, the forward or backward precession, as viewed in the rotating system, occurs at integer multiples of rotational speeds.

Jeffcot investigated the dynamic response of a central unbalanced rotor carried on a flexible shaft supported in rigid bearings. Such a Jeffcot rotor, when supported in rigid bearings having stiffness asymmetry, has been shown to whirl in the backward sense for a speed range lying between the critical speeds [2]. Considering the unequal cross-coupled stiffness coefficients of a hydrodynamic journal bearing and neglecting damping, the backward whirling motion of a Jeffcot rotor supported in a hydrodynamic journal bearing has been shown to occur only when the system has two split critical speeds, and it occurs in between the two critical speeds [24, 29].

The stiffness anisotropy of bearings, in the absence of damping, can cause backward whirling in a Jeffcot rotor, in between the critical speeds, [3, 32]. The stiffness asymmetry of the supporting bearing has a destabilizing influence, and when it is sufficiently small, the backward whirling is still bound to occur in between the critical speeds, [24, 29]. The damping effect of the fluid film which has a significant influence on the dynamics of the rotor was neglected in these investigations.

The damping in such a journal bearing is not negligible and such a rotor has been shown to have at least one critical speed [30]. With both the stiffness and damping characteristics of the journal bearing taken into account, it can be shown that the rotor exhibits backward whirling motion for some particular range of the parameters of the system. Kellenberger [31] considered the anisotropic action of the multi-slide bearing and found that the oil film damping alone is apparently insufficient to prevent backward whirl in the region $\omega/\omega_s = 0.85\ to\ 0.95$. At the present time there are many rigid rotors operating close to this region and it is worthwhile to identify more precisely the system parameters affecting backward whirl so as to minimize the resulting problems. Rajalingham, Ganesan and Prabhu [33], studied the necessary conditions for the occurrence of backward whirling motion of a Jeffcot rotor supported on full cylindrical journal bearings of $b/d = 0.75$ in dimensionless form.

Studies using the stiffness and damping characteristics of the supporting hydrodynamic bearings, showed that the combined influence of the stiffness asymmetry and the damping could suppress the occurrence of the backward whirling, when the flexibility of the rotor is sufficiently small [33]. Further, the backward whirling of the disk could be eliminated either by increasing the slenderness ratio of the bearings or the viscosity of the lubricant, or by reducing the clearance ratio of the bearings. Excessive flexibility of Jeffcot rotor supported on fluid film bearing causes the disk to whirl in the backward sense for a speed range in between the critical speeds. As the disk whirls in the backward sense in between the critical speeds, the journal continues to whirl in the forward sense [34]. Rajalingham, Bhat and Jha [34] showed that, the backward whirl commences at the disk and as the speed increases, it extends over a certain central portion of the shaft and then shrinks back towards the disk before disappearing.

The actual occurrence of backward whirl in turbo-machinery has been doubted in the past [35], but modern instrumentation confirms that it does occur. Backward whirl was experimentally observed by Subbiah et al. [42]. With light damping, backward whirl is excited by rotor imbalance when the rotor speed is between two natural frequencies split by bearing support stiffness asymmetry, for instance, $(\omega_1 < \omega < \omega_2)$, where ω_1 is the eigenvalue associated with the lower stiffness and ω_2 is associated with the higher stiffness. Sufficient damping will make the backward whirl disappear.

Backward whirl is not a defect in itself, but it does occur and is usually indicative of very light damping and operation between two critical speeds. Very severe rotor rubs can produce violent backward whirl that can be quite destructive.

1.3 Experimental Work on Rotor Systems

Compared to the several analytical studies available for the rotor bearing system in the literature, very few experimental investigations are reported. One of the earliest reports on the response of rotors using both analytical and experimental methods on the response of rotors using both analytical and experimental methods was by Yamamoto [36]. He studied the vibrations of a rotor system supported on ball bearings. Most of the refereed work on practical rotors supported on hydrodynamic bearings does not satisfy conditions for a clear backward whirl, hence there were not many experimental investigations on the existence of backward whirling. In 1957, Downham [37] showed that a shaft, rotating in bearings having different support stiffnesses in the vertical and horizontal directions, whirls backward in the range between the critical speeds. He also verified experimentally that there were two critical speeds in rotor systems supported on such anisotropic bearings. He found that the lubricant had a stiffness effect with a consequent increase in critical whirling speed. Hull [38] observed experimentally this backward whirl for a rotor driven by a lathe and supported on an outboard bearing held between two vertical springs in tension giving rise to asymmetric bearing stiffness. By using elementary apparatus and instrumentation, he investigated shaft whirling for three cases involving round and flattened shafts in combination with isotropic or anisotropic bearing supports. Where anisotropic bearings support a round shaft, he found that backward single-frequency whirl is necessary between the two critical speeds because the unbalance phase angle must change from zero to 180 deg. and again to zero twice per shaft revolution. The displacement trace at resonance is a slanted line which involves no angular momentum of whirl. For a second case of symmetrical stiffness bearings supporting an asymmetrical stiffness shaft, he found that three phase changes occur. On passing through the half- critical speed the double frequency, forward-whirl deflection changes 90 deg from in-phase with the soft direction of the shaft stiffness to in-phase with the stiff direction. These phase changes are overridden as the unbalance phase angle approaches zero in preparation for passing through the full- critical speed which is accompanied by the unusual 180-deg phase change. For a third case of asymmetric stiffness bearings supporting an asymmetric stiffness shaft, he found that between the horizontal and vertical half critical speeds the shaft finds itself above critical in horizontal excursions but not when moving in the vertical direction. He observed four 90-deg stiffness phase-angle changes per whirl revolution forcing a backward whirl at twice the shaft angular frequency.

Lund and Orcutt [39] conducted a combined analytical and experimental study of the test rotor, a uniform flexible shaft with disks, supported on two silicone fluid-lubricated tilted pad bearings. They found that peak vibration response did not always occur at the calculated damped critical speed. Cunningham [40] presented the experimental data for the unbalance response of a flexible, ball bearing supported rotor. He compared the values of squeeze film damping coefficients obtained from measured data to those of theoretical values. Subbiah [41] obtained experimentally unbalance response and critical speeds of a laboratory model simple rotor supported on hydrodynamic bearings and compared them with those obtained through theoretical analysis. The experimental results did show a good qualitative agreement with theoretical results. Subbiah, Bhat, Sankar, Rao [42] verified the existence of backward whirling motion experimentally with the aid of a laboratory model of the rotor supported on two identical bearings. They designed the rotor system to exhibit backward synchronous whirl. Non contact type proximity pickups were used to measure the unbalance response. A FFT analyzer was used to obtain the orbital diagram with X-Y plotter. The rotor-bearing system exhibited the split criticals, and they verified the existence of backward whirling between the split criticals by the direction of plotter pen motion on the plotter.

1.4 Scope of the Present Investigation

The objectives of the present investigation are to study the simultaneous forward and backward whirling of a simple rotor mounted on fluid film bearings. To this end, the following studies are carried out.

1. Formulating a finite difference model for the solution of Reynold's equation and calculation of stiffness and damping coefficients of the journal bearing.
2. Response analysis of a *Jeffcot* rotor supported on two identical hydrodynamic bearings and investigation of the simultaneous existence of forward and backward whirling motion.
3. Response analysis of a *Jeffcot* rotor supported on dissimilar hydrodynamic bearings and investigation of the simultaneous existence of forward and backward whirling motion.
4. Experimental investigation of the existence of simultaneous forward and backward whirling motion.

In Chapter 2, the pressure distribution in a journal bearing is computed by solving the Reynold's equation using a finite difference model. Ocvirk's Short Bearing theory and Sommerfeld's Long Bearing analysis are applied to find an approximate solution to Reynold's Equation. The solution is later approximated using one-dimensional analysis and later with two-dimensional approach to obtain the actual pressure distribution. The load carrying capacity of the journal bearing is derived from the hydrodynamic pressures produced in the lubricant by the shearing action of a rotating journal. Stiffness and damping coefficients associated with the journal motion are determined.

In Chapter 3 the unbalance response of a flexible rotor-bearing system, comprising a horizontal shaft and a central rotor, and supported on identical journal bearings at its ends, is investigated. The closed form solution to this problem enables better understanding on the cause of the backward whirling motion of the shaft. Simultaneous forward and backward whirling motion of the shaft, for a speed range in between the critical speeds of the system are studied.

In Chapter 4 the response analysis of a rotor supported on dissimilar bearings is carried out. The governing equations of unbalance response are derived using Euler Bernoulli Beam Theory. Gyroscopic forces are considered in the analysis. The resulting system of linear equations governing the rotor system is solved and the simultaneous forward and backward whirling motion of the rotor is studied.

Chapter 5 deals with the experimental verification of simultaneous forward and backward whiling motions of a laboratory model of a simple rotor supported on two identical journal bearings.

Finally Chapter 6 presents the conclusions and contains suggestions for future investigations.

Chapter 2

Calculation of Stiffness and Damping Coefficients in a Hydrodynamic Bearing

2.1 Introduction

Fluid film bearings commonly used in heavy rotating machines play a significant role in the dynamic behaviour of the rotor. Studies of the dynamic behaviour of rotor rely on an accurate representation of the bearings. The load carrying capacity of fluid film bearings is due to the hydrodynamic pressures developed in the lubricant by the shearing action of the rotating journal. The thin film separating the moving surfaces supports the rotor load, it acts like a spring and also provides damping due to squeeze film effect. The stiffness and damping properties of the oil film significantly alter the critical speeds and out-of-balance response of a rotor. In addition, a form of rotor instability, which is a self excited vibration arising out of the bearing fluid film effects, occurs. Hence, the calculation of stiffness and damping coefficients of the hydrodynamic bearing is of utmost importance for the present investigation. These dynamic coefficients are calculated from a finite difference solution of the governing Reynolds equation for the pressure distribution in the bearing film.

2.2 Finite Difference Model for Solving Reynolds Equation in a Journal Bearing

2.2.1 Reynolds Equation in a Journal Bearing

Reynolds equation which relates the variation of pressure in the lubricating film, is derived under the hydrodynamic lubrication approximation. In bearings, the distance across the film is very small compared to the longitudinal distance along the film. Further, when the reduced Reynolds number is small and Froudes number is large, the effect of inertia and body forces can be neglected. Under this condition, pressure variation across the film is negligible. For Newtonian lubricant with constant viscosity, Reynolds equation reduces to following form:

$$\frac{\partial}{\partial x}\left[\frac{h^3}{12\eta}\frac{\partial p}{\partial x}\right]+\frac{\partial}{\partial z}\left[\frac{h^3}{12\eta}\frac{\partial p}{\partial z}\right]=\frac{\partial}{\partial x}\frac{Uh}{2}-V \tag{2.1}$$

The Reynolds boundary conditions are often considered to be satisfactory for the solution of the Reynolds equation. According to these conditions, the pressure distribution in a journal bearing is assumed to commence from the position of maximum film thickness, and to extend up-to the point where the pressure and the pressure gradient are zero. The solution for the pressure distribution, under the Reynolds boundary conditions, shows an abrupt development of pressure at the inlet of the load carrying film. Since due to the hydrodynamic action the pressure develops smoothly, it is more reasonable to expect the pressure and the pressure gradient to be zero at the inlet of the load carrying film also [43].

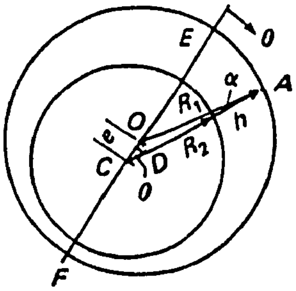

Figure 2.1: Geometry of a Journal Bearing

The Journal Bearing is the most common hydrodynamic bearing in use. It is a circular shaft (or journal) rotating inside a circular bearing. The inner diameter of the bearing is between one and three parts per thousand bigger than the shaft. It is very important to ensure that enough oil gets to the bearing so as to keep it cool. The amount of oil flow is important, as is the size and location of the minimum oil film thickness [47].

The film thickness h at the location θ shown in Fig. (2.1), is given by

$$h = c[1 + \epsilon \cos\theta] \tag{2.2}$$

where $\epsilon = e/c$ and c is radial clearance.

When the shaft and bearing are concentric $\epsilon = 0$ and when they are in contact $\epsilon = 1$. The minimum film thickness h_{min}, at $\theta = \pi$, is given by $c[1 - \epsilon]$.

Approximate solutions of Reynolds Equation are broadly classified into two categories, depending on the assumptions done regarding the bearing geometry as follows.

1. Bearing infinitely long *[The Sommerfeld Bearing]*

2. Bearing infinitely short *[The Ocvirk Bearing]*

The dimensionless Reynolds equation governing the pressure distribution in the lubricating film of a hydrodynamic journal is given as

$$\frac{\partial}{\partial \theta}\left[\frac{\bar{h}^3}{12}\frac{\partial \bar{p}}{\partial \theta}\right] + \frac{\partial}{\partial \bar{z}}\left[\frac{\bar{h}^3}{12}\frac{\partial \bar{p}}{\partial \bar{z}}\right] = \frac{1}{2}\frac{\partial \bar{h}}{\partial \theta} - \bar{V} \tag{2.3}$$

where $\bar{V}$ is the non-dimensional squeeze velocity, given by

$$\bar{V} = -\epsilon' \cos\theta - \epsilon' \beta' \sin\theta \tag{2.4}$$

Here the superscript $(\ )'$ denotes differentiation with respect to ωt

Eqn. (2.3) neglecting the squeeze velocity term $\bar{V}$ can be expressed in non-dimensional form as

$$\frac{\partial^2 \bar{p}}{\partial \theta^2} + \frac{1}{A}\frac{dA}{d\theta}\frac{\partial \bar{p}}{\partial \theta} + \frac{\partial^2 \bar{p}}{\partial \bar{z}^2} + \frac{C}{A} = 0 \tag{2.5}$$

where

$$A = \frac{\bar{h}^3}{12}$$

$$C = -\frac{1}{2}\frac{\partial \bar{h}}{\partial \theta} \tag{2.6}$$

Although Eqn. (2.5) can be solved in two dimensions, a simpler one-dimensional approach will be considered first.

2.2.2 Approximate One-Dimensional Approach for Solving Reynolds Equation in a Journal Bearing

For a Short Bearing, we can assume

$$\frac{\partial \bar{p}}{\partial \theta} \ll \frac{\partial \bar{p}}{\partial \bar{z}} \tag{2.7}$$

Consequently, Eqn. (2.5) reduces to

$$\frac{\partial^2 \bar{p}}{\partial \bar{z}^2} + \frac{C}{A} = 0 \tag{2.8}$$

which can be integrated and further simplified to

$$\bar{p} = \frac{C'^{*} \lambda^2}{2} \left[\frac{2\bar{z}}{\lambda} - \frac{\bar{z}^2}{\lambda^2} \right] \tag{2.9}$$

where, $C'^{*} = \frac{C}{A}$

Pressure at the center line of the bearing ie, at $\bar{z} = b/d = \lambda$ is given by

$$p_0 = \frac{C'^{*} \lambda^2}{2} \tag{2.10}$$

An outcome of Ocvirk's short bearing theory is that the axial pressure profile is parabolic, (Fig. 2.2). The pressure $\bar{p}$ at any arbitrary section AA in Fig. (2.2) is given by

$$\bar{p} = p_0 \left[2\bar{z} - \frac{\bar{z}^2}{\lambda^2} \right] \tag{2.11}$$

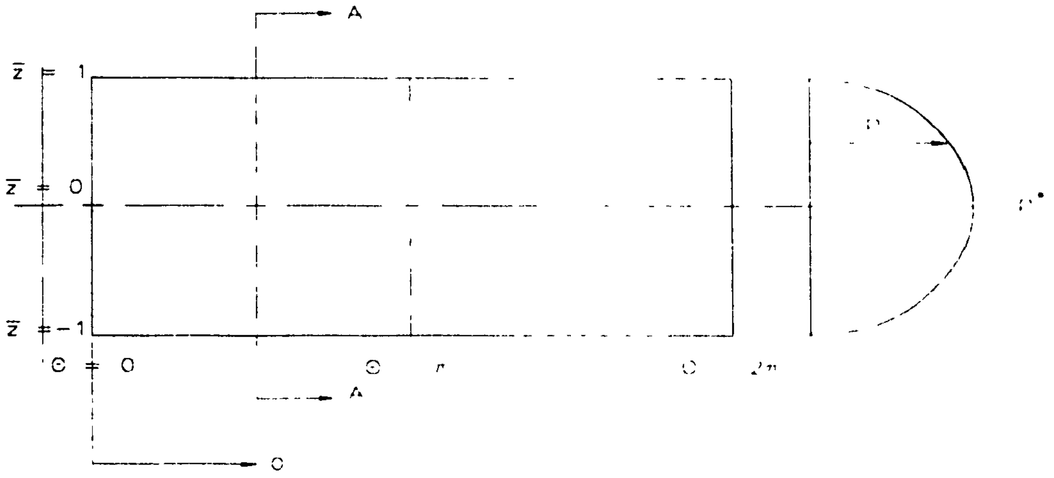

Figure 2.2: Axial Pressure Profile

Figure 2.3: Journal Bearing Domain

In Fig. (2.3) the domain is divided into MX equal lengths of $\delta\overline{x}$ such that $\delta\overline{x} = 2\pi/MX$.

The discrete values of $\overline{p}$ at each node are the solution.

Differentiating Eqn. (2.11) twice with respect to $\overline{z}$

$$\frac{\partial^2\overline{p}}{\partial\overline{z}^2} = p_0\left[-\frac{2}{\lambda^2}\right] \tag{2.12}$$

Substituting Eqn. (2.12) in Eqn. (2.5)

$$\frac{\partial^2\overline{p}}{\partial\theta^2} + \frac{1}{A}\left[\frac{dA}{d\theta}\right]\left[\frac{\partial\overline{p}}{\partial\theta}\right] - p_0\left[\frac{2}{\lambda^2}\right] + C^{*} = 0 \tag{2.13}$$

Considering node i, an approximation to the differential $\partial\overline{p}/\partial\theta$ can be made using the local values:

$$\left[\frac{\partial\overline{p}}{\partial\theta}\right]_i = \frac{\overline{p}_{i+1} - \overline{p}_{i-1}}{2\delta\overline{x}} \tag{2.14}$$

The second order differential also appears in the governing equation. This can be found initially considering the first differential at the half nodes.

$$\left[\frac{\partial\overline{p}}{\partial\theta}\right]_{i+1/2} = \frac{\overline{p}_{i+1} - \overline{p}_i}{\delta\overline{x}} = X_1 \quad (say) \tag{2.15}$$

$$\left[\frac{\partial\overline{p}}{\partial\theta}\right]_{i-1/2} = \frac{\overline{p}_i - \overline{p}_{i-1}}{\delta\overline{x}} = X_2 \quad (say) \tag{2.16}$$

The second differential can be found by differentiating these two values.

$$\frac{\partial^2 \bar{p}}{\partial \theta^2} = \frac{X_1 - X_2}{\delta \bar{x}} = \frac{\bar{p}_{i+1} + \bar{p}_{i-1} - 2\bar{p}_i}{\delta \bar{x}^2} \tag{2.17}$$

Substituting these values in Eqn. (2.13), first approximation at center line of the journal bearing is obtained as

$$\begin{aligned} 2\left[\frac{1}{\delta \bar{x}^2} + \frac{1}{\lambda^2}\right]\bar{p}_i &= \frac{1}{\delta \bar{x}^2}\left[1 + \frac{1}{4}\frac{A_{i+1} - A_{i-1}}{A_i}\right]\bar{p}_{i+1} \\ &+ \frac{1}{\delta \bar{x}^2}\left[1 - \frac{1}{4}\frac{A_{i+1} - A_{i-1}}{A_i}\right]\bar{p}_{i-1} + C^{**} \end{aligned} \tag{2.18}$$

2.2.3 Two dimensional Approach for Solving Reynolds Equation

The domain can be divided into a two-dimensional grid and Reynolds equation (2.5) can be written in finite difference form as :

$$\frac{\bar{p}_{i+1,j} - 2\bar{p}_{i,j} + \bar{p}_{i-1,j}}{\delta \bar{x}^2} + \left[\frac{A_{i+1} - A_{i-1}}{2\delta \bar{x} A_i}\right]\left[\frac{\bar{p}_{i+1,j} - \bar{p}_{i-1,j}}{2\delta \bar{x}}\right] + \frac{\bar{p}_{i,j+1} - 2\bar{p}_{i,j} + \bar{p}_{i,j-1}}{\delta \bar{z}^2} + \frac{C_i}{A_i} = 0 \tag{2.19}$$

Here $\bar{p}_{i,j}$ denotes the pressure at the (i,j) node in the fluid film. The above equation can be simplified to

$$\begin{aligned} \bar{p}_{i,j} &= \frac{1}{2\left(\frac{1}{\delta \bar{x}^2} + \frac{1}{\delta \bar{z}^2}\right)}\left[\frac{1}{\delta \bar{x}^2}\left(1 + \frac{1}{4}\frac{A_{i+1} - A_{i-1}}{A_i}\right)\bar{p}_{i+1,j} + \frac{1}{\delta \bar{x}^2}\left(1 - \frac{1}{4}\frac{A_{i+1} - A_{i-1}}{A_i}\right)\bar{p}_{i-1,j}\right] \\ &+ \frac{1}{2\left(\frac{1}{\delta \bar{x}^2} + \frac{1}{\delta \bar{z}^2}\right)}\left[\frac{1}{\delta \bar{z}^2}\left(\bar{p}_{i,j+1} + \bar{p}_{i,j-1}\right) + \frac{C_i}{A_i}\right] \end{aligned} \tag{2.20}$$

The first approximation for the two-dimensional analysis is calculated using the short bearing approximation [46]

$$\overline{p} \approx \overline{p}_m(\theta)\left(1 - \frac{\overline{z}}{\lambda^2}\right) \tag{2.21}$$

where $\overline{p}_m$ is the pressure at the center plane NZ, as calculated by one dimensional analysis, from Eqn. (2.18).

Considering i represent $\overline{x}$ direction and j represent $\overline{z}$ direction, from *1 to NX* (Fig. 2.3), the pressure distribution in the $\overline{z}$ direction can be calculated using Eqn. (2.21).

The pressure distribution $\overline{p}_{i,j}$ obtained in this way can be further refined using a two-dimensional solution Eqn. (2.20).

2.3 Calculation of Bearing Characteristics

2.3.1 Steady State Characteristics

From the steady state locus of the journal, it is seen that although the load applied on the rotor is always vertically down, the journal center does not move vertically up or down. If the load is respectively released or increased, as in a conventional spring system, the journal bearing behaves like an asymmetric spring offering also a horizontal motion in addition to a vertical motion. The bearing is anisotropic in character, offering different stiffnesses in different radial directions. Furthermore, if the journal is oscillating, the velocity of the journal introduces time dependent terms on the right hand side of the Reynolds equation which gives rise to squeeze film forces corresponding to damping forces in a viscous dash-pot. These forces are also asymmetric and should be accounted for in calculating the unbalance response of a rotor. Unlike the material damping in the rotor which is small, the damping offered by a fluid film bearing could be substantial and it is important to consider film damping in any analysis of the unbalance response of a rotor mounted on fluid film bearings. These stiffness and damping properties have also a considerable influence on the instability of a rotor, leading to a dangerous oil whip phenomenon observed in such rotors.

The load carrying capacity of fluid-film bearings derives from the hydrodynamic pressures produced in the lubricant by the shearing action of the rotating journal. At any given speed and, for a given value of lubricant viscosity, the film reaction force, is a function of the journal center position relative to the bearing center (eccentricity). In addition, it depends on the instantaneous journal center velocity (the squeeze effect).

2.3.2 Derivation of Dynamic Coefficients from Reynolds Equation

Reynolds equation with the inclusion of squeeze film term has the following form

$$\frac{\partial}{\partial\theta}\left[\frac{\bar{h}^3}{12}\frac{\partial\bar{p}}{\partial\theta}\right]+\frac{\partial}{\partial\bar{z}}\left[\frac{\bar{h}^3}{12}\frac{\partial\bar{p}}{\partial\bar{z}}\right]=\Gamma-\frac{1}{2}\frac{\partial\bar{h}}{\partial\theta} \tag{2.22}$$

The Reynolds pressure boundary conditions for the pressure distribution in the load carrying region are as follows [43]:

$$\begin{aligned}
\theta &= 0 && \bar{p}=0\\
\bar{z} &= \frac{b}{d} && \bar{p}=0\\
\theta &= \theta_2\,(\bar{z}) && \bar{p}=0,\quad \frac{\partial\bar{p}}{\partial\theta}=0\\
\bar{z} &= -\frac{b}{d} && \bar{p}=0
\end{aligned} \tag{2.23}$$

Since $\bar{p}=0$ at $\theta=\theta_2(\bar{z})$, the component of the pressure gradient in the tangential direction to the outlet boundary is zero. The condition $\theta=\theta_2(\bar{z})$, $\partial\bar{p}/\partial\theta=0$ is therefore trivial only when the tangent to the outlet boundary is in the circumferential direction and, except for this trivial case, both the components of the pressure gradient are seen to vanish on the outlet boundary.

The known solutions of Eqn. (2.22), obtained by using the boundary conditions (2.23), show the commencement of pressure development from $\theta = 0$, under an adverse pressure gradient, and this is meaningful only when the lubricant addition takes place precisely at $\theta = 0$. This discontinuity in the pressure gradient could be removed by restating the pressure boundary conditions as given below.

$$\begin{aligned} \theta &= \theta_1 (\bar{z}) & \bar{p} = 0, \quad \frac{\partial \bar{p}}{\partial \theta} = 0 \\ \bar{z} &= \frac{b}{d} & \bar{p} = 0 \\ \theta &= \theta_2 (\bar{z}) & \bar{p} = 0, \quad \frac{\partial \bar{p}}{\partial \theta} = 0 \\ \bar{z} &= -\frac{b}{d} & \bar{p} = 0 \end{aligned} \qquad (2.24)$$

Since $\theta = \theta_1 (\bar{z})$ and $\theta = \theta_2 (\bar{z})$ are not pre-specified boundaries, the additional conditions $\theta = \theta_1 (\bar{z})$, $\partial \bar{p} / \partial \theta = 0$ and $\theta = \theta_2 (\bar{z})$, $\partial \bar{p} / \partial \theta = 0$ could be considered as conditions necessary to define the inlet and outlet boundaries.

Reynolds equation can be simplified to

$$\frac{\partial}{\partial \theta} \left[\frac{\bar{h}^3}{12} \frac{\partial p^*}{\partial \theta} \right] + \frac{\partial}{\delta \bar{z}} \left[\frac{\bar{h}^3}{12} \frac{\partial p^*}{\partial \bar{z}} \right] + \frac{1}{2} \epsilon \left[\sin \theta - \epsilon^* \cos \theta \right] = 0 \qquad (2.25)$$

where

$$\epsilon^* = \frac{2\epsilon'}{\epsilon((1 - 2\beta')}$$

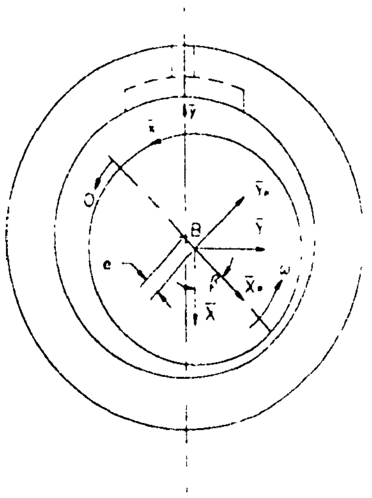

Figure 2.4: Journal Bearing

Figure 2.5: Lubricant Film

$$p^* = \frac{\bar{p}}{((1 - 2\beta')}$$

(2.26)

Given ϵ and ϵ^* and $\lambda = b/d$ the above Eqn. (2.25) could be solved with the modified pressure distribution p^*, using the modified pressure boundary conditions listed below [43]:

$$\begin{aligned}
\theta &= \theta_1\,(z) \quad p^* = 0, \quad \frac{\partial p^*}{\partial \theta} = 0 \\
z &= \frac{b}{d} \qquad p^* = 0 \\
\theta &= \theta_2\,(z) \quad p^* = 0, \quad \frac{\partial p^*}{\partial \theta} = 0 \\
z &= -\frac{b}{d} \qquad p^* = 0
\end{aligned}$$

(2.27)

The radially inward and the transverse force components P_c and P_s acting on the journal due to the hydrodynamic pressure are given by

$$\begin{aligned}
\frac{\bar{P}_c}{(1 - 2\beta')} &= P_c^* = \frac{1}{4b/d} \int\!\!\int p^* \cos\theta \, d\theta \, dz \\
\frac{\bar{P}_s}{(1 - 2\beta')} &= P_s^* = \frac{1}{4b/d} \int\!\!\int p^* \sin\theta \, d\theta \, dz
\end{aligned}$$

(2.28)

Now P^*_c and P^*_s are functions of ϵ and ϵ^* and b/d. For sufficiently small ϵ^*, the modified force components P_c^* and P_s^* can be approximated as [43],

$$P_c^* = S_c + \epsilon^* D_c$$

$$P_s^* = S_s + \epsilon^* D_s$$

(2.29)

S_c, S_s, D_c and D_s are independent of ϵ^*. Using Eqn. (2.28), Eqn. (2.29) can be rewritten in the alternate form as

$$P_c^* = S_c\,(1 - 2\beta') + \epsilon^*\,(1 - 2\beta')\,D_c$$

$$P_s^* = S_s\,(1 - 2\beta') + \epsilon^*\,(1 - 2\beta')\,D_s$$

(2.30)

substituting

$$\epsilon^*\,(1 - 2\beta') = \frac{2\epsilon'}{\epsilon}$$

$$P_c^* = S_c^* + \frac{2}{\epsilon} D_c^* \epsilon' - \frac{2}{\epsilon} S_c^* \epsilon \beta'$$
$$P_s^* = S_s^* + \frac{2}{\epsilon} D_s^* \epsilon' - \frac{2}{\epsilon} S_s^* \epsilon \beta'$$

(2.31)

For the steady state, $\epsilon' = 0$ and $\epsilon\beta' = 0$. Thus the Sommerfeld number and the attitude angle are given by

$$S_0 = \sqrt{S_c^{*2} + S_s^{*2}} \qquad (2.32)$$

$$\beta_0 = \tan^{-1}\left(\frac{S_s^*}{S_c^*}\right) \tag{2.33}$$

Displacements in the radial and tangential direction are given by

$$\overline{X}_p = \frac{X_p}{c} = \delta\epsilon$$

$$\overline{Y}_p = \frac{Y_p}{c} = \epsilon\delta\beta \tag{2.34}$$

The restoring force component for displacement X_p.

$$\begin{aligned} \delta S_{X_p} &= \frac{\partial S_c^*}{\partial\epsilon}\partial\epsilon + S_s^*\delta\beta \\ \delta S_{Y_p} &= \frac{\partial S_s^*}{\delta\epsilon}\partial\epsilon + S_c^*\delta\beta \end{aligned} \tag{2.35}$$

or

$$\begin{aligned} \frac{\delta S_{X_p}}{S_o} &= \frac{1}{S_0}\frac{\partial S_c^*}{\partial\epsilon}\delta\epsilon + \frac{S_s^*}{S_0\epsilon}\epsilon\delta\beta \\ \frac{\delta S_{Y_p}}{S_o} &= \frac{1}{S_0}\frac{\partial S_s^*}{\partial\epsilon}\delta\epsilon + \frac{S_c^*}{S_0\epsilon}\epsilon\delta\beta \end{aligned} \tag{2.36}$$

The stiffness coefficient matrix with respect to the radial-transverse frame $J\overline{X}_p\overline{Y}_p$, shown in Fig. (2.4), can be evaluated from S_c^* and S_s^* as

$$\overline{K}_p = \frac{1}{S_0}\begin{bmatrix} (\partial S_c^*/\partial\epsilon) & (S_s^*/\epsilon) \\ -(\partial S_s^*/\partial\epsilon) & (S_c^*/\epsilon) \end{bmatrix} \tag{2.37}$$

From Eqn. (2.30), the damping coefficient matrix with respect to the radial-transverse frame can be written as

$$\bar{\mathcal{C}}_p = \frac{2}{\epsilon.S_0} \begin{bmatrix} D_c{}^* & -S_c{}^* \\ -D_s{}^* & S_s{}^* \end{bmatrix} \tag{2.38}$$

Transforming the stiffness and damping coefficient matrices from $J\mathcal{X}_p\mathcal{Y}_p$ to $J\mathcal{X}\mathcal{Y}$ frame as shown in Fig. (2.4) results in

$$[\bar{\mathcal{K}}] = [T]^T[\bar{\mathcal{K}}_p][T] \tag{2.39}$$

and

$$[\bar{\mathcal{C}}] = [T]^T[\bar{\mathcal{C}}_p][T] \tag{2.40}$$

where

$$[T] = \begin{bmatrix} \cos\beta & \sin\beta \\ -\sin\beta & \cos\beta \end{bmatrix} \tag{2.41}$$

2.4 Numerical Computation

For given values of b/d, ϵ and ϵ^*, Eqn. (2.25) was solved for p^*, using the modified boundary conditions (2.27), by means of a finite difference scheme. Intervals of $\pi/45$ and 0.05 in the circumferential and axial directions, respectively, were used with an over-relation factor of 1.5. The computations were carried out for b/d = *0.25, 0.50, 0.75 and 1.00,* ϵ = 0.10, 0.15, 0.20,......, 0.90 and ϵ^* = -0.2, -0.1, 0.0, and 0.2. The modified force components $P_c{}^*$ and $P_s{}^*$ were evaluated using Simpson's rule.

By fitting the fourth degree polynomials in ϵ^* for P_c^* and P_s^* the quantities S_c, S_s, D_c, and D_s are evaluated. The derivatives of the quantities $S_c(1-\epsilon^2)^2$ $S_s(1-\epsilon^2)^2$ with respect to ϵ were evaluated by fitting the piecewise cubic interpolation polynomials and the derivatives of S_c and S_s with respect to ϵ were deduced. The stiffness and damping coefficients were finally evaluated and the computations were repeated using the Reynolds boundary conditions.

2.5 Results and Conclusions

The present computational scheme utilizes a more accurate method for the determination of the derivatives and is less prone to truncation error. Pressure distribution in the journal bearing using short bearing, long bearing, finite bearing approach is evaluated, and a comparison between short bearing and long bearing is done for different b/d ratio's, and represented in Figs. (2.6 - 2.13).

In Fig. (2.6) pressure distribution in a journal bearing for a b/d ratio of 0.25 is plotted using the short bearing approximation. For the purpose of comparison, the measured pressure distribution by the finite bearing approach is shown in dotted line. Similar results are shown in Figs. (2.7 - 2.9) for bearing of b/d ratio's 0.50, 0.75 and 1.00, respectively. In all cases short bearing approximation gives a much larger value of pressure around $\theta = 165°$. An approximation to pressure distribution in a journal bearing is also made with long bearing approach and the results are depicted in Figs. (2.10 - 2.13). Comparison is made to finite bearing distribution in dotted line in the same plot. The results are represented for b/d ratios of 0.25, 0.75, 1.00 respectively. The long bearing approximation gives a smaller value of pressure in all the cases discussed.

In a bearing the make-up flow, ie. the top side leakage, is a very important quantity which is the oil that has to be pumped into the bearing to keep it full. This flow is made up of two components, the first is the difference between the oil flowing at the start of the pressure curve and the finish. The second part is the oil that flows out of the bearing near the entry, due to the pressure feeding. The Fig. (2.14) represents the plot of flow rate vs. eccentricity ratio ϵ for a *b/d* ratio of 0.75.

There is a direct relationship between Sommerfeld number *So* and eccentricity ratio ϵ. As ϵ increases, so does Sommerfeld number proportionately. Fig. (2.15) shows a plot of Sommerfeld number vs. eccentricity ratio for a bearing of *b/d* ratio of 0.75.

In Fig. (2.16) the complete computed results of eccentricity ratio vs. attitude angle are plotted for a journal bearing of *b/d* ratio of 0.75. Such a plot is often called '*the equilibrium semi circle*'. This plot enables the location of h_{min} to be determined for a particular *b/d* ratio.

Variation of direct stiffness coefficients $\overline{K}_{xx}$. $\overline{K}_{yy}$ and direct damping coefficients $\overline{C}_{xx}$, $\overline{C}_{yy}$ with respect to Sommerfeld number *So* is shown in Fig. (2.17) for a bearing of *b/d = 0.25*. The value of the direct stiffness $\overline{K}_{xx}$ is found to increase with the increase of Sommerfeld number, whereas $\overline{K}_{yy}$ decreases slightly, remaining almost constant over a wide range of Sommerfeld number. Direct damping coefficient $\overline{C}_{xx}$ decreases with increase in Sommerfeld number to a limiting value of Sommerfeld number, and with any increase above this value, $\overline{C}_{xx}$ also increases, whereas $\overline{C}_{yy}$ decreases gradually with the increase in Sommerfeld number.

Cross coupled stiffness and damping coefficients variation is represented in Fig. (2.18). Cross coupled stiffness $\overline{K}_{xy}$ decreases with an increase in Sommerfeld number, and increases after a certain value of *So*. Negative value of the stiffness coefficient $\overline{K}_{yx}$ over a wide range of Sommerfeld number is one of the major factors in causing the backward whirling motion of the rotor. Cross coupled stiffness $\overline{K}_{yx}$ does take a positive value at a higher range of Sommerfeld number. These results are computed for journal bearings having *b/d* ratios of 0.50, 0.75 and 1.00 respectively, and direct and cross coupled stiffness and damping coefficients are plotted in Figs. (2.19 - 2.24).

Stiffness and damping coefficients of hydrodynamic bearings influence the unbalance response of the rotor supported on them. The anisotropic nature of stiffness coefficient results in backward whirling of the rotor between the critical speeds. It is observed that the asymmetry of the damping coefficients remain negligible under the modified boundary conditions. The stiffness and damping coefficients thus calculated in this chapter are used in the following chapters in finding the unbalance response of the rotor supported on hydrodynamic bearings and the occurrence of simultaneous forward and backward whirling motion. In Chapter 3, the unbalance response and the simultaneous forward and backward whirling motion of a Jeffcot rotor supported on two identical bearings are analyzed and discussed.

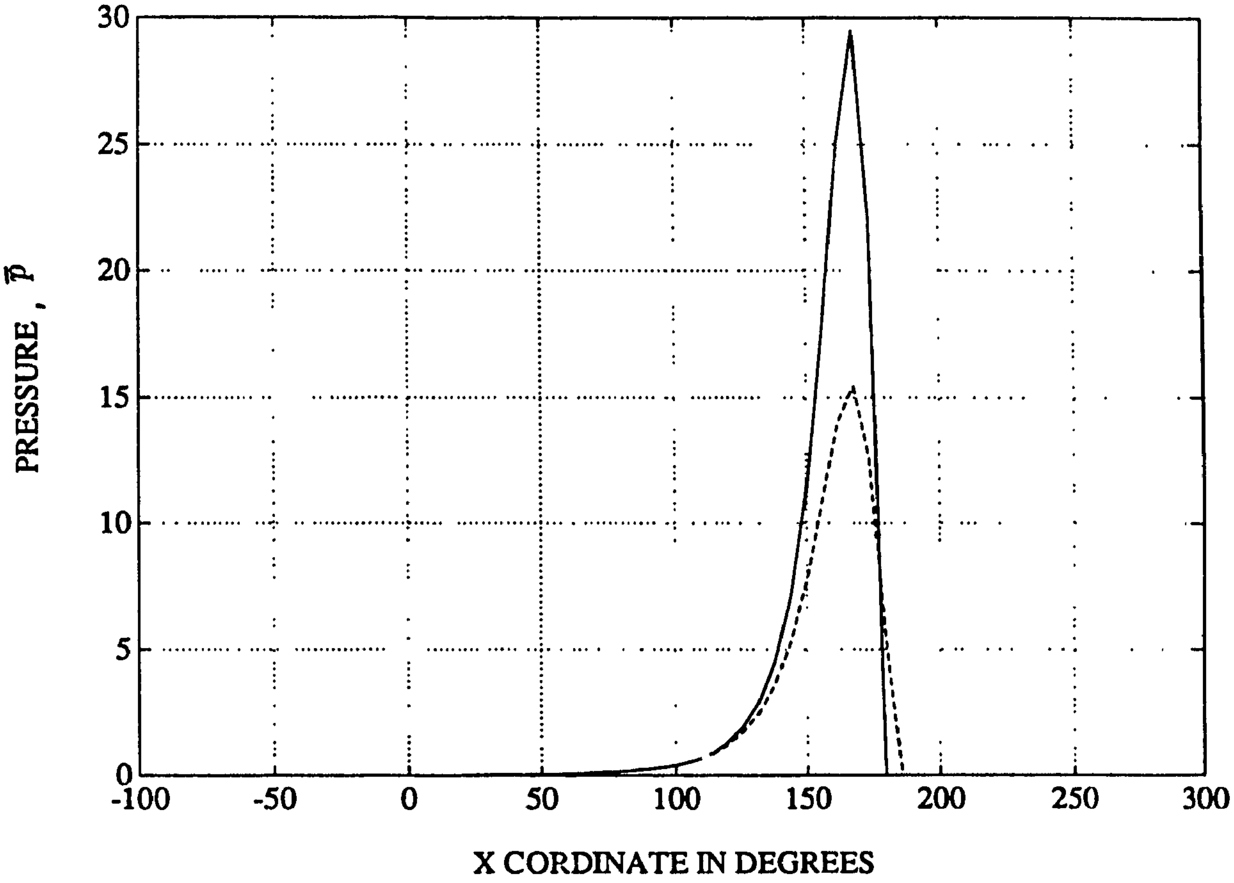

Figure 2.6: Pressure Distribution around the Journal by the Short Bearing Approximation : b/d = 0.25

——— Short Bearing Approximation
.... Finite Difference Approximation

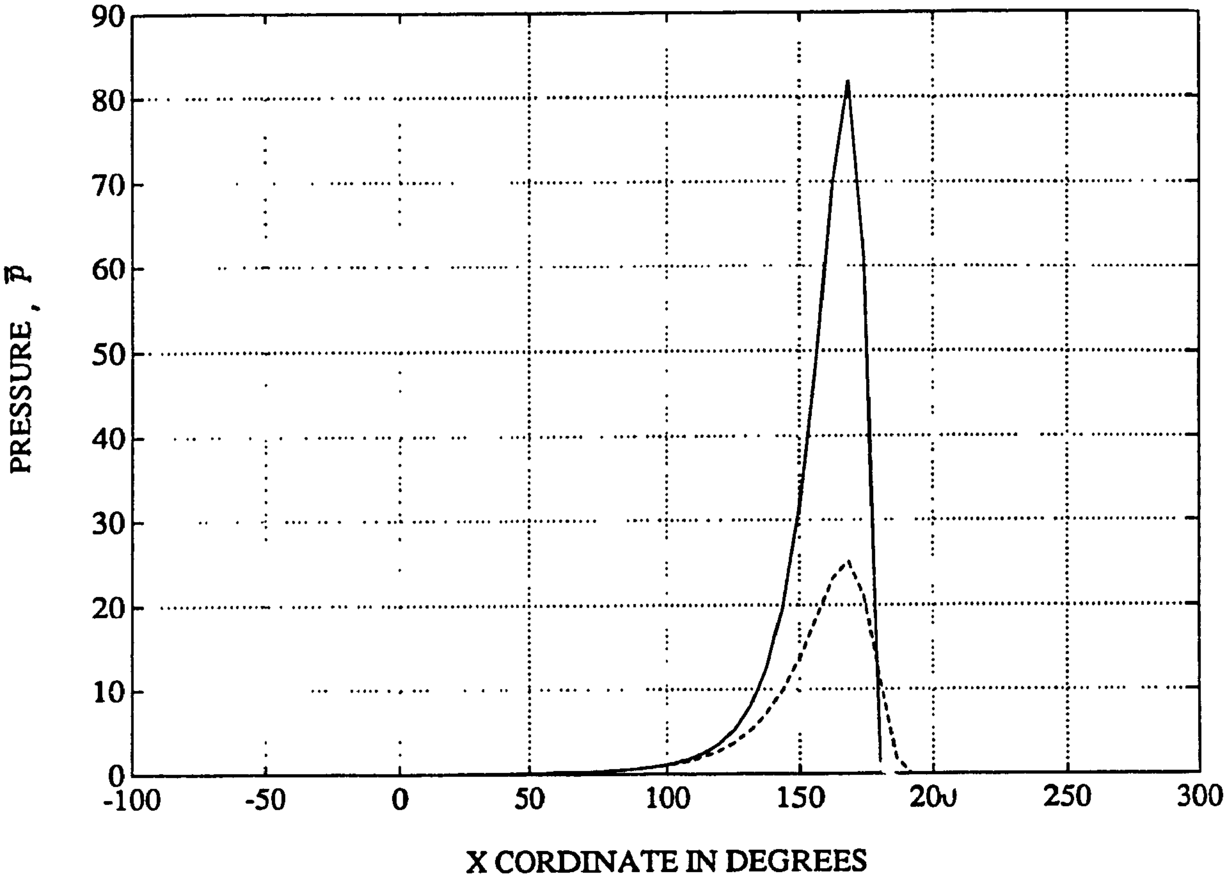

Figure 2.7: Pressure Distribution around the Journal by the Short Bearing Approximation : b/d = 0.50

———— Short Bearing Approximation
.... Finite Difference Approximation

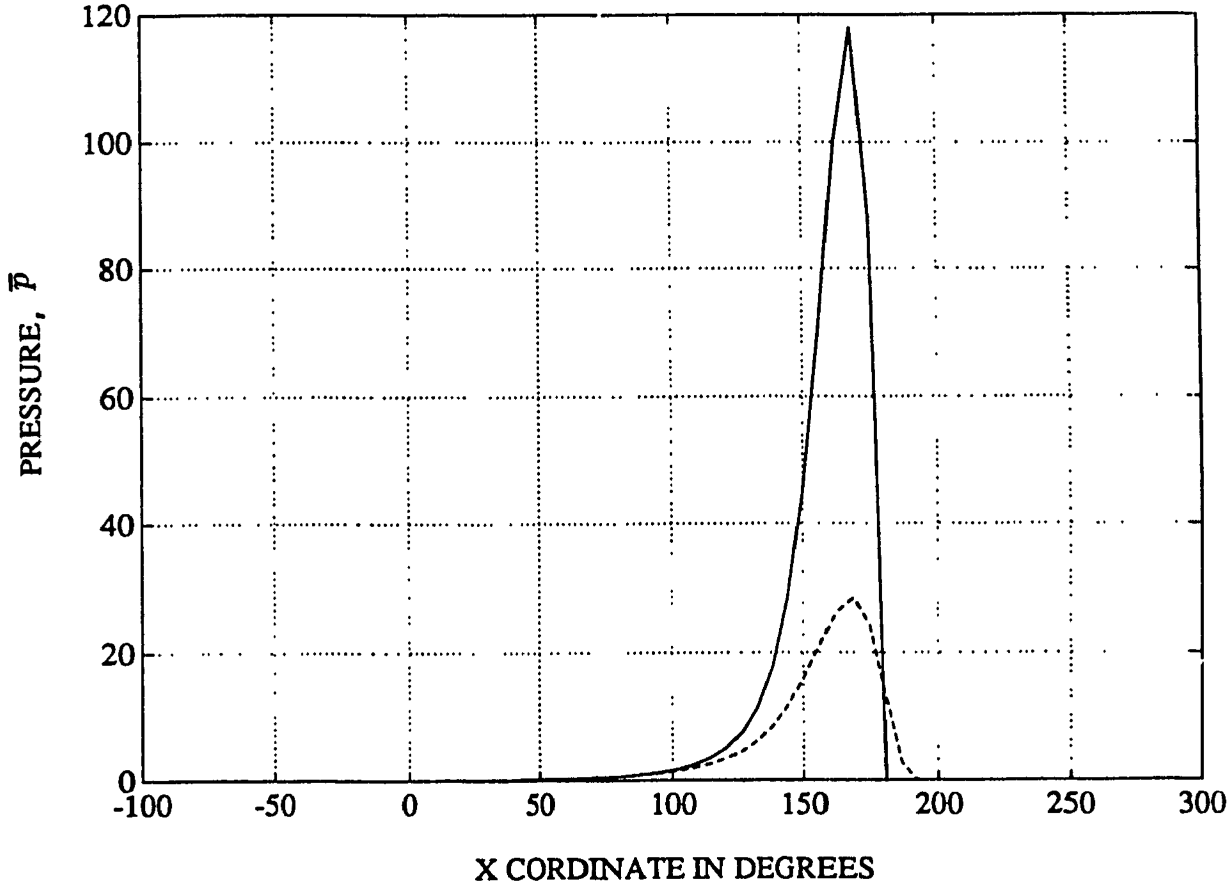

Figure 2.8: Pressure Distribution around the Journal by the Short Bearing Approximation : b/d = 0.75

———— Short Bearing Approximation
.... Finite Difference Approximation

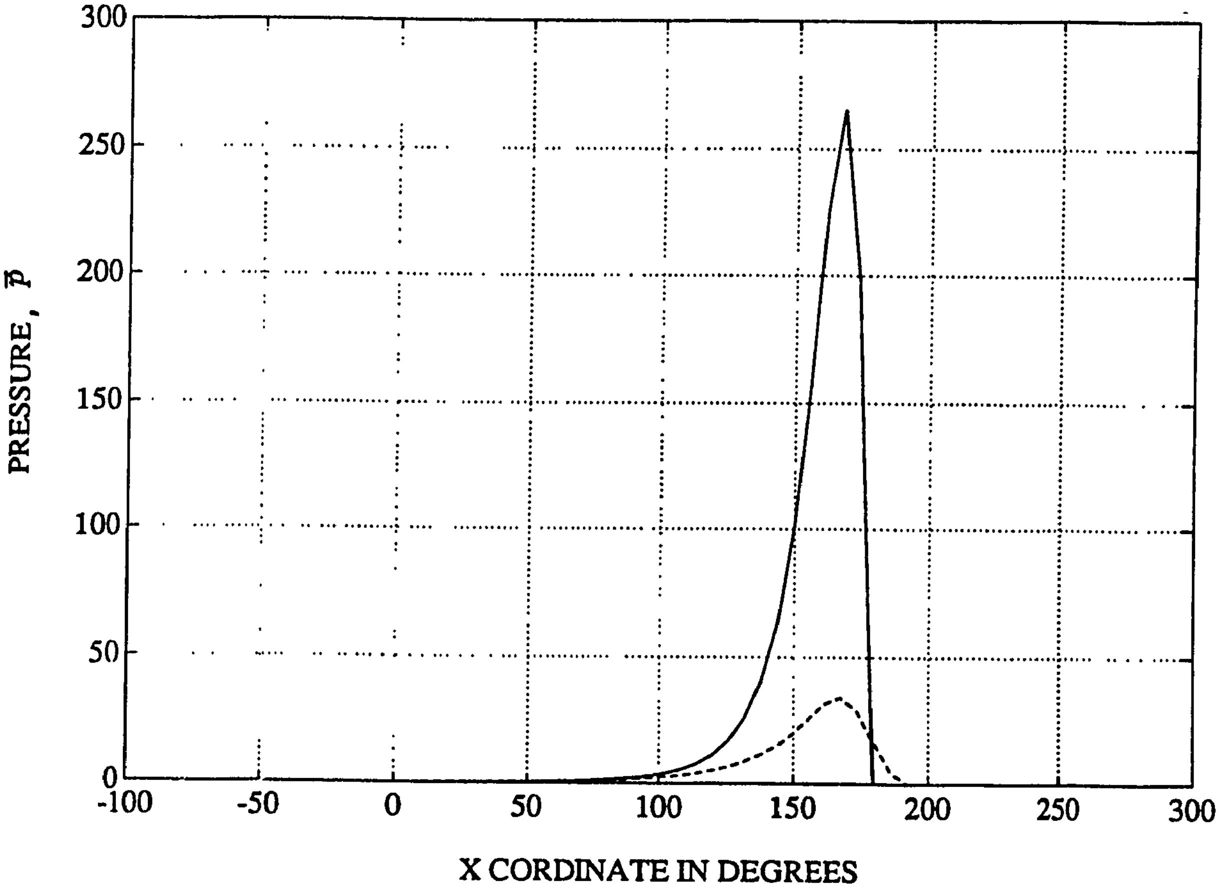

Figure 2.9: Pressure Distribution around the Journal by the Short Bearing Approximation : b/d = 1.00

——— Short Bearing Approximation

……….. Finite Difference Approximation

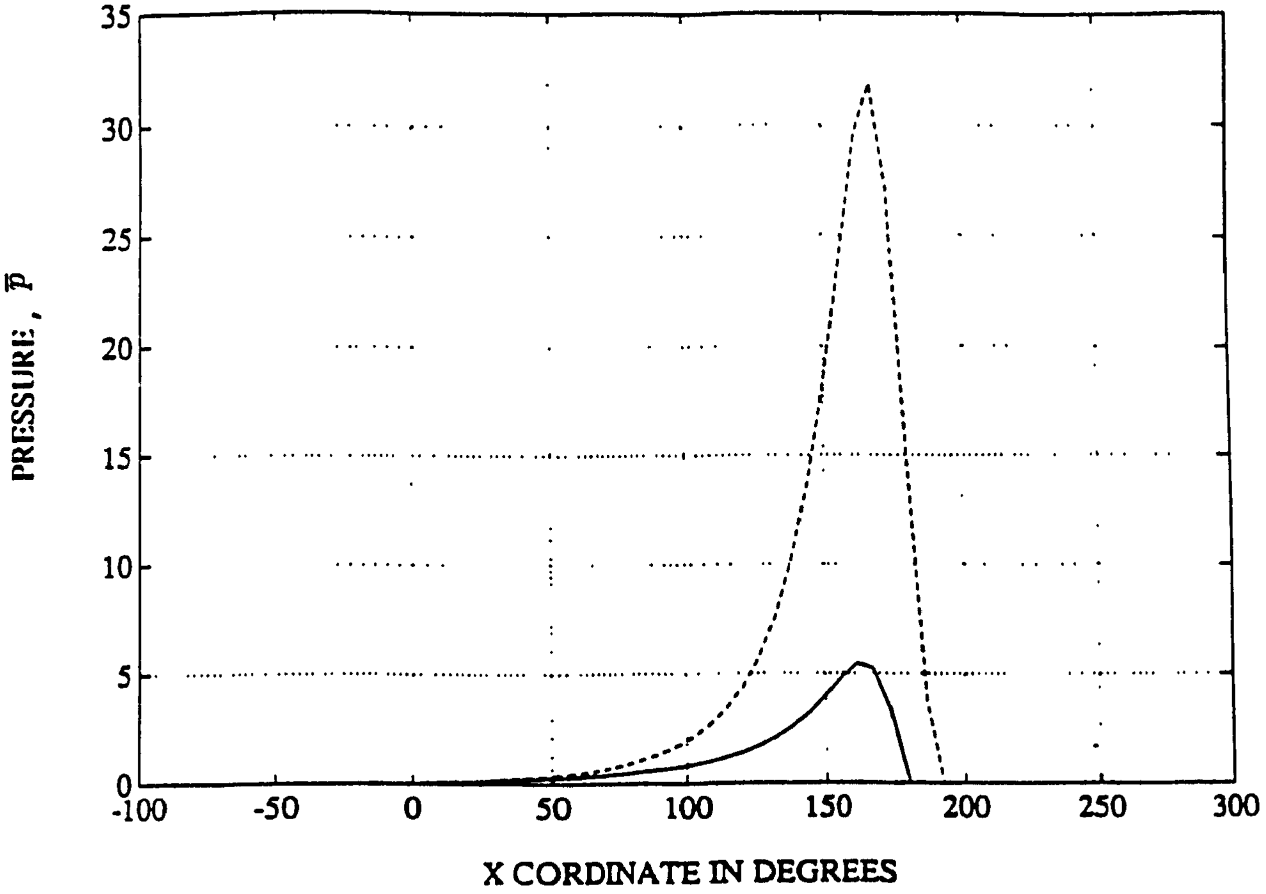

Figure 2.10: Pressure Distribution around the Journal by the Long Bearing Approximation : b/d = 0.25

——— Long Bearing Approximation

.... Finite Difference Approximation

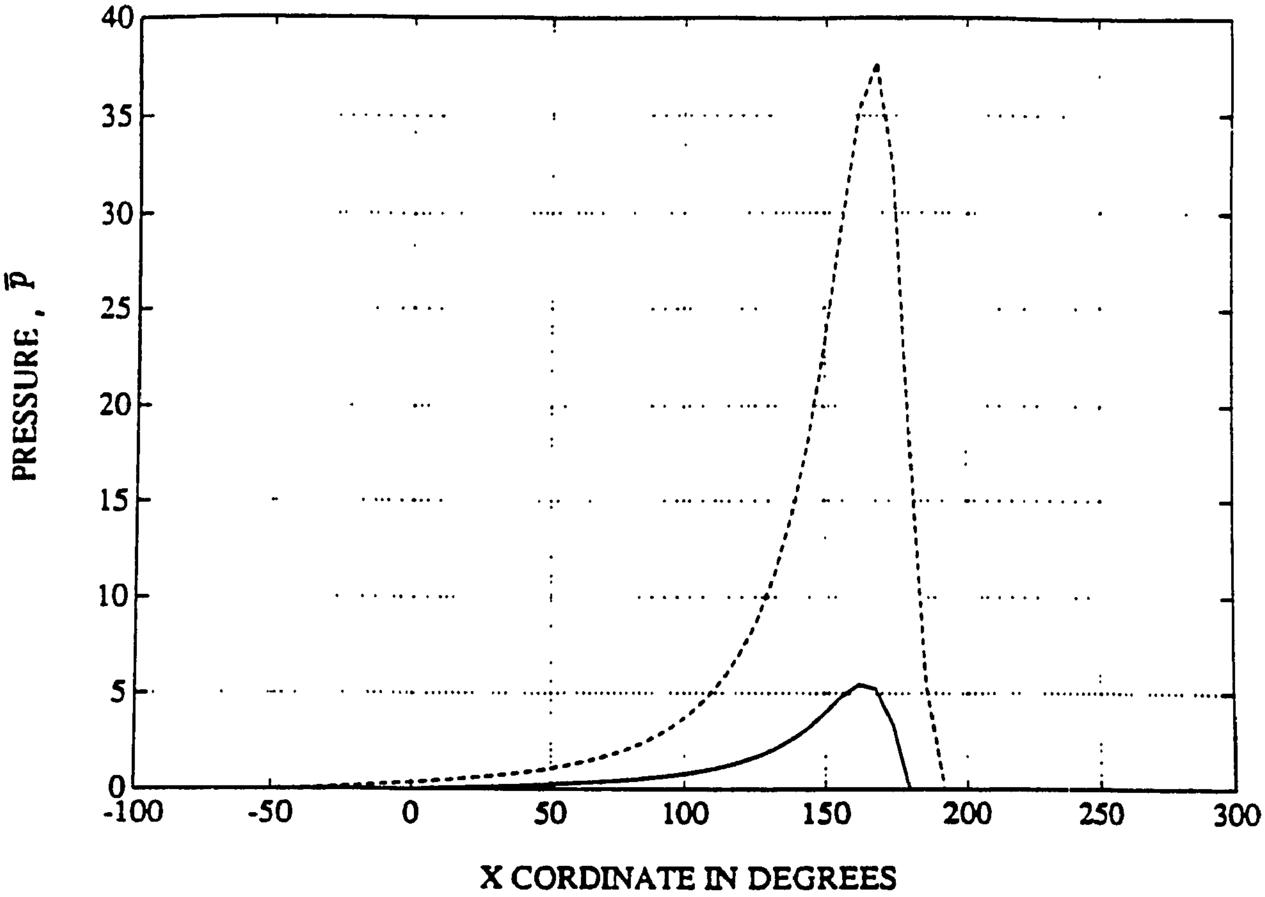

Figure 2.11: Pressure Distribution around the Journal by the Long Bearing Approximation : b/d = 0.50

——— Long Bearing Approximation
.... Finite Difference Approximation

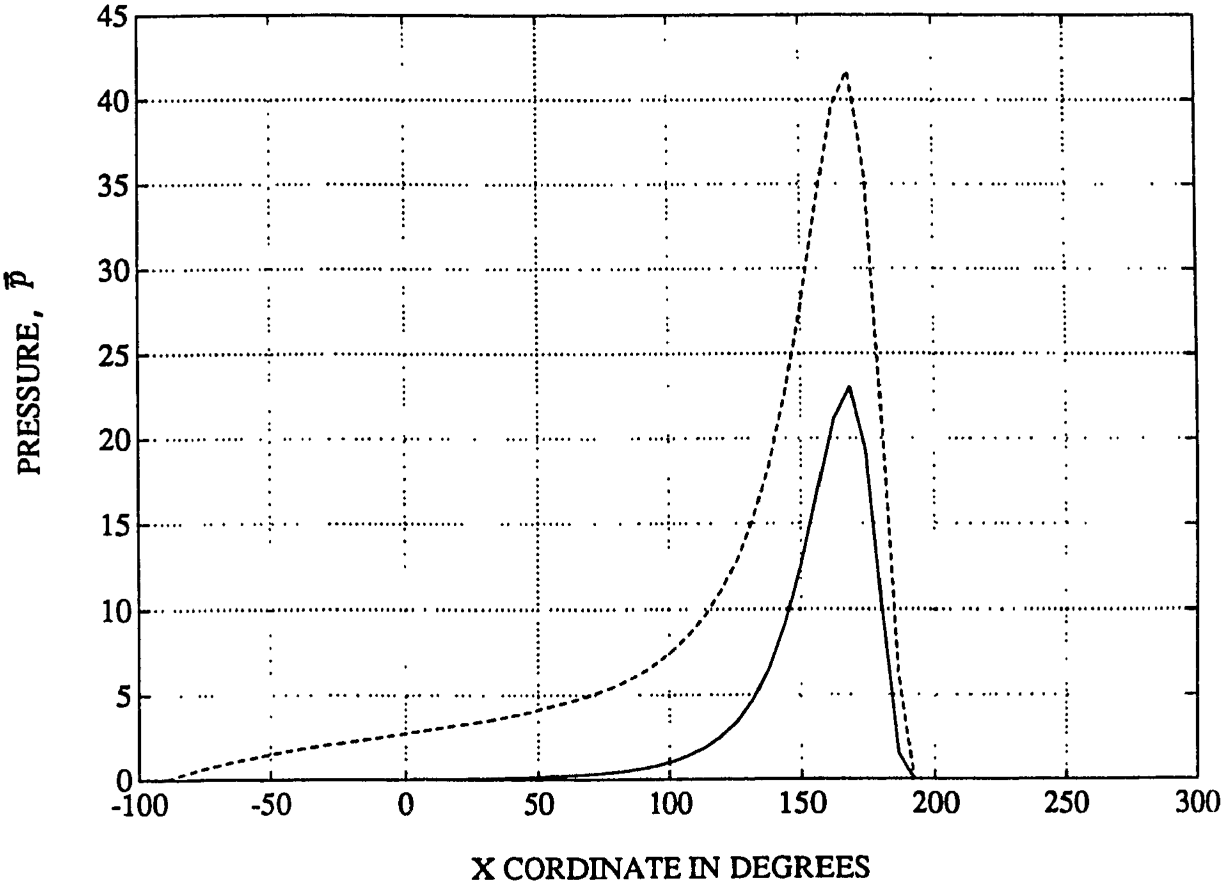

Figure 2.12: Pressure Distribution around the Journal by the Long Bearing Approximation : b/d = 0.75

——— Long Bearing Approximation
.... Finite Difference Approximation

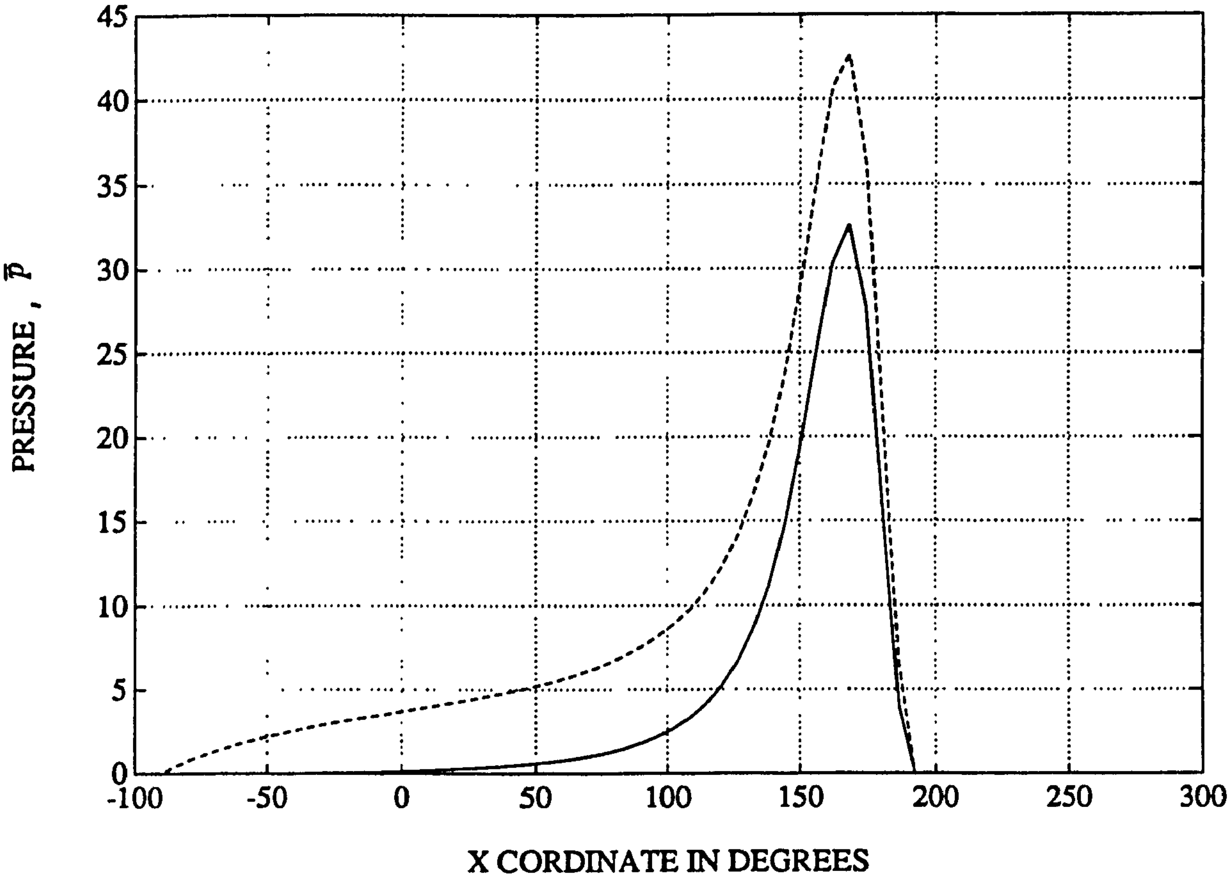

Figure 2.13: Pressure Distribution around the Journal by the Long Bearing Approximation : b/d = 1.00

——— Long Bearing Approximation
.... Finite Difference Approximation

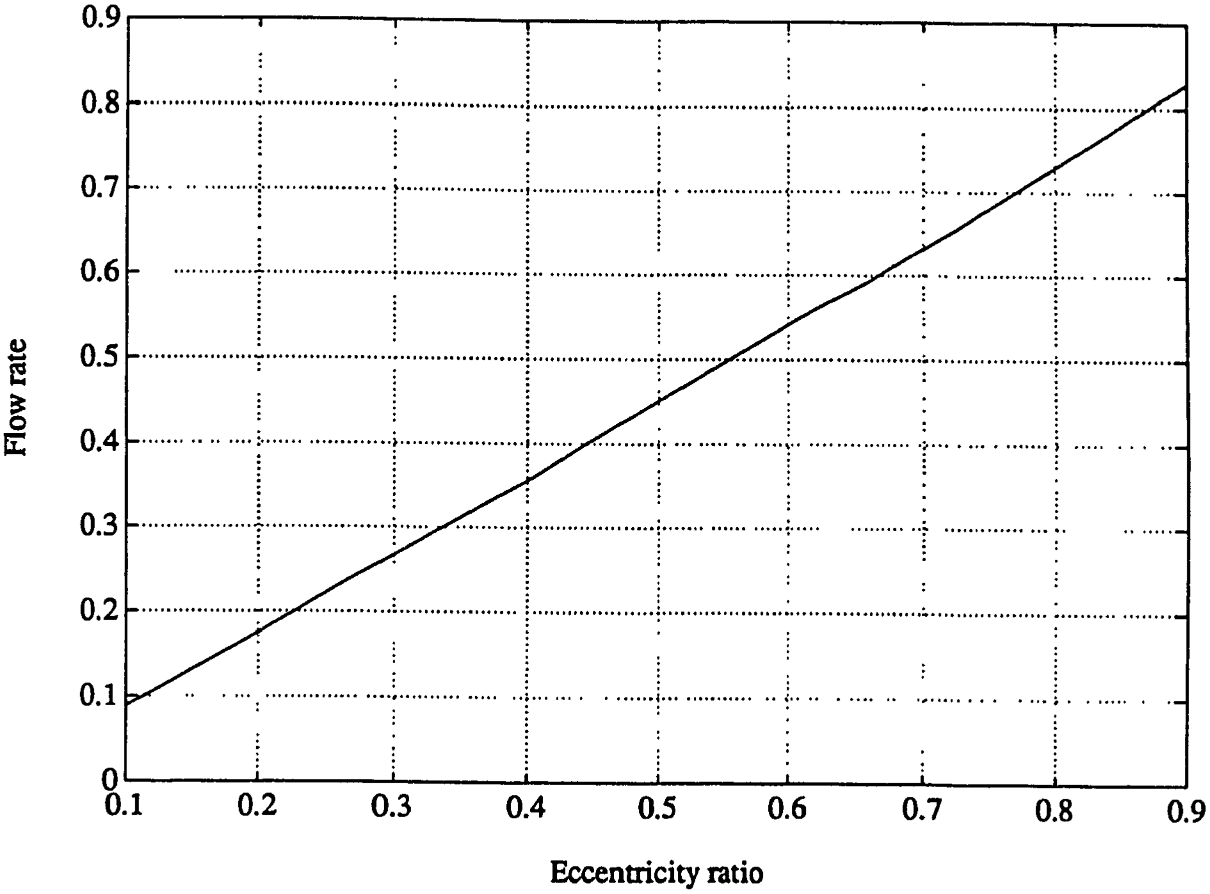

Figure 2.14: Plot of Flow Rate $\overline{Q}$ vs. Eccentricity Ratio ϵ : b/d = 0.75

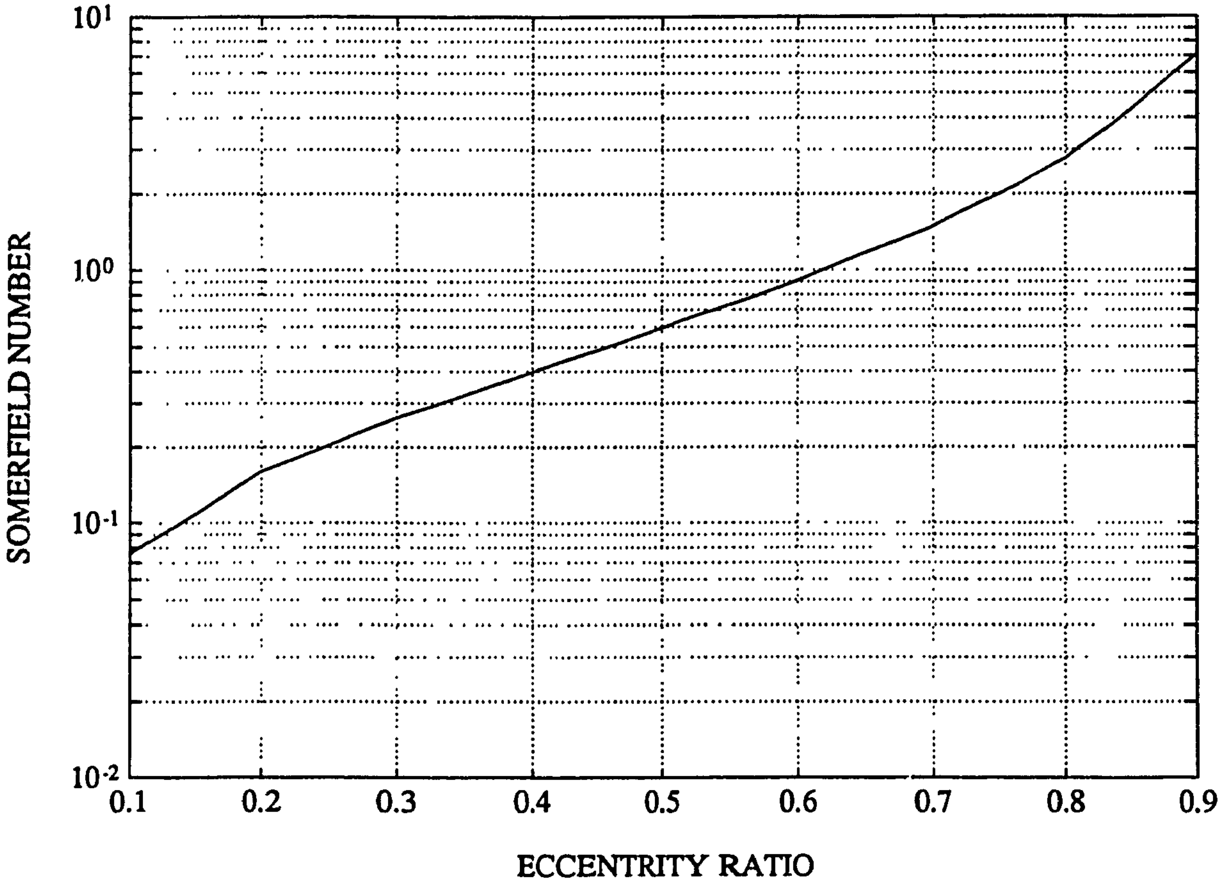

Figure 2.15: Plot of Sommerfeld Number So_0 vs. Eccentricity Ratio ϵ : b/d = 0.75

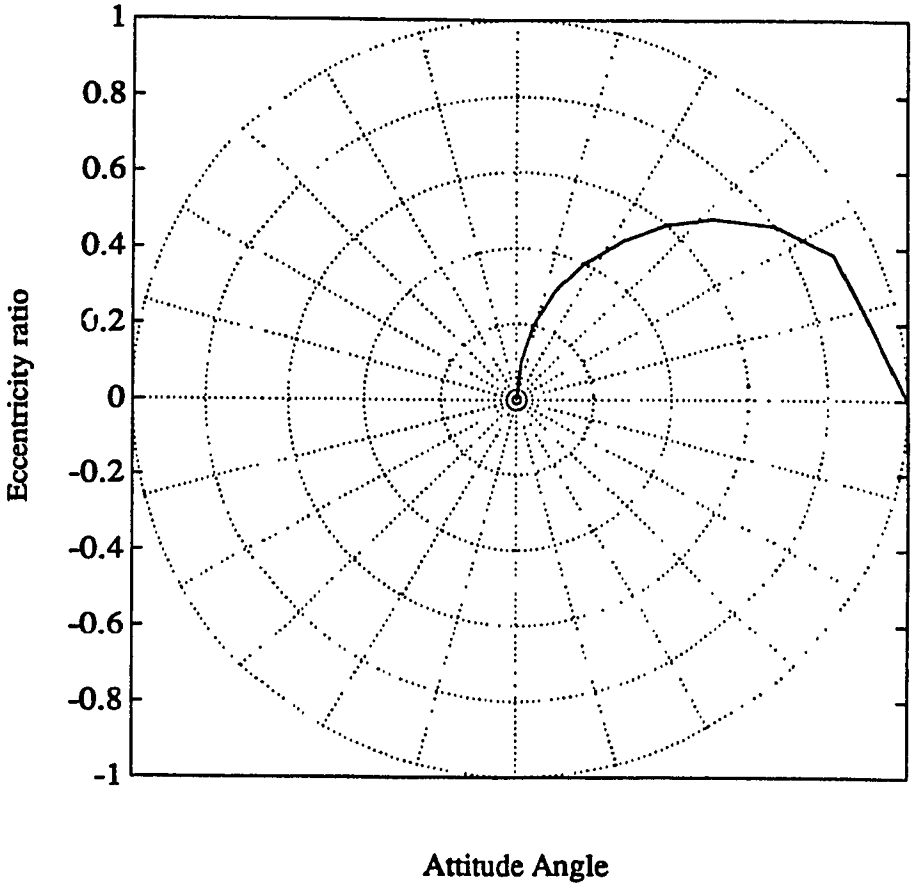

Figure 2.16: Plot of Eccentricity Ratio ϵ vs. Attitude angle β : b/d = 0.75

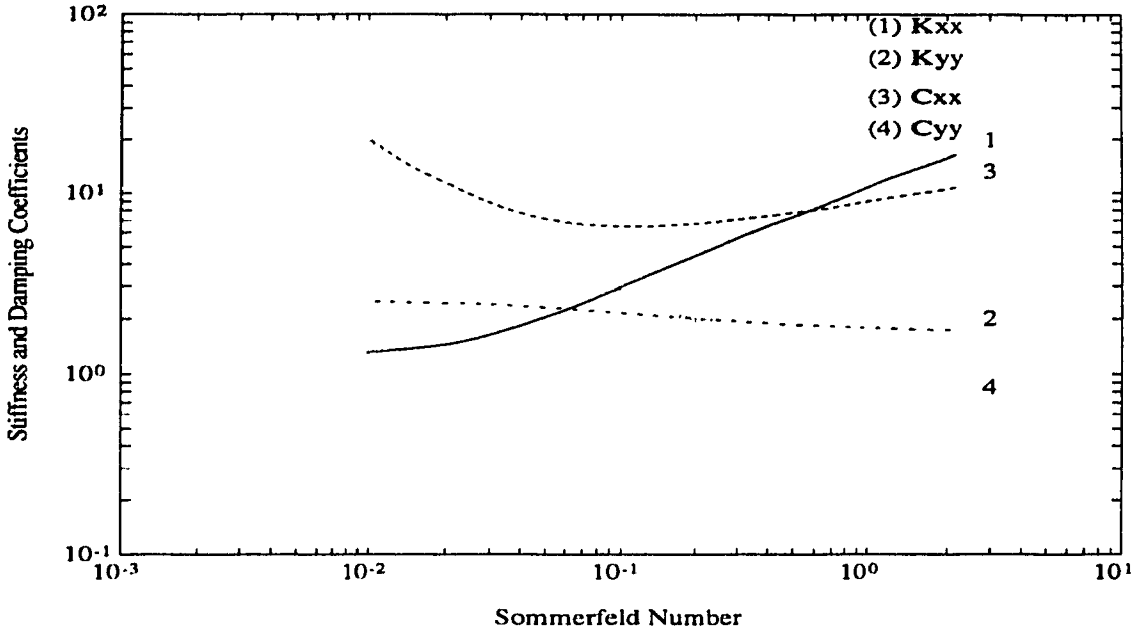

Figure 2.17: Plot of Non-Dimensional Direct Stiffness and Damping Coefficients of a Cylindrical Bearing Vs. Sommerfeld Number S_{ω_0} : b/d = 0.25

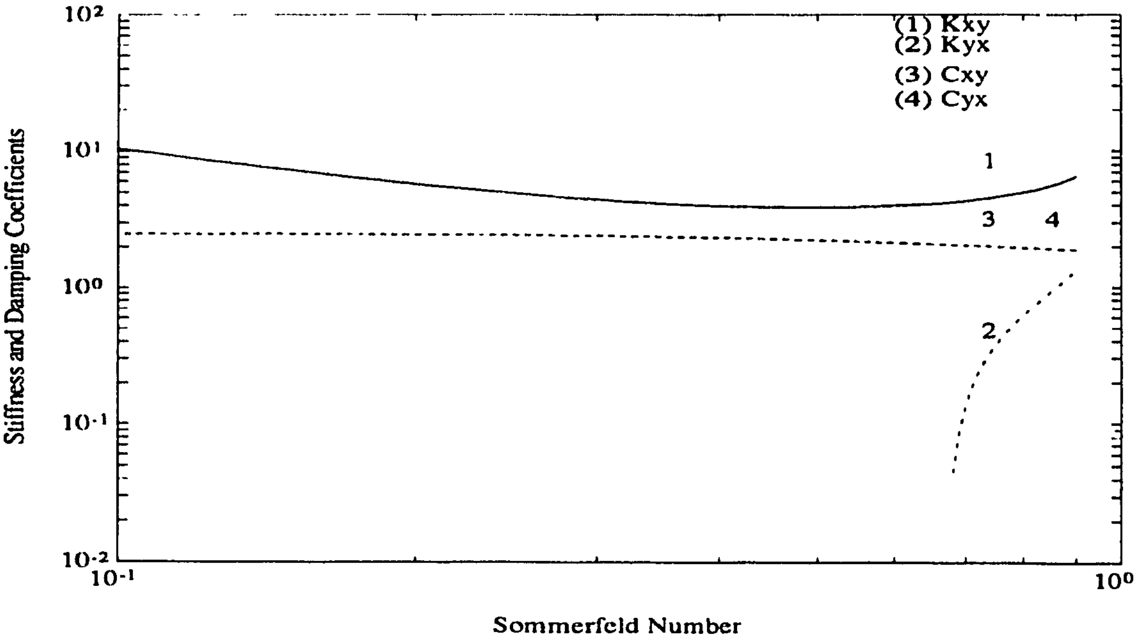

Figure 2.18: Plot of Non-Dimensional Cross Coupled Stiffness and Damping Coefficients of a Cylindrical Bearing Vs. Sommerfeld Number S_{ω_0} : b/d = 0.25

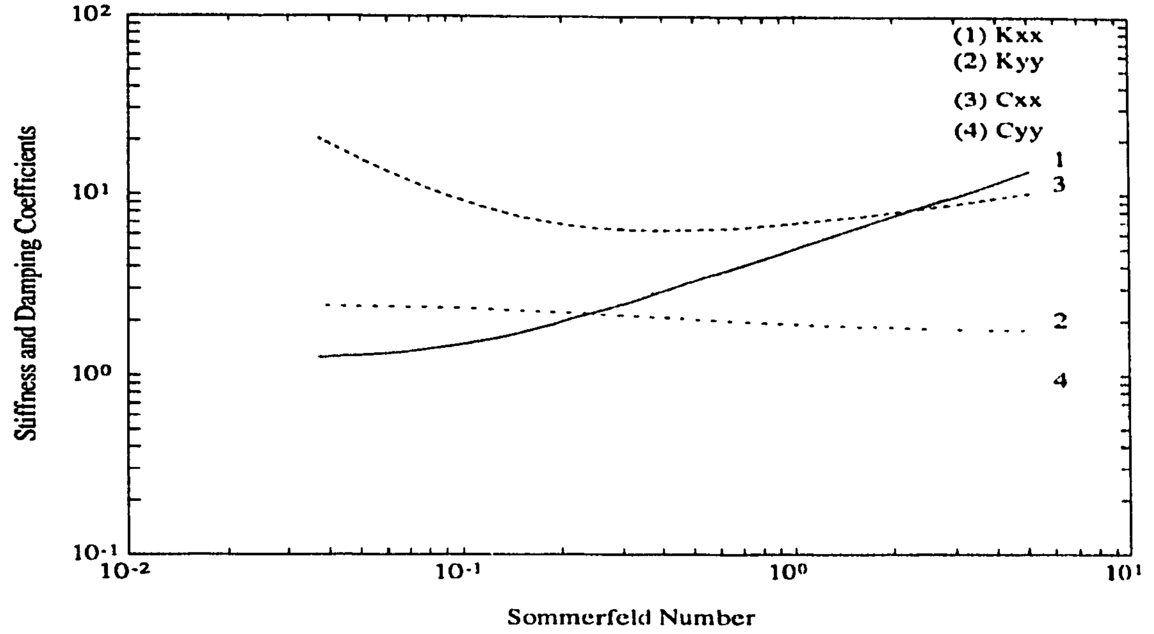

Figure 2.19: Plot of Non-Dimensional Direct Stiffness and Damping Coefficients of a Cylindrical Bearing Vs. Sommerfeld Number $S\alpha_0$: b/d = 0.50

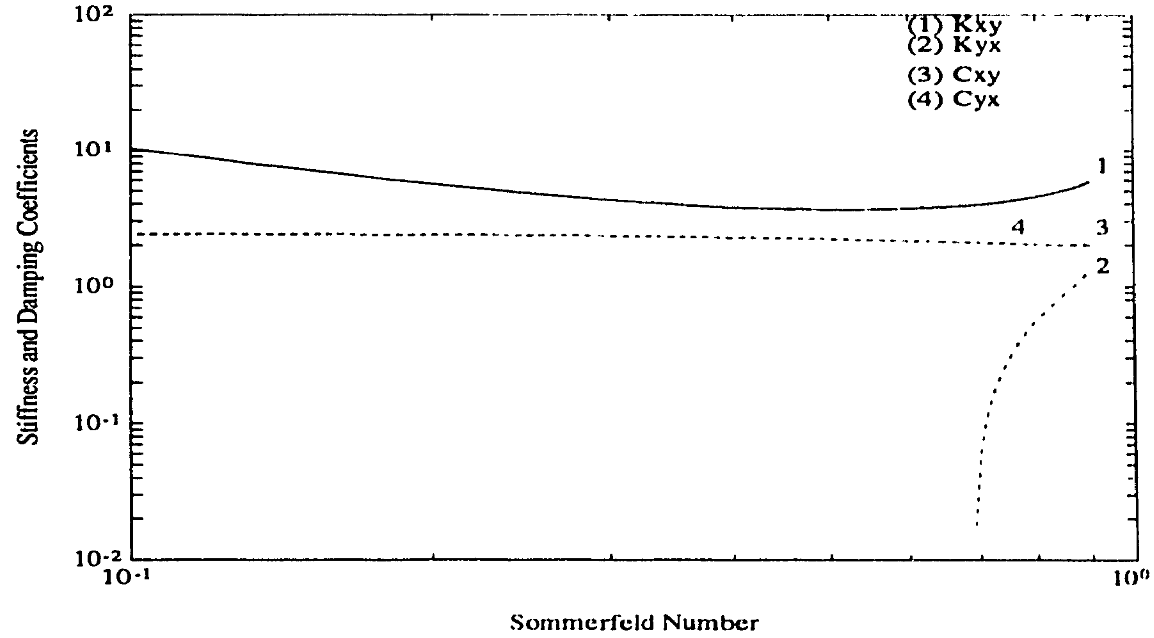

Figure 2.20: Plot of Non-Dimensional Cross Coupled Stiffness and Damping Coefficients of a Cylindrical Bearing Vs. Sommerfeld Number $S\alpha_0$: b/d = 0.50

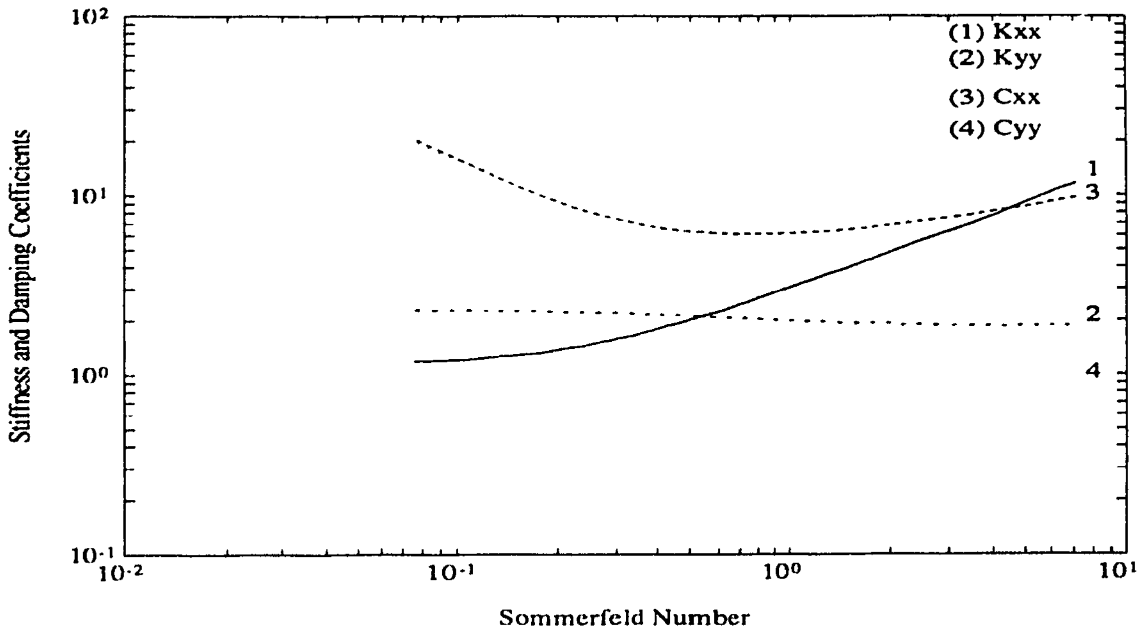

Figure 2.21: Plot of Non-Dimensional Direct Stiffness and Damping Coefficients of a Cylindrical Bearing Vs. Sommerfeld Number So_0 : b/d = 0.75

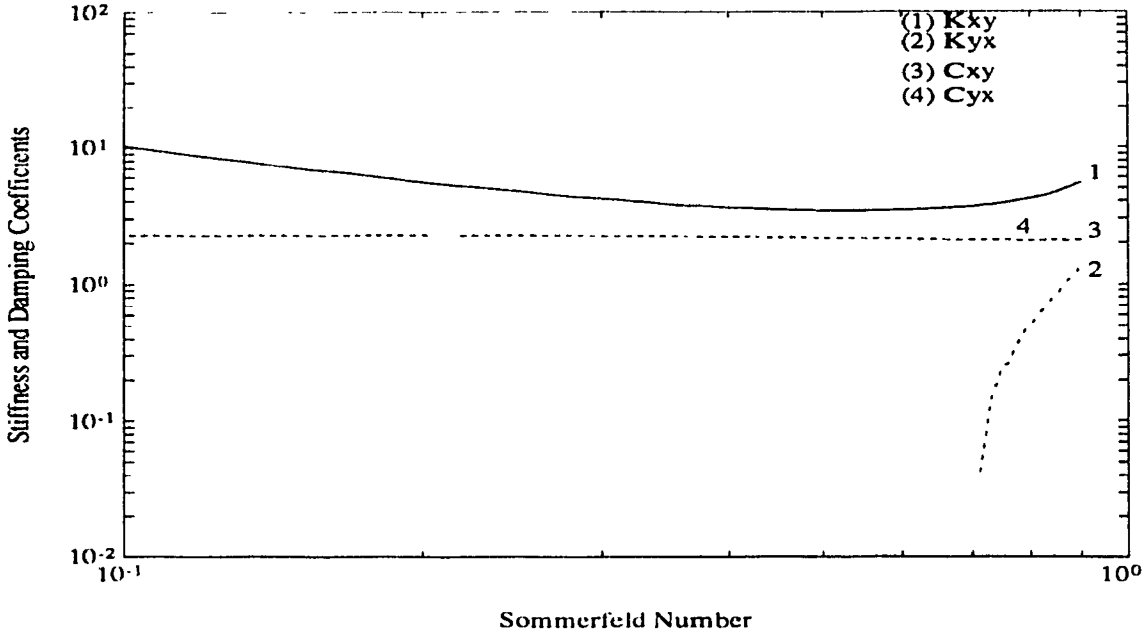

Figure 2.22: Plot of Non-Dimensional Cross Coupled Stiffness and Damping Coefficients of a Cylindrical Bearing Vs. Sommerfeld Number So_0 : b/d = 0.75

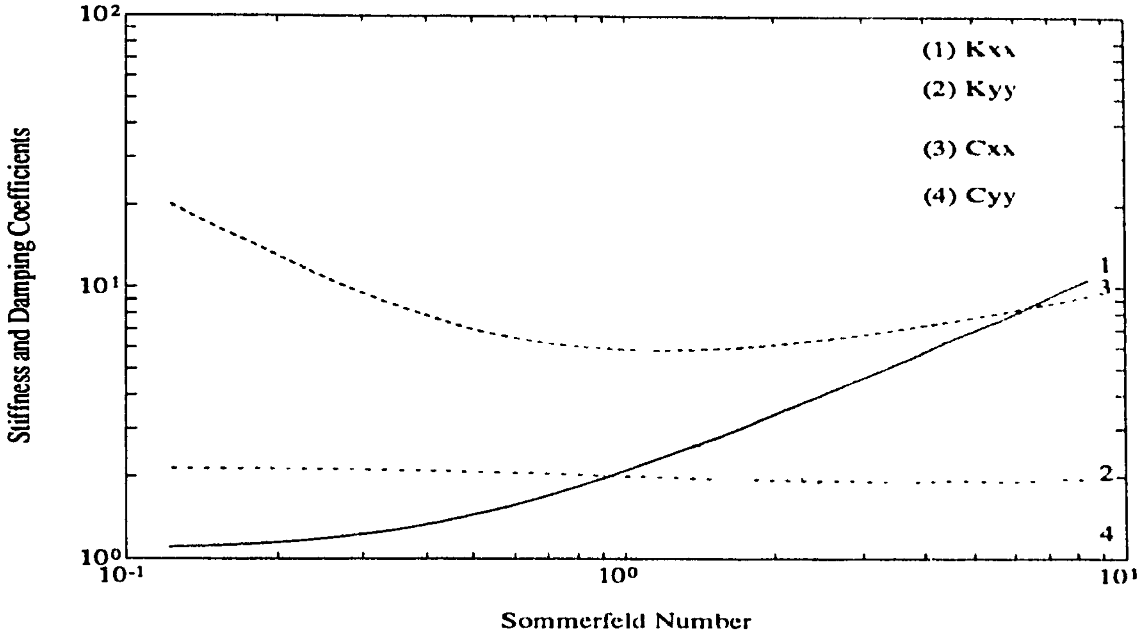

Figure 2.23: Plot of Non-Dimensional Direct Stiffness and Damping Coefficients of a Cylindrical Bearing Vs. Sommerfeld Number S_{o} : b/d = 1.00

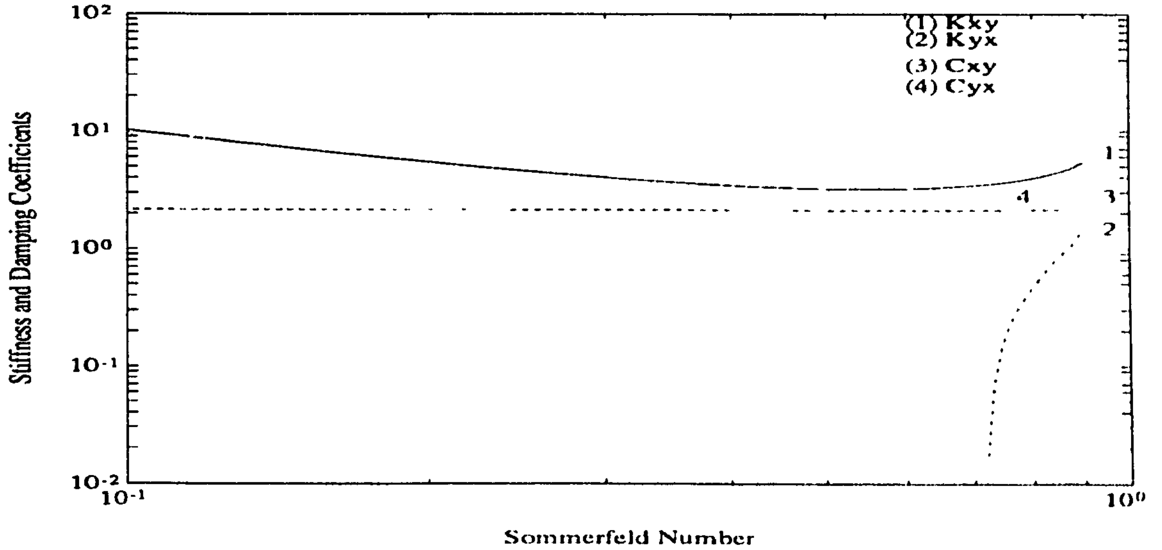

Figure 2.24: Plot of Non-Dimensional Cross Coupled Stiffness and Damping Coefficients of a Cylindrical Bearing Vs. Sommerfeld Number S_{o} : b/d = 1.00

Chapter 3

Simultaneous Forward and Backward Whirling Motion of Rotor

3.1 Introduction

For a rotor supported on fluid film bearings, the reaction force of the lubricating film depends on the position and velocity of the journal in the bearing. When the journal displacement is small, the fluid film reaction can be represented by eight bearing coefficients. A review of the concept of bearing coefficients is given in [22]. For a chosen bearing type, the non-dimensional bearing coefficients can be obtained by solving Reynolds equation with appropriate boundary conditions, [23] In this linearized representation of the fluid film reaction, the stiffness matrix is found to be anisotropic. Consequently, the spring effect of the fluid film reaction either accumulates or dissipates energy depending on whether the journal whirling motion is in the forward or backward sense. This active spring effect of the fluid film reaction renders the rotor-bearing system unstable when the speed exceeds a certain threshold speed of instability.

The stiffness anisotropy of the bearings, in the absence of damping, can cause the undesirable backward whirling motion of the rotor, for a speed range in between the critical speeds of the system. Under certain conditions, the stiffness anisotropy and the damping effect of the bearing can suppress the occurrence of this backward whirling motion of the rotor. A *Jeffcot* rotor supported on two identical fluid film bearings is a suitable rotor-dynamic model for such investigations.

In the present chapter, response analysis of a horizontal *Jeffcot* rotor supported on two identical fluid film bearings is carried out. Conditions for the backward whirl motion of the rotor lying in between the two critical speeds is derived. The investigation shows that the journal center always orbits in the forward sense, and that excessive flexibility of the rotor and bearing anisotropy are the cause for the backward whirling motion of the rotor.

3.2 Study of Simultaneous Backward and Forward Whirling motion of Disk and Journal in a Jeffcot Rotor Supported on Two Identical Hydrodynamic Bearings

3.2.1 Governing Equations

A flexible shaft, carrying a central rotor and supported on identical journal bearings at its ends, as shown in Fig. (3.1), is considered for the theoretical investigation. Since the aim of the study is to investigate the influence of the bearings on the synchronous unbalance response of the rotor, this investigation is restricted to the symmetrical whirling motion of the rotor. When the whirl amplitude is sufficiently small, the fluid film force on the journal can be represented by eight stiffness and damping coefficients. For rotor dynamic investigations it is convenient to have these bearing coefficients tabulated as functions of the Sommerfeld number.

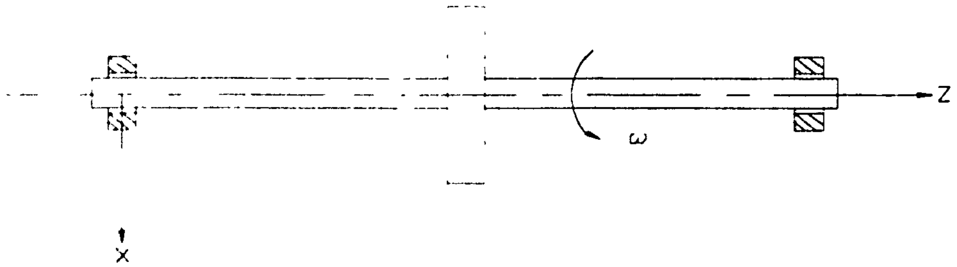

Figure 3.1: Rotor Bearing System

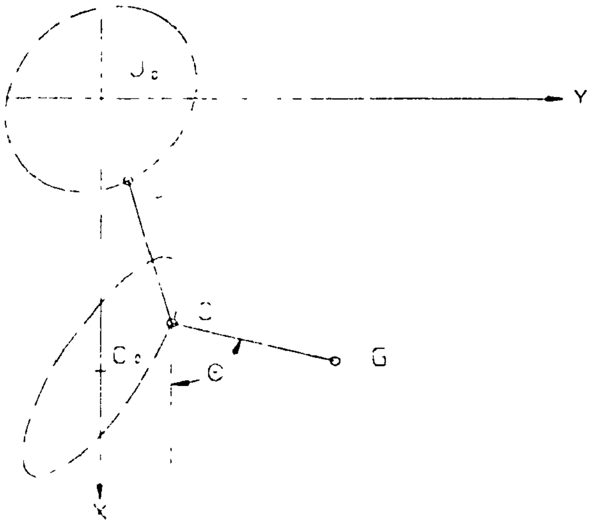

Figure 3.2: Reference Frame

For the rotor system rotating at a constant speed ω with respect to the Cartesian reference frame J_0XY as shown in Fig. (3.2), the equations of motion given by

$$m\ddot{x}_r + k_s(x_r - x_j) = m\omega^2\delta\cos\omega t + mg \tag{3.1}$$

$$m\ddot{y}_r + k_s(y_r - y_j) = m\omega^2\delta\sin\omega t \tag{3.2}$$

$$k_s(x_r - x_j) = 2(k_{xx}x_j + k_{xy}y_j + c_{xx}\dot{x}_j + c_{xy}\dot{y}_j) + mg \tag{3.3}$$

$$k_s(y_r - y_j) = 2(k_{yx}x_j + k_{yy}y_j + c_{yx}\dot{x}_j + c_{yy}\dot{y}_j) \tag{3.4}$$

The subscripts *j* and *r* in Eqn. (3.1 - 3.4) refer to the journal and the rotor respectively. The steady state positions of the journal and disk centers are

$$x_j = 0; \qquad y_j = 0$$

$$x_r = mg/k_s; \qquad y_r = 0$$

In the derivation of the above equations, all damping effects, other than that provided by the bearings, are neglected. The equations of motion (3.1 - 3.4) can be rewritten in non-dimensional form as

$$\bar{x}_r'' + \left(\frac{\omega_s^2}{\omega^2}\right)(\bar{x}_r - \bar{x}_j) = \frac{\delta}{c}\cos\omega t \tag{3.5}$$

$$\bar{y}_r'' + \left(\frac{\omega_s^2}{\omega^2}\right)(\bar{y}_r - \bar{y}_j) = \frac{\delta}{c}\sin\omega t \tag{3.6}$$

$$(\bar{x}_i - \bar{x}_j) = \left(\frac{\omega_o^2}{\omega_s^2}\right)\left(\bar{K}_{xx}\bar{x}_j + \bar{K}_{xy}\bar{y}_j + \bar{C}_{xx}\bar{x}_j' + \bar{C}_{xy}\bar{y}_j'\right) \tag{3.7}$$

$$\left(\bar{y}_i - \bar{y}_j\right) = (\frac{\omega_o^2}{\omega_s^2})\left(\bar{K}_{yx}\bar{x}_j + \bar{K}_{yy}\bar{y}_j + \bar{C}_{yx}\bar{x}_j' + \bar{C}_{yy}\bar{y}_j'\right) \tag{3.8}$$

In Eqns. (3.5 - 3.8) the superscript ( )' denotes differentiation with respect to ωt. The terms on the right hand side of Eqns. (3.5, 3.6) represent the synchronous unbalance excitation of the rotor-bearing system. From a stability point of view, the response of the system can be regarded as the superposition of the characteristic transient whirling motion and the synchronous unbalance response associated with the excitation.

3.2.2 Unbalance Whirling Motion

Under steady state conditions, the unbalance response could be expressed as

$$\bar{x}_j = \left(\frac{\delta}{c}\right)\{a_{jx}\cos\omega t + b_{jx}\sin\omega t\} \tag{3.9}$$

$$\bar{y}_j = \left(\frac{\delta}{c}\right)\{a_{jy}\cos\omega t + b_{jy}\sin\omega t\} \tag{3.10}$$

$$\bar{x}_i = \left(\frac{\delta}{c}\right)\{a_{ix}\cos\omega t + b_{ix}\sin\omega t\} \tag{3.11}$$

$$\bar{y}_i = \left(\frac{\delta}{c}\right)\{a_{iy}\cos\omega t + b_{iy}\sin\omega t\} \tag{3.12}$$

The eight coefficients a_{jx}, a_{jy}, ... etc in the above steady state solutions can be obtained as follows. Substituting solution (3.9, 3.11) into the Eqn. (3.5) and equating the sine and cosine coefficients results in

$$\Lambda\,(a_{rx} - a_{jx}) = \mu_s\,(a_{jx} + 1) \tag{3.13}$$

$$\Lambda\,(a_{ry} - a_{jy}) = \mu_s a_{jy} \tag{3.14}$$

where,

$$\mu_s = \frac{\omega_o'^2}{\omega_s'^2} = \frac{\delta_s}{c}$$

$$\Lambda = \left(\frac{\omega_o'^2}{\omega^2} - \frac{\omega_o'^2}{\omega_s'^2}\right)$$

Since μ_s is the ratio of the static deflection of the rotor shaft to the bearing (radial) clearance, it is termed as the flexibility parameter of the rotor-bearing system.

Similarly for y co-ordinate, substitution of Eqn. (3.10, 3.12), in to Eqn. (3.6) results in

$$\Lambda\,(b_{rx} - b_{jx}) = \mu_s b_{jx} \tag{3.15}$$

$$\Lambda\,(b_{ry} - b_{jy}) = \mu_s\,(b_{jy} + 1) \tag{3.16}$$

Eqn. (3.13 - 3.16) can be rewritten in matrix notation as

$$\begin{bmatrix} a_{rx} \\ a_{ry} \end{bmatrix} = \left(1 + \frac{\mu_s}{\Lambda}\right) \begin{bmatrix} a_{jx} \\ a_{jy} \end{bmatrix} + \left(\frac{\mu_s}{\Lambda}\right) \begin{bmatrix} 1 \\ 0 \end{bmatrix} \tag{3.17}$$

$$\begin{bmatrix} b_{rx} \\ b_{ry} \end{bmatrix} = \left(1 + \frac{\mu_s}{\Lambda}\right) \begin{bmatrix} b_{jx} \\ b_{jy} \end{bmatrix} + \left(\frac{\mu_s}{\Lambda}\right) \begin{bmatrix} 0 \\ 1 \end{bmatrix} \tag{3.18}$$

Substituting Eqns. (3.9 - 3.12) into Eqn. (3.7, 3.8) results in

$$(a_{rx} - a_{jx}) = \mu_s\left(\overline{K}_{xx}a_{jx} + \overline{K}_{xy}a_{jy} + \overline{C}_{xx}b_{jx} + \overline{C}_{xy}b_{jy}\right) \quad (3.19)$$

$$(a_{ry} - a_{jy}) = \mu_s\left(\overline{K}_{yx}a_{jx} + \overline{K}_{yy}a_{jy} + \overline{C}_{yx}b_{jx} + \overline{C}_{yy}b_{jy}\right) \quad (3.20)$$

$$(b_{rx} - b_{jx}) = \mu_s\left(-\overline{C}_{xx}a_{jx} - \overline{C}_{xy}a_{jy} + \overline{K}_{xx}b_{jx} + \overline{K}_{xy}b_{jy}\right) \quad (3.21)$$

$$(b_{ry} - b_{jy}) = \mu_s\left(-\overline{C}_{yx}a_{jx} - \overline{C}_{yy}a_{jy} + \overline{K}_{yx}b_{jx} + \overline{K}_{yy}b_{jy}\right) \quad (3.22)$$

The eight linear simultaneous equations (3.17 - 3.22) in the eight unknown coefficients can be used to solve for the unknown coefficients.

Substituting Eqn. (3.13 - 3.16) in Eqn. (3.19 - 3.22) results in

$$(a_{jx} + 1) = \wedge\left(\overline{K}_{xx}a_{jx} + \overline{K}_{xy}a_{jy} + \overline{C}_{xx}b_{jx} + \overline{C}_{xy}b_{jy}\right)$$

$$a_{jy} = \wedge\left(\overline{K}_{yx}a_{jx} + \overline{K}_{yy}a_{jy} + \overline{C}_{yx}b_{jx} + \overline{C}_{yy}b_{jy}\right)$$

$$b_{jx} = \wedge\left(-\overline{C}_{xx}a_{jx} - \overline{C}_{xy}a_{jy} + \overline{K}_{xx}b_{jx} + \overline{K}_{xy}b_{jy}\right)$$

$$(b_{jy} + 1) = \wedge\left(-\overline{C}_{yx}a_{jx} - \overline{C}_{yy}a_{jy} + \overline{K}_{yx}b_{jx} + \overline{K}_{yy}b_{jy}\right)$$

The above equation can be rewritten in matrix form as

$$\begin{bmatrix} a_{jx} \\ a_{jy} \end{bmatrix} + \begin{bmatrix} 1 \\ 0 \end{bmatrix} = \wedge \begin{bmatrix} \overline{K}_{xx} & \overline{K}_{xy} \\ \overline{K}_{yx} & \overline{K}_{yy} \end{bmatrix} \begin{bmatrix} a_{jx} \\ a_{jy} \end{bmatrix} + \wedge \begin{bmatrix} \overline{C}_{xx} & \overline{C}_{xy} \\ \overline{C}_{yx} & \overline{C}_{yy} \end{bmatrix} \begin{bmatrix} b_{jx} \\ b_{jy} \end{bmatrix} \qquad (3.23)$$

$$\begin{bmatrix} b_{jx} \\ b_{jy} \end{bmatrix} + \begin{bmatrix} 0 \\ 1 \end{bmatrix} = -\wedge \begin{bmatrix} \overline{C}_{xx} & \overline{C}_{xy} \\ \overline{C}_{yx} & \overline{C}_{yy} \end{bmatrix} \begin{bmatrix} a_{jx} \\ a_{jy} \end{bmatrix} + \wedge \begin{bmatrix} \overline{K}_{xx} & \overline{K}_{xy} \\ \overline{K}_{yx} & \overline{K}_{yy} \end{bmatrix} \begin{bmatrix} b_{jx} \\ b_{jy} \end{bmatrix} \qquad (3.24)$$

Symbolically, Eqns. (3.23, 3.24) can be written as

$$A_j + U_1 = \wedge\overline{K}A_j + \wedge\overline{C}B_j \qquad (3.25)$$

$$B_j + U_2 = -\wedge\overline{C}A_j + \wedge\overline{K}B_j \qquad (3.26)$$

Using the notation

$$\tilde{A}_j = A_j - jB_j$$

$$\tilde{K} = \overline{K} + j\overline{C}$$

$$\tilde{U} = U_1 - jU_2$$

Eqn. (3.25, 3.26) reduces to

$$\tilde{A}_j = \left[\wedge\tilde{K} - I\right]^{-1}\tilde{U} \qquad (3.27)$$

The inverse of the matrix $[\wedge\tilde{K} - I]$ can be expressed as

$$\left[\wedge \bar{K} - I\right]^{-1} = \frac{1}{D_1 + jD_2} \begin{bmatrix} \wedge(\overline{K}_{yy} + j\overline{C}_{yy}) - 1 & -\wedge(\overline{K}_{xy} + j\overline{C}_{xy}) \\ -\wedge(\overline{K}_{yx} + j\overline{C}_{yx}) & \wedge(\overline{K}_{xx} + j\overline{C}_{xx}) - 1 \end{bmatrix} \tag{3.28}$$

where

$$D_1 = 1 - \wedge J_1 + \wedge^2 (J_3 - J_4)$$

$$D_2 = -\wedge J_2 + \wedge^2 J_5$$

Substitution of Eqn. (3.28) into Eqn. (3.27) gives the expression for A_j as

$$A_j = \frac{D_1 - jD_2}{D} \begin{bmatrix} \{\wedge(\overline{K}_{yy} - \overline{C}_{xy}) - 1\} + j\wedge(\overline{K}_{xy} + j\overline{C}_{yy}) \\ -\wedge(\overline{K}_{yx} - \overline{C}_{xx}) - j\{\wedge(\overline{K}_{xx} + \overline{C}_{yx}) - 1\} \end{bmatrix} \tag{3.29}$$

where

$$D = \left\{1 - \wedge J_1 + \wedge^2 (J_3 - J_4)\right\}^2 + \wedge^2 \{J_2 - \wedge J_5\}^2 \tag{3.30}$$

Equating the real and imaginary parts of Eqn. (3.29) results in

$$\begin{bmatrix} a_{jx} \\ a_{jy} \end{bmatrix} = \frac{1}{D} \begin{bmatrix} D_1\{\wedge(\overline{K}_{yy} - \overline{C}_{xy}) - 1\} + D_2\wedge(\overline{K}_{xy} + \overline{C}_{yy}) \\ -D_1\wedge(\overline{K}_{yx} - \overline{C}_{xx}) - D_2\{\wedge(\overline{K}_{xx} + \overline{C}_{yx}) - 1\} \end{bmatrix} \tag{3.31}$$

$$\begin{bmatrix} b_{jx} \\ b_{jy} \end{bmatrix} = \frac{1}{D} \begin{bmatrix} -D_1\wedge(\overline{K}_{xy} + \overline{C}_{yy}) + D_2\{\wedge(\overline{K}_{yy} - \overline{C}_{xy}) - 1\} \\ D_1\{\wedge(\overline{K}_{xx} + \overline{C}_{yx}) - 1\} - D_2\wedge(\overline{K}_{yx} - \overline{C}_{xx}) \end{bmatrix} \tag{3.32}$$

3.2.3 Orbit of the Journal Center

The algebraic area enclosed by the elliptic orbit of the journal center can be written as $\pi\delta^2(a_{jx}b_{jy} - b_{jx}a_{jy})$ (See appendix A). Thus the orbit of the journal center in the forward sense when, $(a_{jx}b_{jy} - b_{jx}a_{jy})$ is positive and is backward when $(a_{jx}b_{jy} - b_{jx}a_{jy})$ is negative.

Substituting for a_{jx}, a_{jy}, b_{jx}, b_{jy} (3.31 and 3.32), gives

$$a_{jx}b_{jy} - b_{jx}a_{jy} = G_1(\Lambda) \tag{3.33}$$

where

$$G_1(\Lambda) = 1 - \Lambda(J_1 - J_7) + \Lambda^2(J_3 + J_4 - J_9) \tag{3.34}$$

By investigating the sign of the quadratic expression G_1, it is possible to establish whether the journal is executing backward whirling motion or the forward whirl. The quantity G_1 is found to be positive for all values of Λ and for values of $\epsilon = 0.10, \ldots, 0.90$. Thus for the eccentricity ratios in the working range of hydrodynamic journal bearings the whirling is always forward.

3.2.4 Orbit of the Rotor Center

The orbit of the rotor center is in the forward or backward sense according as

$$(a_{rx}b_{ry} - b_{rx}a_{ry}) \gtrless 0 \tag{3.35}$$

The co-ordinates $\bar{x}$, $\bar{y}$ at any point on the rotor shaft are given by the expression (See Appendix B)

$$\begin{aligned} \bar{x} &= \bar{x}_j + \nu(\bar{x}_r - \bar{x}_j) \\ \bar{y} &= \bar{y}_j + \nu(\bar{y}_r - \bar{y}_j) \end{aligned} \tag{3.36}$$

Using Eqn. (3.36), expression for $(a_{rx}b_{ry} - b_{rx}a_{ry})$ can be written as

$$\begin{aligned} a_{rx}b_{ry} - b_{rx}a_{ry} &= [a_{jx} + \nu(a_{rx} - a_{jx})]\,[b_{jy} + \nu(b_{ry} - b_{jy})] \\ &- [b_{jx} + \nu(b_{rx} - b_{jy})]\,[a_{jy} + \nu(a_{ry} - a_{jy})] \qquad (3.37) \end{aligned}$$

This can be simplified to

$$\begin{aligned} a_{rx}b_{ry} - b_{rx}a_{ry} &= (a_{jx}b_{jy} - b_{jx}a_{jy}) \\ &+ \nu\,(a_{sx}b_{jy} + a_{jx}b_{sy} - b_{jx}a_{sy} - b_{sx}a_{jy}) \\ &+ \nu^2\,(a_{sx}b_{sy} - b_{sx}a_{sy}) \qquad (3.38) \end{aligned}$$

Here $(a_{sx} - b_{sy})$ represent relative displacement of the rotor with respect to the journal, which is given by

$$\begin{aligned} a_{sx} &= a_{rx} - a_{jx} \\ a_{sy} &= a_{ry} - a_{jy} \\ b_{sx} &= b_{rx} - b_{jx} \\ b_{sy} &= b_{ry} - b_{jy} \end{aligned}$$

Using Eqn. (3.13 - 3.16), the Eqn. (3.38) can be written in an alternate form as

$$\begin{aligned} a_{rx}b_{ry} - b_{rx}a_{ry} &= (a_{jx}b_{jy} - b_{jx}a_{jy}) \\ &+ \frac{\nu\mu_s}{\Lambda}\{(a_{jx} + 1)b_{jy} + a_{jx}(b_{jy} + 1) - b_{jx}a_{jy} - b_{jx}a_{jy}\} \\ &+ \frac{\nu^2\mu_s^2}{\Lambda^2}\{(a_{jx} + 1)(b_{jy} + 1) - a_{jy}b_{jx}\} \qquad (3.39) \end{aligned}$$

The whirling of the rotor is forward or backward according as

$$(a_{jx}b_{jy} - b_{jx}a_{jy}) + \frac{\nu\mu_s}{\Lambda}\{(a_{jx} + b_{jy}) + 2(a_{jx}b_{jy} - b_{jx}a_{jy})\}$$

$$+ \frac{\nu^2 \mu_s^2}{\Lambda^2} \{1 + (a_{jx} + b_{jy}) + (a_{jx} b_{jy} - b_{jx} a_{jy})\} \gtrless 0 \qquad (3.40)$$

Using Eqn. (3.31, 3.32), the various terms in Eqn. (3.40) can be simplified as follows:

$$(a_{jx} + b_{jy}) = \frac{1}{D} [\{\Lambda(J_1 - J_7) - 2\} D_1 + \Lambda(J_2 + J_6) D_2]$$

$$(a_{jx} b_{jy} - b_{jx} a_{jy}) = \frac{1}{D} \left[1 + \Lambda(J_1 - J_7) + \Lambda^2 (J_3 + J_4 - J_9)\right]$$

$$\begin{aligned}
(a_{jx} + b_{jy}) + 2\,(a_{jx} b_{jy} - b_{jx} a_{jy}) &= \frac{1}{D} \Lambda\, [(J_1 + J_7) \\
&\quad - \Lambda(J_1^2 + J_2^2 - J_1 J_7 - J_2 J_6 - 4 J_4 + 2 J_9) \\
&\quad + \Lambda^2 \{(J_1 - J_7)(J_3 - J_4) + J_5 (J_2 - J_6)\}] \\
&= \frac{\Lambda}{D} G_2(\Lambda) \qquad (3.41)
\end{aligned}$$

$$\begin{aligned}
1 + (a_{jx} + b_{jy}) + (a_{jx} b_{jy} - b_{jx} a_{jy}) &= \frac{\Lambda^2}{D} [(J_3 + J_4 + J_1 J_7 - J_2 J_6 - J_9) \\
&\quad - \Lambda\{(J_1 + J_7)(J_3 - J_4) + J_5 (J_2 - J_6)\} \\
&\quad + \Lambda^2 \{(J_3 - J_4)^2 + J_5^2\}] \\
&= \frac{\Lambda^2}{D} G_3(\Lambda) \qquad (3.42)
\end{aligned}$$

Substituting these values in Eqn. (3.40), the point on the rotor whirls in the forward or backward sense according as

$$G(\Lambda) = G_1(\Lambda) + \nu\mu_s G_2(\Lambda) + \nu^2\mu_s^2 G_3(\Lambda) \gtrless 0 \qquad (3.43)$$

where

$$G_1(\Lambda) = 1 - \Lambda(J_1 - J_7) + \Lambda^2(J_3 + J_4 - J_9) \qquad (3.44)$$

$$\begin{aligned} G_2(\Lambda) &= (J_1 + J_7) - \Lambda(J_1^2 + J_2^2 - J_1 J_7 + J_2 J_6 - 4J_4 + 2J_9) \\ &+ \Lambda^2\{(J_1 - J_7)(J_3 - J_4) + J_5(J_2 - J_6)\}] \end{aligned} \qquad (3.45)$$

$$\begin{aligned} G_3(\Lambda) &= (J_3 + J_4 + J_1 J_7 - J_2 J_6 - J_9) \\ &- \Lambda\{(J_1 + J_7)(J_3 - J_4) + J_5(J_2 - J_6)\} \\ &+ \Lambda^2\{(J_3 - J_4)^2 + J_5^2\} \end{aligned} \qquad (3.46)$$

From conditions (3.34, 3.43), one can easily verify that for the case of a very stiff shaft or a rigid rotor (μ_s), the journal center and the rotor center orbit in the same sense. For any given $\mu_s > 0$, the admissible values of Λ must satisfy the condition $(\Lambda + \mu_s) = (\omega_o^2/\omega^2) > 0$.

Thus, from condition (3.43), one can deduce that the transition from forward whirl to backward whirl, or *vice versa*, occurs when Λ *and* μ_s satisfy the conditions

$$G_1 + G_2\mu_s + G_3\mu_s^2 = 0, \quad \mu_s > 0, \quad (\Lambda + \mu_s) > 0 \qquad (3.47)$$

3.3 Numerical Computation

Computations are carried out for b/d = *0.25, 0.50, 0.75* and 1.00; and ϵ = *0.10,* *0.15,....0.90*. For chosen values of *b/d* and ϵ, the values of $\wedge$ for which $G_1 = 0$, $G_2 = 0$, $G_3 = 0$ and $(G_2^2 - 4G_1G_3) = 0$ are obtained. The range of $\wedge$ for which $(G_1 + G_2\mu_s + G_3\mu_s^2) = 0$ has at-least one positive real root for μ_s, is then computed using a $\wedge$ interval of 0.001. For every value of this ϵ, the roots of $G(\wedge) = 0$ corresponding to the flexibility parameter, μ_s = *0.001, 0.005, 0.01, 0.05, 0.1, 0.5, 1.0, 5.0, 10, 50* and z/l = *0.05, 0.10, ..., 0.50* were noted, and the values of speed ratio ω/ω_s and load parameter So_0, were evaluated from the relations $\omega/\omega_s = \mu_s/(\wedge + \mu_s)^{\frac{1}{2}}$ and $So_0 = So/(\wedge + \mu_s)^{\frac{1}{2}}$.

3.4 Results and Discussion

The quantity $G_1(\wedge)$ is found to be positive for all values of $\wedge$, implying that the journal center orbits in the forward sense always. However for sufficiently large values of $\epsilon \geq 0.70$, the Eqns. $G_2(\wedge) = 0$ and $G_3(\wedge) = 0$ were found to have real roots for $\wedge$ and hence condition (3.43) is satisfied. When μ_s is small, i.e. for a rigid rotor, the rotor center orbits in the forward sense and therefore the region of backward whirling motion of the rotor center will become prominent only if the value of μ_s exceeds the minimum value required for backward whirling.

The variations of limiting values of So_0 for given values of *b/d* and μ_s, defines whether backward whirling is possible or not during the motion of a given rotor-bearing system. The speed range corresponding to the backward whirl is likely to be reduced or suppressed, in the presence of additional external damping.

The variations of the flexibility parameter with load parameter at the onset of the backward whirling given by the coincident root condition of $G = 0$ at a point of the shaft, is shown in Figs. (3.3 - 3.6). The different values of ratio *z/l* represent the various location along the length of rotor for the onset of the backward whirling. Flexibility parameter and load parameter values for a particular rotor configuration determine whether the existence of backward whirling is possible or not. The region above the curves signifies the region of backward whirling motion of the rotor center. Clearly there cannot be backward whirling if the flexibility is less than the minimum value corresponding to the disk for that load. When the flexibility exceeds this minimum value, there can be backward whirling of the shaft at the disk and its vicinity. The results are computed for various configuration of *b/d* ratios of the journal bearing. Fig. (3.3) represents the variation of minimum flexibility parameter for a *b/d = 0.25*. Similarly Figs. (3.4 - 3.6) represents the flexibility parameter variation with load parameter for *b/d = 0.50, 0.75, 1.00* respectively.

The load parameter, So_0 , has been plotted against the speed ratio, ω/ω_s, for different values of the flexibility parameter, μ_s in Figs. (3.7 - 3.10), at the disk location. The plot of load parameter vs. speed ratio forms an envelope of region which separates the zone of the backward whirling from forward. For the region below this envelope, there cannot be backward whirl and it can exist for values of load parameter or speed ratio above this region. It is seen that for a given load, the disk whirls in the backward sense for a range of speed when the flexibility of the rotor is sufficiently large. Similar transition curves could be drawn for points of the shaft and this clearly supplements the observation made in Figs. (3.3 - 3.6). It is also observed that when flexibility parameter is very small, the load parameter has to be sufficiently large to have backward whirling motion which is not the case when the flexibility parameter of the rotor is sufficiently high. Fig. (3.7) represents the transition curves for disk for *b/d* ratio of 0.25. Figs. (3.8 - 3.10) represent similar results of variation of load parameter vs. speed ratio for *b/d* = 0.50, 0.75, 1.00. It is clearly evident that with the increase in *b/d* ratio, backward whirling region shifts to higher load parameter region, indicating that one possibility of avoiding backward whirling phenomenon is to have a bearing of higher *b/d* ratio.

For the flexibility parameter $\mu_s = 1$, transition curves for the rotor are plotted. These plots are repeated for various shaft locations, i.e. for different values of *z/l* values and shown in Fig. (3.11). It is seen that for a given flexibility when the load is sufficiently large to cause backward whirling, the backward whirling commences at the disk, and as the speed increases, extends over to a portion of the shaft and then shrinks back towards the disk before disappearing completely. The speed ratio for occurrence of the backward whirl remains at a high value of 0.75 to 1.0. The same results are represented in Figs. (3.12 - 3.14) for *b/d* ratio of 0.50, 0.75 and 1.00. With the increase of *b/d* ratio, the load parameter shifts towards higher range for the occurrence of backward whirl.

Transition curves for rotor for different shaft locations are repeated in Figs. (3.15 - 3.18) for a higher flexibility parameter $\mu_s = 5.0$ for *b/d* ratio of 0.25, 0.50, 0.75, 1.00. Commencement of the backward whirling motion follows the same above pattern. The increase in the flexibility parameter of rotor has a direct effect on increase in the range of speed ratio over which the possibility of backward whirling occurs, from 0.4 to 1.0. Also backward whirl does occur at a lower load parameter, and only increase in *b/d* does compensate this.

The effect of increasing the flexibility parameter to a considerably high value of $\mu_s = 50$ is depicted in Figs. (3.19 - 3.22) for values of *b/d* of 0.25, 0.50, 0.75 and 1.0 respectively. The result of making the rotor more flexible, results in increase in speed ratio range over which backward whirl can occur from 0.1 to 1.0, and there is also an decrease in the load·parameter.

The orbital behaviour of the rotor resulting from the unbalance response when $S\sigma_0 = 2.0$ and $\mu_s = 1.5$ at the speed $\omega/\omega_s = 0.9168$ is shown in Figs. (3.23 - 3.28), for different locations in the shaft. For these system parameters, the rotor will exhibit backward whirling motion between the critical speeds as represented by Fig.

(3.6). Fig. (3.23) represents the orbit of the rotor at the disk i.e., at $z/l = 0$. Figs. (3.24 - 3.28) represents the orbit for different location away from the disk. The whirling is backward over approximately the central two-fifths of the shaft. At the point of transition from backward to forward whirling, represented in Fig. (3.26) for $z/l = 0.3$, the whirl orbit becomes a straight line. The point of transition from forward to backward whirl may be different for different set of system parameters.

Response plots for the rotor supported on identical bearings are shown in Figs. (3.29, 3.30). For a rotor, with the load parameter of So_0 = 0.5 and flexibility parameter of μ_q = = 1.5, rotor exhibits single critical speed at 2650 rpm as shown in Fig. (3.29). Rotor exhibits split criticals when parameters So_0 and μ_q are changed to 3.0 and 2.0 respectively as shown in Fig. (3.30). The orbital motion of the rotor bearing system as the direction of whirling motion changes from backward at disk to forward at a shaft location is discussed in Appendix E.

3.5 Elimination of Backward Whirling Motion

Backward whirling motion of the rotor bearing system can be eliminated, by increasing b/d and by reducing So_0 and μ_q, as shown in the results presented in this chapter. Hence the designer can suppress the backward whirling motion by increasing b/d or η and by reducing c. The next chapter will discuss the dynamic behaviour of rotors supported on dissimilar bearings.

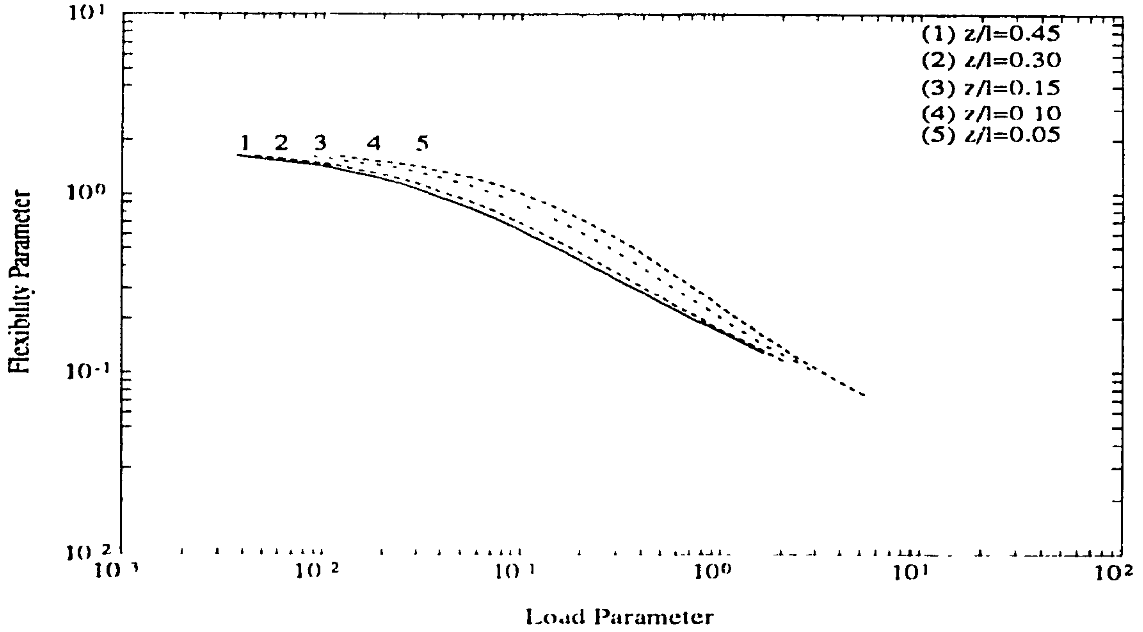

Figure 3.3: Variation of Minimum Flexibility Parameter μ_s for Backward Whirling Motion, Plot of Flexibility Parameter μ_s Vs. Load Parameter $S\alpha_0$: b/d = 0.25

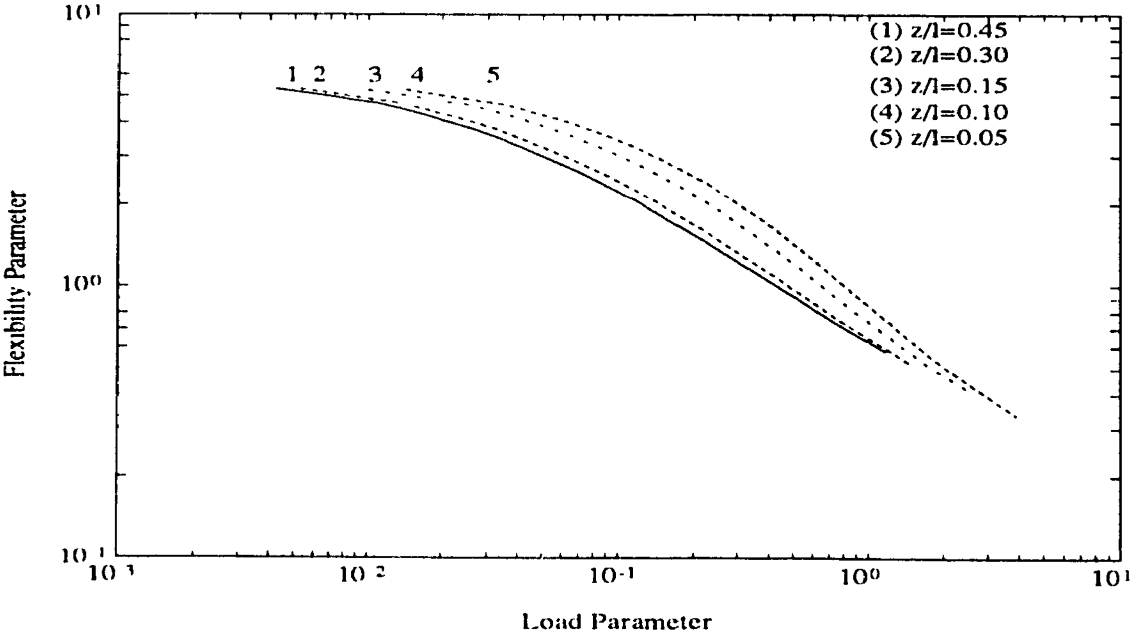

Figure 3.4: Variation of Minimum Flexibility Parameter μ_s for Backward Whirling Motion, Plot of Flexibility Parameter μ_s Vs. Load Parameter $S\alpha_0$: b/d = 0.50

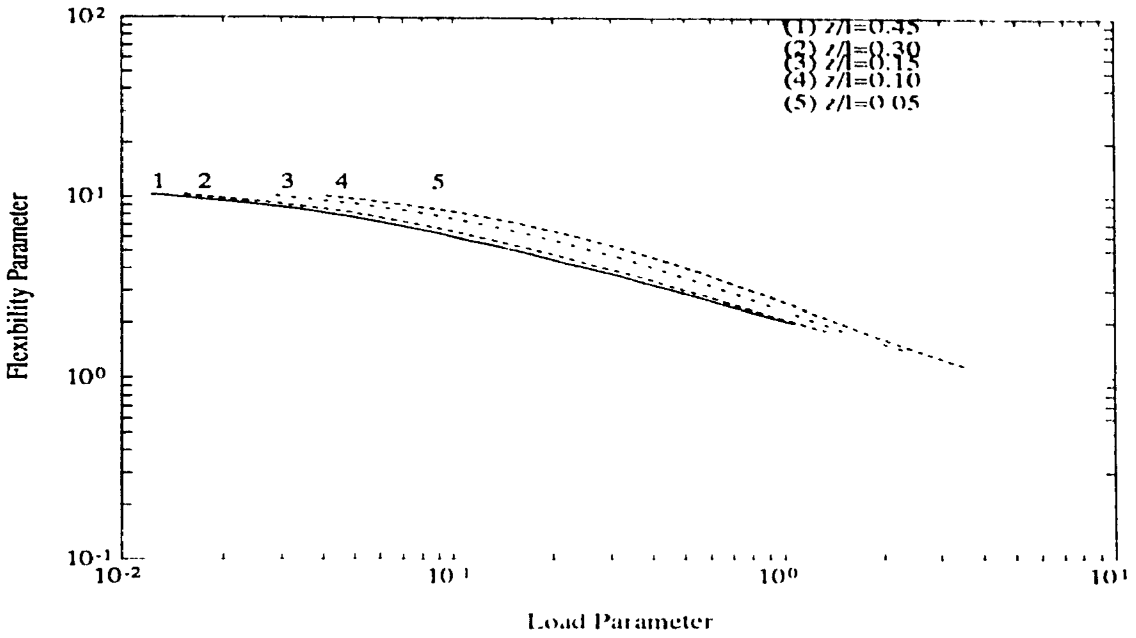

Figure 3.5: Variation of Minimum Flexibility Parameter μ_s for Backward Whirling Motion, Plot of Flexibility Parameter μ_s Vs. Load Parameter S_{o_0} : b/d = 0.75

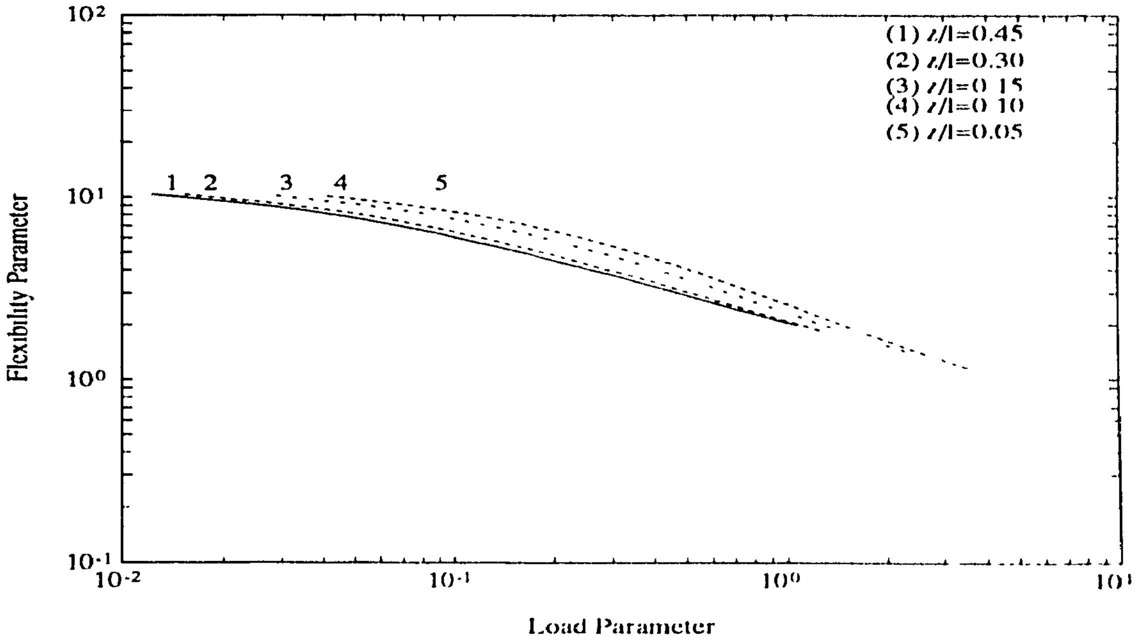

Figure 3.6: Variation of Minimum Flexibility Parameter μ_s for Backward Whirling Motion, Plot of Flexibility Parameter μ_s Vs. Load Parameter S_{o_0} : b/d = 1.00

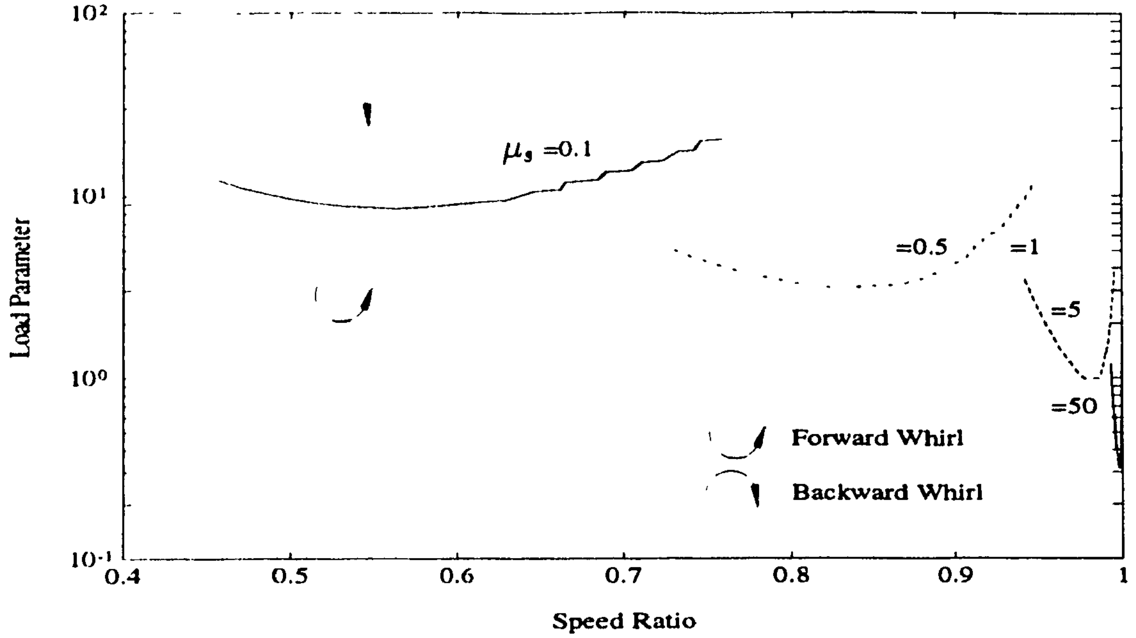

Figure 3.7: Transition Curves for Disk : Plot of Load Parameter So_0 vs. Speed Ratio ω/ω_q, for b/d = 0.25

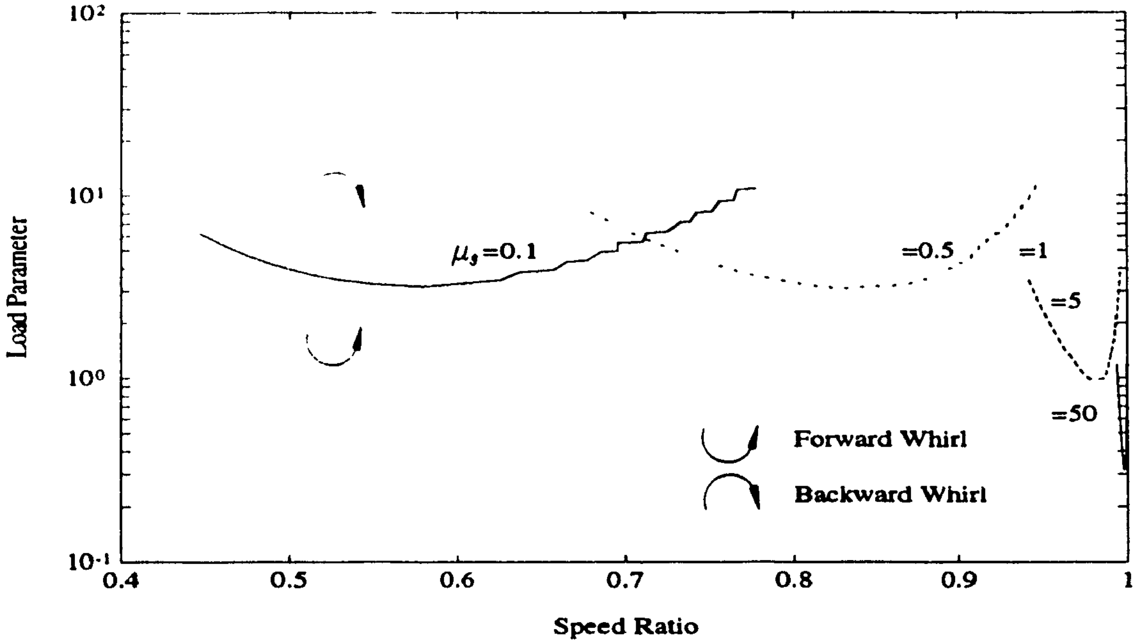

Figure 3.8: Transition Curves for Disk : Plot of Load Parameter So_0 vs. Speed Ratio ω/ω_q, for b/d = 0.50

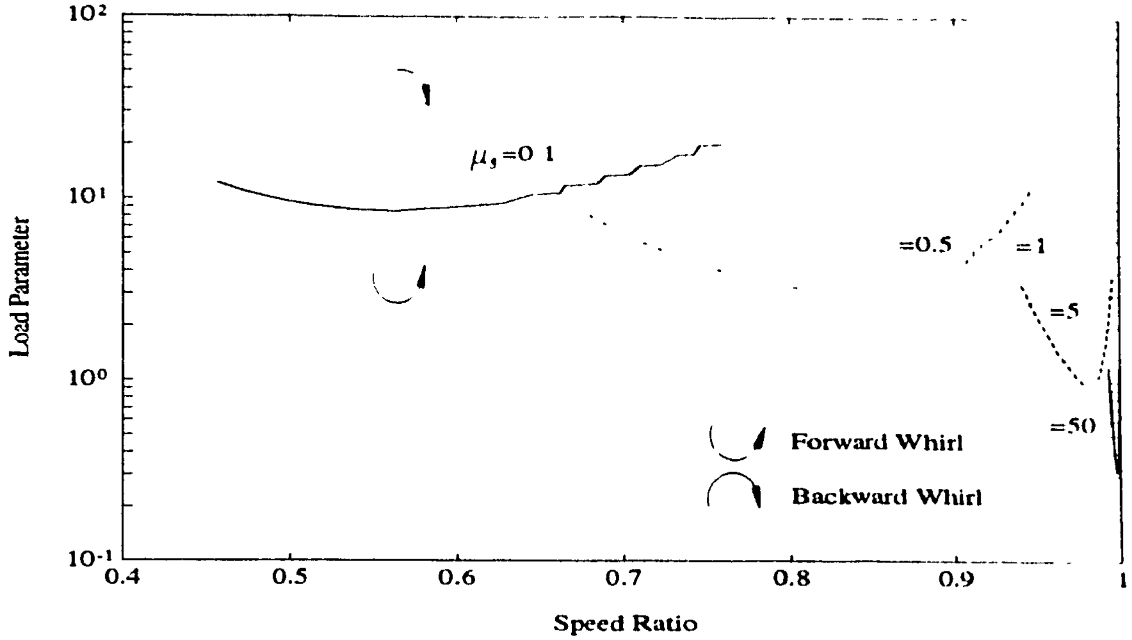

Figure 3.9: Transition Curves for Disk : Plot of Load Parameter $S\alpha_0$ vs. Speed Ratio ω/ω_s, for b/d = 0.75

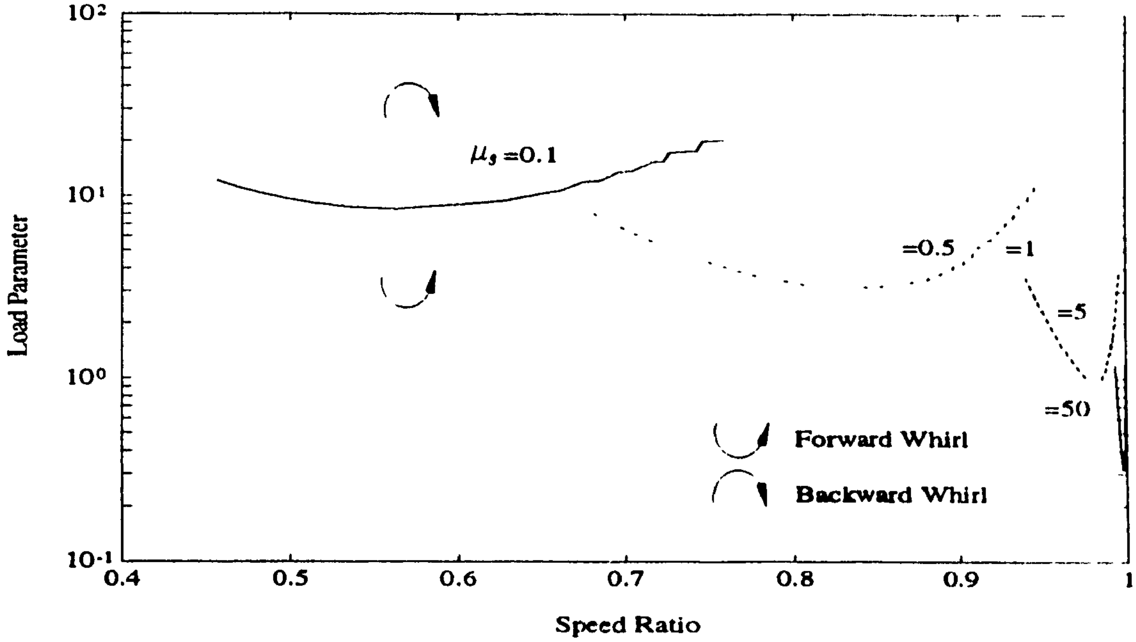

Figure 3.10: Transition Curves for Disk : Plot of Load Parameter $S\alpha_0$ vs. Speed Ratio ω/ω_s, for b/d = 1

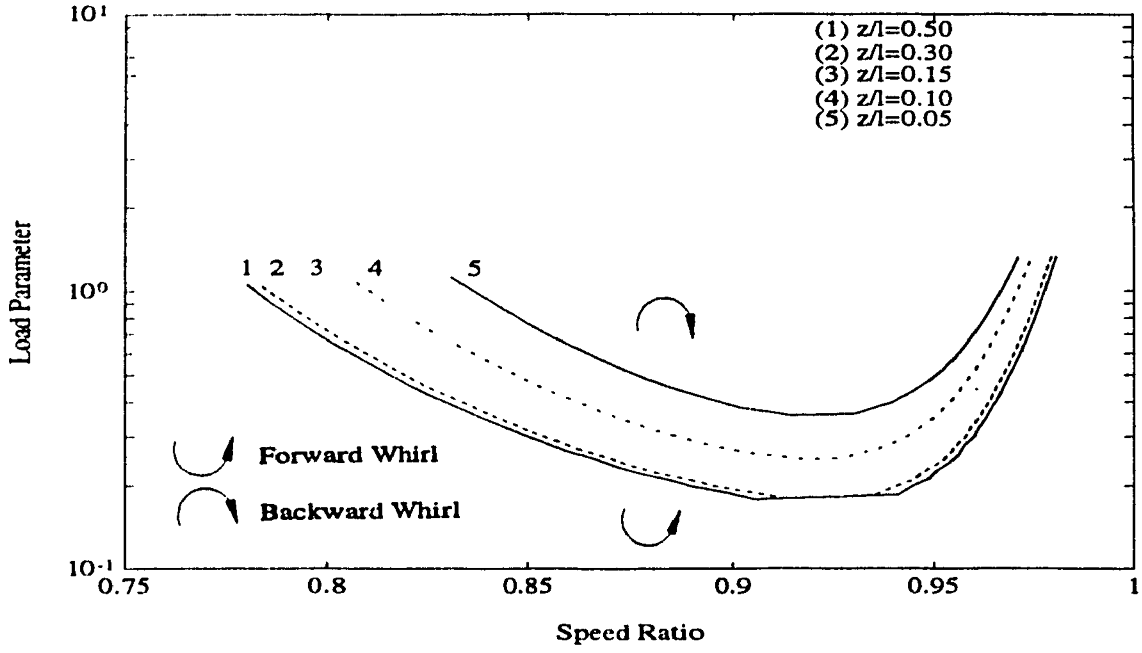

Figure 3.11: Transition Curves for Rotor : Plot of Load Parameter $S\alpha_0$ vs. Speed Ratio ω/ω_s, μ_s = 1.0 and b/d = 0.25

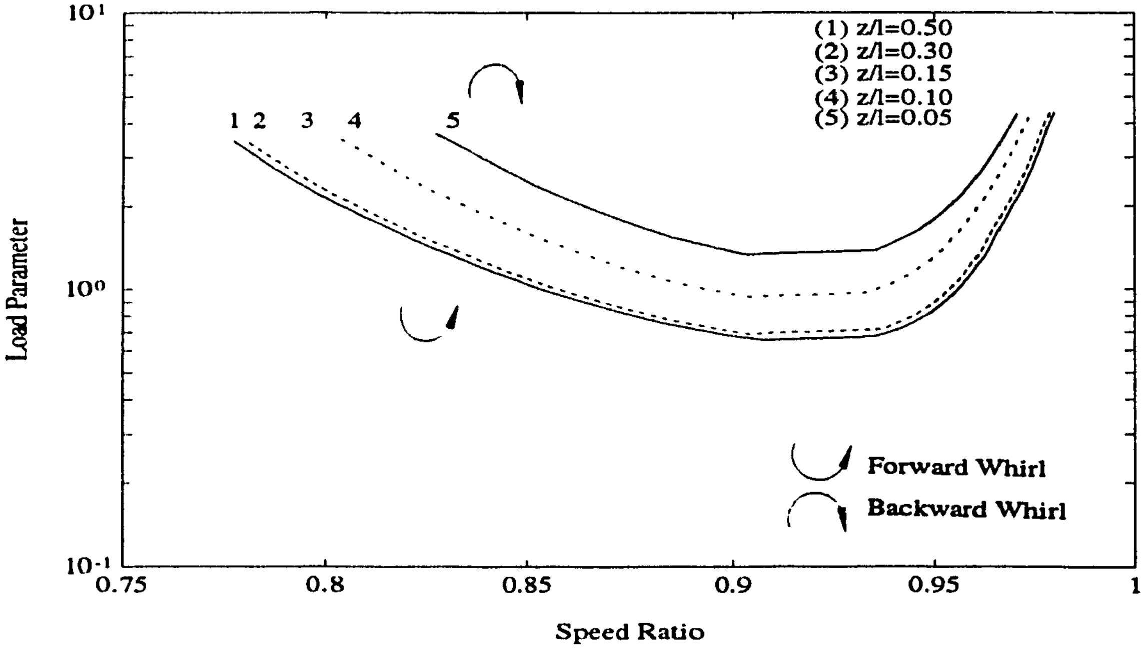

Figure 3.12: Transition Curves for Rotor : Plot of Load Parameter $S\alpha_0$ vs. Speed Ratio ω/ω_s, μ_s = 1.0 and b/d = 0.50

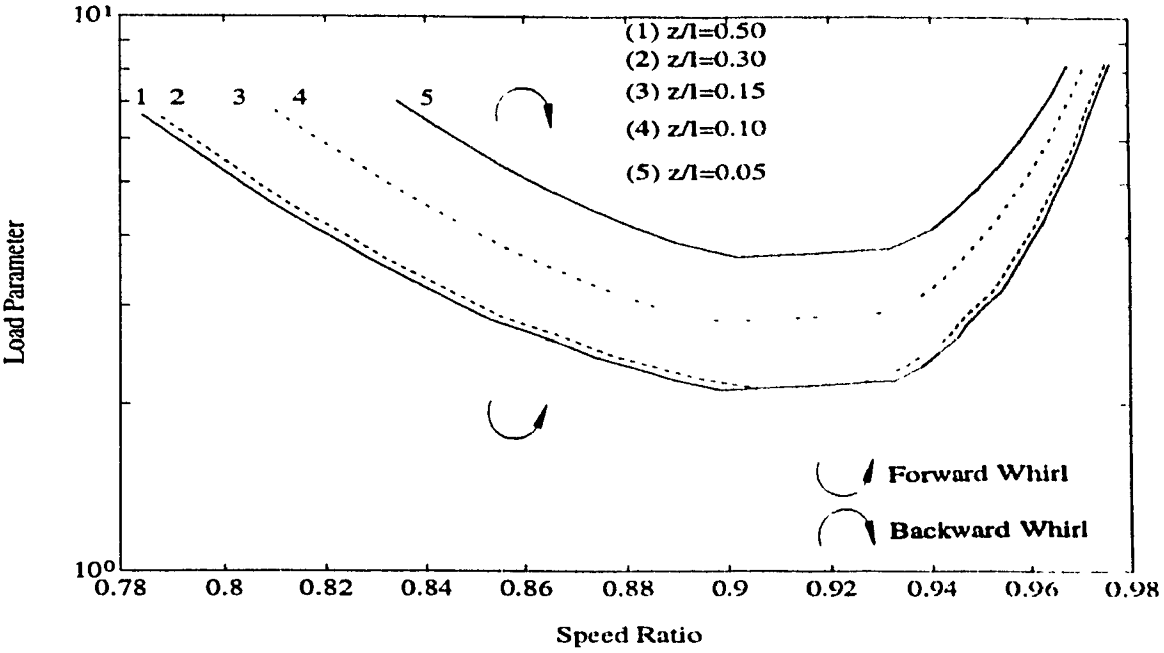

Figure 3.13: Transition Curves for Rotor : Plot of Load Parameter $S\alpha_0$ vs. Speed Ratio ω/ω_q, μ_q = 1.0 and b/d = 0.75

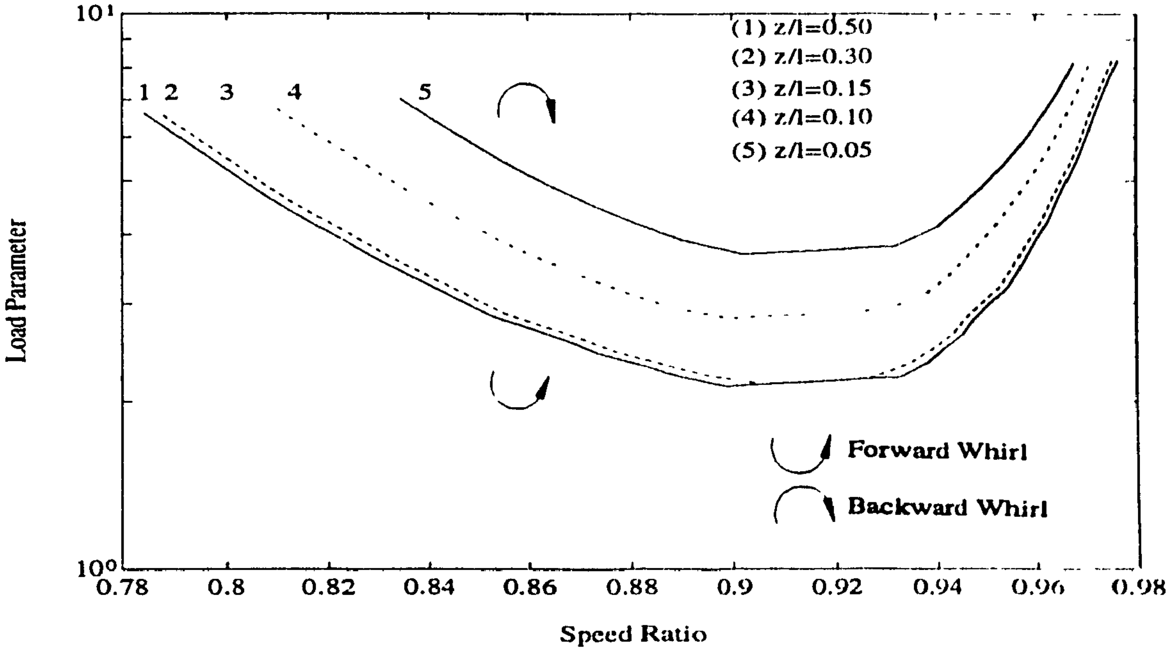

Figure 3.14: Transition Curves for Rotor : Plot of Load Parameter $S\alpha_0$ vs. Speed Ratio ω/ω_q, μ_q = 1.0 and b/d = 1

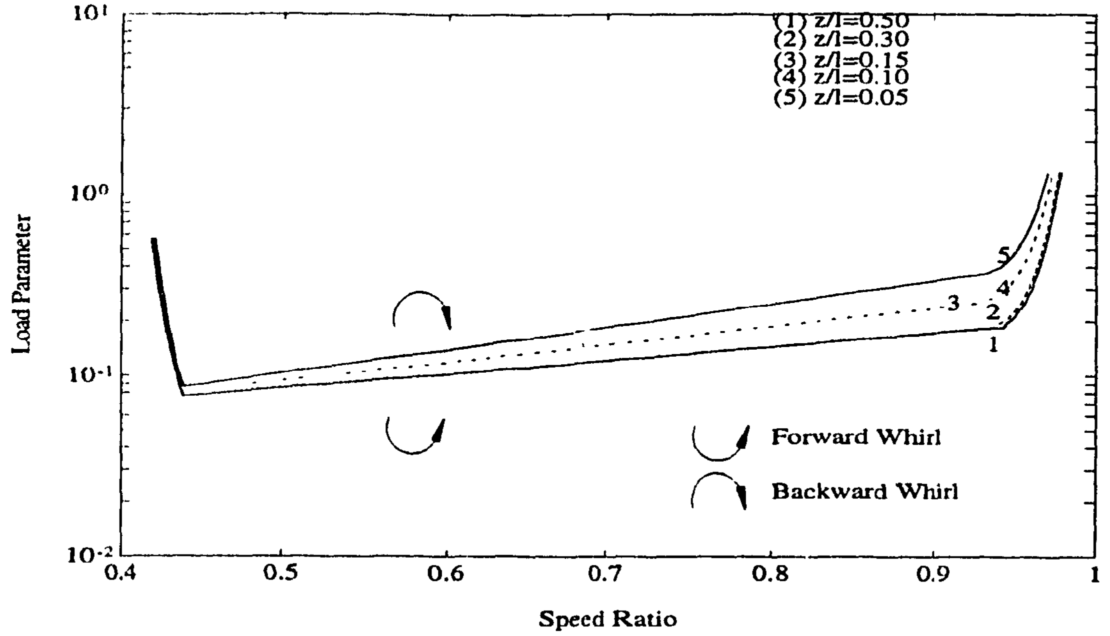

Figure 3.15: Transition Curves for Rotor : Plot of Load Parameter So_0 vs. Speed Ratio ω/ω_s, $\mu_s = 5.0$ and b/d = 0.25

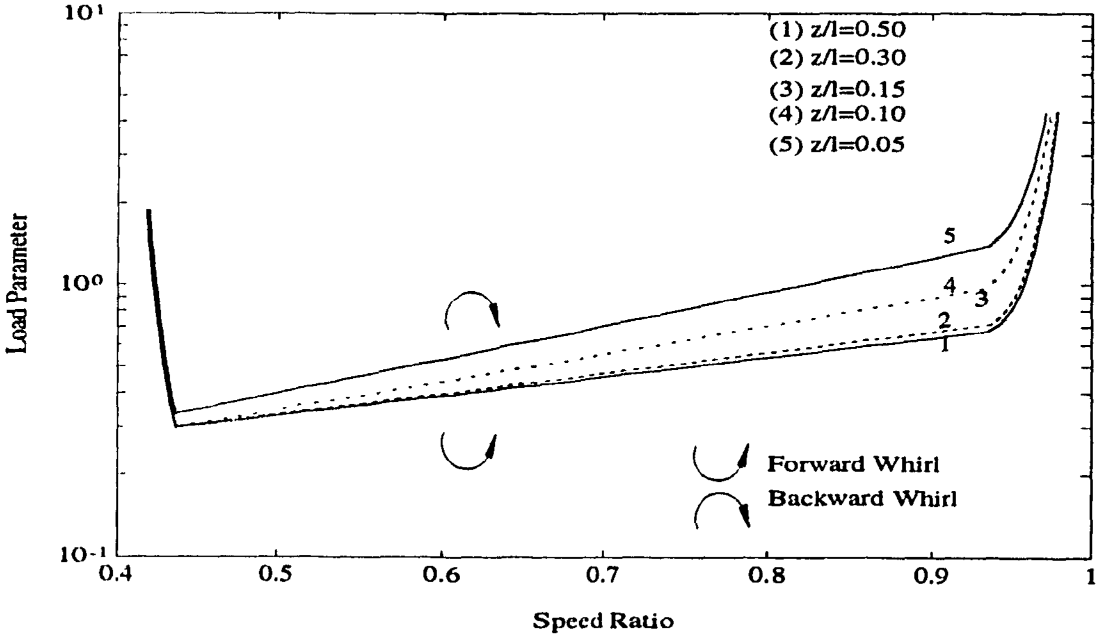

Figure 3.16: Transition Curves for Rotor : Plot of Load Parameter So_0 vs. Speed Ratio ω/ω_s, $\mu_s = 5.0$ and b/d = 0.50

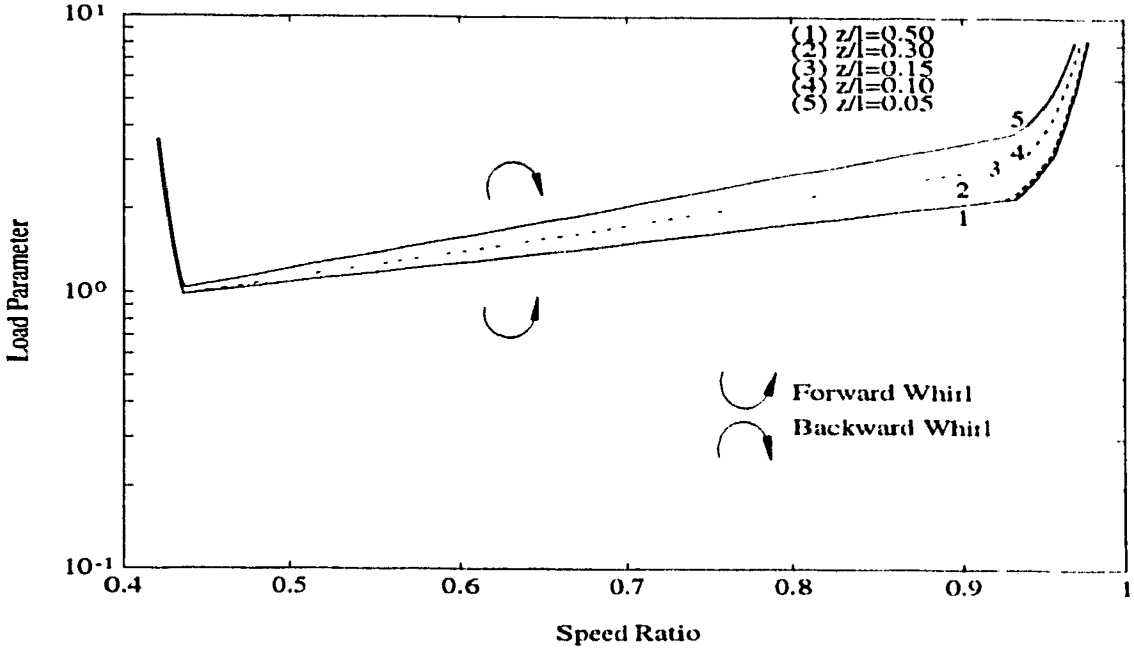

Figure 3.17: Transition Curves for Rotor : Plot of Load Parameter $S\alpha_0$ vs. Speed Ratio ω/ω_s, μ_s = 5.0 and b/d = 0.75

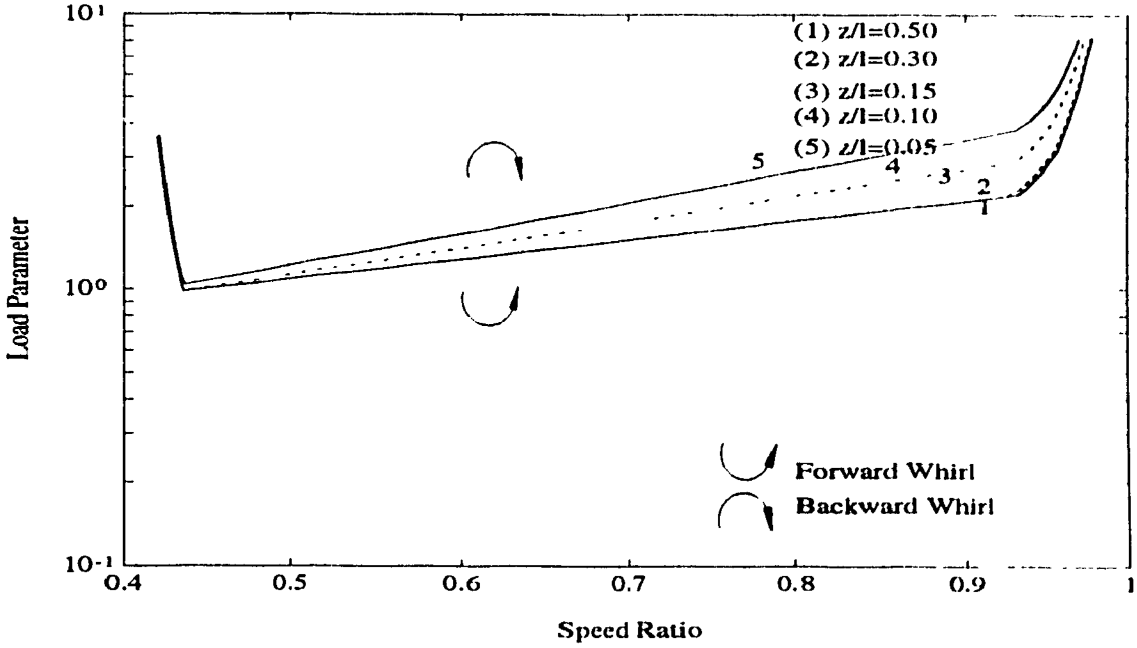

Figure 3.18: Transition Curves for Rotor : Plot of Load Parameter $S\alpha_0$ vs. Speed Ratio ω/ω_s, μ_s = 5.0 and b/d = 1

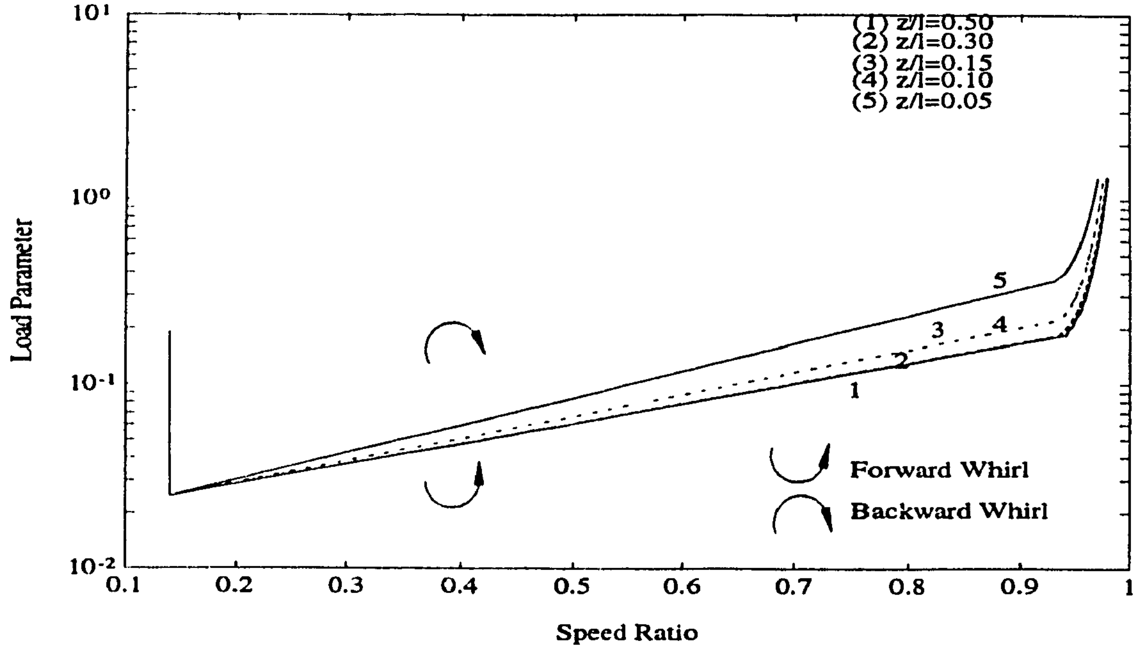

Figure 3.19: Transition Curves for Rotor : Plot of Load Parameter So_0 vs. Speed Ratio ω/ω_q, μ_q = 50.0 and b/d = 0.25

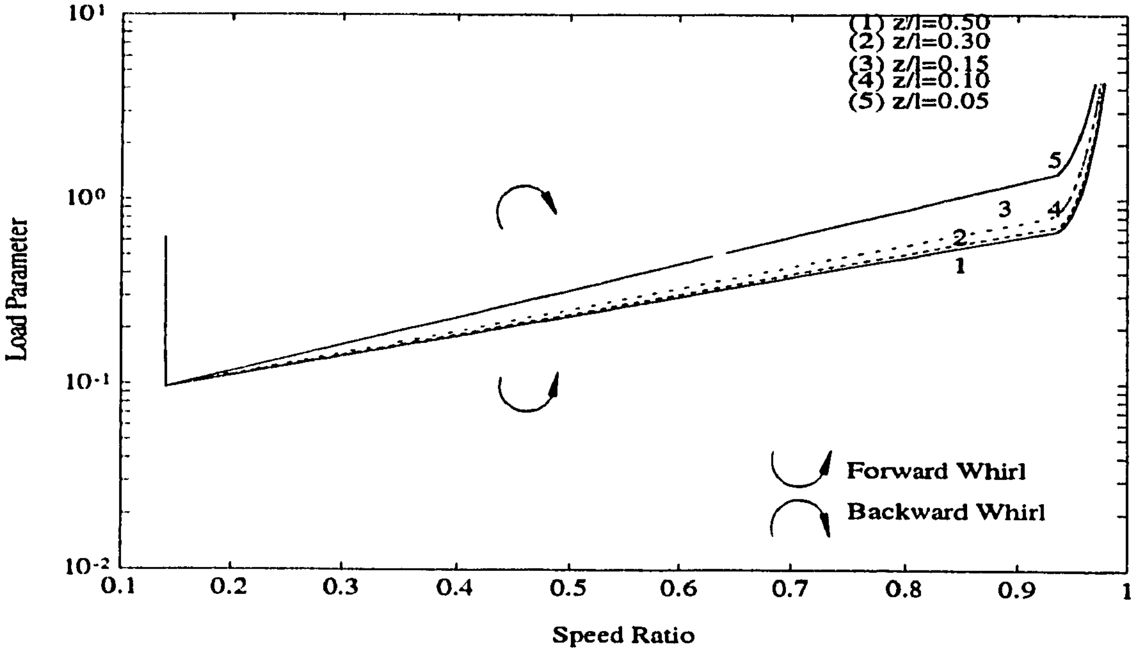

Figure 3.20: Transition Curves for Rotor : Plot of Load Parameter So_0 vs. Speed Ratio ω/ω_q, μ_q = 50.0 and b/d = 0.5

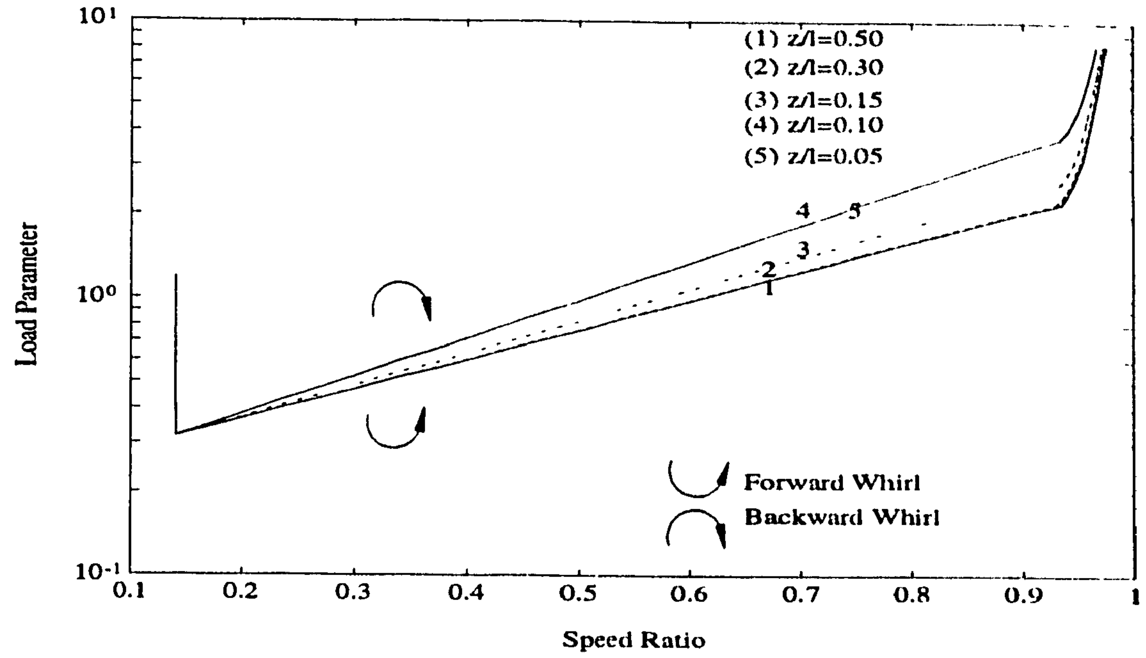

Figure 3.21: Transition Curves for Rotor : Plot of Load Parameter $S\alpha_0$ vs. Speed Ratio ω/ω_s, μ_s = 50.0 and b/d = 0.75

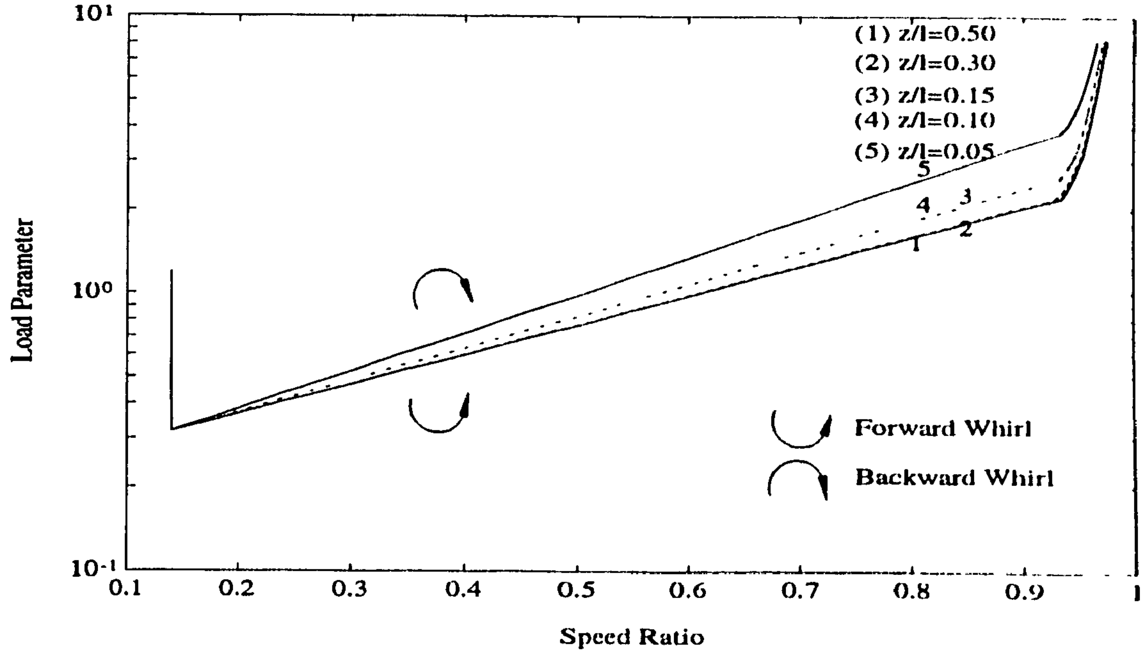

Figure 3.22: Transition Curves for Rotor : Plot of Load Parameter $S\alpha_0$ vs. Speed Ratio ω/ω_s, μ_s = 50.0 and b/d = 1

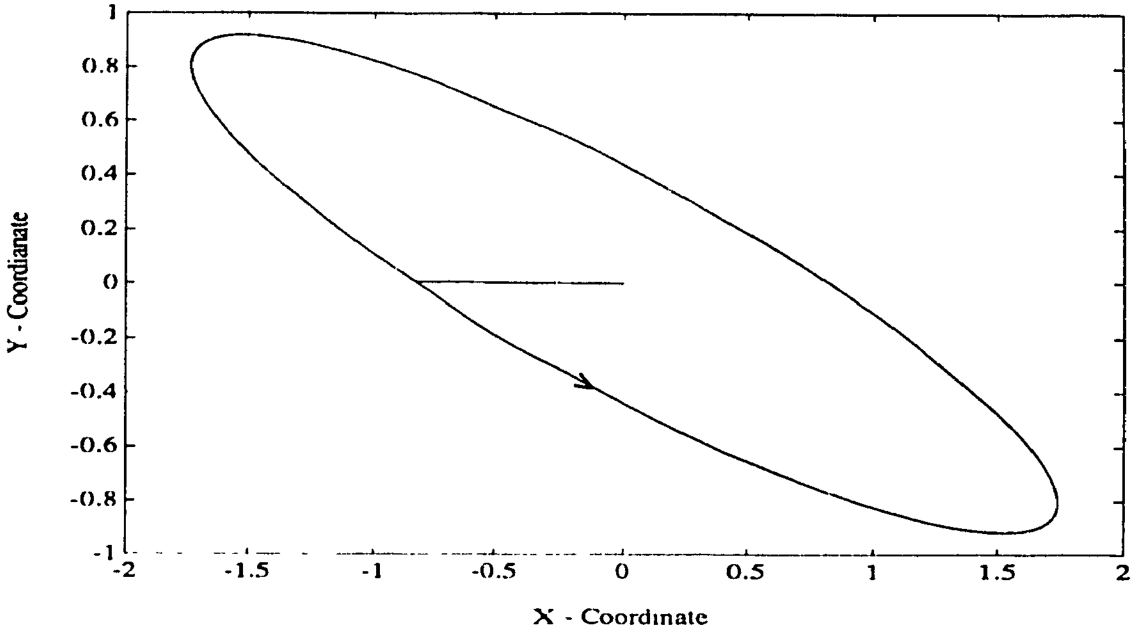

Figure 3.23: Non-Dimensional Unbalance Orbit of the Rotor, So_0 = 2.0, μ_s = 1.5, z/l = 0.0, and b/d = 1

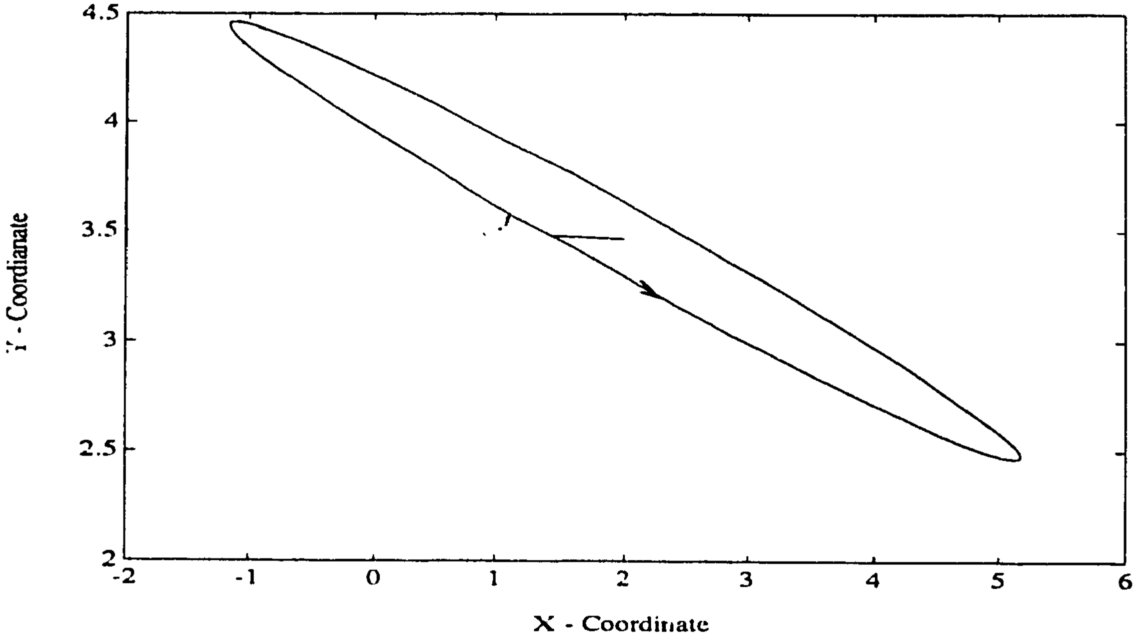

Figure 3.24: Non-Dimensional Unbalance Orbit of the Rotor, So_0 = 2.0, μ_s = 1.5, z/l = 0.1, and b/d = 1

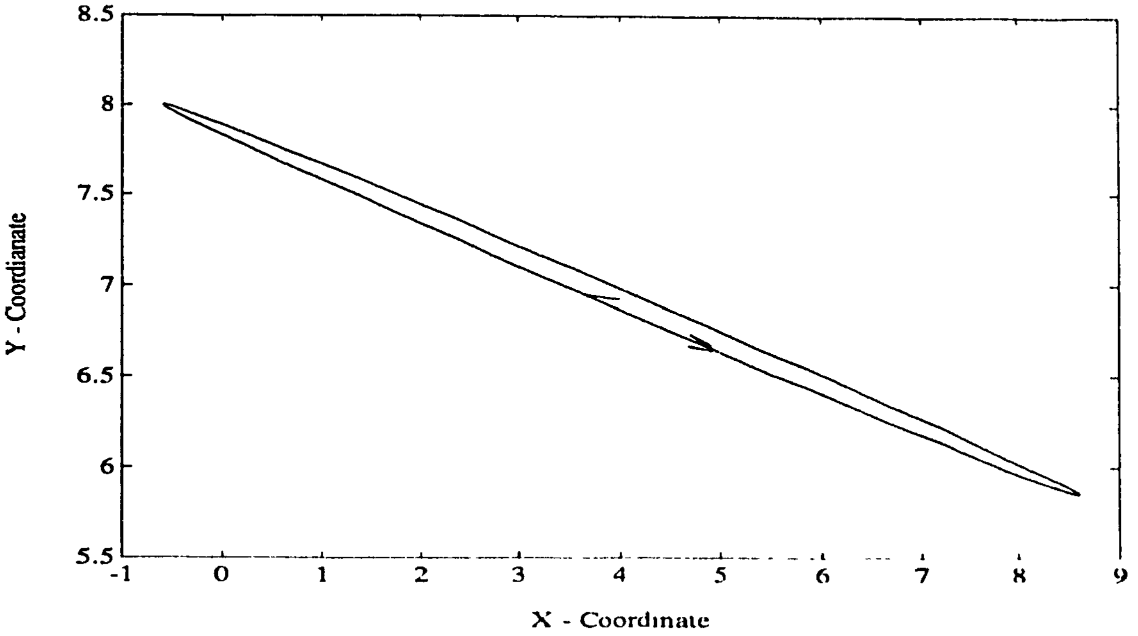

Figure 3.25: Non-Dimensional Unbalance Orbit of the Rotor, $S\omega_0$ = 2.0, μ_s = 1.5, z/l = 0.2, and b/d = 1

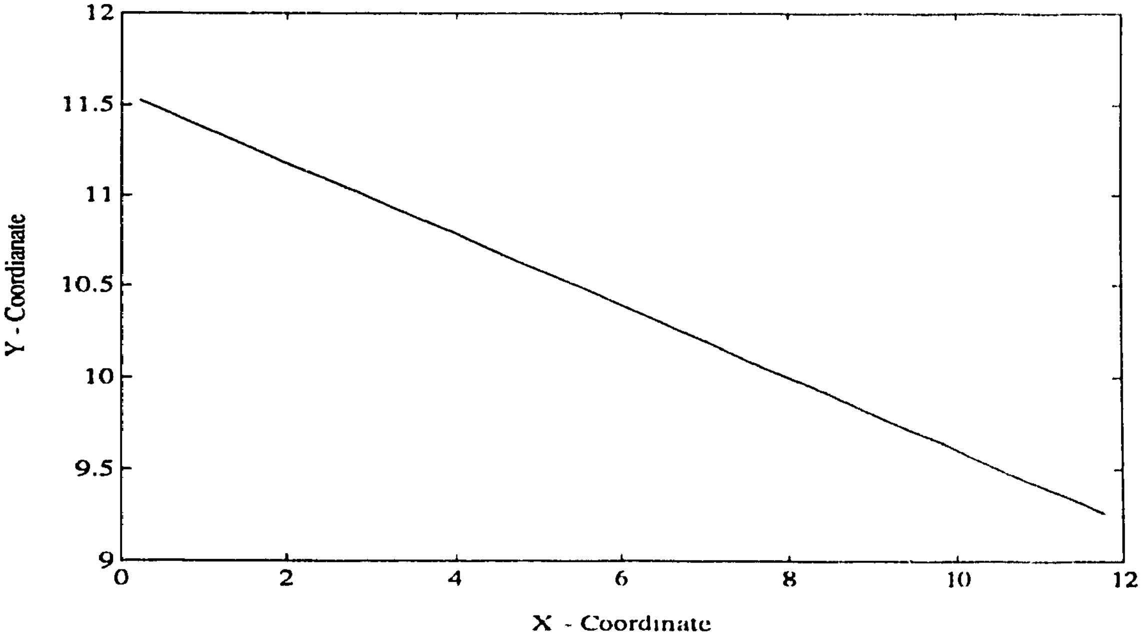

Figure 3.26: Non-Dimensional Unbalance Orbit of the Rotor, $S\omega_0$ = 2.0, μ_s = 1.5, z/l = 0.3, and b/d = 1

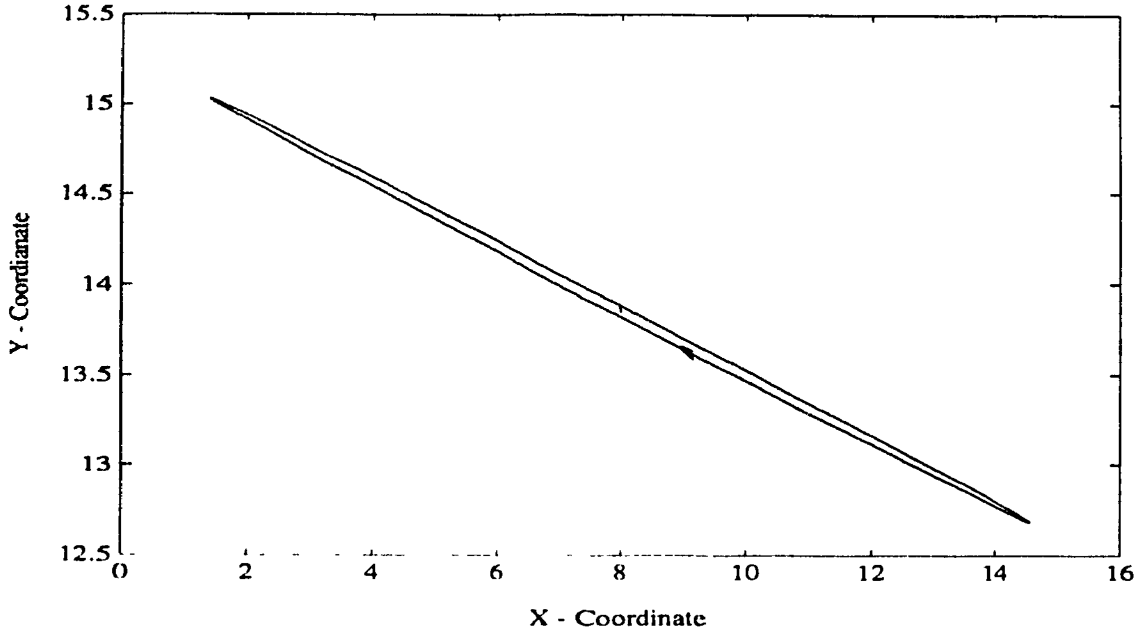

Figure 3.27: Non-Dimensional Unbalance Orbit of the Rotor, So_0 = 2.0, μ_s = 1.5, z/l = 0.4, and b/d = 1

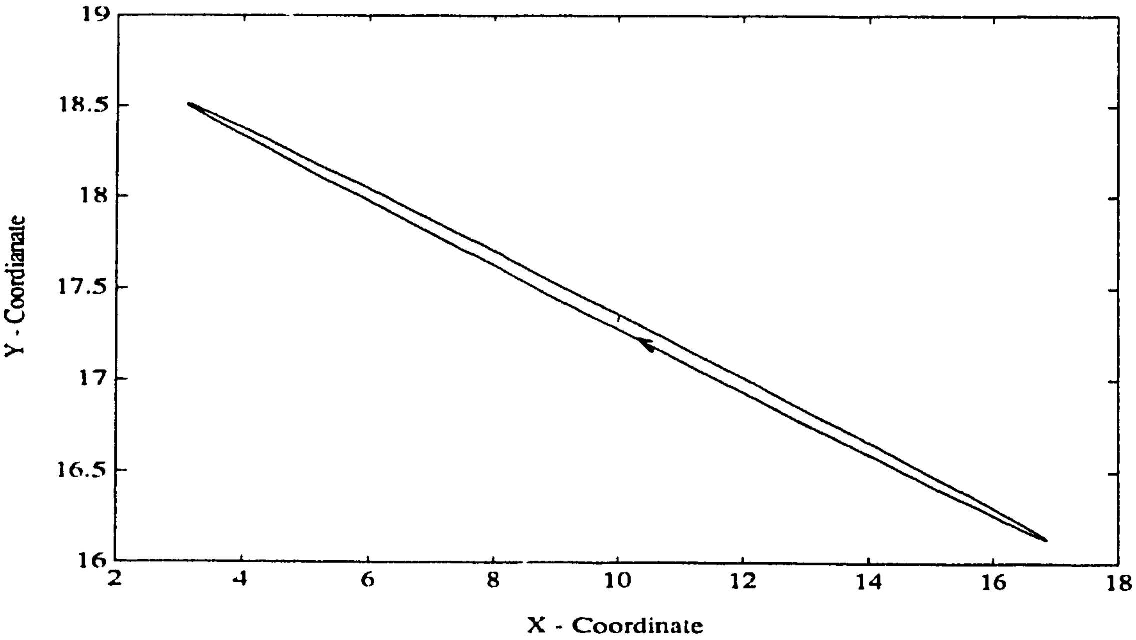

Figure 3.28: Non-Dimensional Unbalance Orbit of the Rotor, So_0 = 2.0, μ_s = 1.5, z/l = 0.5, and b/d = 1

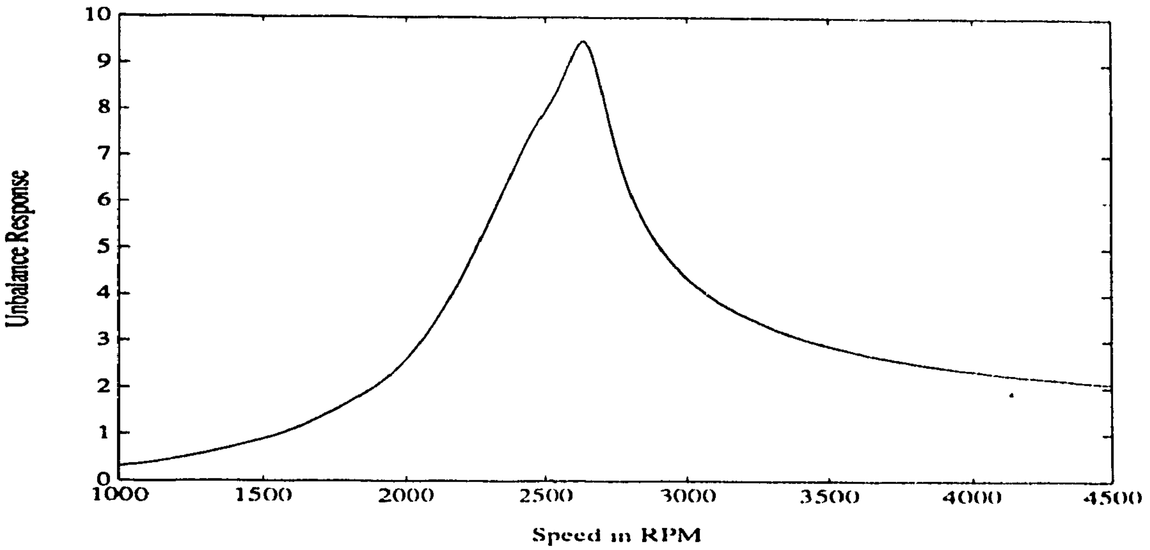

Figure 3.29: Unbalance Response, $\overline{R}$ of a Rotor Supported on Identical bearings : Load Parameter $\overline{S0}_0$ = 0.5, Flexibility Parameter μ_s = 1.5

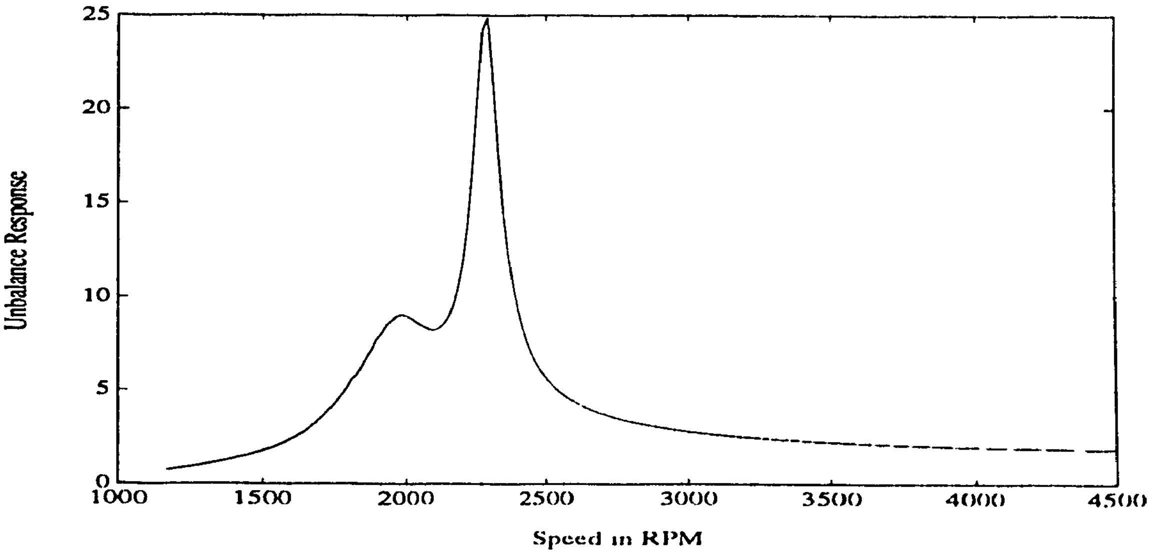

Figure 3.30: Unbalance Response, $\overline{R}$ of a Rotor Supported on Identical bearings : Load Parameter $\overline{S0}_0$ = 3.0, Flexibility Parameter μ_s = 2.0

Chapter 4

Response Analysis of Rotor Supported on Dissimilar Hydrodynamic Bearings

4.1 Introduction

The response analysis of a Jeffcot rotor supported on two dissimilar bearings is studied in the present chapter. The dissimilarities may have been introduced in the design itself in the form of different loads on the two bearings or different bearing geometries. Moreover, even if the two bearings are identical by design, the manufacturing precision difficulties, wear, variation in lubricant flow rate and oil temperature could introduce dissimilarity in the supportive bearings. The equations of motion of the disk are derived using the influence coefficient method and the force balance at journal is used to formulate the remaining governing equations. Euler-Bernoulli beam theory is used to obtain the necessary influence coefficients associated with the displacement and rotation components at the disk location. Gyroscopic couples are also considered in the analysis. The solution for unbalance response is determined by solving the resulting system of linear equations numerically.

The data corresponding to laboratory model of a single mass rotor supported on dissimilar bearings are used to obtain the unbalance response for different combinations of bearing clearances. The critical speeds of the rotor-bearing system are identified from the displacement components at the journal and the disk. Existence of the simultaneous forward and backward whirling motion at the disk location is verified.

When a rotor is supported on identical bearings the analysis becomes fairly simple due to the symmetry about the central plane. Also in the case of rotor supported on identical bearings, slopes at the bearings are not considered and displacement components at the two bearings are equal. All these factors make the analysis in Chapter 3 a special case of the present investigation. In the case of a rotor supported on dissimilar bearings, the rotation at the disk center should also be taken into consideration in addition to deflection . Also the displacements at the two bearings are unequal. Thus the analysis is carried out using a continuous system model.

4.2 Study of Simultaneous Forward and Backward Whirling Motion of Disk and Journal of a Jeffcot Rotor Supported on Dissimilar Hydrodynamic Bearings

4.2.1 Equations of Motion

Figure (4.1) shows a schematic representation of a typical single mass rotor supported on dissimilar hydrodynamic bearings at the two ends. The force and moment component on this rotor is also shown in the figure. The bending moments at a distance z is expressed as (Appendix C)

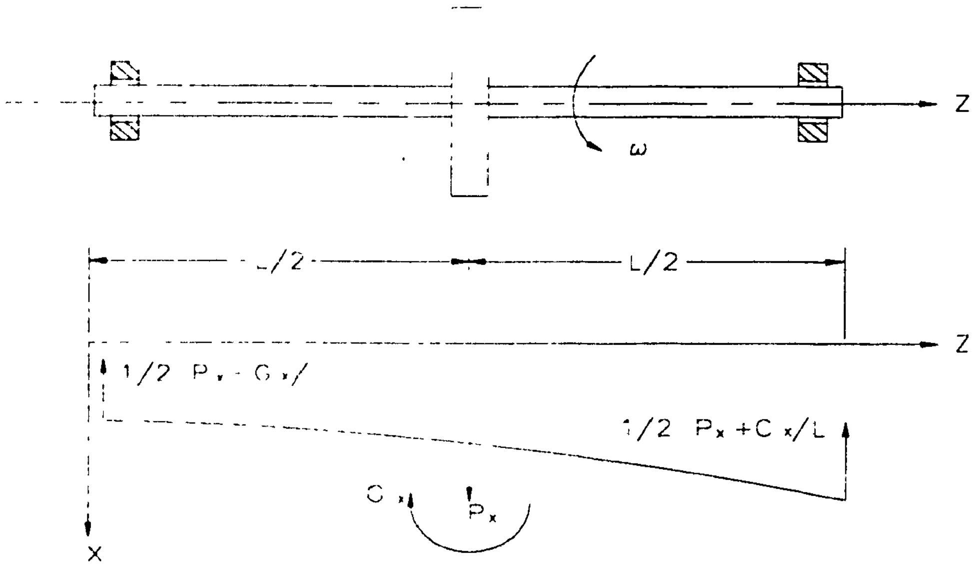

Figure 4.1: Bending Moment Diagram for X - Z Plane

$$EI\frac{d^2\xi_x}{dz^2} = -\left(\frac{1}{2}P_x - \frac{1}{l}G_x\right)z + P_x\left[z - \frac{l}{2}\right] - G_x\left[z - \frac{l}{2}\right]^0 \qquad (4.1)$$

where the closed rectangular brackets, [ ] is Macaulays notation [51], where the expression within the box bracket is considered only when it is positive.

Integration of Eqn. (4.1) gives

$$EI\frac{d\xi_x}{dz} = -\left(\frac{1}{2}P_x - \frac{1}{l}G_x\right)\frac{z^2}{2} + \frac{1}{2}P_x\left[z - \frac{l}{2}\right]^2 - G_x\left[z - \frac{l}{2}\right] + A_1 \qquad (4.2)$$

$$EI\xi_x = -\left(\frac{1}{2}P_x - \frac{1}{l}G_x\right)\frac{z^3}{6} + \frac{1}{6}P_x\left[z - \frac{l}{2}\right]^3 - \frac{1}{2}G_x\left[z - \frac{l}{2}\right]^2 + A_1z + A_2 \qquad (4.3)$$

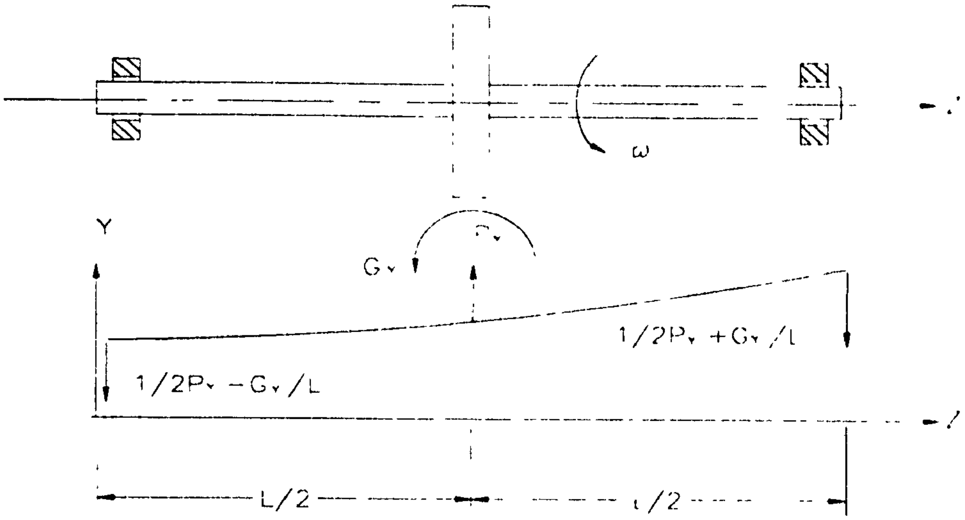

Figure 4.2: Bending Moment Diagram for Y - Z Plane

Using the boundary conditions at $z=0$, $\xi_y = \xi_{yl}$ and at $z=l$, $\xi_y = \xi_{yr}$ and simplification yields the constants of integration as

$$A_1 = \frac{EI}{l}(\xi_{yr} - \xi_{yl}) + \left(\frac{1}{2}P_y - \frac{1}{l}G_y\right)\frac{l^2}{6} - \frac{1}{6}P_y\frac{l^2}{8} + \frac{1}{2}G_y\frac{l}{4} \tag{4.4}$$

$$A_2 = EI\xi_{yl} \tag{4.5}$$

Substituting the boundary conditions at $z = l/2$, $\xi_y = \xi_{yc}$ in Eqn. (4.3) and simplifying results in

$$EI(2\xi_{yc} - \xi_{yr} - \xi_{yl}) = \frac{1}{24}P_y l^3 \tag{4.6}$$

Using the boundary conditions at $z = l/2$, $d\xi_y/dz = \theta_{yc}$ in Eqn. (4.2) and simplifying using Eqn. (4.4) results in

$$EI\left(\theta_{yc} - \frac{\xi_{yr} - \xi_{yl}}{l}\right) = -\frac{1}{12}G_y l \tag{4.7}$$

Similarly for *'y-z'* plane (Fig. 4.2), the governing equations reduces to

$$EI\,(2\xi_{yc} - \xi_{yr} - \xi_{yl}) = \frac{1}{24}P_y l^3 \tag{4.8}$$

$$EI\left(\theta_{yc} - \frac{\xi_{yr} - \xi_{yl}}{l}\right) = \frac{1}{12}G_y l \tag{4.9}$$

The expression for the force components P_x, P_y and the moment components G_x, G_y at the disk location are given by

$$P_x = M\omega^2\delta_c\cos\omega t - M\ddot{\xi}_{xc} + Mg \tag{4.10}$$

$$P_y = M\omega^2\delta_c\sin\omega t - M\ddot{\xi}_{yc} \tag{4.11}$$

$$G_x = -J\omega\dot{\theta}_{yc} \tag{4.12}$$

$$G_y = J\omega\dot{\theta}_{xc} \tag{4.13}$$

Substituting the expression for the force component P_x from Eqn. (4.10), into Eqn. (4.6) gives

$$(2\xi_{xc} - \xi_{xr} - \xi_{xl}) = \frac{2\mu_s}{\omega_0^2}\left(\omega^2\delta_c\cos\omega t - \ddot{\xi}_{xc} + g\right) \tag{4.14}$$

Similarly eliminating P_y from Eqn. (4.7) using Eqn. (4.11) results in

$$(2\xi_{yc} - \xi_{yr} - \xi_{yl}) = \frac{2\mu_s}{\omega_0^2}\left(\omega^2\delta_c\sin\omega t - \ddot{\xi}_{yc}\right) \tag{4.15}$$

Substitution of the moment components G_x, G_y from Eqns. (4.12, 4.13) in Eqns. (4.8, 4.9) yields

$$\left(\theta_{xc} - \frac{\xi_{xr} - \xi_{xl}}{l}\right) = -\frac{4\mathcal{J}}{\omega_s}\left(\omega\dot{\theta}_{yc}\right) \tag{4.16}$$

$$\left(\theta_{yc} - \frac{\xi_{yr} - \xi_{yl}}{l}\right) = \frac{4\mathcal{J}}{\omega_s}\left(\omega\dot{\theta}_{xc}\right) \tag{4.17}$$

When $\delta_c = 0$, the particular solution

$$\begin{array}{llll} & \xi_{xl} = 0 & \xi_{yl} = 0 & \theta_{xc} = 0 \\ & \xi_{xr} = 0 & \xi_{yr} = 0 & \theta_{yc} = 0 \\ & & \xi_{xc} = \frac{\mu_s g}{\omega_0^2}, & \xi_{yc} = 0 \end{array}$$

satisfies Eqns. (4.14 - 4.17).

Eqn. (4.14) can be simplified to

$$2\left(\frac{\xi_{xc} - \frac{\mu_s g}{\omega_0^2}}{c}\right) - \frac{c_r}{c}\left(\frac{\xi_{xr}}{c_r}\right) - \frac{c_l}{c}\left(\frac{\xi_{xl}}{c_l}\right) = \frac{2\mu_s}{\omega_0^2}\left(\omega^2\frac{\delta_c}{c}\cos\omega t - \frac{\ddot{\xi}_{xc}}{c}\right) \qquad (4.18)$$

Eqn. (4.18) can be written in non-dimensional form as

$$2\frac{\omega^2}{\omega^2_s}\overline{\xi}_{xc}'' + 2\overline{\xi}_{xc} - \overline{c_r}\overline{\xi}_{xr} - \overline{c_l}\overline{\xi}_{xl} = 2\frac{\omega^2}{\omega^2_s}\overline{\delta_c}\cos\omega t \qquad (4.19)$$

Similarly Eqn. (4.15) in non-dimensional form may be obtained as

$$2\frac{\omega^2}{\omega^2_s}\overline{\xi}_{yc}'' + 2\overline{\xi}_{yc} - \overline{c_r}\overline{\xi}_{yr} - \overline{c_l}\overline{\xi}_{yl} = 2\frac{\omega^2}{\omega^2_s}\overline{\delta_c}\sin\omega t \qquad (4.20)$$

Eqns. (4.16, 4.17) considering gyroscopic couple can be written in non-dimensional form as

$$\overline{\theta}_{xc} - \overline{c_r}\overline{\xi}_{xr} + \overline{c_l}\overline{\xi}_{xl} = -4\overline{J}\frac{\omega^2}{\omega_s^2}\overline{\theta}_{yc}' \qquad (4.21)$$

$$\overline{\theta}_{yc} - \overline{c_r}\overline{\xi}_{yr} + \overline{c_l}\overline{\xi}_{yl} = 4\overline{J}\frac{\omega^2}{\omega_s^2}\overline{\theta}_{xc}' \qquad (4.22)$$

4.2.2 Force Balance at the Bearing

Force balance at the bearings is expressed as

$$\frac{1}{2}P_x - \frac{G_x}{l} - \frac{W}{2} = K_{xx,l}\xi_{xl} + K_{xy,l}\xi_{yl} + C_{xx,l}\dot{\xi}_{xl} + C_{xy,l}\dot{\xi}_{yl} \tag{4.23}$$

$$\frac{1}{2}P_y - \frac{G_y}{l} = K_{yx,l}\xi_{xl} + K_{yy,l}\xi_{yl} + C_{yx,l}\dot{\xi}_{xl} + C_{yy,l}\dot{\xi}_{yl} \tag{4.24}$$

$$\frac{1}{2}P_x + \frac{G_x}{l} - \frac{W}{2} = K_{xx,r}\xi_{xr} - + K_{xy,r}\xi_{yr} + C_{xx,r}\dot{\xi}_{xr} + C_{xy,r}\dot{\xi}_{yr} \tag{4.25}$$

$$\frac{1}{2}P_y - \frac{G_y}{l} = K_{yx,r}\xi_{xr} + K_{yy,r}\xi_{yr} + C_{yx,r}\dot{\xi}_{xr} + C_{yy,r}\dot{\xi}_{yr} \tag{4.26}$$

Substituting the force component term P_x and P_y from Eqns. (4.6,4.7) in Eqns. (4.23, 4.24) results in

$$\begin{aligned}\frac{12EI}{l^3}(2\xi_{xc} - \xi_{xr} - \xi_{xl}) - \frac{12EI}{l^2}\left(\theta_{xc} - \frac{\xi_{xr} - \xi_{xl}}{l}\right) - \frac{W}{2} &= K_{xx,l}\xi_{xl} + K_{xy,l}\xi_{yl} \\ &+ C_{xx,l}\dot{\xi}_{xl} + C_{xy,l}\dot{\xi}_{yl}\end{aligned} \tag{4.27}$$

$$\begin{aligned}\frac{12EI}{l^3}(2\xi_{yc} - \xi_{yr} - \xi_{yl}) - \frac{12EI}{l^2}\left(\theta_{yc} - \frac{\xi_{yr} - \xi_{yl}}{l}\right) &= K_{yx,l}\xi_{xl} + K_{yy,l}\xi_{yl} \\ &+ C_{yx,l}\dot{\xi}_{xl} + C_{yy,l}\dot{\xi}_{yl}\end{aligned} \tag{4.28}$$

Similarly substitution for the moment components G_x from Eqn. (4.8), and G_y from (4.9) in Eqn. (4.25), (4.26) yields

$$\begin{aligned}\frac{12EI}{l^3}(2\xi_{xc} - \xi_{xr} - \xi_{xl}) + \frac{12EI}{l^2}\left(\theta_{xc} - \frac{\xi_{xr} - \xi_{xl}}{l}\right) - \frac{W}{2} &= K_{xx,r}\xi_{xr} + K_{xy,r}\xi_{yr} \\ &+ C_{xx,r}\dot{\xi}_{xr} + C_{xy,r}\dot{\xi}_{yr}\end{aligned} \tag{4.29}$$

$$\frac{12EI}{l^3}\left(2\xi_{yc}-\xi_{yr}-\xi_{yl}\right)+\frac{12EI}{l^2}\left(\theta_{yc} - \frac{\xi_{yr}-\xi_{yl}}{l}\right) = K_{yx,r}\xi_{xr}+K_{yy,r}\xi_{yr} + C_{yx,r}\dot{\xi}_{xr}+C_{yy,r}\dot{\xi}_{yr} \quad (4.30)$$

Using the non-dimensional stiffness and damping coefficients, Eqn. (4.27 - 4.30) can be written in non-dimensional form as

$$2\left(\bar{\xi}_{xc} - \overline{c_l}\bar{\xi}_{xl}\right) - \bar{\theta}_{xc} = 2\mu_s\left(\bar{K}_{xx,l}\bar{\xi}_{xl}+\bar{K}_{xy,l}\bar{\xi}_{yl}\right) + 2\mu_s\left(\bar{C}_{xx,l}\bar{\xi}_{xl}'+\bar{C}_{xy,l}\bar{\xi}_{yl}'\right) \quad (4.31)$$

$$2\left(\bar{\xi}_{yc} - \overline{c_l}\bar{\xi}_{yl}\right) - \bar{\theta}_{yc} = 2\mu_s\left(\bar{K}_{yx,l}\bar{\xi}_{xl}+\bar{K}_{yy,l}\bar{\xi}_{yl}\right) + 2\mu_s\left(\bar{C}_{yx,l}\bar{\xi}_{xl}'+\bar{C}_{yy,l}\bar{\xi}_{yl}'\right) \quad (4.32)$$

$$2\left(\bar{\xi}_{xc} - \overline{c_r}\bar{\xi}_{xr}\right) + \bar{\theta}_{xc} = 2\mu_s\left(\bar{K}_{xx,r}\bar{\xi}_{xr}+\bar{K}_{xy,r}\bar{\xi}_{yr}\right) + 2\mu_s\left(\bar{C}_{xx,r}\bar{\xi}_{xr}'+\bar{C}_{xy,r}\bar{\xi}_{yr}'\right) \quad (4.33)$$

$$2\left(\bar{\xi}_{yc} - \overline{c_r}\bar{\xi}_{yr}\right) + \bar{\theta}_{yc} = 2\mu_s\left(\bar{K}_{yx,l}\bar{\xi}_{xl}+\bar{K}_{yy,l}\bar{\xi}_{yl}\right) + 2\mu_s\left(\bar{C}_{yx,r}\bar{\xi}_{xr}'+\bar{C}_{yy,r}\bar{\xi}_{yr}'\right) \quad (4.34)$$

4.2.3 Unbalance Whirling Motion

Under steady state conditions the unbalance response can be expressed as

$$\begin{aligned}
\bar{\xi}_{xl} &= \frac{\delta_c}{c}\left(a_{xl}\cos\omega t + b_{xl}\sin\omega t\right)\\
\bar{\xi}_{xr} &= \frac{\delta_c}{c}\left(a_{xr}\cos\omega t + b_{xr}\sin\omega t\right)\\
\bar{\xi}_{yl} &= \frac{\delta_c}{c}\left(a_{yl}\cos\omega t + b_{yl}\sin\omega t\right)
\end{aligned}$$

$$
\begin{aligned}
\overline{\xi}_{yr} &= \frac{\delta_c}{c}\left(a_{yr}\cos\omega t + b_{yr}\sin\omega t\right)\\
\overline{\xi}_{xc} &= \frac{\delta_c}{c}\left(a_{xc}\cos\omega t + b_{xc}\sin\omega t\right)\\
\overline{\xi}_{yc} &= \frac{\delta_c}{c}\left(a_{yc}\cos\omega t + b_{yc}\sin\omega t\right)\\
\overline{\theta}_{xc} &= \frac{\delta_c}{c}\left(c_{xc}\cos\omega t + d_{xc}\sin\omega t\right)\\
\overline{\theta}_{yc} &= \frac{\delta_c}{c}\left(c_{yc}\cos\omega t + d_{yc}\sin\omega t\right)
\end{aligned}
\tag{4.35}
$$

Substitution of the steady state solution (4.35) into the equation of motion and equating $\cos\omega t$ and $\sin\omega t$ terms from the left and right hand sides of Eqns. (4.19 - 4.22) results in

$$2a_{xc}\left(1 - \frac{\omega^2}{\omega_s{}^2}\right) - \overline{\tau}_r a_{xr} - \overline{\tau}_l a_{xl} = 2\frac{\omega^2}{\omega_s{}^2} \tag{4.36}$$

$$2b_{xc}\left(1 - \frac{\omega^2}{\omega_s{}^2}\right) - \overline{\tau}_r b_{xr} - \overline{\tau}_l b_{xl} = 0 \tag{4.37}$$

$$2a_{yc}\left(1 - \frac{\omega^2}{\omega_s{}^2}\right) - \overline{\tau}_r a_{yr} - \overline{\tau}_l a_{yl} = 0 \tag{4.38}$$

$$2b_{yc}\left(1 - \frac{\omega^2}{\omega_s{}^2}\right) - \overline{\tau}_r b_{yr} - \overline{\tau}_l b_{yl} = 2\frac{\omega^2}{\omega_s{}^2} \tag{4.39}$$

$$c_{xc} - \overline{\tau}_r a_{xr} + \overline{\tau}_l a_{xl} = -4\overline{J}\frac{\omega^2}{\omega_s{}^2}d_{yc} \tag{4.40}$$

$$d_{xc} - \overline{\tau}_r b_{xr} + \overline{\tau}_l b_{xl} = 4\overline{J}\frac{\omega^2}{\omega_s{}^2}c_{yc} \tag{4.41}$$

$$c_{yc} - \overline{\tau}_r a_{yr} + \overline{\tau}_l a_{yl} = 4\overline{J}\frac{\omega^2}{\omega_s{}^2}d_{xc} \tag{4.42}$$

$$d_{yc} - \overline{\tau}_r b_{yr} + \overline{\tau}_l b_{yl} = -4\overline{J}\frac{\omega^2}{\omega_s{}^2}c_{xc} \tag{4.43}$$

Similarly, the substitution of (4.35) in equation of force balance at the bearing and equating $\cos\omega t$ and $\sin\omega t$ terms in Eqns. (4.31 - 4.34) results in

$$\begin{aligned} 2a_{xc} - 2\bar{c}_l a_{xl} - c_{xc} &= 2\mu_s \overline{K}_{xx,l} a_{xl} + 2\mu_s \overline{K}_{xy,l} a_{yl} \\ &+ 2\mu_s \overline{C}_{xx,l} b_{xl} + 2\mu_s \overline{C}_{xy,l} b_{yl} \end{aligned} \tag{4.44}$$

$$\begin{aligned} 2b_{xc} - 2\bar{c}_l b_{xl} - d_{xc} &= 2\mu_s \overline{K}_{xx,l} b_{xl} + 2\mu_s \overline{K}_{xy,l} b_{yl} \\ &- 2\mu_s \overline{C}_{xx,l} a_{xl} - 2\mu_s \overline{C}_{xy,l} a_{yl} \end{aligned} \tag{4.45}$$

$$\begin{aligned} 2a_{yc} - 2\bar{c}_l a_{yl} - c_{xc} &= 2\mu_s \overline{K}_{yx,l} a_{xl} + 2\mu_s \overline{K}_{yy,l} a_{yl} \\ &+ 2\mu_s \overline{C}_{yx,l} b_{xl} + 2\mu_s \overline{C}_{yy,l} b_{yl} \end{aligned} \tag{4.46}$$

$$\begin{aligned} 2b_{yc} - 2\bar{c}_l b_{yl} - d_{yc} &= 2\mu_s \overline{K}_{yx,l} b_{xl} + 2\mu_s \overline{K}_{yy,l} b_{yl} \\ &- 2\mu_s \overline{C}_{yx,l} a_{xl} - 2\mu_s \overline{C}_{yy,l} a_{yl} \end{aligned} \tag{4.47}$$

$$\begin{aligned} 2a_{xc} - 2\bar{c}_r a_{xr} + c_{xc} &= 2\mu_s \overline{K}_{xx,r} a_{xr} + 2\mu_s \overline{K}_{xy,r} a_{yr} \\ &+ 2\mu_s \overline{C}_{xx,r} b_{xr} + 2\mu_s \overline{C}_{xy,r} b_{yr} \end{aligned} \tag{4.48}$$

$$\begin{aligned} 2b_{xc} - 2\bar{c}_r b_{xr} + d_{xc} &= 2\mu_s \overline{K}_{xx,r} b_{xr} + 2\mu_s \overline{K}_{xy,r} b_{yl} \\ &+ -2\mu_s \overline{C}_{xx,r} a_{xr} - 2\mu_s \overline{C}_{xy,r} a_{yr} \end{aligned} \tag{4.49}$$

$$\begin{aligned} 2a_{yc} - 2\bar{c}_r a_{yr} + c_{xc} &= 2\mu_s \overline{K}_{yx,r} a_{xr} + 2\mu_s \overline{K}_{yy,r} a_{yr} \\ &+ 2\mu_s \overline{C}_{yx,r} b_{xr} + 2\mu_s \overline{C}_{yy,r} b_{yr} \end{aligned} \tag{4.50}$$

$$\begin{aligned} 2b_{yc} - 2\bar{c}_r b_{yr} + d_{yc} &= 2\mu_s \overline{K}_{yx,r} b_{xr} + 2\mu_s \overline{K}_{yy,r} b_{yr} \\ &- 2\mu_s \overline{C}_{yx,r} a_{xr} - 2\mu_s \overline{C}_{yy,r} a_{yr} \end{aligned} \tag{4.51}$$

Disk mass,	11 kg
Type of bearings	Plain Cylindrical
Bearing diameter	0.0254 m
Bearing L/D ratio	1
Modulus of elasticity of the material of shaft	2.15*$10^{11}\, N/m^2$
Viscosity of oil	0.0241 N. sec/m^2
Length of the rotor	0.5105 m
Disk diameter	0.2032 m
Shaft diameter	0.022 m

Table 4.1: Data for Computation

4.3 Numerical Computation

The system of Eqns. (4.36 - 4.51) thus derived in the above analysis, represents typical single mass rotor system whose configuration is given in table 4.1.

The above analysis is carried out to obtain the damped critical speed and unbalance response of the simple rotor in consideration. For the case, where the supporting bearing clearances are unequal, the parameter $\delta = (c_l - c_r)/c$, where $c = (c_r + c_l)/2$, is used to express the dissimilarity of the end bearings in non-dimensional form. For the bearing of $b/d = 1.00$, stiffness and damping coefficients thus computed in Chapter 2 are used. The unknown coefficients $a_{xl}.\ b_{xl}.\ ....\ c_{yc}, c_{dc}$ in Eqns. (4.36 - 4.51) are computed by solving the real general system of linear equations, using the IMSL subroutine LSLRG.

4.3.1 Sense of Whirling Motion

The unbalance response of the rotor can be calculated thus using the computed value of coefficients $a_{xl}.\ ....\ c_{dc}$ in Eqn. (4.35). Similar to the analysis of a rotor supported on identical bearings in Chapter 3, the area of the elliptic orbit at the left bearing is evaluated from the expression $\pi\delta_c^2(a_{xl}b_{yl} - b_{xl}a_{yl})$ (see Appendix A). When the sign of this expression is positive, the whirl is forward and when it is negative, the whirl is backward.

Similarly the sense of whirling motion at the right bearing and at the disk location are evaluated from the area of the respective elliptical orbits, $\pi\delta_c^2\,(a_{xr}b_{yr} - b_{xr}a_{yr})$ and $\pi\delta_c^2(a_{xc}b_{yc} - b_{xc}a_{yc})$. Once again the sign of the area determines whether the whirl is forward or backward depending on it being positive or negative.

4.4 Results and Discussion

In hydrodynamic bearings, the variations in bearing clearances alter the Sommerfeld number which in turn, influences the bearing stiffness and damping coefficients. Using the data for computation of the laboratory model, the computed value of load parameter and flexibility parameter respectively are 1.06 and 1.43. which with reference to Fig. (3.6), the rotor is seen to lie in a region of forward whirl. The unbalance response for this rotor is depicted Fig. (4.3) which shows a single critical speed. The corresponding area of the whirl orbit at the disk and bearings is positive over the range of speed, of rotor operation indicating forward mode of whirling for these system parameters of the rotor, Figs. (4.4, 4.5).

Considering a rotor model supported on identical bearings ie, keeping the dissimilarity parameter $\delta = 0$. the load parameter $S\omega_0$ and flexibility parameter μ_s are varied such that the rotor exhibits split criticals. For the value of $S\omega_0 = 3.0$ and $\mu_s = 2.0$, the rotor exhibits a split criticals, the first minor critical speed at 1900 rpm and the second major critical speed at 2400 rpm as shown in Fig. (4.6). Area of the whirl orbit remains positive at the supporting bearings, indicating a forward whirling motion as shown in Fig. (4.9). Area of the whirl orbit at the disk goes negative between the two critical speeds, indicating the existence of simultaneous forward whirling motion at the bearings and backward whirling motion at the disk as shown in Fig. (4.7). Response at the bearing location is shown in Fig. (4.8). Response at the right and left bearings are equal since the dissimilarity parameter is taken to be zero.

Keeping the load parameter So_0 and flexibility parameter μ_s the same at 3.0 and 2.0 respectively, the dissimilarity in the supporting bearing is introduced by making the parameter δ = 0.005. Change in the dissimilarity parameter to a smaller value does not considerably affect the response at the disk and area of the whirl orbit as represented in Figs. (4.10, 4.11). However the peak amplitude of response at the right bearing, whose clearance is lowered with respect to the left bearing comes down as shown in Fig. (4.12). The corresponding area of the whirl orbit at the bearing location is positive over the range of speed, of rotor operation indicating forward mode of whirling at bearings, Fig. (4.13).

For the same system parameters, varying the dissimilarity parameter to a value of 0.05 results in increase of peak amplitude of response at the disk, however the critical speed peaks shift towards the lower rotor speeds as shown in Fig. (4.14). The same trend is observed in the area of the orbit at the disk and existence of the backward whirling motion for a range in between the two critical speeds at the disk is verified in Fig. (4.15). Peak amplitude at the right bearing drops down considerably compared to the left bearing as depicted in Fig. (4.16). However the area of the whirl orbit at the bearing location remains positive as shown in Fig. (4.17) indicates that the whirl orbit is forward.

The effect of increasing the dissimilarity factor further to a value of 0.1 results in critical speed peaks falling down to 1700 and 2000 rpm at the rotor, with the increase in peak amplitude of response at the disk as observed in Figs. (4.18, 4.19). Response at the right bearing drops down drastically with the peak amplitude of response for the second critical speed being smaller than the first one. At the left bearing location, peak amplitude of response for the first critical speed was observed to drop down compared to second critical speed with the increase in dissimilarity parameter δ as depicted in Fig. (4.20). Corresponding area of the whirl orbit remains positive at bearing locations indicating a forward whirl, Fig. (4.21).

Increasing the value of δ to 0.15, the analysis is repeated and the results of which are shown in Figs. (4.22 - 4.25). Increasing the value of δ to 2.0, the response at the disk and bearings does not follow the regular trend and the rotor becomes highly unstable.

The orbital diagram for the rotor with system parameters, $S_{\omega_0} = 3.0$ and $\mu_s = 2.0$ and dissimilarity parameter $\delta = 0.1$ are studied, because the rotor exhibits split criticals and hence the whirl patterns of the system at different rotor speeds are of interest. The orbital diagram provide the amplitude and direction of whirl orbit, indicating whether the whirling motion is forward or backward at any defined location of the rotor system. The orbital diagram for the rotor resulting from the unbalance response is shown in Figs. (4.26 - 4.30), for different locations in the shaft for a rotor speed of 2300 rpm. Fig. (4.26) represents the orbit of the rotor at disk, i.e. at $z/l = 0$. Figs. (4.26, 4.27) shows that whirling motion is backward over approximately the central one-fifths of the shaft. At the point of transition from backward to forward whirling, represented in Fig.(4.28) for $z/l = 0.15$, the whirl orbit becomes a straight line. The point of transition from forward to backward whirl occurs at a point on the rotor much in advance than in the case of identical bearings. This is due to variation in flexibility and load parameter and also due to the introduction of dissimilarity in the bearings.

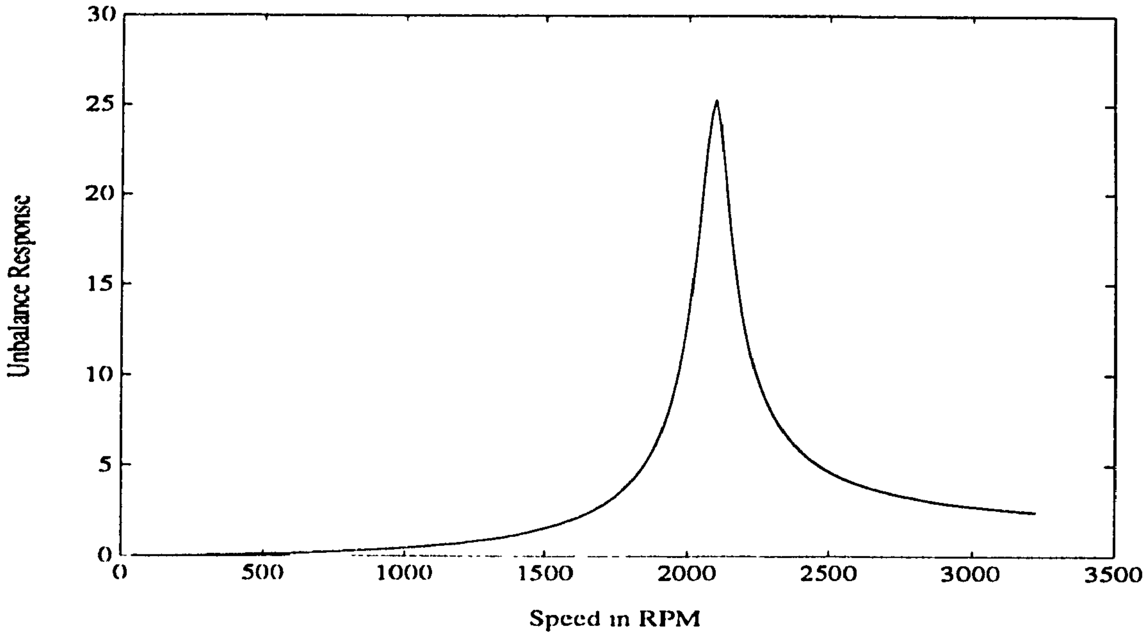

Figure 4.3: Unbalance Response, $\overline{R}$ at the Disk : $S\omega_0 = 0.10$, $\mu_s = 2.43$ and $\delta = 0$

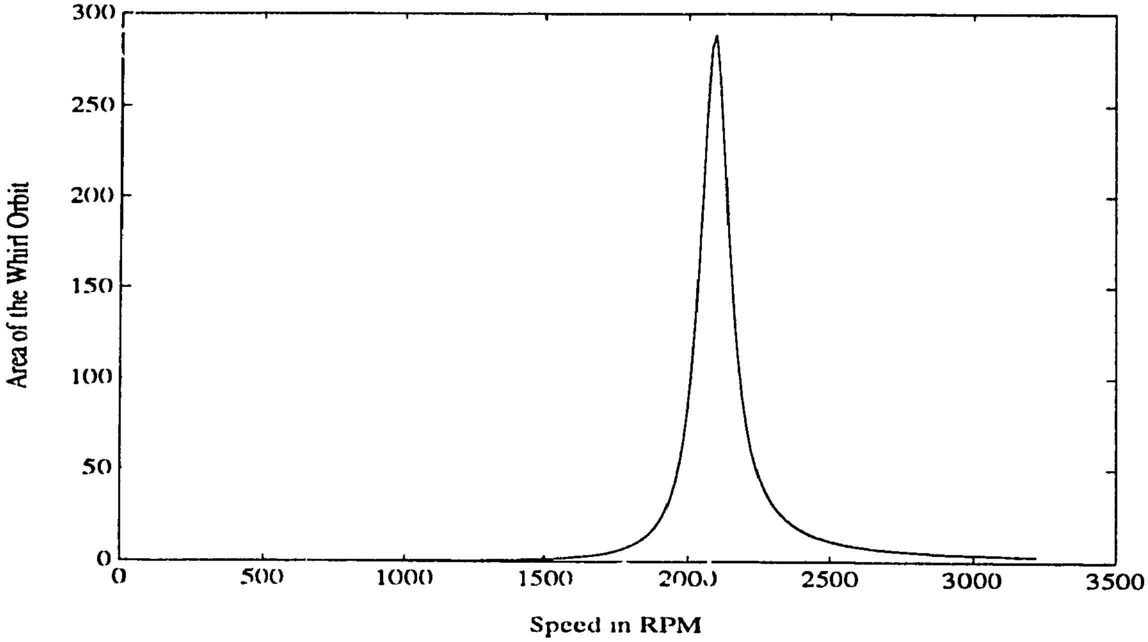

Figure 4.4: Area of the Whirl Orbit at the Disk, $\overline{A}$: $S\omega_0 = 0.10$, $\mu_s = 2.43$ and $\delta = 0$

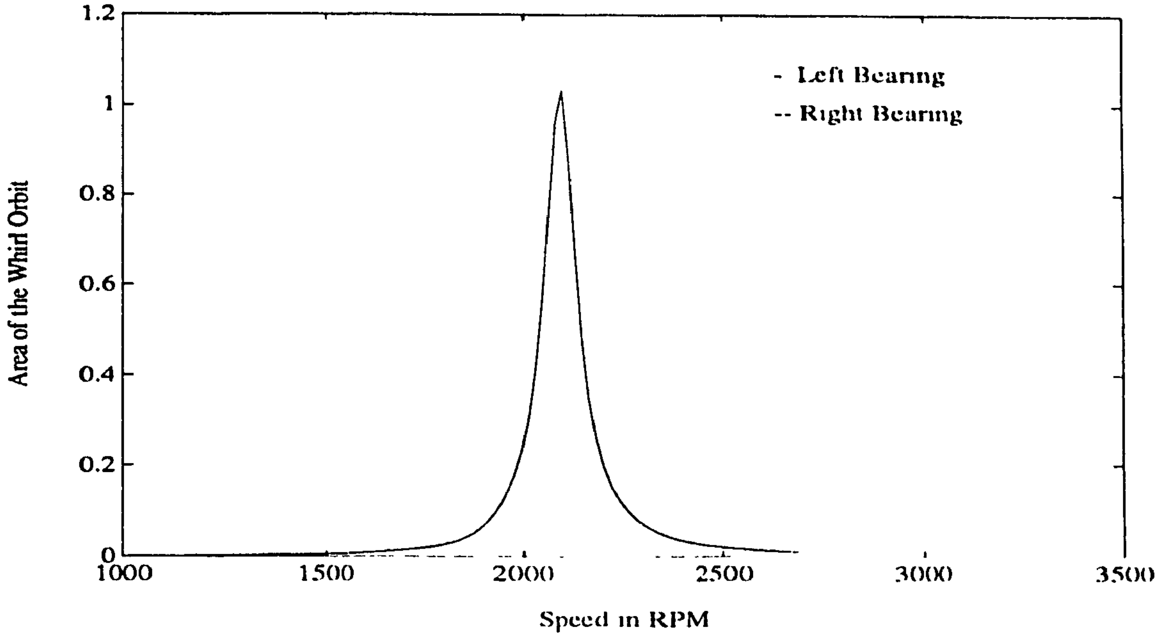

Figure 4.5: Area of the Whirl Orbit at the Bearing Location, $\overline{A}$: $S\omega_0 = 0.10$, $\mu_s = 2.43$ and $\delta = 0$

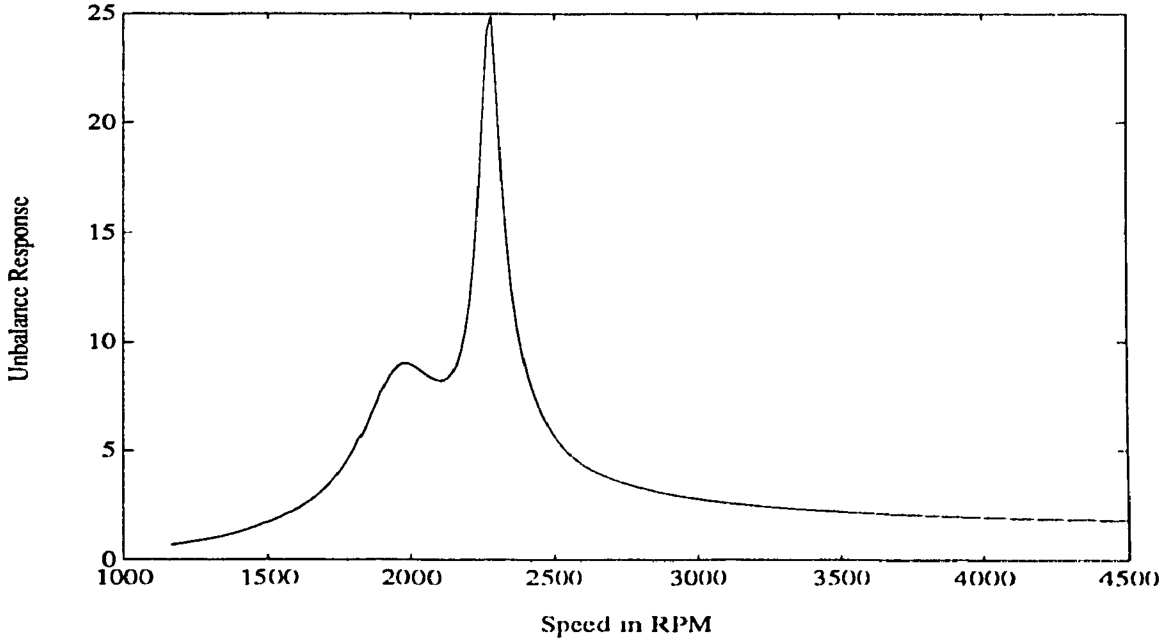

Figure 4.6: Unbalance Response, $\overline{R}$ at the Disk : Load Parameter $S\omega_0 = 3.0$, Flexibility Parameter $\mu_s = 2.0$ and Dissimilarity Parameter $\delta = 0$

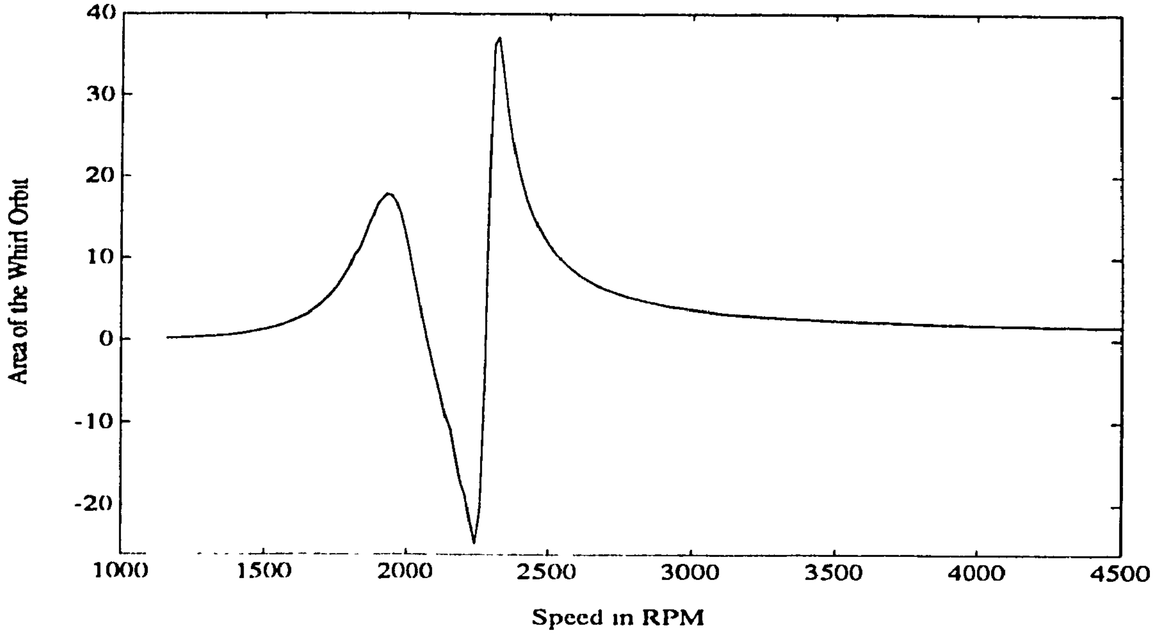

Figure 4.7: Area of the Whirl Orbit at the Disk, $\overline{A}$: So_0 = 3.0, μ_s = 2.0 and δ = 0

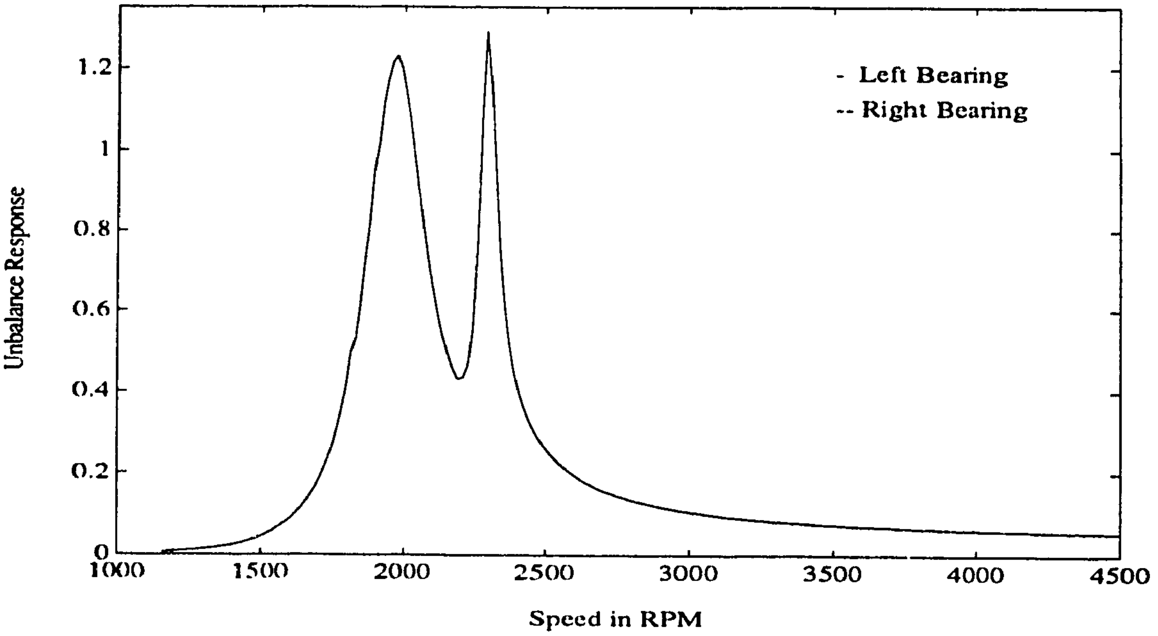

Figure 4.8: Unbalance Response, $\overline{R}$ at the Bearing Location : So_0 = 3.0, μ_s = 2.0 and δ = 0

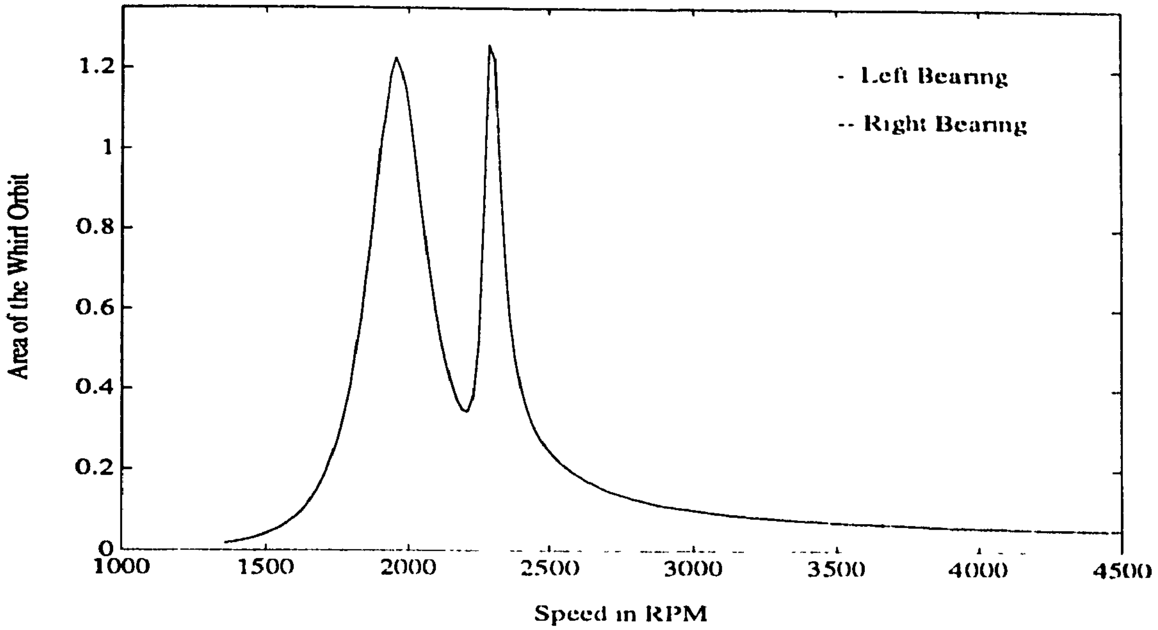

Figure 4.9: Area of the Whirl Orbit at the Bearing Location, $\overline{A}$: $S_{O_0} = 3.0$, $\mu_s = 2.0$and $\delta = 0$

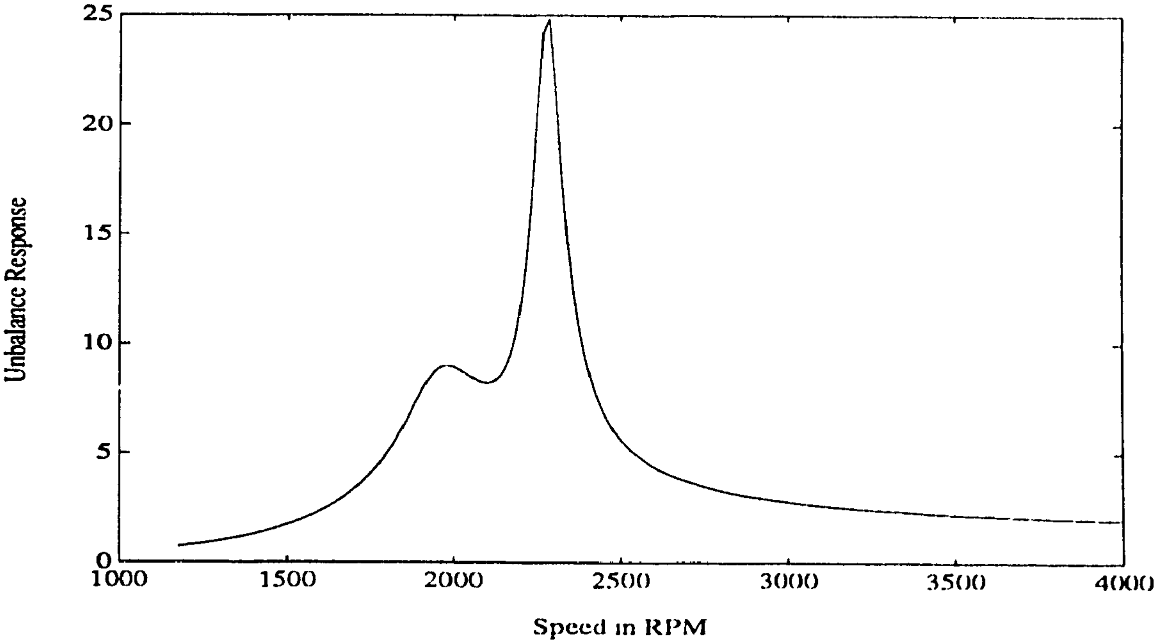

Figure 4.10: Unbalance Response, $\overline{R}$ at the Disk : Load Parameter $S_{O_0} = 3.0$, Flexibility Parameter $\mu_s = 2.0$ and Dissimilarity Parameter $\delta = 0.005$

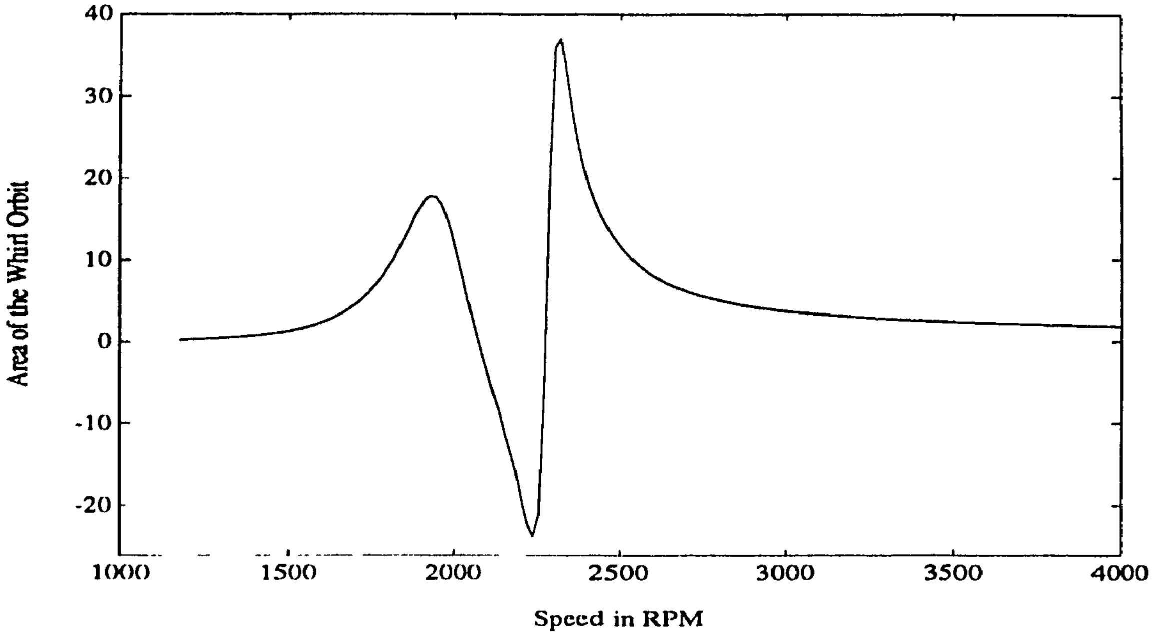

Figure 4.11: Area of the Whirl Orbit at the Disk, $\overline{A}$: So_0 = 3.0, μ_s = 2.0 and δ = 0.005

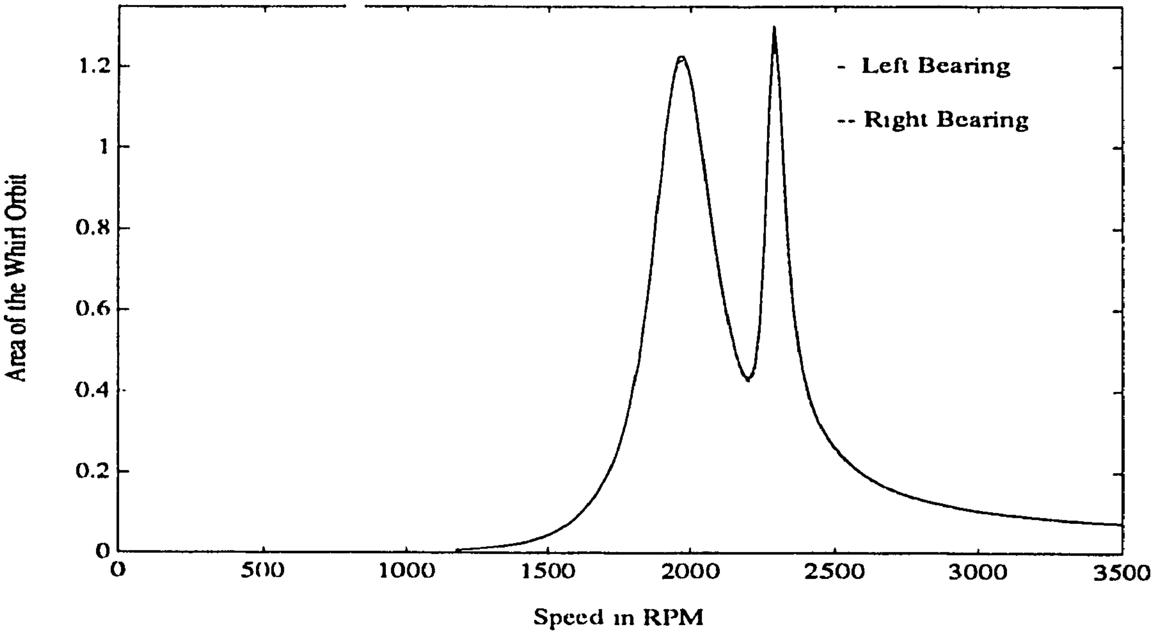

Figure 4.12: Unbalance Response, $\overline{R}$ at the Bearing Location : So_0 = 3.0, μ_s = 2.0 and δ = 0.005

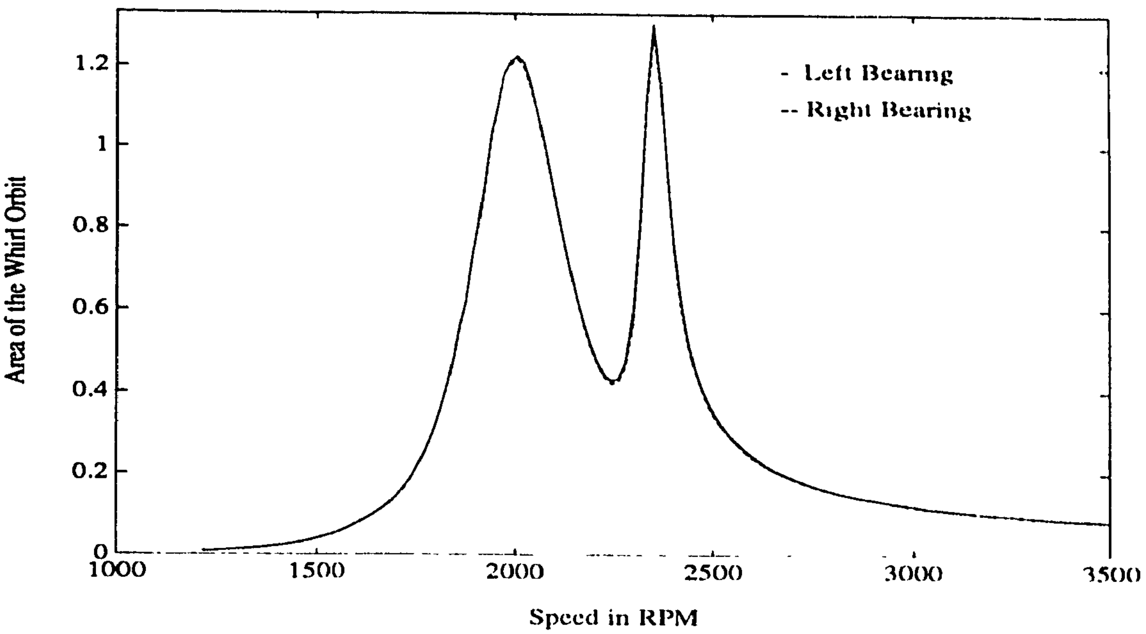

Figure 4.13: Area of the Whirl Orbit at the Bearing Location, $\overline{A}$: $S\sigma_0$ = 3.0, μ_s = 2.0 and δ = 0.005

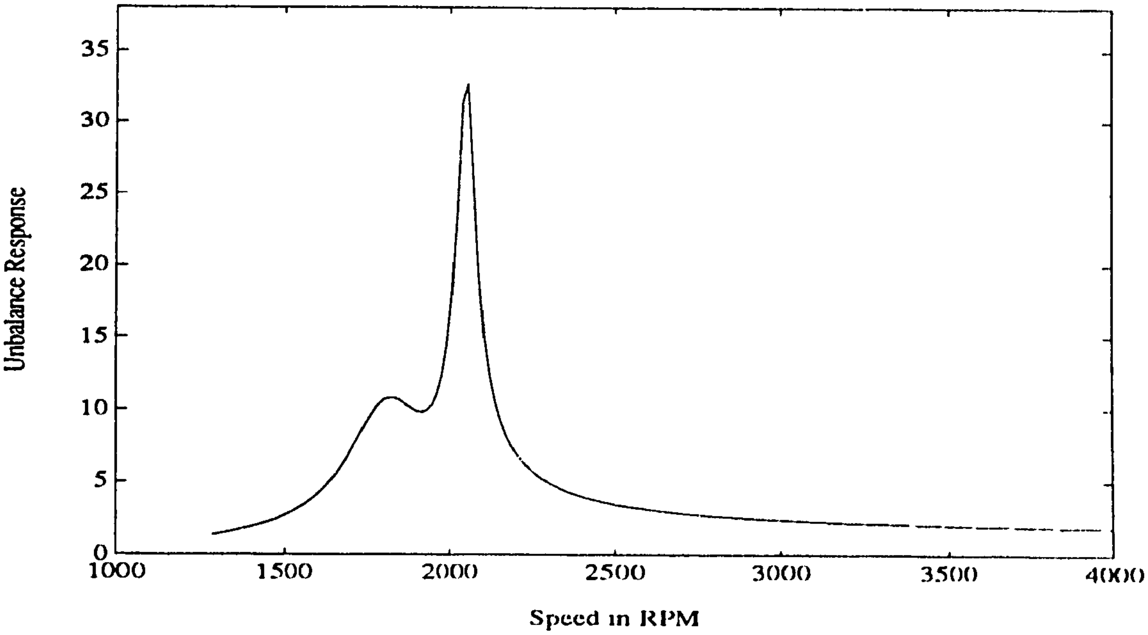

Figure 4.14: Unbalance Response, $\overline{R}$ at the Disk : Load Parameter $S\sigma_0$ = 3.0, Flexibility Parameter μ_s = 2.0 and Dissimilarity Parameter δ = 0.05

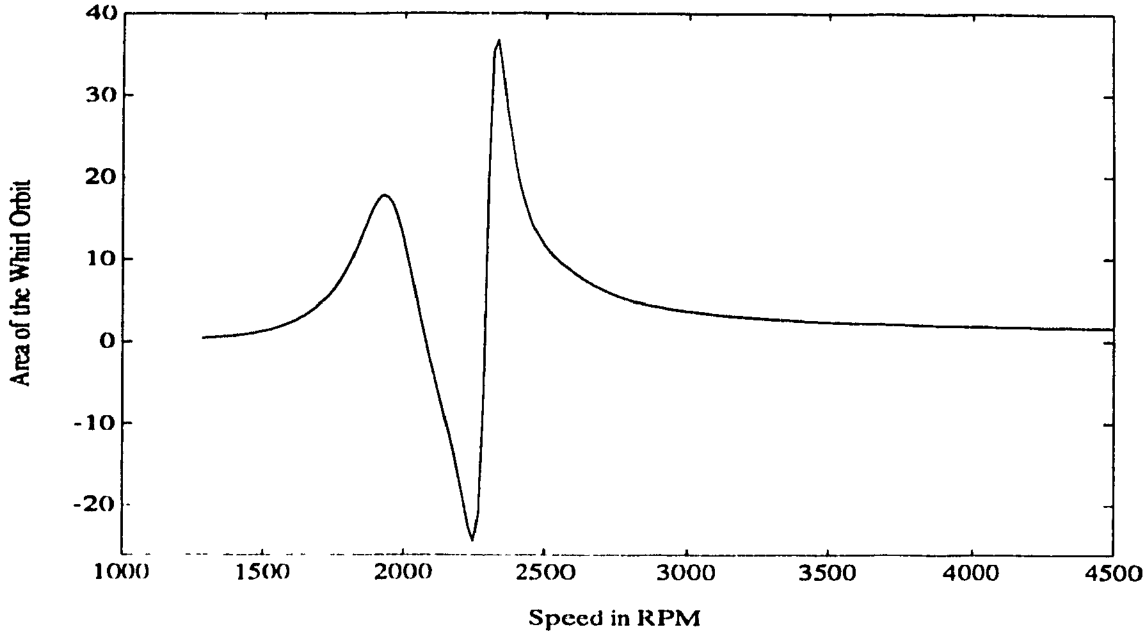

Figure 4.15: Area of the Whirl Orbit at the Disk, $\overline{A}$: So_0 = 3.0, μ_s = 2.0 and δ = 0.05

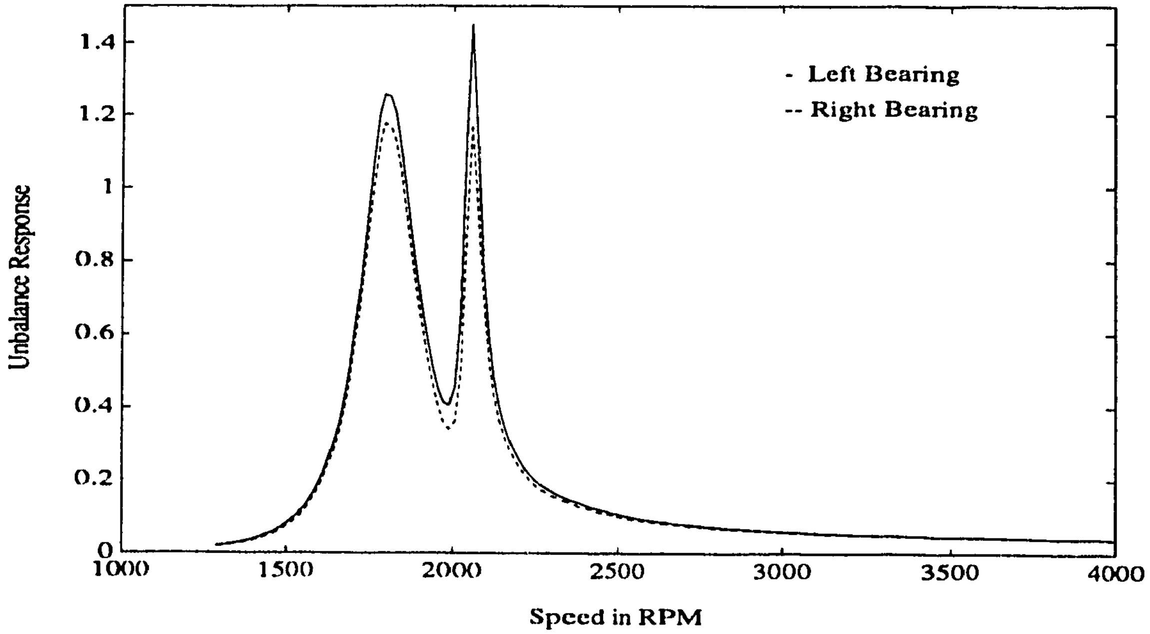

Figure 4.16: Unbalance Response, $\overline{R}$ at the Bearing Location : So_0 = 3.0, μ_s = 2.0 and δ = 0.05

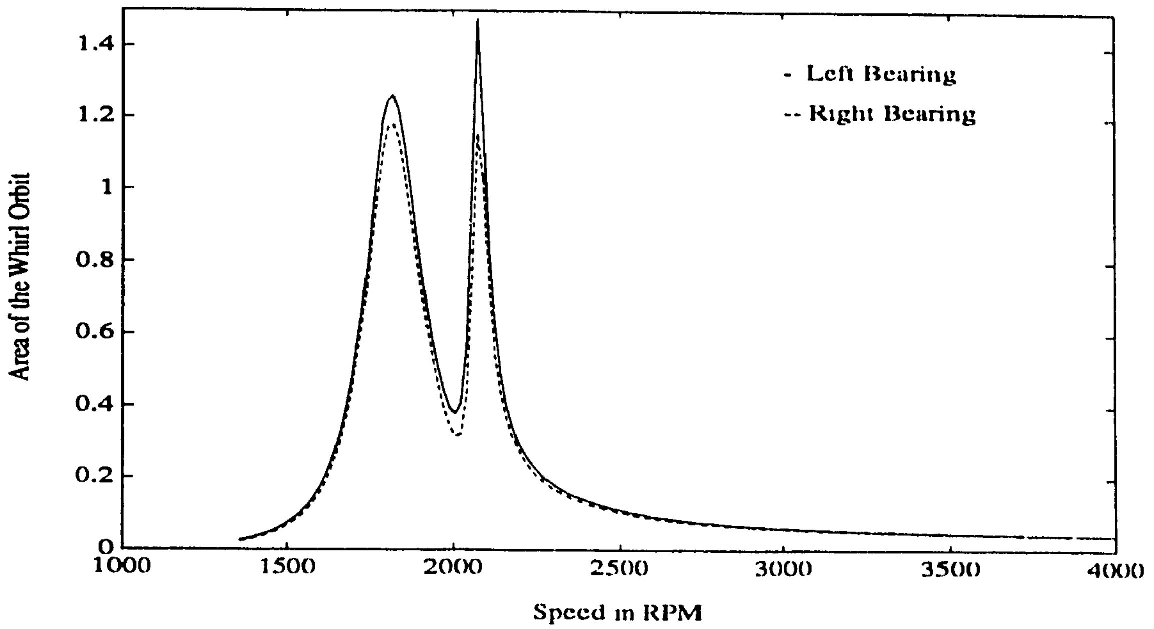

Figure 4.17: Area of the Whirl Orbit at the Bearing Location, $\overline{A}$: $S\sigma_0$ = 3.0, μ_s = 2.0 and δ = 0.05

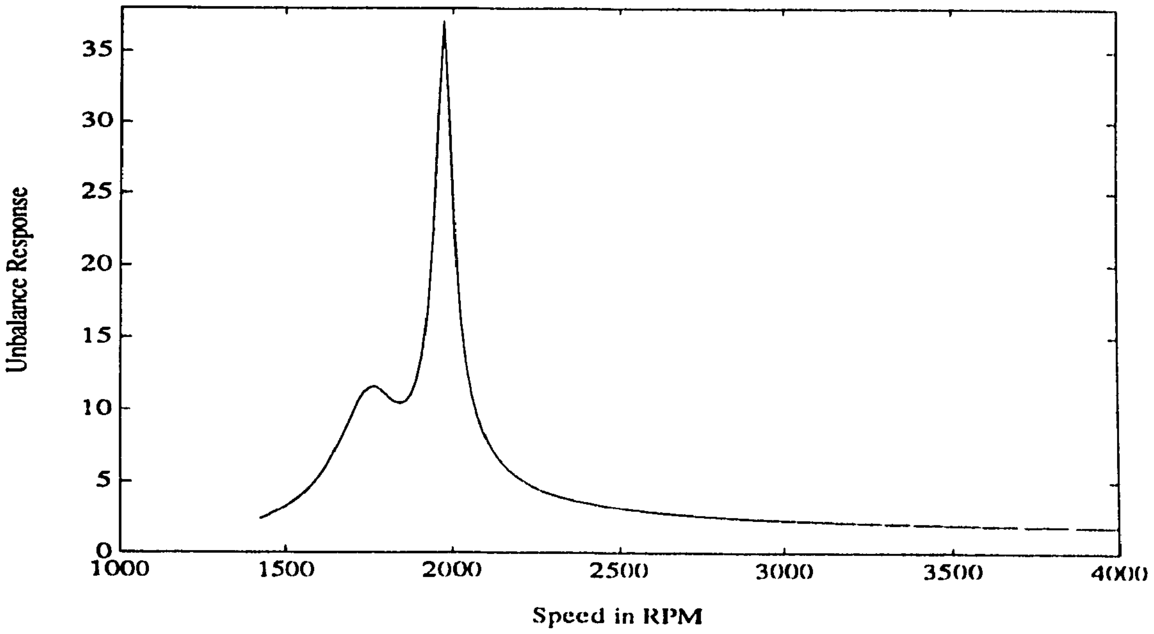

Figure 4.18: Unbalance Response, $\overline{R}$ at the Disk : Load Parameter $S\sigma_0$ = 3.0, Flexibility Parameter μ_s = 2.0 and Dissimilarity Parameter δ = 0.1

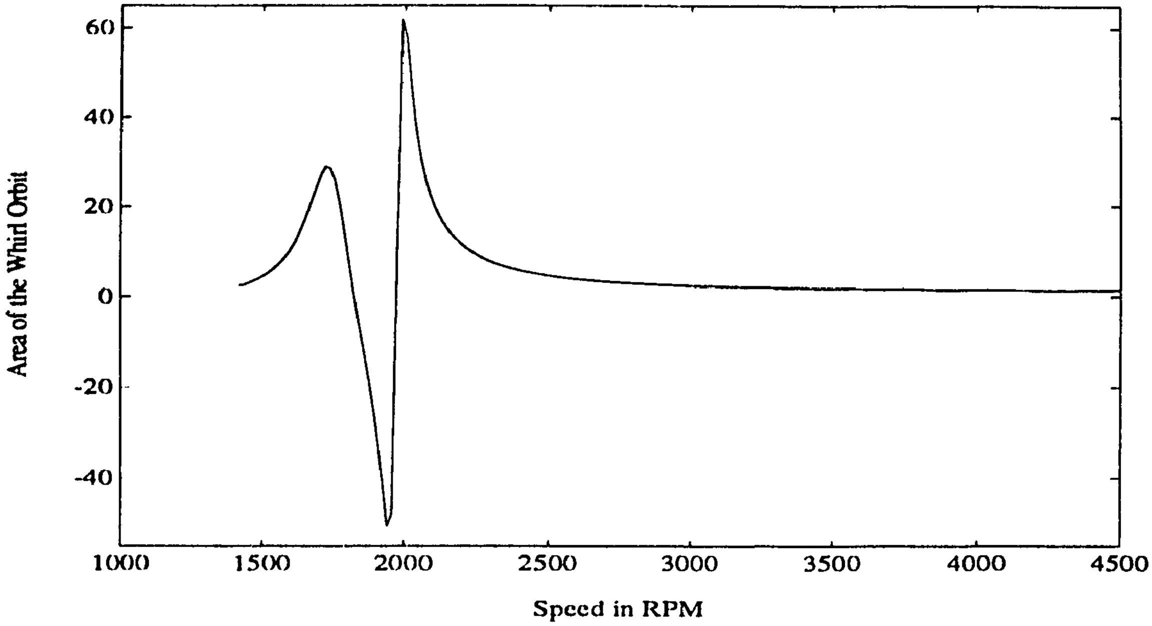

Figure 4.19: Area of the Whirl Orbit at the Disk, $\overline{A}$: $So_0 = 3.0$, $\mu_s = 2.0$ and $\delta = 0.1$

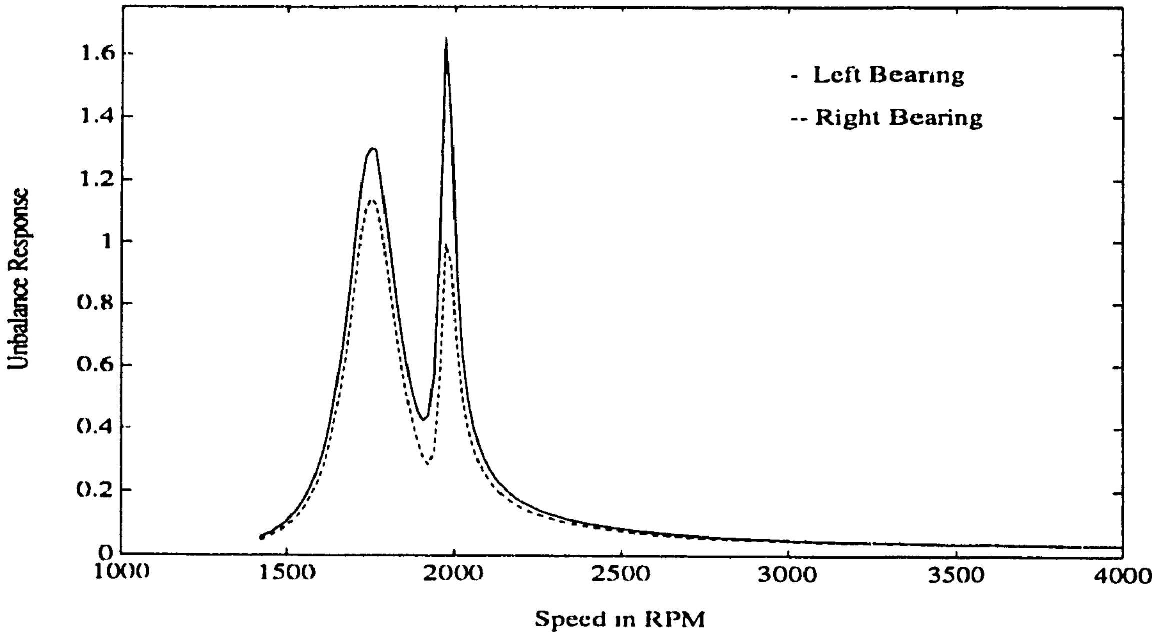

Figure 4.20: Unbalance Response, $\overline{R}$ at the Bearing Location : $So_0 = 3.0$, $\mu_s = 2.0$ and $\delta = 0.1$

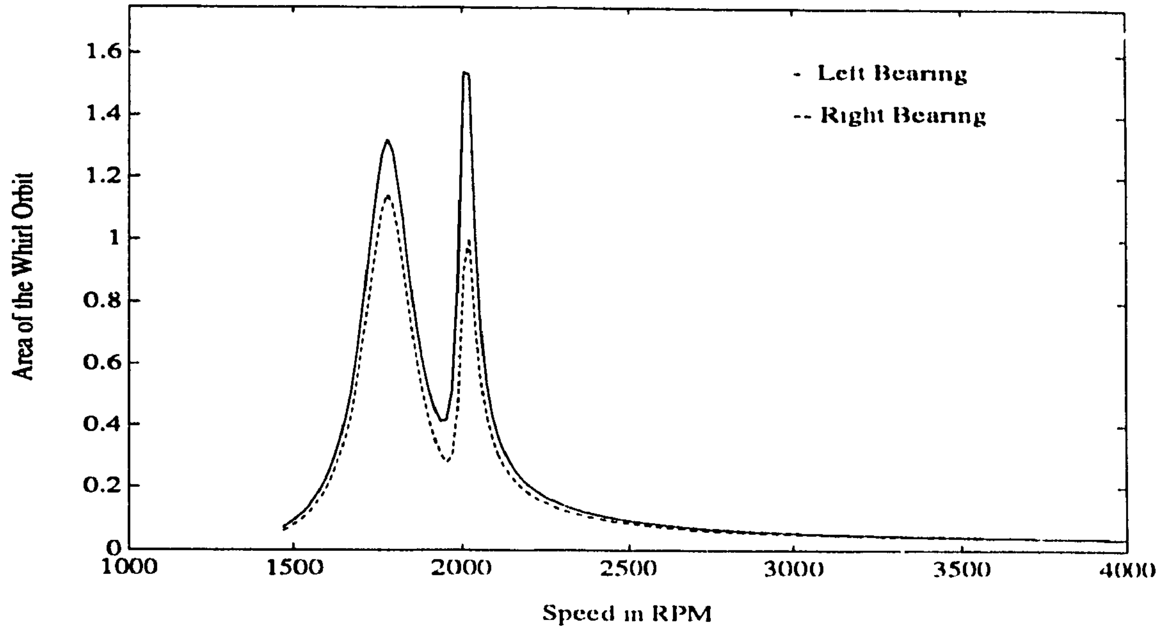

Figure 4.21: Area of the Whirl Orbit at the Bearing Location, $\overline{A}$: $S_{o0} = 3.0$, $\mu_s = 2.0$ and $\delta = 0.1$

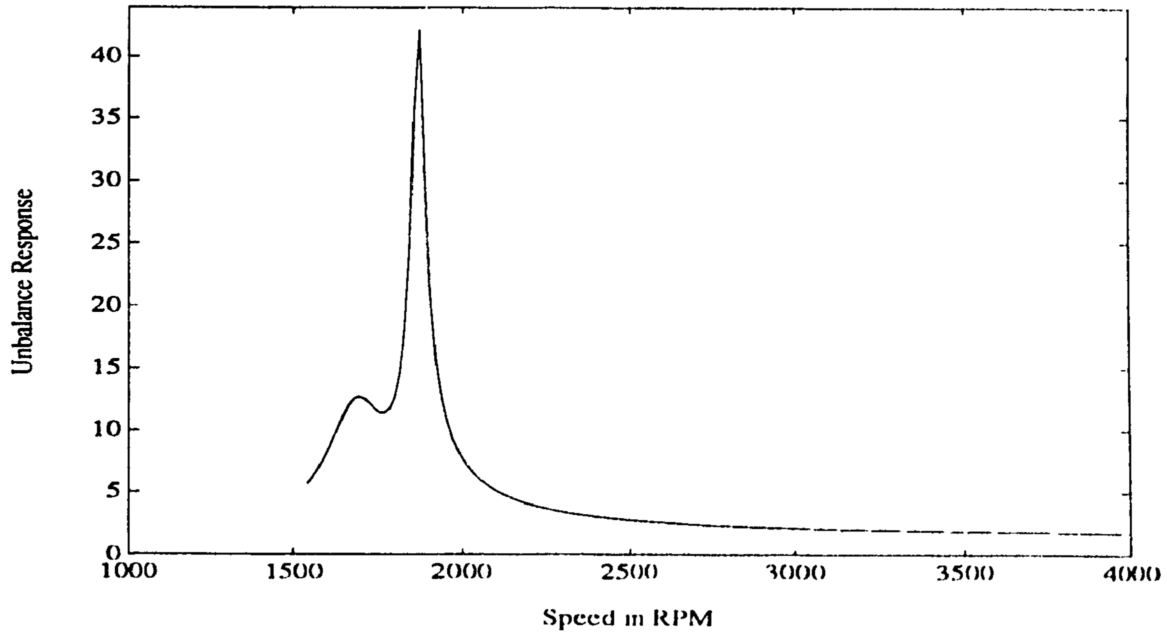

Figure 4.22: Unbalance Response, $\overline{R}$ at the Disk : Load Parameter $S_{o0} = 3.0$, Flexibility Parameter $\mu_s = 2.0$ and Dissimilarity Parameter $\delta = 0.15$

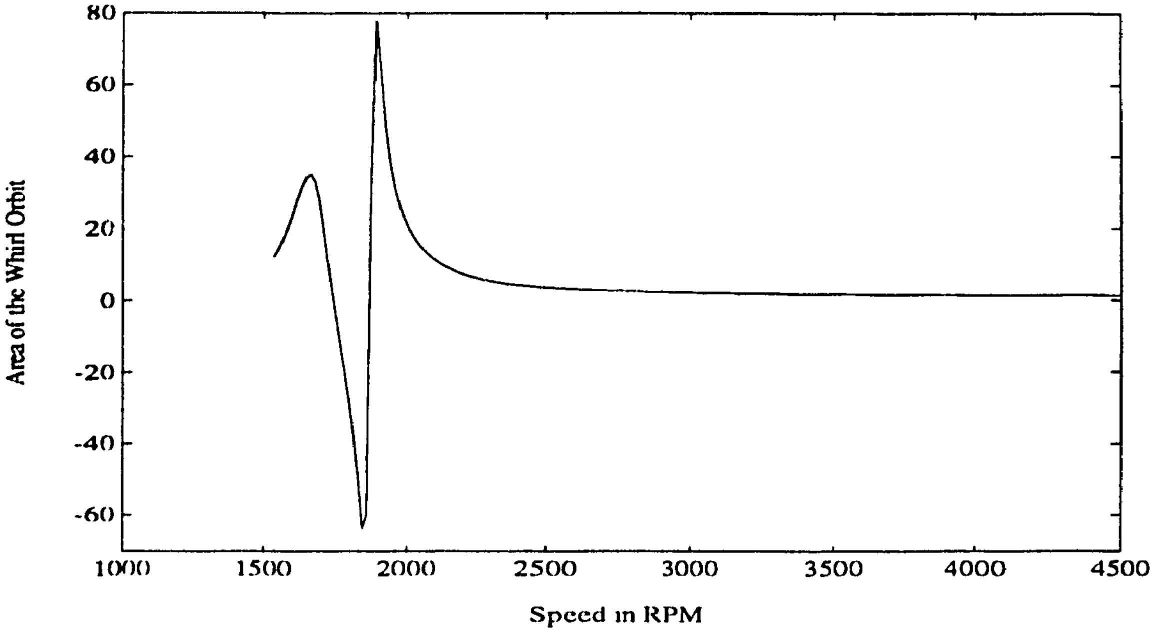

Figure 4.23: Area of the Whirl Orbit at the Disk, $\overline{A}$: $S\alpha_0$ = 3.0, μ_s = 2.0 and δ = 0.15

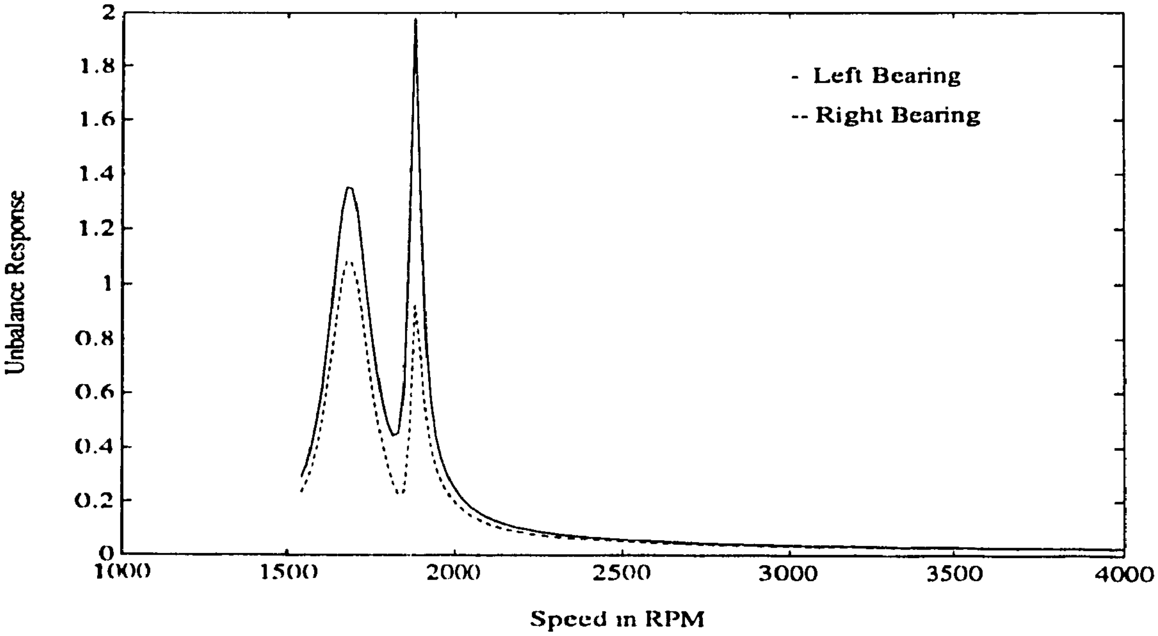

Figure 4.24: Unbalance Response, $\overline{R}$ at the Bearing Location : $S\alpha_0$ = 3.0, μ_s = 2.0 and δ = 0.15

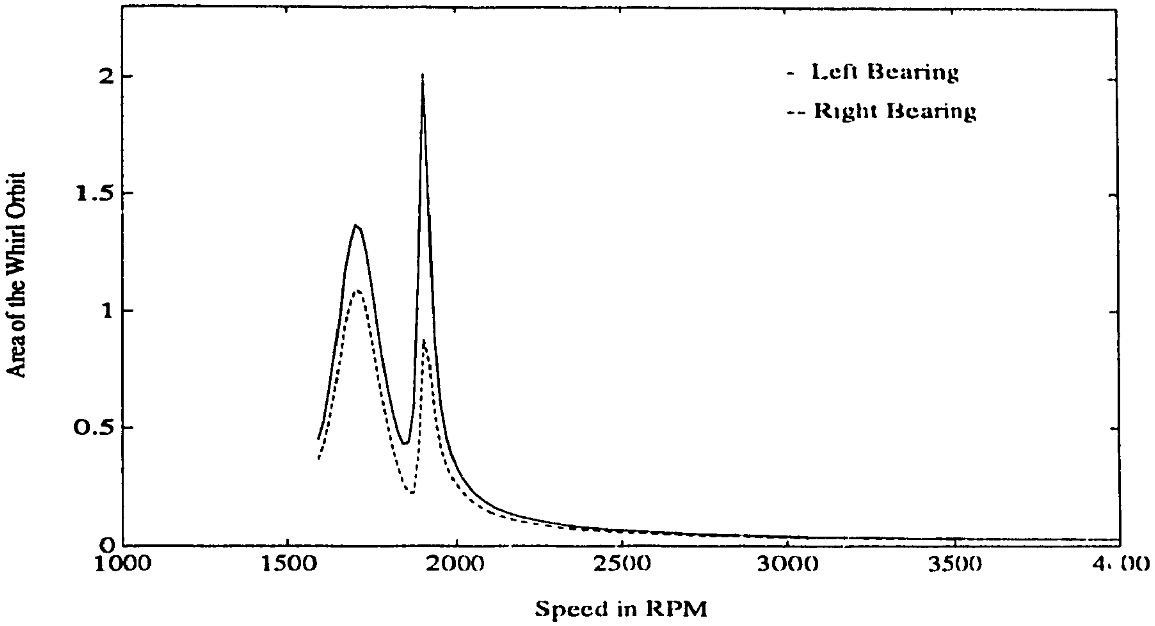

Figure 4.25: Area of the Whirl Orbit at the Bearing Location, $\overline{A}$: $S\alpha_0$ = 3.0, μ_s = 2.0 and δ = 0.15

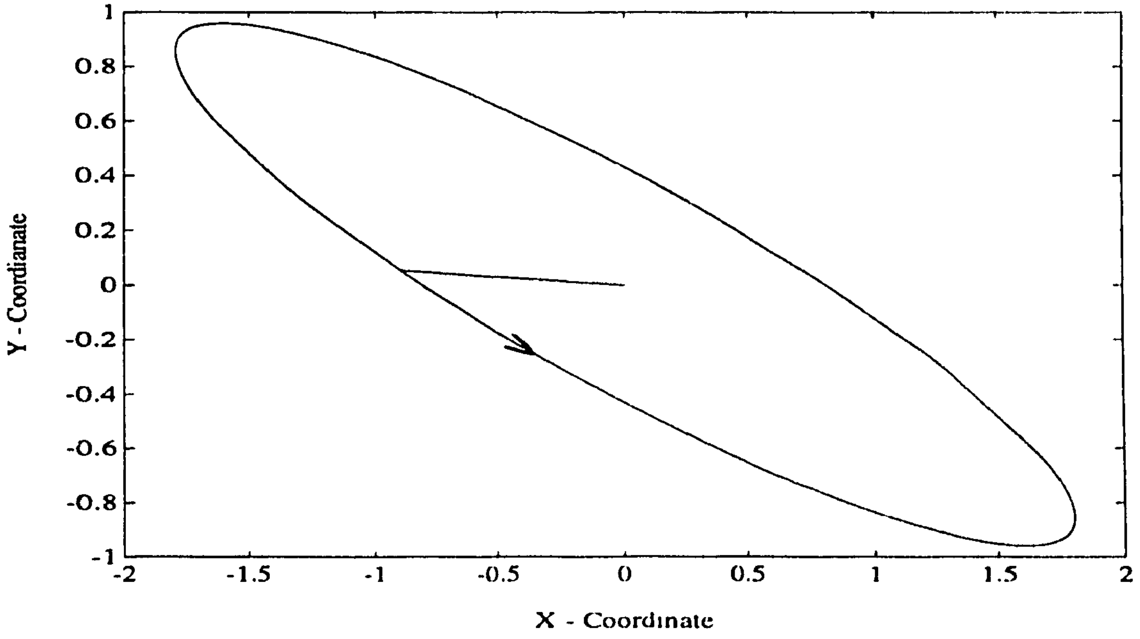

Figure 4.26: Non-Dimensional Unbalance Orbit of the Rotor, $S\alpha_0$ = 3.0, μ_s = 2.0, z/l = 0.0

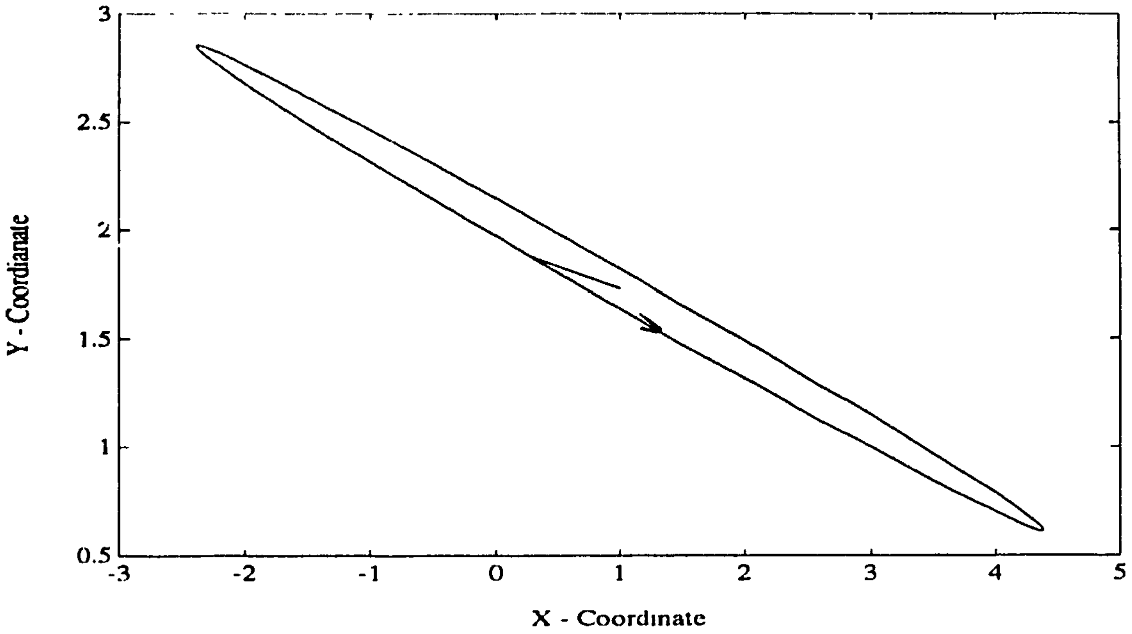

Figure 4.27: Non-Dimensional Unbalance Orbit of the Rotor, So_0 = 3.0, μ_s = 2.0, z/l = 0.05

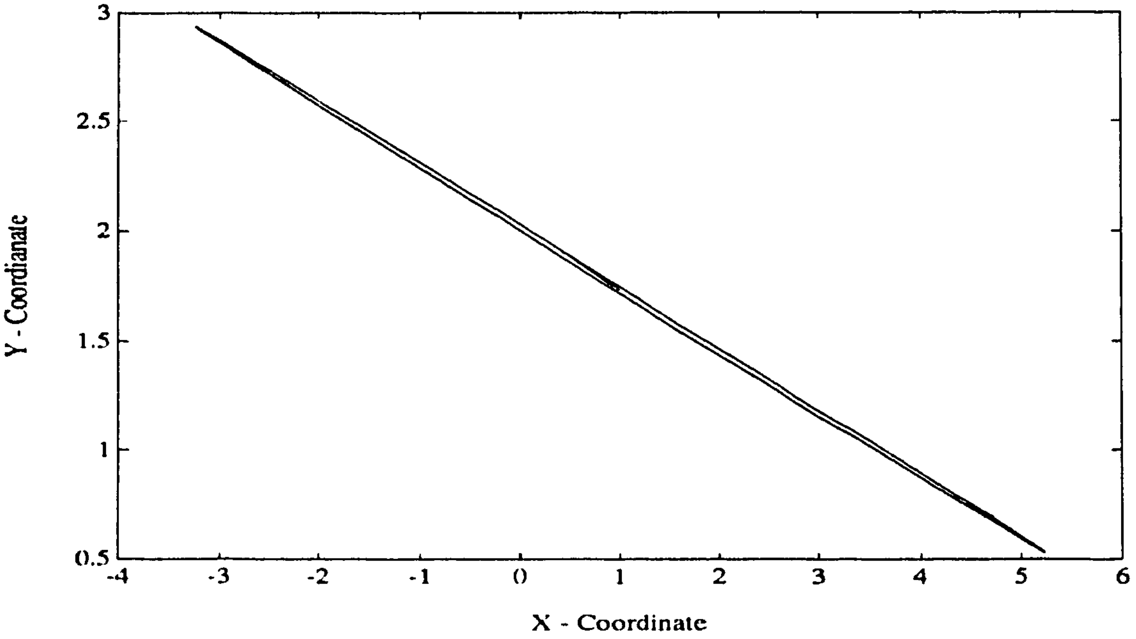

Figure 4.28: Non-Dimensional Unbalance Orbit of the Rotor, So_0 = 3.0, μ_s = 2.0, z/l = 0.1

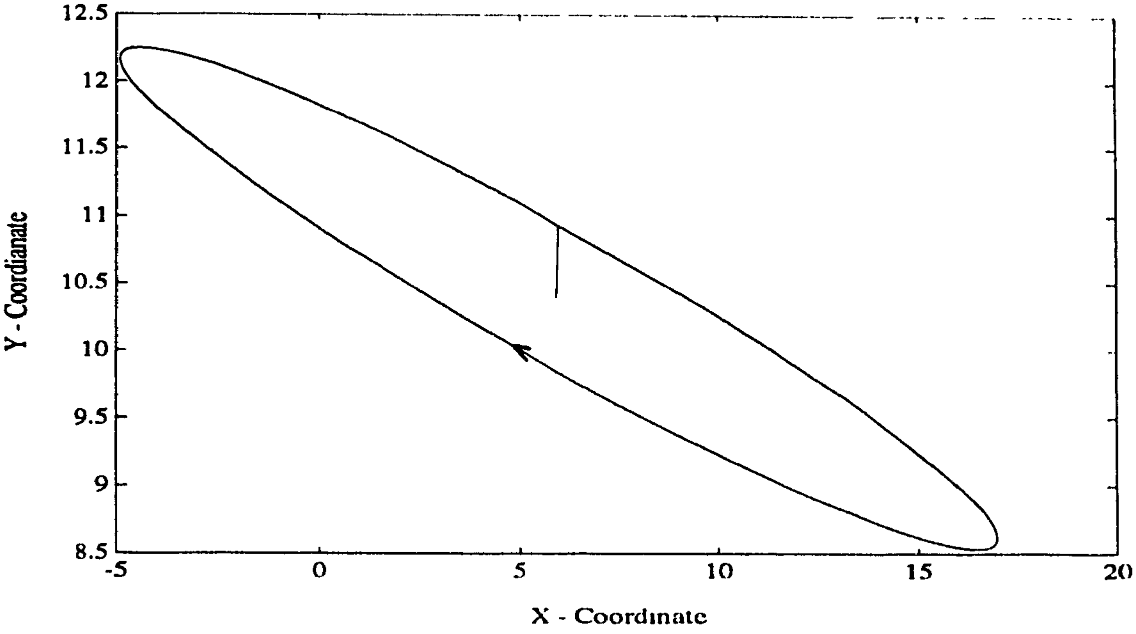

Figure 4.29: Non-Dimensional Unbalance Orbit of the Rotor, $S_{00} = 3.0$, $\mu_s = 2.0$, z/l = 0.3

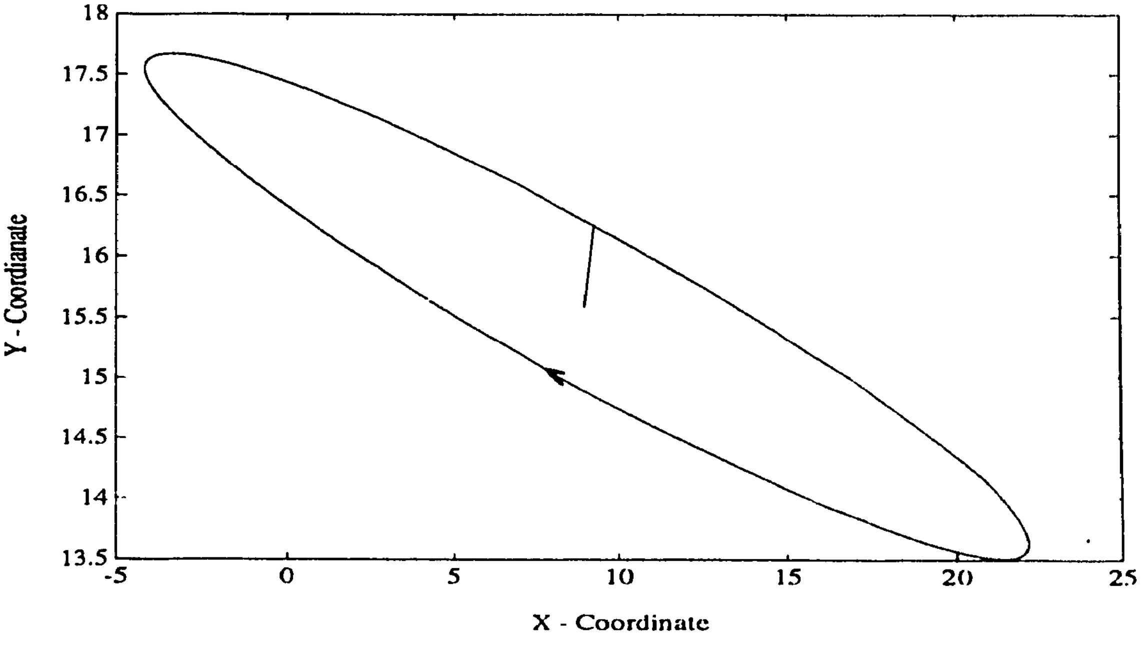

Figure 4.30: Non-Dimensional Unbalance Orbit of the Rotor, $S_{00} = 3.0$, $\mu_s = 2.0$, z/l = 0.5

Chapter 5

Experimental Investigation of Simultaneous Forward and Backward Whirling Motion of Laboratory Model of Rotor Supported on Identical Journal Bearings

5.1 Introduction

The existence of backward and forward whirling motion of the rotor supported on identical and dissimilar bearings is theoretically investigated in Chapters 3 and 4. However, very few experimental studies have been reported to support this theoretical analysis. Subbiah, Bhat, Sankar and Rao [42] verified the existence of the backward whirling motion experimentally for a laboratory model of the rotor supported on identical bearings. Non-contact type proximity pickups are used to measure the unbalance response. A FFT analyzer was used to obtain the orbital diagram with a x-y plotter. From the direction of plotter pen motion while plotting the orbital diagrams they could verify the existence of backward whirling for a small range in between two critical speeds. In the present investigation, a differentiator-multiplier circuit is employed to determine the direction of the whirl orbit.

Fig. (5.1) represents the elliptical orbit of whirling motion of the rotor. The area of this orbit is given by,

$$A = \int x\dot{y}dt \tag{5.1}$$

The displacement components x, y are represented by

$$\begin{aligned} x &= a_x \cos\omega t + b_x \sin\omega t \\ y &= a_y \cos\omega t + b_y \sin\omega t \end{aligned} \tag{5.2}$$

The integrand of Eqn. 5.1 simplifies to

$$x\dot{y} = \omega\left[\frac{1}{2}(a_x b_y - b_x a_y) + \frac{1}{2}(a_x b_y + b_x a_y)\cos 2\omega t + \frac{1}{2}(-a_x a_y + b_x b_y)\sin 2\omega t\right] \tag{5.3}$$

Fig. (5.2) represents the schematic representation of the differentiator multiplier circuit. The response amplitude y is differentiated first in a differentiator and then multiplied with the amplitude signal x in the multiplier. From Eqn. (5.3), the resulting signal has two components; an average or *DC* component $\frac{1}{2}(a_x b_y - b_x a_y)$ and a *AC* component $\frac{1}{2}\left((a_x b_y + b_x a_y)\cos 2\omega t + (-a_x a_y + b_x b_y)\sin 2\omega t\right)$. By filtering out the *AC* component from the resultant signal, the *DC* component can be separated. The sense of whirling motion can be determined from the sign of the *DC* component. The sign of the *DC* component is positive for forward whirling motion and negative for backward whirling motion.

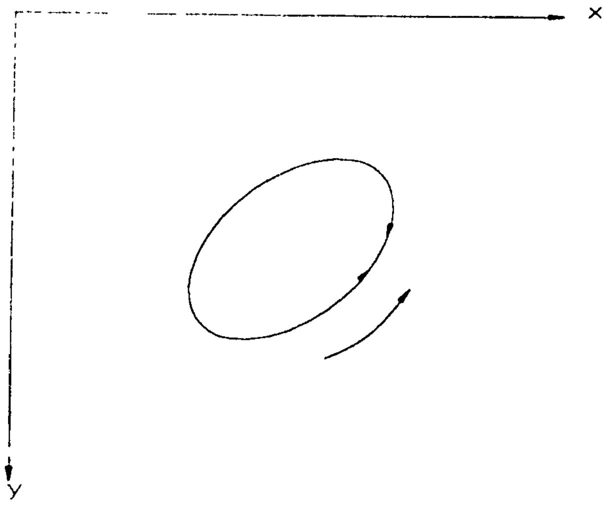

Figure 5.1: Typical Whirl Orbit

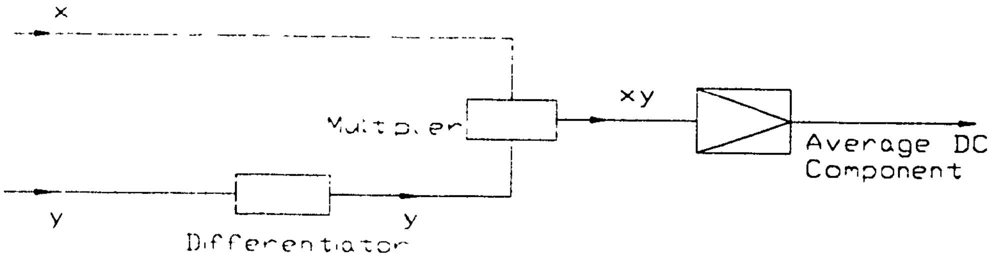

Figure 5.2: Schematic Representation of Differentiator-Multiplier Circuit

5.2 General Description of the Experimental Setup

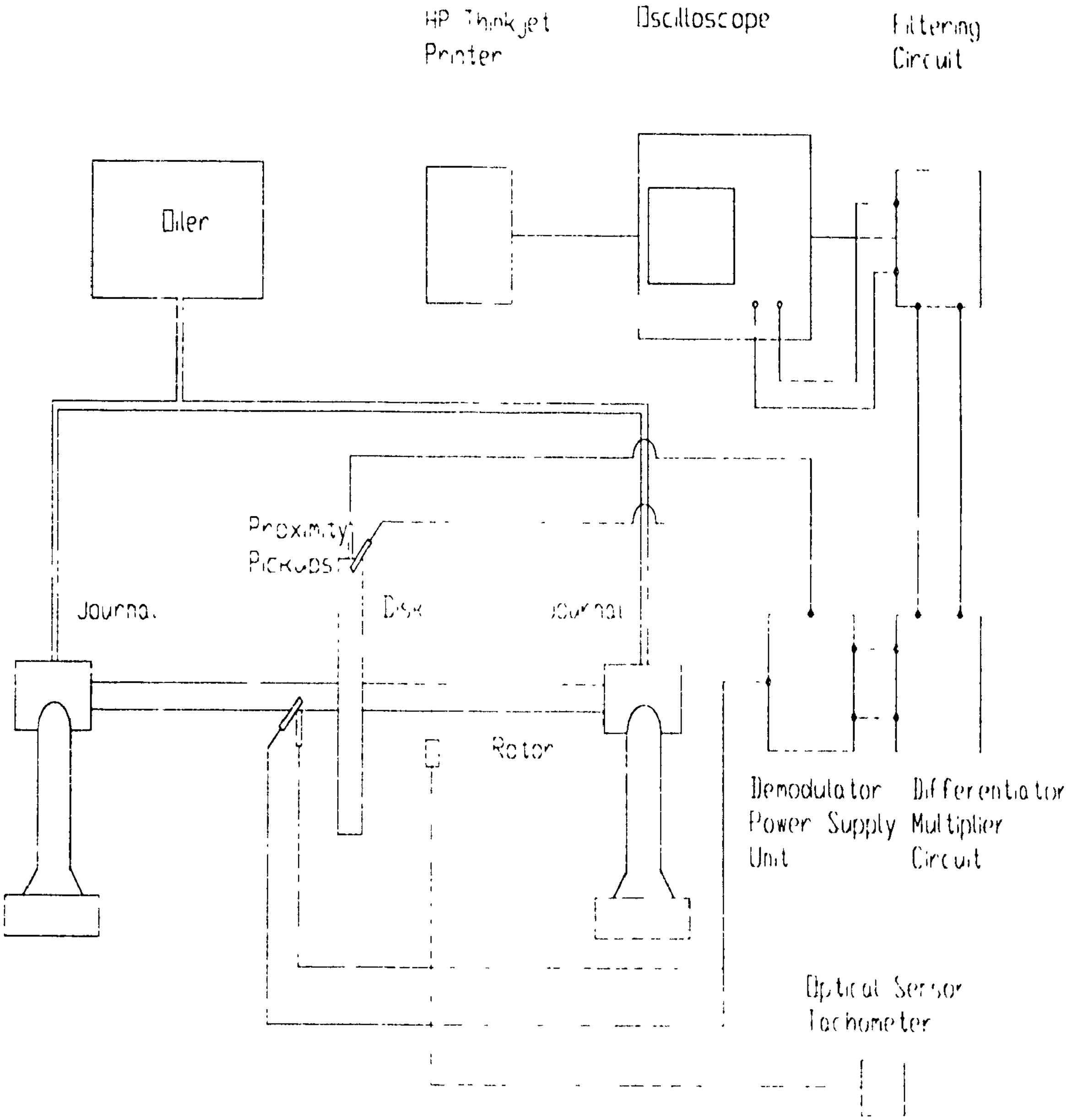

Figure 5.3: Schematic Representation of Experimental Setup

In order to verify the theoretical analysis for the existence of forward and backward whirl motions, an experimental facility was established. Fig. (5.3) shows the schematic representation of the experimental setup. It consists of a flexible shaft of circular cross-section, a central disk, supported at its ends on two identical cylindrical journal bearings and the are lubricated through gravity feed. The rotor-bearing system is supported on cast-iron pedestals at the two ends. and the entire system is mounted on a heavy steel frame which in turn is fastened to the floor on rubber padding for damping vibration.

The rotor is driven by a variable speed motor through a timer belt. The rotor speed is measured using a panel-mounted optical tachometer. Two non-contacting type displacement transducers which operate on the eddy current principle are used to measure whirl amplitude signals. Orbit of the whirling motion is detected using a differentiator-multiplier and filtering circuit which operates in conjunction with the setup. A Digital oscilloscope is used to process the results.

5.3 Design Features

5.3.1 Rotor Shaft

The details of the steel rotor shown in Fig. (5.3) are:

Shaft length	0.51 m
Shaft diameter	0.022 m
Disk diameter	0.20 m
Disk width	.04 m
Disk mass	11 kg

5.3.2 Bearings

The rotor is supported on two identical journal bearings having the following details.

Type of bearing	Plain cylindrical
Bearing-bush width	0.025 m
Bearing-bush outer diameter	0.04 m
Oil hole diameter	8 mm

Case A

Shaft diameter at left bearing	0.022167 m
Left bearing-bush diameter	0.022214 m
Shaft diameter at right bearing	0.022171 m
Right bearing-bush diameter	0.022223 m

Case B

Shaft diameter at left bearing	0.022167 m
Left bearing-bush diameter	0.022185 m
Shaft diameter at right bearing	0.022171 m
Right bearing-bush diameter	0.022180 m

The material of the bearing is phosphor-bronze. The inner surface of the bushes are jig-bored and the dimensions of the inner diameter were measured using the digital vernier calipers to an accuracy of ± $0.5\mu m$. The right hand side bearing is covered with an teflon bearing cover.

5.3.3 Drive

The drive unit consists of a variable speed DC motor, driven by a speed controller and a timer belt drive for power transmission.

The details of the motor are below:

Motor manufacturer	Boston Gear
Type of Motor	DC
Rated power	1/3 Hp
Rated voltage	110 V at 50 Hz
Rated current	5-14 A
Speed range	0-1750 rpm

Speed control unit specifications are:

Speed control unit	Ratiotrol DC motor
Line input	120 V AC at 6 A / 60 CPS
DC output	Field 100 V, Armature 90 V
Rated current	Field 1 A, Armature 3.6 A
Speed range	0-1750 rpm

The motor is mounted on a base plate which is hinged at one end and supported on two jack-bolts on the other, for drive belt tensioning. The power transmission from the motor to the rotor is accomplished through a timer belt with a speed transmission ratio of 2:1.

5.3.4 Lubricant Circulation

The lube Devices Inc. multiple feed full flow dispenser is designed to serve as a central reservoir for lubricating the bearings. The reservoir is mounted on the central mounting shank. The reservoir provides a full flow of oil to two valves which can be manually shut off by flipping the toggle at the top of the reservoir to a horizontal position. Feed rate of drip is individually set at each valve. The reservoir is of transparent lucite which provides a 360° viewing and has a capacity of 3.25 litres. The reservoir is mounted at a height of one metre to supply lubricant under gravity. The oil is fed to the bearings from the reservoir through polythene tubes. The oil flow rate is maintained continuous so that the bearing does not run dry. The lubricant specification is SAE 30 whose viscosity is 96.7 centi-stoke at $40°C$.

5.3.5 Instrumentation

Displacement Transducers

Non-contacting displacement transducers (also known as proximity probes) are used to measure the relative shaft displacement non-intensively. As the shaft moves relative to the sensor, the eddy current energy changes, modulating the oscillator voltage. This signal is demodulated, providing an output signal proportional to the displacement. Transducers convert the measured quantity into a voltage, which can be displayed on an oscilloscope, recorded, plotted, or analyzed by a computer. The voltage output of most transducers is an "analog signal" i.e., it is a time-varying continuous voltage analogous to the quantity being measured. Only a scale factor (calibration constant) is required to determine the magnitude of the measured quantity at any time.

A Kaman Instrumentation Displacement Measuring System Model KD-2310 was used to make the precision non-contact displacement measurements in the present experiment. The system includes a sensor, a 10 ft (3.1 m) coaxial cable and a signal conditioning electronics package. Zero, gain and linearity adjustments are provided on the electronics package. The system uses the principle of impedance variation caused by eddy currents induced in a conductive metal target. The coupling between a coil in a sensor and a target is dependent upon their displacement (gap). The output voltage of the system is proportional to the distance between the face of the sensor and any metallic (conductive) target. The electronics consists of an oscillator, linearization network, amplifiers and a demodulator which provides an analog voltage directly proportional to displacement. It uses modern electronics (Eddy current operating principle) to replace LVDTs, air gauges, capacitance systems, dial indicators and micrometers.

KD-2310 systems are most stable when the target is near the face of the sensor. Sensitivity to the cable movement, dielectric constant, magnetic fields, etc., are greatest when the target is at full scale displacement. Parallelism between the target and sensor is not critical as long as the angle between the sensor face and the target is within approximately 15 degrees. Each sensor type has been designed to provide an offset between the face of the sensor and the start of the measuring range (zero point) to provide clearance for a moving target and to avoid contact pressure errors. For highly curved targets, improved linearity and stability over the full range may be obtained by reducing the offset. The sensor model which is being used in the present experimental setup is the 2S type with a measurement range of 0 - 80 mils, a recommended offset of 15 mils, and a voltage output of 0 - 0.800 V and a sensitivity of 10 mV/mil.

Optical Tachometer

Panel-mount optical tachometer made by Cole-Parmer make is used for rotor speed measurements. The tachometer unit is equipped with an integral light source, photodetector, and signal conditioning circuitry to provide a 5 V compatible pulse upon receipt of an image from a reflective marker. Power requirement is +5 VDC at 75 mA. The remote optical sensor, can detect a reflected pulse from a target consisting of reflective tape at a distance up to 3 feet from the rotor shaft. Output from the sensor is displayed on the panel, which has also an option to feed directly to a computer for plotting rotor response.

Specification of the tachometer:

Model type	L-08212-20
Measuring range	50 to 20,000 rpm
Input	Single pulse/rev
Resolution	1 rpm
Accuracy	±1 rpm
Display	5 digit LED, 1/2″

Multiplier-Differentiator Circuitry

A schematic diagram of the Multiplier-Differentiator circuit is represented in Fig. (5.4). The circuitry consists of chip AD 533JH, which is an analog integrated circuit multiplier. The multiplier operation is accomplished by closing the loop around the internal *op amp* with the Z input connected to the output. The X_o null potentiometer balances the X input channel to minimize Y feed-through and similarly the Y_o potentiometer minimizes the X feed-through. The Z_o potentiometer nulls the output op amp offset voltage and the gain pot sets the full scale output level.

Trim Procedures:

1. With X = Y = 0 volts, adjust Z_o for 0 VDC output.
2. With Y = 20 volts p-p (at f = 50Hz) and X = 0 V, adjust X_o for minimum AC output.
3. With X = 20 Volts p-p (at f = 50Hz) and Y = 0 V, adjust Y_o for minimum AC output.
4. Readjust Z_o for 0 VDC output.
5. With X = +10 VDC and Y = 20 volts p-p (at f = 50Hz), adjust gain for output = Y_{in}

The multiplier circuit was calibrated alone with the steps given in the trim procedures. With X = 10 VDC and Y = 20 VAC at 50 Hz, the multiplier output was found to be equal to *XY/10 = 20 VAC*. Similarly the circuit was checked for different values of *X and Y* inputs, it was found to be functional.

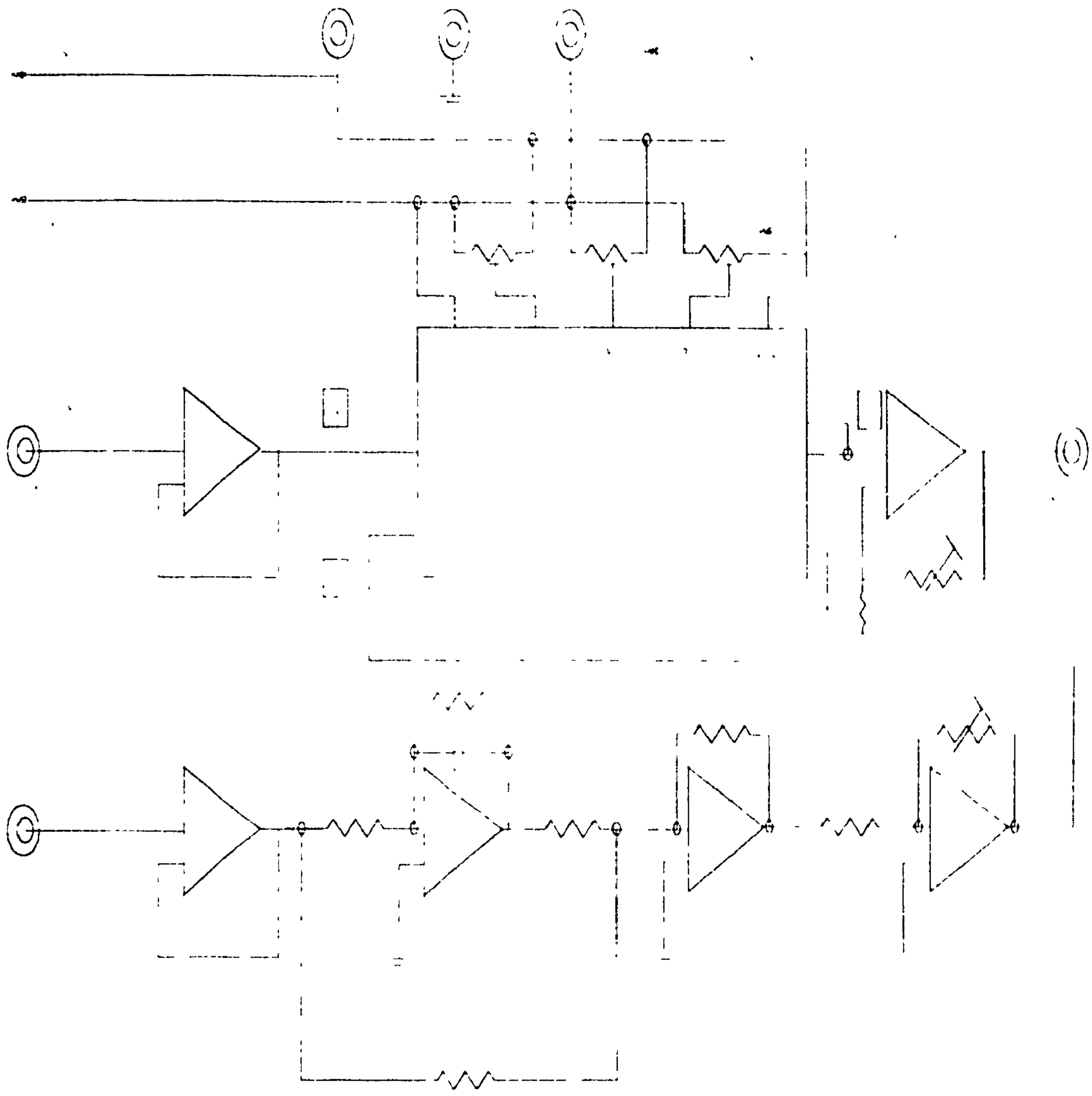

Figure 5.4: Schematic Multiplier-Differentiator circuit

The *op-amp B/2* combination with a capacitance and resistors shown in the Fig. (5.4), operates as the differentiator in the circuit. The differential differentiator is formed by adding to the noninverting input a network which is identical to the feedback network. In each network a gain-limiting resistor R_1 is added to the basic elements in order to ensure frequency stability. As expressed, the differential differentiator takes the difference between two signals and differentiates the result. In this way the output of a floating source can be differentiated with out its common-mode signal.

A major problem encountered with differentiator circuits is high noise. This results from the increasing gain of the differentiator frequency response and the resulting high-gain of the amplification of the amplifier noise. To reduce this noise an indirect method of computing the derivative of a signal can be used, as in Fig. (5.4). In this case, the derivative of the signal is derived from the signal and its integral. The differentiator response approximation ends at frequency $f = 1/2\pi R_1 C$ [49]. The op-amp C/2 with the trim potentiometer of 100 K is used to give the necessary gain to the differentiated signal so that it can be compatible with the multiplier.

The capacitance and resistor across the *op-amp B/2* is varied to achieve the necessary differentiation effect and the circuit was found to work as a differentiator with a capacitance value of *4.7 nf* and resistance of *13 K*. The circuit was checked by giving a square pulse as input resulting in the output of a triangular pulse, since differentiation results in rate of change with respect to time of the input signal. Similarly, a sine pulse resulted in an output having a spike waveform. This circuit is used to identify the direction of the whirling motion of the rotor. Two separate differentiator-multiplier circuits were designed and utilized to find the sense of whirl orbit.

Filtering Circuit

One of the major problems encountered while analyzing the output from the differentiator multiplier circuit was noise. In order to avoid this, a filtering circuit was designed whose schematic representation is given in Fig. (5.5).

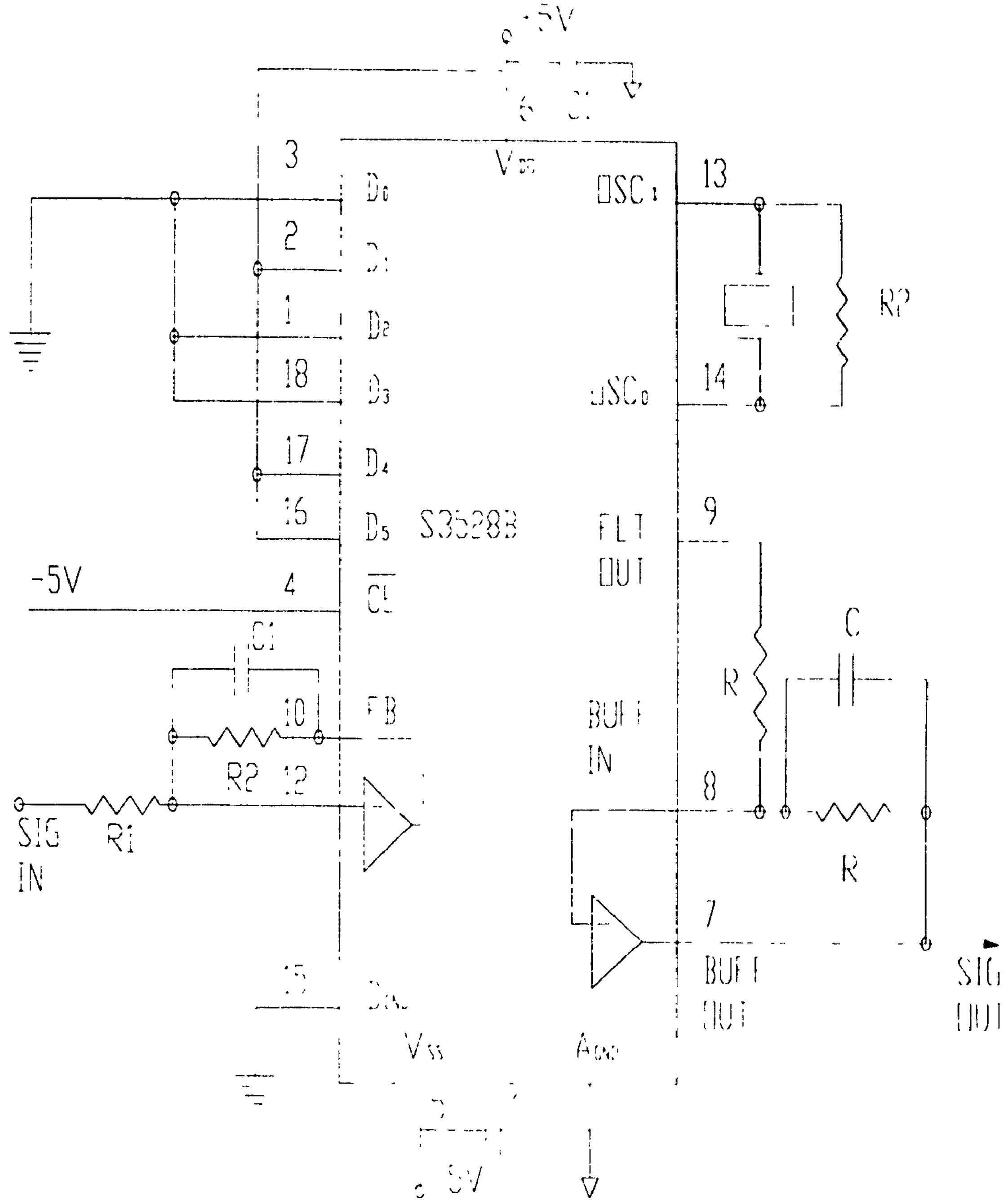

Figure 5.5: Filtering circuit

S3528B Filter is a CMOS Switched Capacitor Filter device designed to provide a very accurate, very flat programmable filter that can be used in fixed applications where only one cutoff frequency is required, or in dynamic applications where logic or

Pin Name	Number	Function
V_{DD}	6	Positive supply voltage pin, +5 V ± 10%
V_{SS}	5	Negative supply voltage pin, -5 V ± 10%
A_{GND}	11	Analog ground reference point for analog input and output signals, connected to ground
D_{GND}	15	Digital ground reference point for digital input and output signals, connected to ground
D_0 D_1 D_2 D_3 D_4 D_5	3 2 1 18 17 16	Control word inputs: The set of six bits allows selection of one of sixty four cutoff frequencies
$\overline{CE}$	4	Tied to V_{ss}, -5 V
OSC_1 OSC_0	13 14	Oscillator in Oscillator Out: Placing a crystal and a 10M resistor across these pins create the time base oscillator 3.58MHz TV outburst crystal is used
SIG IN	12	Signal Input
FB	10	Feedback point for the input op amp. The feed back back resistor$\geq 10K$
FLT OUT	9	The high impedance output of the programmable low pass filter
BUFF IN	8	The inverting input of the buffer amplifier
BUFF OUT	7	The buffer amplifier output

Table 5.1: Pin Function Description

a microprocessor can select any one of 64 different cutoff frequencies. It is clocked by an inexpensive TV color burst crystal and provides the required cut off frequencies. The accessories involved in the design of this circuit is a 10 M resistor, the 3.58 MHz TV crystal, and some resistors and capacitors around the input and output amplifiers to set the gain, anti-aliasing, and smoothing. The Data Bus pins are programmed with either a "1" (+5 V) or "0" (ground or -5 V) for the desired cutoff frequency. The $\overline{CE}$ pin is tied low, to V_{ss} [Fig. 5.5].

By connecting the pins D_0 *to* D_5 to either ground or to +5 *V*, different combination of cutoff frequencies can be selected, which is set at 250 Hz for the present experiment.

Four filtering circuits are designed to filter out the signals *X*, *Y* from four proximity pick-ups at the rotor shaft and the disk locations.

Digital Oscilloscope

The Hewlett Packard type 54503A Digital Oscilloscope is a high frequency high sensitivity laboratory instrument providing accurate measurements in the range from DC to 500 MHz.

The HP 54503A specifications:

Repetitive Bandwidth	500 MHz
Single Shot Bandwidth	dc to 2 MHz
Maximum Vertical Sensitivity	1 mV/div
Maximum Sample Rate	20 MSa/s
Number of Channels	4
Memory Depth	1 K/channel

The features of viewing the signal events prior to trigger, auto-scale for automatic setup, four nonvolatile setup and waveform memories make this instrument ideal for the present experimentation. The feature of waveform math (+, -, *, vs, invert, only) makes it possible to perform the mathematical operation on the signal from the multiplier-differentiator circuit. The feature of instant hardcopy output enables the output of the oscilloscope display, whirl orbit and mode of whirling to print on the compatible printer. With the feature of quad screen display capability the four signal output from the four proximity pick-ups can be simultaneously viewed on the screen and the required mathematical operation can be performed on them individually.

Printer

The output from the oscilloscope display is printed on the Hewlett-Packard Thinkjet printer. The oscilloscope is connected to the printer with a standard cable. The printer is calibrated to the oscilloscope compatibility. The printer receives a copy of the oscilloscope display, including the measurements and setup information.

5.4 Experimental Investigation

5.4.1 Rotor Alignment on the Bearing

Journal bushes are mounted on the pedestal and are aligned with respect to the steel frame, with the help of height and dial gages so that the journal centers are in the same line. The rotor shaft is then mounted on the journal and care is taken so that the shaft center is aligned with the journal centers. The inner surface of the bushes are jig-bored in order to get the necessary clearance between bush and the rotor shaft. The steel frame supporting the rotor is levelled with the help of mercury level gage. Rotor is coupled to the motor with the help of timer belt and care is taken to align the rotor shaft pulley with respect to the motor pulley. Lubrication lines are connected to the bearing inlet and care is taken to keep the bearings properly lubricated.

5.4.2 Proximity Pickup Installation and Calibration

Two proximity pickup sensors are mounted to measure the unbalance response displacement amplitude in both *X and Y* directions at a point along the rotor shaft closer to the disk. These pickups can be moved along the length of the shaft on the guideway provided. Two more pickups are mounted on the fixture provided, on the disk location in *X and Y* direction to measure the amplitude of the whirl orbit at the disk. Once the proximity pickups are installed they are calibrated for proper operation. The calibration procedure is given below.

1. Set the FINE LINEARITY control to mid range. With the target at full scale displacement (plus offset), adjust COARSE LINEARITY CONTROL control to the desired full scale output voltage.
2. With the target at "Zero" displacement (at the recommended offset from the face of the sensor), adjust the ZERO control until the output is zero volts.
3. Move the target away from the sensor to the displacement equal to one-half of the chosen full range (plus offset). Adjust the GAIN control to obtain half scale output voltage.
4. Move the target to the chosen full scale displacement point (plus offset), read the output and note the difference between the actual reading and the desired reading. Using the COARSE LINEARITY control, adjust the output to the desired setting and then continue past the desired setting by an amount equal to the noted difference.
5. Repeat steps 2 through 4 as many times as necessary until calibration is attained. When finer setting of linearity is required, the FINE LINEARITY control may be used.

5.4.3 Experimentation

Whirl Orbit

Signal from the sensors are routed into the electronics package which consists of an oscillator, linearization network, amplifiers and a demodulator. The output from the demodulators are displayed on the oscilloscope. By using waveform math-mode function *'versus'* which draws a volts versus volts display of the two selected operands, input signal from two sensors on the shaft location are plotted resulting in the whirl orbit at the rotor shaft. Similarly the whirl orbit is plotted for the disk, from the signal inputs from the sensors located at the disk location. Whirl orbits for the shaft and disk are displayed on oscilloscope for different operating speeds and is printed on HP Thinkjet printer.

Direction of the Whirl Orbit

Displacement signals from the sensors are modulated in the oscillator-demodulator unit. The output from the demodulator which is an analog voltage is directly proportional to displacement. Modulated signal from demodulator corresponding to X signal from the sensor on the shaft location is input x into the differentiator circuit (Fig. 5.4). The differentiated signal *x out* becomes the *SIG IN* input of the filter circuit (Fig. 5.5). The filtering circuit is incorporated to filter out the noise component of the output from the differentiator. The output from the filter circuit, *SIG OUT* which is in the range of 0 to 200 Hz is the *Channel 1* input into the oscilloscope. The Demodulator output corresponding to signal y from the sensor on the shaft location becomes the input *SIG IN* to the second filtering circuit. The output *SIG.OUT* from the filtering circuit becomes input to Channel 3 of the oscilloscope.

The oscilloscope wave-form math menu defines two functions. Channel 1 and 3 waveforms correspond to sensors at the shaft location are multiplied in waveform math-mode which represent the function *f1* and is displayed on function 1 viewing area on the oscilloscope. Mathematical results of the average value of the DC component of the function is displayed on the bottom half of the oscilloscope screen. For the forward whirling motion, the value of DC component of the function *f1* corresponding to the shaft location is positive if the whirling motion is forward and in the case of backward whirling motion, this value is observed to be negative.

Similarly signals *x and y* from sensors located at the disk locations after passing through differentiator and filtering circuit becomes input signals to Channel 2 and 4 respectively of the oscilloscope. Channel 2 and 4 waveform are multiplied and the resulting function *f2* is viewed on the oscilloscope. The sign of the average value of DC component determines the sense of the whirling motion.

As a check to the operation of the differentiator-multiplier circuit rotor was run in clockwise direction which is considered in the experiment as positive direction of the whirling motion. Resulting functions *f1 and f2* were both on the positive side and average DC components of the functions were observed to be positive. With the reversal in the direction of the rotor motion, for backward whirling motion, the functions *f1 and f2* were both on the negative side and the average DC component is observed to be negative.

5.5 Experimental Results and Discussion

Occurrence of the backward whirling motion which is due to the anisotropic nature of the fluid film stiffness and damping properties in rotors supported on fluid film bearings. In order for the rotor to exhibit backward whirl, the rotor has to be designed to have split critical speeds. The flexibility and the load parameters are the two important factors in deciding whether the occurrence of backward whirl is possible for the particular configuration of the rotor. Variation of the bearing clearance does have a direct effect on the flexibility parameter, which can be increased by decreasing the clearance. The backward whirling motion of the rotor is possible by the variation of viscosity of the lubricant. By lowering the viscosity of the lubricant, the corresponding load parameter increases to simulate the rotor into the region of backward whirling.

The effect of variation of the clearance of the supportive bearings on the simultaneous forward and backward whirling motion of the rotor supported on identical bearings is studied experimentally. For the first set of bearings, the bearing clearance value at the left and right bearing is calculated as 0.0047 and 0.0052 cm. Using the average value of radial clearance, 0.005 cm at the supportive bearings, the flexibility parameter μ_s and load parameter So_o are calculated as 1.43 and 1.06 respectively. For a rotor supported on identical bearings with the mean clearance of 0.005 cm, Fig. (3.6) shows that the sense of whirl of the rotor with the above combination of flexibility parameter and Sommerfeld number is always forward. Fig. (5.6) shows this rotor has only one critical speed at 2100 rpm.

To investigate the orbital whirling motion, experiment is carried out on the laboratory model and the rotor speed was varied from 0 to 4200 rpm and the displacement components at shaft and disk locations are measured by the sensors. The combination of oscillator, demodulator and amplifier converts the displacement into voltage signal which is used to generate the whirl orbit on the oscilloscope. Figs. (5.7 - 5.9) shows the rotor and disk orbits at 1500, 2150 and 4000 rpm respectively. Orbits of whirling motion at a operating speed of 2150 rpm in the proximity of critical speed is shown in Fig. (5.8). It can be seen that the magnitude of the whirl orbit at the shaft and disk locations are much larger than that corresponding to the speed of 1500 rpm.

To analyze sense of the whirling motion, x, y voltage signals corresponding to displacement signals from sensors at the rotor shaft and disk are routed through a combination of differentiator-multiplier and filtering circuit. The function *f1 and f2* from the differentiated-multiplied and the filtered signal signifying the whirl orbit direction at the rotor shaft and disk location are represented in the Figs. (5.10 - 5.12). Whirl orbit direction waveform for a rotor speed of 1500 rpm is shown in Fig. (5.10). The function *f1 and f2* are positive and the average DC component value at 38.973 mv and 16.429 mv, indicates that the whirling motion is in forward sense for the rotor shaft. With a rotor operating speed of 2150 rpm, whirl direction waveforms *f1 and f2* are positive with the average DC component value of 19.155 mv and 3.178 mv, indicates that the whirling motion continues in forward sense, Fig. (5.11). Fig. (5.12) represents the function *f1 and f2* for a rotor speed of 4000 rpm, value of DC component at 17.942 mv and 6.800 mv marks the whirling motion continues to remain in forward sense for this rotor configuration.

For another set of bearings whose clearances are 0.0018 and 0.0013 cm respectively at left and right bearing, the sense of whirling motion is studied. Using the mean radial clearance of 0.001 cm, flexibility and load parameters are calculated as 2.43 and 1.02 respectively. For these values of the system parameters, rotor supported on identical bearings with mean clearance of 0.001 cm, Fig. (3.6) shows that the rotor whirls in the backward mode for a certain range of speed, and the rotor has two critical speeds, the minor critical speed at 1900 rpm and the major critical speed at 2400 rpm as shown in Fig. (5.13).

Experimental analysis is carried out by supporting the rotor on these pair of bearings and is operated through a full range of speed from 0 to 4250 rpm. Presence of the first critical speed was not distinguishable, whereas the second critical speed is seen clearly at 2750 rpm marked by excessive vibration and resonance on the rotor. Figs. (5.14 - 5.17) shows orbital diagrams of the whirling motions at shaft and disk locations at 1500, 2750, 2950 and 4250 rpm respectively. Orbital diagrams in the vicinity of critical speed of 2750 rpm is shown in Fig. (5.15), marked by a increase in magnitude of the whirl orbit at shaft and disk locations.

The sense of the whirling motion is measured using the differentiator-multiplier - filter circuit. The waveform of the function *f1 and f2* representing the whirl orbit direction at rotor shaft and disk locations are shown in Figs. (5.18 - 5.21). For a rotor speed of 1500 rpm the whirling motion direction function *f1 and f2* both are positive with average DC component voltage value of 16.638 mv and 5.606 mv at rotor shaft and disk location respectively, indicates that the sense of the whirling motion is forward for the rotor shaft at this speed of operation, Fig. (5.18). However, in the case of disk, the waveform of the function *f2* remains positive through a large range of speed except for a short range of speed just before the second critical. Rotor speed is varied and the functions *f1 and f2* are observed for transition in to the backward whirling motion. With the rotor speed of 2700 rpm, the function *f2* was observed to take a negative value with average DC voltage component voltage at 2.235 mv and -1.020 mv at rotor shaft and disk locations respectively, marking the onset of the backward whirling motion at the disk where as the sense of whirling motion continues to be forward at the rotor shaft location as seen in Fig. (5.19). The existence of simultaneous forward and backward whirling motion continues for a range of speed from 2700 rpm to 2950 rpm. This is in accordance with the theoretical analysis of Chapter 3 for the rotor supported on identical bearings with the given system parameters, the rotor will exhibit the backward whirling motion between the split criticals. Sense of whirling motion at the rotor disk becomes forward at a rotor speed of 2950 rpm as shown in Fig. (5.20), with the DC component value of 4.605 mv and 168 mv respectively for functions *f1 and f2*. Whirling motion remains forward for the remaining speed range of rotor operation, Fig. (5.21) represents the forward sense of the whirling motion at rotor operation speed of 4250 rpm.

5.6 Summary

Simultaneous existence of forward and backward whirling motion is studied experimentally for a rotor supported on identical journal bearings. The effect of variation of bearing clearances on the onset of backward whirl is investigated by finding the sense of whirling motion using a differentiator multiplier circuit. For a rotor supported on bearings with clearances of 0.0047 and 0.0052 cm at left and right bearing, the whirling motion was observed to be in the forward direction throughout the operating speed range of the rotor. Experimentation was repeated by varying the bearing clearances to a value of 0.0018 and 0.0013 cm at left and right bearing respectively. The rotor system was observed to have split criticals, with the sense of whirl going backward at the disk location for a speed range of 250 rpm, while the direction of whirling motion elsewhere in the shaft location remains forward.

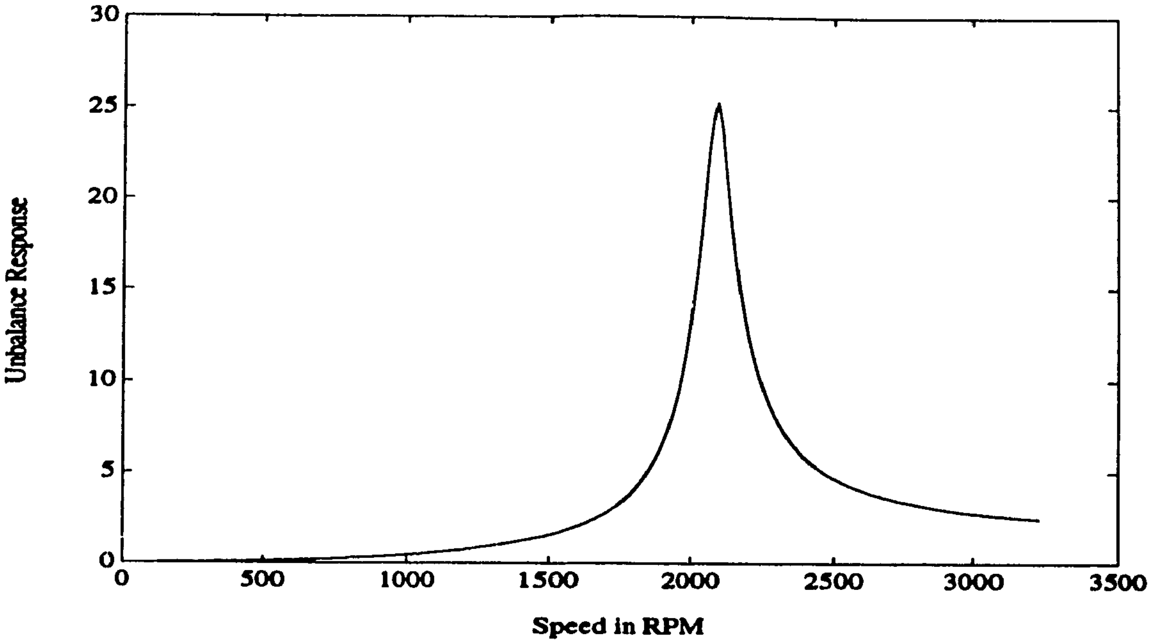

Figure 5.6: Unbalance Response of Rotor - Bearing Clearance = 0.005cm

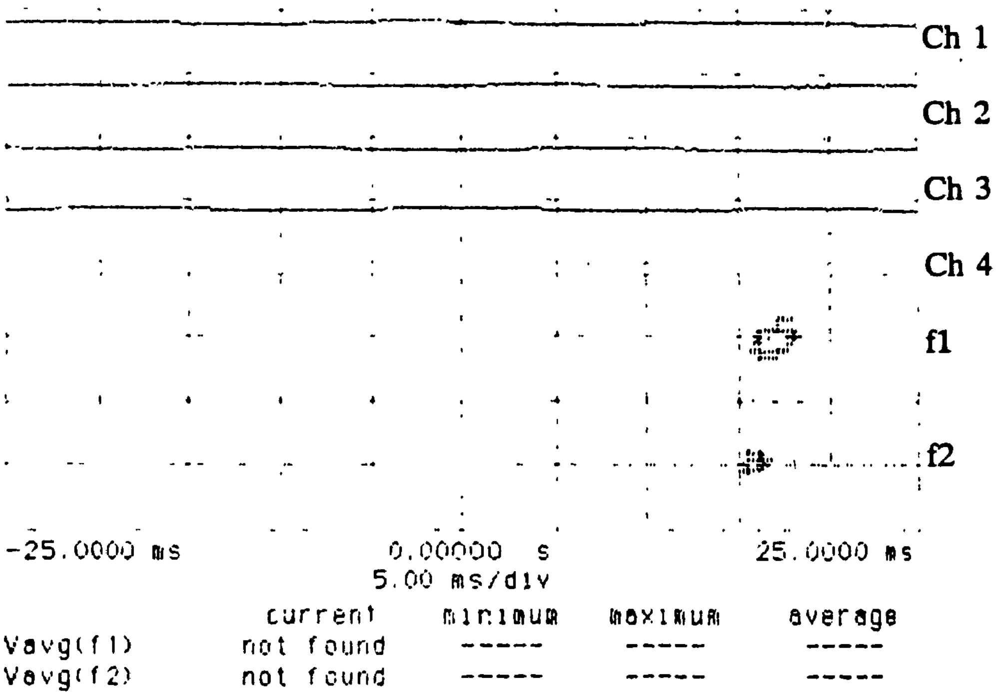

```
                   current      minimum    maximum    average
Vavg(f1)          not found      -----      -----      -----
Vavg(f2)          not found      -----      -----      -----
```

Figure 5.7: Whirl Orbit at the Rotor Shaft and Disk Locations : Bearing Clearance = 0.005cm, Rotor Speed 1500 rpm

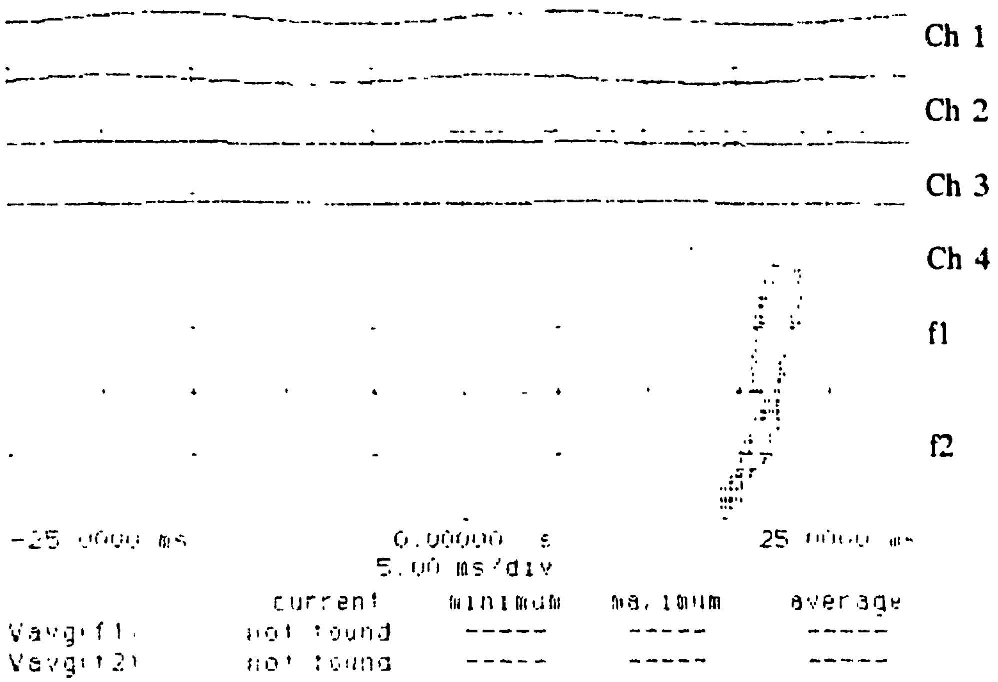

```
-25.0000 ms              0.00000  s            25.0000 ms
                         5.00 ms/div
                current      minimum     maximum     average
Vavg(f1)        not found    -----       -----       -----
Vavg(f2)        not found    -----       -----       -----
```

Figure 5.8: Whirl Orbit at the Rotor Shaft and Disk Locations : Bearing Clearance = 0.005cm, Rotor Speed 2150 rpm

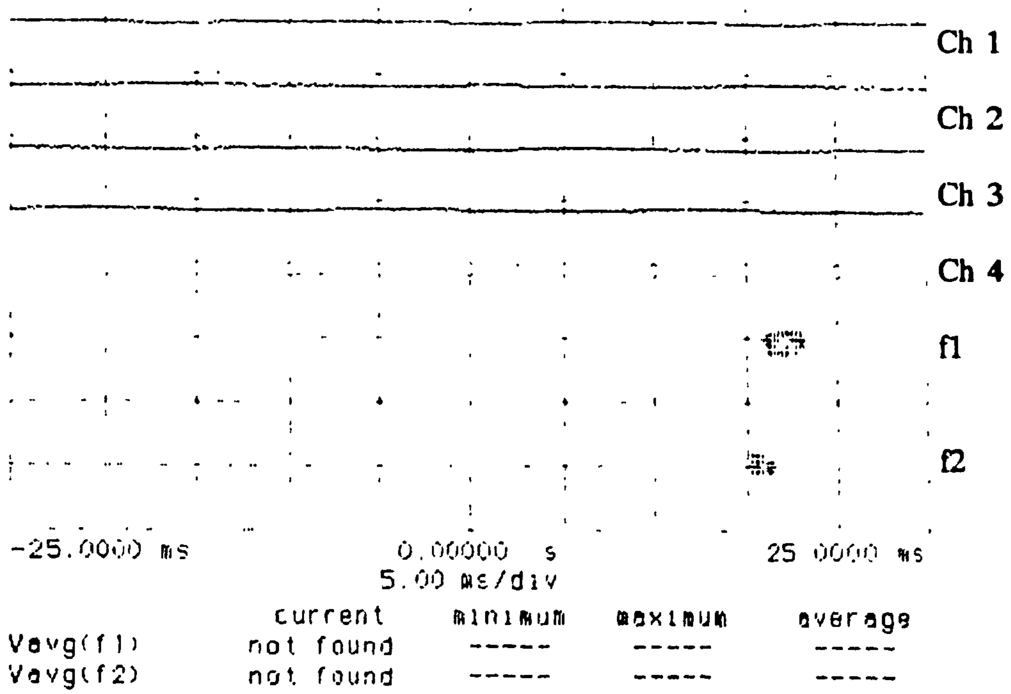

```
-25.0000 ms              0.00000  s            25.0000 ms
                         5.00 ms/div
                current      minimum     maximum     average
Vavg(f1)        not found    -----       -----       -----
Vavg(f2)        not found    -----       -----       -----
```

Figure 5.9: Whirl Orbit at the Rotor Shaft and Disk locations : Bearing Clearance = 0.005cm, Rotor Speed 4000 rpm

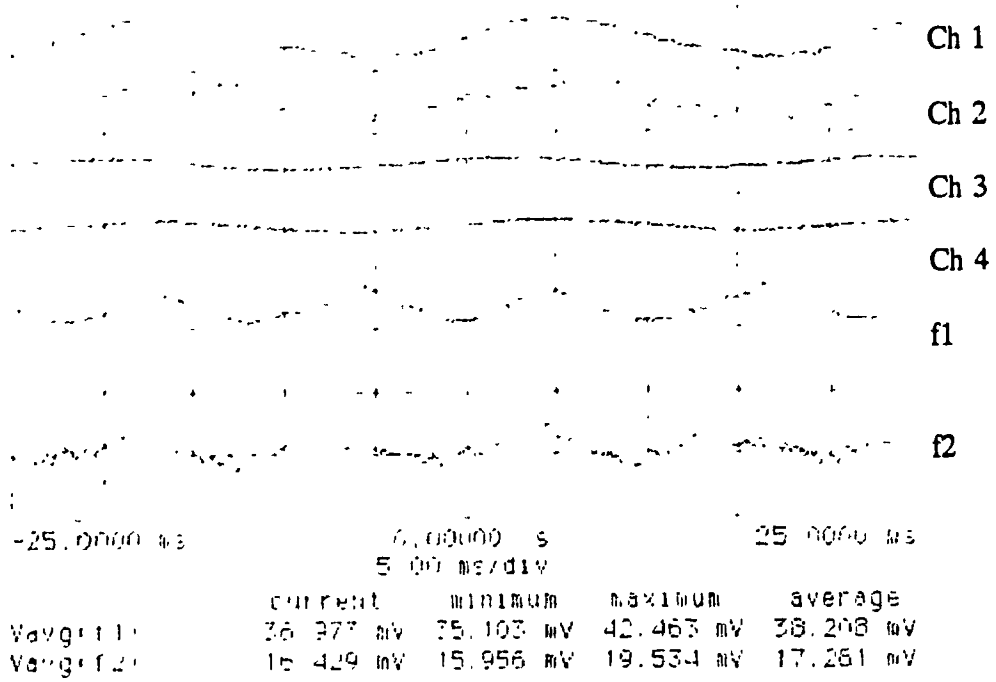

```
              current     minimum     maximum     average
Vavg(f1)    36.377 mV   35.103 mV   42.463 mV   38.208 mV
Vavg(f2)    16.429 mV   15.956 mV   19.534 mV   17.261 mV
```

Figure 5.10: Differentiator-Multiplier Signal - Whirl Orbit Direction : Bearing Clearance = 0.005cm, Rotor Speed 1500 rpm

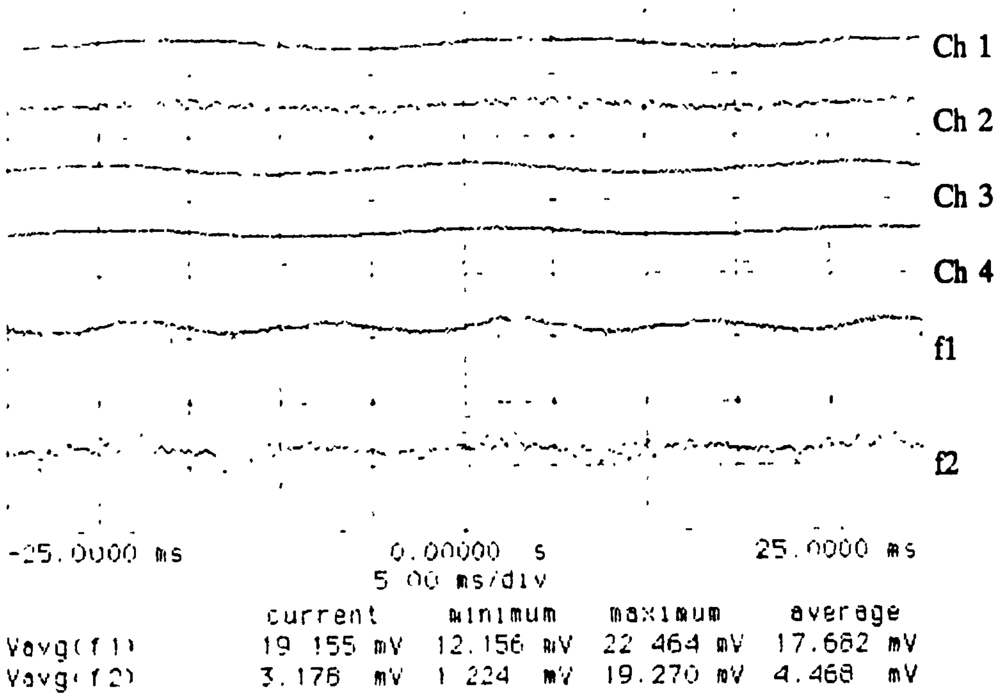

```
              current     minimum     maximum     average
Vavg(f1)    19.155 mV   12.156 mV   22.464 mV   17.682 mV
Vavg(f2)    3.176  mV   1.224  mV   19.270 mV   4.468  mV
```

Figure 5.11: Differentiator-Multiplier Signal - Whirl Orbit Direction : Bearing Clearance = 0.005cm, Rotor Speed 2150 rpm

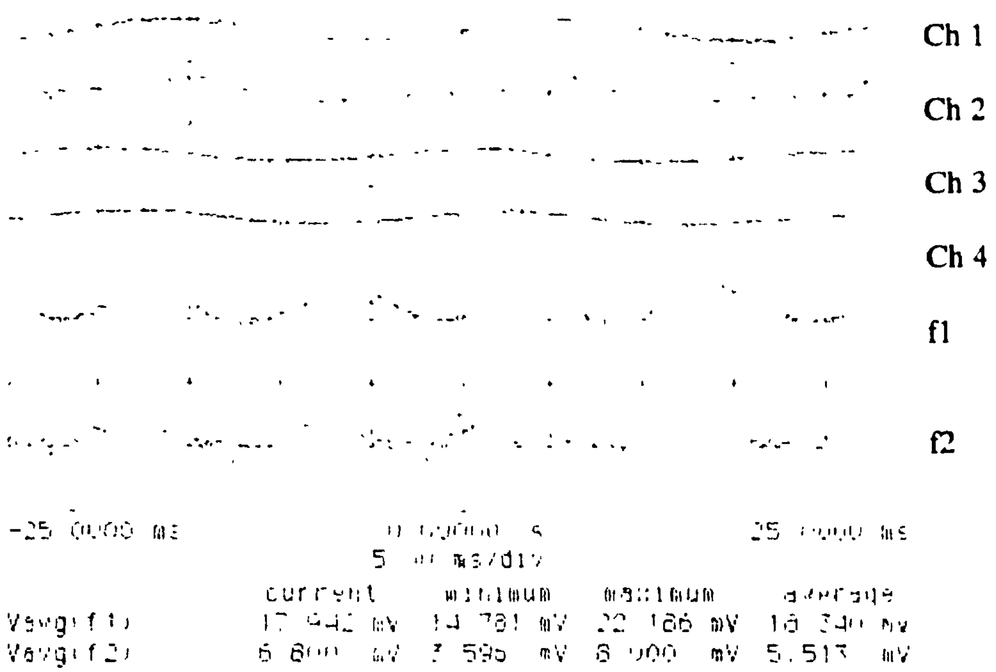

```
-25.0000 ms              0.00000 s                25.0000 ms
                         5.00 ms/div
                    current     minimum     maximum     average
Vavg(f1)            17.942 mV   14.781 mV   22.186 mV   18.340 mV
Vavg(f2)            6.800  mV   3.595  mV   8.000  mV   5.513  mV
```

Figure 5.12: Differentiator-Multiplier Signal - Whirl Orbit Direction : Bearing Clearance = 0.005cm, Rotor Speed 4000 rpm

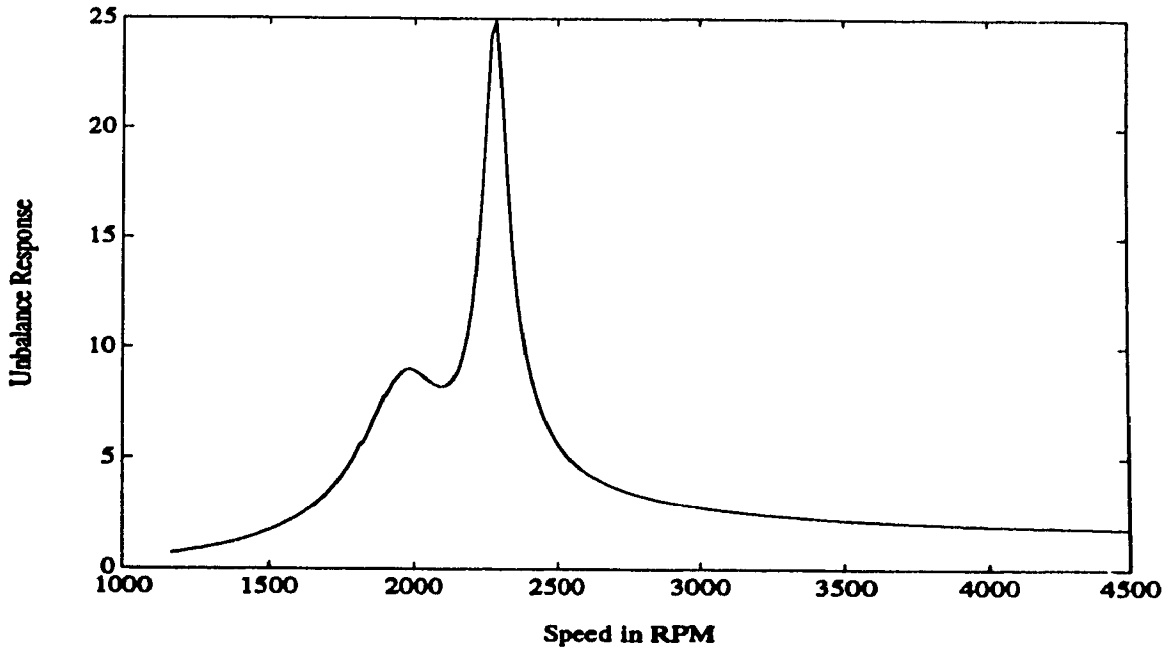

Figure 5.13: Unbalance Response of Rotor - Bearing Clearance = 0.001cm

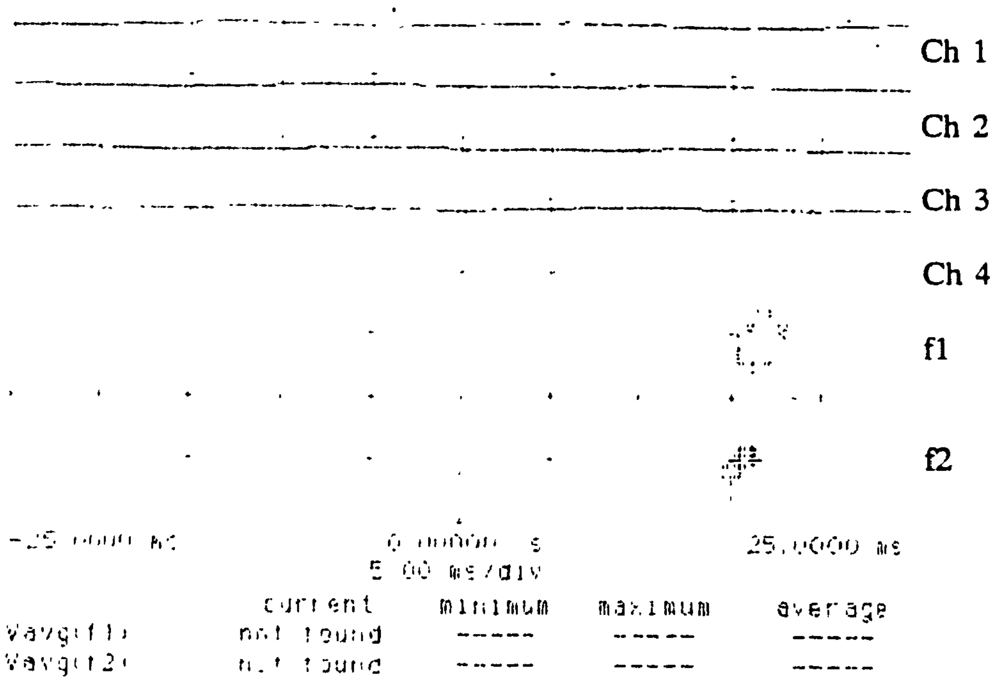

Figure 5.14: Whirl Orbit at the Rotor Shaft and Disk Locations : Bearing Clearance = 0.001cm, Rotor Speed 1500 rpm

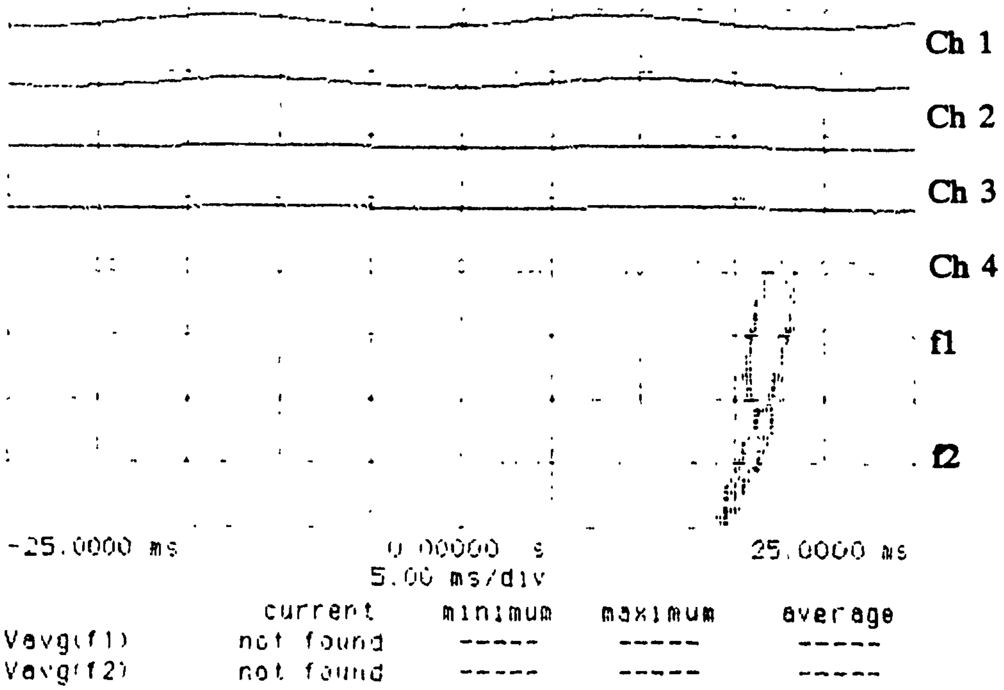

Figure 5.15: Whirl Orbit at the Rotor Shaft and Disk Locations : Bearing Clearance = 0.001cm, Rotor Speed 2750 rpm

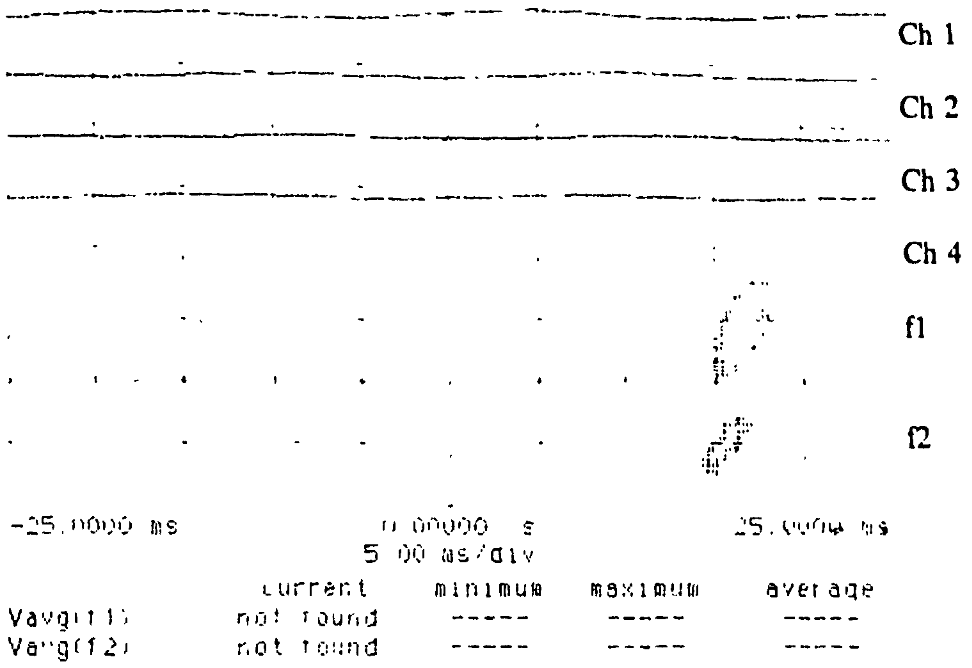

```
-25.0000 ms              0.00000  s              25.0000 ms
                         5.00 ms/div
                    current     minimum    maximum     average
Vavg(f1)           not found     -----      -----       -----
Vavg(f2)           not found     -----      -----       -----
```

Figure 5.16: Whirl Orbit at the Rotor Shaft and Disk locations : Bearing Clearance = 0.001cm, Rotor Speed 2950 rpm

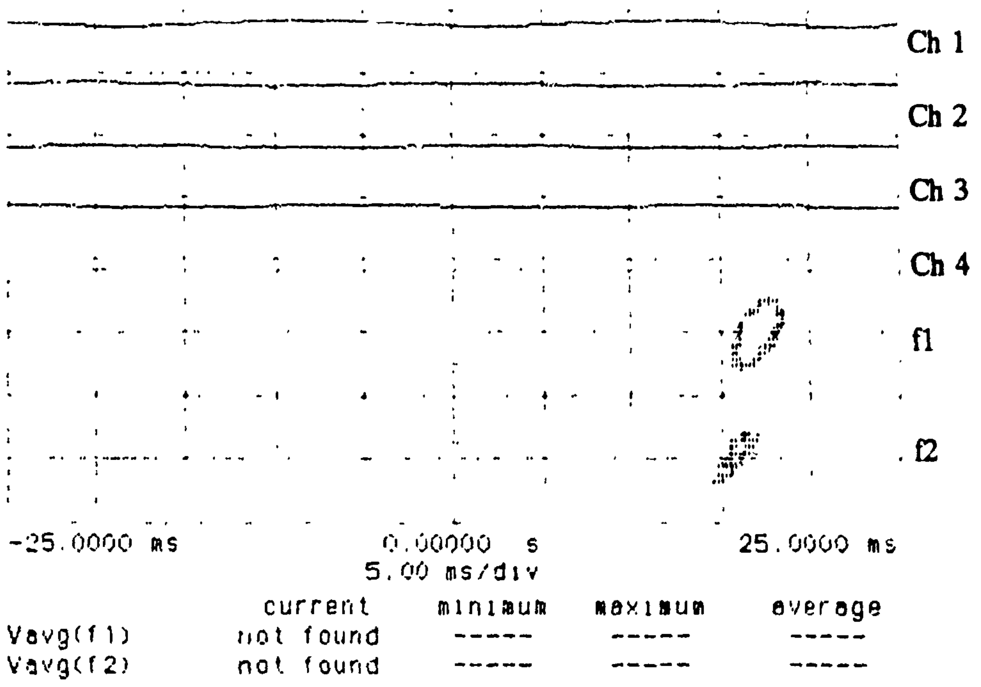

```
-25.0000 ms              0.00000  s              25.0000 ms
                         5.00 ms/div
                    current     minimum    maximum     average
Vavg(f1)           not found     -----      -----       -----
Vavg(f2)           not found     -----      -----       -----
```

Figure 5.17: Whirl Orbit at the Rotor Shaft and Disk locations : Bearing Clearance = 0.001cm, Rotor Speed 4250 rpm

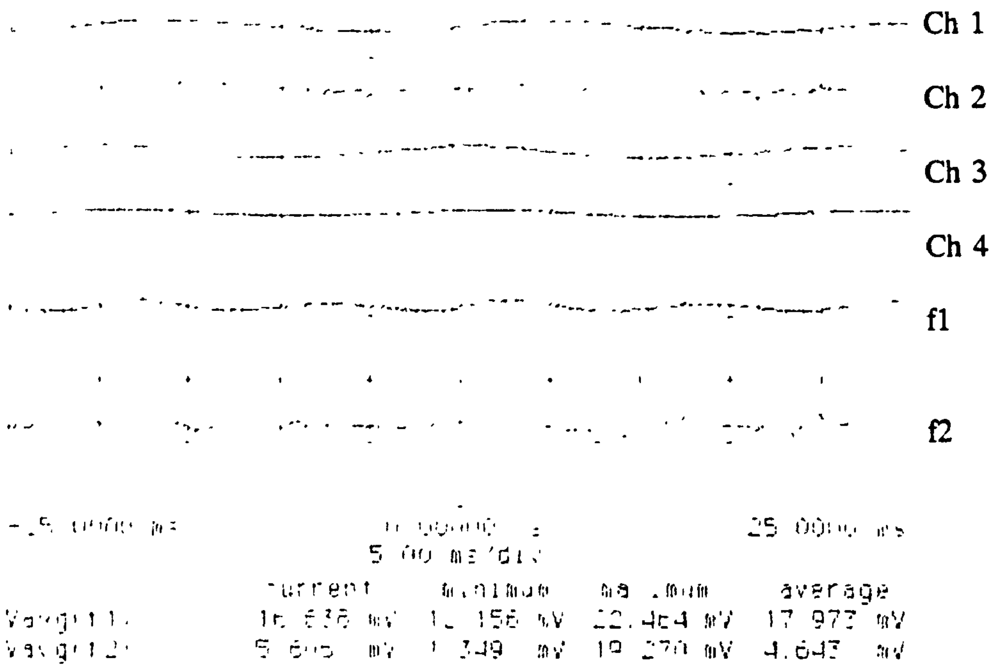

```
                 current     minimum     maximum     average
Vavg(f1)        16.538 mV   12.156 mV   22.464 mV   17.972 mV
Vavg(f2)         5.605 mV    1.349 mV   19.270 mV    4.643 mV
```

Figure 5.18: Differentiator-Multiplier Signal - Whirl Orbit Direction : Bearing Clearance = 0.001cm, Rotor Speed 1500 rpm

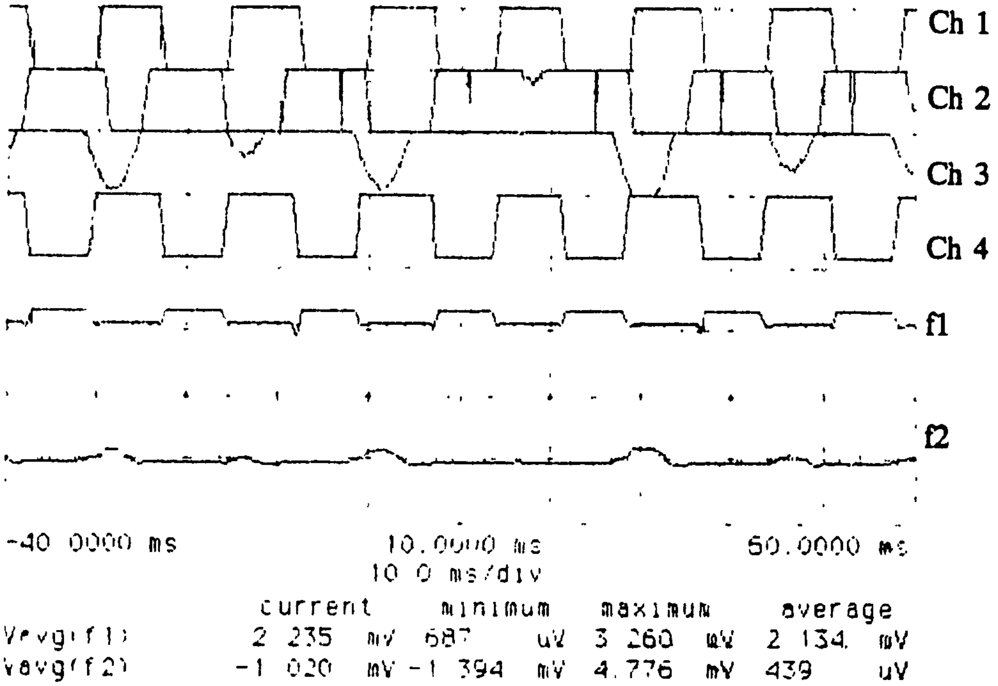

```
                 current      minimum      maximum     average
Vavg(f1)        2.235 mV     687   uV    3.260 mV    2.134 mV
Vavg(f2)       -1.020 mV   -1.394 mV     4.776 mV    439    uV
```

Figure 5.19: Differentiator-Multiplier Signal - Whirl Orbit Direction : Bearing Clearance = 0.001cm, Rotor Speed 2700 rpm

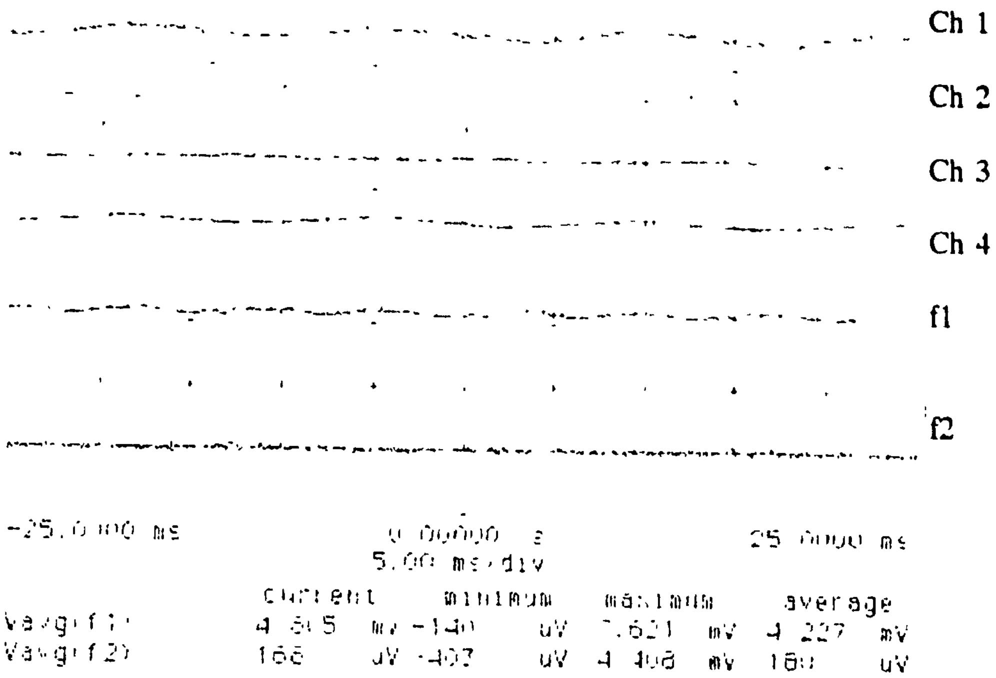

```
                      current      minimum      maximum      average
Vavg(f1)              4 515  mV  -140    uV   7.621  mV   4 227  mV
Vavg(f2)              166    uV  -407    uV   4 408  mV   168    uV
```

Figure 5.20: Differentiator-Multiplier Signal - Whirl Orbit Direction : Bearing Clearance = 0.001cm, Rotor Speed 2950 rpm

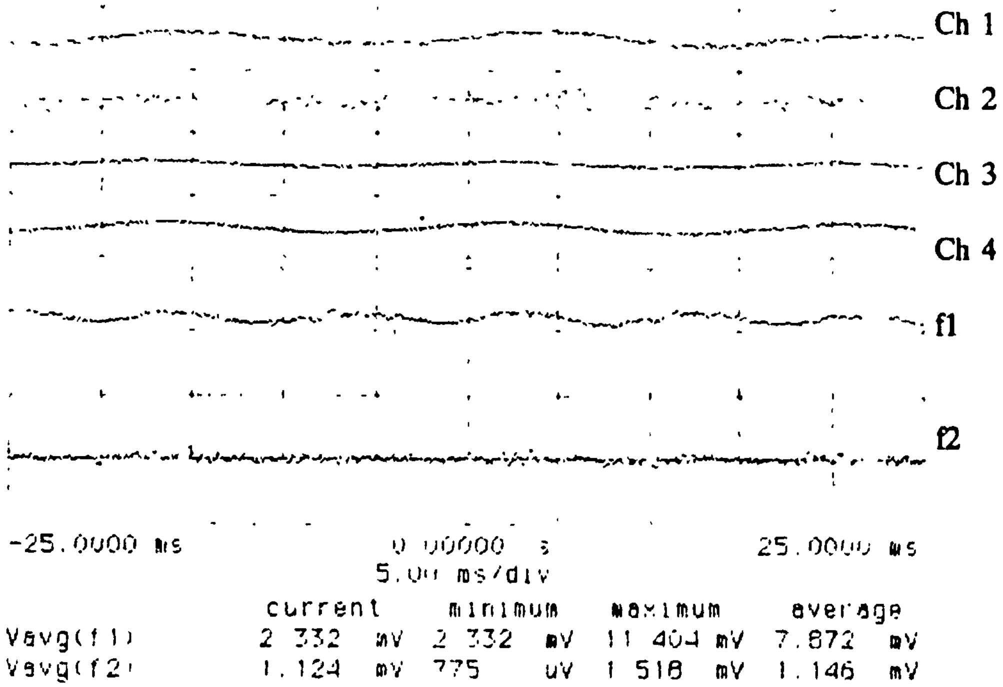

```
                      current      minimum      maximum      average
Vavg(f1)              2 332  mV   2 332  mV   11 404 mV   7.872  mV
Vavg(f2)              1.124  mV   775    uV   1 518  mV   1.146  mV
```

Figure 5.21: Differentiator-Multiplier Signal - Whirl Orbit Direction : Bearing Clearance = 0.001cm, Rotor Speed 4250 rpm

Chapter 6

Conclusions and Recommendations

6.1 Conclusions

The dynamic behaviour of a simple rotor system supported on hydrodynamic bearings is studied. Response analysis of the rotor supported on identical and dissimilar bearings are analyzed.

For a *Jeffcot rotor* supported on hydrodynamic bearings:

1. Simultaneous existence of forward and backward whirling motion of *Jeffcot rotor* supported on identical hydrodynamic bearing is investigated.
2. The response analysis of the rotor supported on dissimilar bearings is also analyzed. Dissimilarity of the bearing is due to the difference in the clearances of the supporting bearings.
3. To verify this aspect experimentally, a laboratory model of *Jeffcot Rotor* mounted on identical journal bearings, driven by a variable speed motor is developed.

Proximity pickups are used to make precision non-contact x and y displacement measurements of shaft whirling orbit. The electronics consists of an oscillator, linearization network, amplifiers and a de-modulator which provides an analog voltage directly proportional to displacement. A *Multiplier - Differentiator - filter circuit* is designed to identify the direction of the whirling motion.

4. Based on the results of the above investigations the following conclusions are drawn:

5. For a *Jeffcot rotor* supported on two identical fluid film bearings excessive flexibility causes the disk to whirl in the backward sense for a speed range in between the critical speeds. As the disk whirls in the backward sense in between the critical speeds, the journal continues to whirl in the forward sense. It is also observed that the backward whirl commences at the disk and as the speed increases, it extends over a certain central portion of the shaft and then shrinks back towards the disk before disappearing.

6. Studies using the stiffness and damping characteristics of the supporting hydrodynamic bearings, showed that the combined influence of the stiffness asymmetry and the damping could suppress the occurrence of the backward whirling, when the flexibility of the rotor is sufficiently small. Further, the backward whirling of the disk could be eliminated either by increasing the slenderness ratio of the bearings or the viscosity of the lubricant, or by reducing the clearance ratio of the bearings.

7. Existence of the simultaneous forward and backward whirling motion at the disk location is verified for a rotor supported on dissimilar bearings. Effect of dissimilarity effects the peak amplitude of response and the critical speed peaks shifts towards lower speed of the rotor.

8. The existence of simultaneous forward and backward whirl is verified experimentally.

6.2 Recommendations for Future Work

Some suggestions for the possible future work are given below:

1. **Analytical and Experimental and Investigation of whirling phenomenon of a rotor supported on three or more bearings.**

   A transfer matrix or finite element analysis of whirling phenomenon of a rotor supported on three or more bearing. When more than two bearings are used, factors such as the bearing misalignment, initial bending in the rotor shaft etc. must be given proper consideration. For laboratory studies an initially straight rotor setup can be used, and the influence of the bearing misalignment on the whirling motion of the rotor can be investigated.

2. **Application of thermo-hydrodynamic characteristics of the lubricant for unbalance response analysis of the rotor.**

   In the present investigation, the bearing characteristics like Sommerfeld number, stiffness and damping coefficients are computed assuming viscosity of the lubricant remains a constant with variation of temperature. The viscous heat generation in the lubricant film of a hydrodynamic journal bearing causes a rise in temperature of the fluid film. The variation of lubricant viscosity which depends strongly on temperature, must be taken into account for an accurate evaluation of bearing characteristics. Such a thermohydrodynamic analysis reduces the mathematical problem to the simultaneous solution of a generalized Reynolds equation and an energy equation with the appropriate boundary conditions. The solution of the simultaneous partial differential equations is difficult and time consuming. Application of finite element analysis techniques can be used to solve these simultaneous equations and the bearing characteristics are determined. These modified characteristics can be employed to investigate the whirling phenomenon of a rotor.

3. **Application of Condition Monitoring techniques in rotor bearing experimentation.**

   The effect of rotor bearing system parameters on the rotor operation can be studied experimentally for comparison with the existing condition monitoring techniques. In condition monitoring techniques, the critical parameters that are usually decided in advance and programmed, are monitored continuously and analyzed by suitable techniques. The rotating machinery are highly complex dynamic systems and are very sensitive to slight changes in operating conditions. The condition of the machine is reflected by parameters such as frequencies of vibration, direction of predominant amplitude, location of predominant amplitude, magnitude of response to speed variation, influence of loading, oil pressure and temperature. The procedure for continuous condition monitoring and diagnosis therefore boils down to obtaining the signature of the rotating machinery at suitable predetermined locations and analyzing this signature for determining the health of the machine. The data thus obtained can be used to analyze the effect of various parameters such as bearing clearance. flexibility parameter, lubricant viscosity etc. in rotor bearing system operation.

4. **Application of micromechatronic accelerometer sensors in Active control of rotor bearing system.**

   Application of micromechatronic sensors in rotor bearing experimentation is fairly a new concept. In present investigation, the experimentation is done using non-contact type proximity pickups, which can be replaced by lighter micromechatronic accelerometer sensors. The advantage of using micromechatronic sensors is, they are economic and accurate. The active control of unbalance response of rotor system can be done using actuators.

Bibliography

[1] W. J. Rankine, "On the Centrifugal Force of Rotating Shafts," Engineer, Vol. 27, p. 249 (1869)

[2] H. H. Jeffcot, "The Lateral Vibration of Loaded Shafts in the Neighborhood of a Whirling Speed: The Effect of Want of Balance," Philosophical Magazine, Series 6, Vol 37, p. 304 (1919)

[3] A. Tondl, "Some Problems of Rotor Dynamics", Chapman and Hall, London (1965)

[4] J. W. Lund, "Rotor Bearing Dynamic Design Technology", Part III: Design Handbook For Fluid Film Bearings. Mechanical Technology Inc., Latham, New York AFAPL-Tr-65-45 (1965)

[5] O. Pinkus, "Experimental Investigation of Resonant whip", Trans. ASME, Vol. 78, pp. 975-983 (1956)

[6] H. Poritsky, "Contribution to the Theory of Oil Whip", Trans. ASME, pp. 1153-1161 (1953)

[7] A. C. Hagg and P. C. Warner, "Oil Whip of Flexible Rotors", Trans. ASME, Vol. 75, pp. 1339-1344 (1953)

[8] E. J. Gunter, "Dynamic Stability of Rotor-Bearing Systems", NASA SP-113 (1966)

[9] Y. Hori, "Theory of Oil Whip", Journal of Applied Mechanics, Vol. 26, Trans. ASME, Series E, Vol. 81, p. 189 (1959)

[10] R. H. Badgley, "Turborotor Instability - Dynamic Unbalance, Gyroscopic, and Variable-Speed Effects with Finite-Length, Cavitated, Fluid-Film Bearings", Ph.D. Dissertation, Cornell University (1967)

[11] J. W. Lund, "The Stability of an Elastic Rotor in Journal Rotor in Journal Bearings with Flexible, Damped Supports", Journal of Applied Mechanics, Trans. ASME, Series E, Vol. 87, No. 4, pp. 911-920 (1965)

[12] E. J. Gunter, "The Influence of Flexibility Mounted Rolling Element Bearings on Rotor Response", Part 1: Linear Analysis, Journal of Lubrication Technology, Trans. ASME, pp. 59-75 (1970)

[13] R. G. Kirk, P. D. Choudhury and E. J. Gunter, "The effect of Support Flexibility on the Stability of Rotors Mounted in Plain Cylindrical Journal Bearings", Symposium Lyngby/Denmark, International Union of Theoretical and Applied Mechanics, Aug. 12-16 (1974)

[14] J. W. Lund, "Rotor Bearing Dynamic Design Technology", Part V: Computer Program Response and Stability. Mechanical Technology Inc., Latham, New York AFAPL-Tr- 65-45 (1965)

[15] E. C. Pestel and F. A. Leckie, "Matrix Methods in Elasto Mechanics", McGraw-Hill, New York (1963)

[16] W. D. Pilkey and P. Y. Chang, "Modern Formulas for Statics and Dynamics", McGraw-Hill, New York (1978)

[17] E. Kramer, "Computation of Unbalance Vibrations of Turbo rotors", ASME Publication, 77-DET-13 (1977)

[18] J. S. Rao, "Out of Balance Response of Turbo Alternator Rotors", Computer Program, Bharat Heavy Electricals Ltd., Hyderabad, India (1980)

[19] H. D. Nelson and J. N. McVaugh, "The Dynamics of Rotor Bearing Systems Using Finite Elements", Journal of Engineering for Industry, ASME., Vol. 98, p. 593 (1976)

[20] P. G. Morton, "Influence of Coupled Asymmetric Bearings on the Motion of a Massive Flexible Rotor", Proc. Inst. Mech. Engng, 182, p. 255 (1967)

[21] R. G. Kirk and E. J. Gunter, "The Effect of Flexibility and Damping on the Synchronous Response of a Single Mass Flexible Rotor", J. Engg. Ind. ASME 221 (1972)

[22] J. W. Lund, "Review of the concept of Dynamic Coefficients for Fluid Film Journal Bearings", ASME Journal of Tribology, Vol. 109, pp. 37-41 (1987)

[23] C. Rajalingham, N. Ganesan and B. S. Prabhu, "The Effect of Modified Inlet Boundary Conditions on the Stiffness and Damping Characteristics of Finite Hydrodynamic Journal Bearings", Wear 108, pp. 203-211 (1986)

[24] J. S. Rao, "Conditions for Backward Synchronous Whirl of a Flexible Rotor in Hydrodynamic Bearings", Mechanisms and Machine Theory Journal, Vol.17, pp. 143-152 (1982)

[25] J. S. Rao, R. B. Bhat and T S. Sankar, ‘Effect of Damping on the Synchronous Whirl of a Rotor Hydrodynamic Bearings", CSME Transactions, Vol.6, No. 3, pp. 155-161 (1980-81)

[26] T. Yamamoto, H. Ota and K. Kono, "On the Unstable Vibrations of a Shaft with Unsymmetrical Rotor", Applied Mechanics, p. 313 (1968)

[27] D. Ardayfio and D. A. Frohrib, "Vibration of an Asymmetrically Mounted Rotor with Gyroscopic Effects", Transactions of the ASME, Journal of Engineering for Industry, p. 327 (1976)

[28] R. Subbiah, R. B. Bhat and T. S. Sankar, "Unbalance Response of a Single Mass Rotor Mounted on Dissimilar Hydrodynamic Bearings", Presented at 53rd Shock and Vibration held at Danvers, MA. (1982)

[29] J. S. Rao, "Rotor Dynamics", Wiley Eastern, New Delhi (1983)

[30] C. Rajalingham, N. Ganesan and B. S. Prabhu, "Dissipation Coefficient and its Application to Flexible Rotor-Bearing System Design", Wear 107, pp. 343-354 (1986)

[31] W. Kellenberger, "Double-Frequency Accelerations in Turbo-Generator Rotors Resulting from Anisotropy in the Bearings", Proceedings of the Institution of Mechanical Engineers Vibrations in Rotating machinery (London), pp. 415-420

[32] F. M. Dimintberg, "Flexural Vibrations of Rotating Shafts", Butterworth's Publishing House, London (1961)

[33] C. Rajalingham, N. Ganesan and B. S. Prabhu, "Conditions of Backward whirling motion of a Flexible Rotor Supported on Hydrodynamic Journal Bearings", Journal of Sound and Vibration, Vol. 111, pp. 29-36 (1986)

[34] C. Rajalingham, R. B. Bhat and V. K. Jha, "Simultaneous Backward and Forward whirling motion of Disk and Journal in a Jeffcot Rotor Supported on Fluid Film Bearings ", 60th Shock and Vibration Symposium, Virginia Beach, U.S.A (1989)

[35] J. M. Vance, "Rotor of Turbo-machinery", A Wiley-Interscience Publication, U.S.A (1988)

[36] T. Yamamoto, "On the Critical Speeds of a Shaft", Memoirs of the Faculty of Engineering, Nagoya University, Japan, Vol. 6, No. 2, pp. 106-174 (1954)

[37] E. Downham, "Theory of Shaft Whirling, A Fundamental Approach to Shaft Whirling", The Engineer, 518-522, 552-555 and 660-665 (1957)

[38] E. H. Hull, "Shaft Whirling as influenced by stiffness asymmetry", J. Engg. Ind., ASME 83, p. 219 (1961)

[39] J. W. Lund and K. K. Orcutt, "Calculations and Experiments on the Unbalance Response of a Flexible Rotor", Journal of Engineering for Industry, Trans. ASME, 89, No. 4, pp. 785-796 (1967)

[40] R. E. Cunningham, "Steady-State Unbalance Response of a Three-Disk Flexible Rotor on Flexible Damped Supports", Journal of Mechanical Design, Trans. ASME, Vol. 100, pp. 785-796 (1978)

[41] R. Subbiah, "Dynamic Behaviour of Rotor Systems with a Comprehensive Model for the Hydrodynamic Bearing Supports Using Modal Analysis and Testing", Phd Dissertation, Department of Mechanical Engineering, Concordia University, Montreal, Quebec (1985)

[42] R. Subbiah, R. B. Bhat, T. S. Sankar and J. S. Rao, "Backward Whirl in a Simple Rotor Supported on Hydrodynamic Bearings", NASA Conference Publication 2409, Proceedings of a Symposium Sponsored by Bently Rotor Dynamics Research Corporation and held in Carson City, Nevada June 10-14 (1985)

[43] C. Rajalingham, "Some Studies on Non-Newtonian and Thermal Influence on Steady State and Dynamic Performance of Journal Bearings", Phd Dissertation, Department of Applied Mechanics, Indian Institute of Technology, Madras, India (1987)

[44] J. P. Den Hartog, "Mechanical Vibrations", 4th ed., p. 265, McGraw-Hil, New York (1956)

[45] R. G. Loewy and V. J. Piarulli "The Dynamics of Rotating Shafts", SVM No. 4, The Shock and Vibration Information Center, Washington D.C. (1970)

[46] S. Z. Szeri "Tribology: Friction, Lubrication and Wear", McGraw-Hill (1980)

[47] Alastair Cameron "Basic Lubrication Theory", 3rd edition, Ellis Horward Limited (1981)

[48] J. Thomson "Theory of Vibration with Application", Prentice - Hall (1981)

[49] J. G. Graeme "Application of Operational Amplifiers", Third Generation Techniques, pp 76-78, McGraw Hill (1973)

[50] J. S. Rao "Future Perspective Condition Monitoring with Special emphasis on expert Systems", National Seminar on Frontiers of Tribology and Condition Monitoring, Indian Institute of Technology, Madras, India, Tata McGraw-Hill (1993)

[51] John Case and A. H. Chilver "Strength of Materials and Structures : An Introduction to the Mechanics of Solids and Structures", Edward Arnold, London (1971)

Appendix A

The Elliptic Orbit

Let the co-ordinates of the moving point p at time t, with respect to an orthogonal Cartesian frame Oxy be,

$$x = a_x \cos \omega t + b_x \sin \omega t \qquad (A.1)$$

$$y = a_y \cos \omega t + b_y \sin \omega t \qquad (A.2)$$

where a_x, a_y, b_x, b_y and ω are constants. From the periodicity of $\sin \omega t$ and $\cos \omega t$, one can infer that the point P describes a closed curve at frequency ω.

Eliminating ωt from Eqns. (A.1 and A.2) gives the equation to the locus of P as

$$(a_y^2 + b_y^2)x^2 - 2(a_x a_y + b_x b_y)xy + (a_x^2 + b_x^2)y^2 = (a_x b_y - b_x a_y)^2 \qquad (A.3)$$

The above equation is an ellipse whose centre is at the origin. When $(a_x b_y - b_x a_y) = 0$, the ellipse degenerates to a segment of a straight line. When $(a_x/b_y) = (b_x/a_y) = \pm 1$, the ellipse becomes a circle.

Using Eqns. (A.1 and A.2), one can deduce the relation

$$x^2 + y^2 = A\cos 2\omega t + B\sin 2\omega t + C \tag{A.4}$$

where

$$A = \frac{1}{2}[a_x^2 + a_y^2 - b_x^2 - b_y^2] \tag{A.5}$$

$$B = [a_x b_x + a_y b_y] \tag{A.6}$$

$$C = \frac{1}{2}[a_x^2 + a_y^2 + b_x^2 + b_y^2] \tag{A.7}$$

(A.8)

Using Eqns. (A.5 - A.7) the following results could be deduced.

$$C^2 - (A^2 + B^2) = (a_x b_x + a_y b_y)^2 \geq 0 \tag{A.9}$$

Eqn. (A.4) can be rewritten in the alternate form as

$$x^2 + y^2 = \sqrt{(A^2 + B^2)}\cos 2(\omega t - \theta) + C \tag{A.10}$$

where

$$\theta = \tan^{-1}[B/(A + \sqrt{(A^2 + B^2)})] \tag{A.11}$$

From Eqn. (A.10), the major and minor axes of the ellipse can be expressed as $\sqrt{\left[C + \sqrt{(A^2 + B^2)}\right]}$ and $\sqrt{\left[C - \sqrt{(A^2 + B^2)}\right]}$, respectively.

Area enclosed by the x, y coordinates of amplitude of the whirl rotation is an ellipse can be obtained from Eqns. (A.1 and A.2) as

$$\begin{aligned} Area &= \oint x\,dy \\ &= \delta^2 \int_0^{2\pi} (a_x \cos\theta + b_x \sin\theta)\,(-a_y \sin\theta + b_y \cos\theta)\,d\theta \\ &= \delta^2 \int_0^{2\pi} \left(-a_x a_y \sin\theta\cos\theta + a_x b_y \cos^2\theta - b_x a_y \sin^2\theta + b_x b_y \sin\theta\cos\theta\right) \\ &= 2\pi\delta^2\,(a_x b_y - b_x a_y) \end{aligned}$$

(A.12)

The area enclosed by the elliptical orbit of the journal centre is given by

$$\oint x_j dy_j = \pi\delta^2 \left(a_{jx}b_{jy} - b_{jx}a_{jy}\right) \tag{A.13}$$

Thus the orbit of P on the ellipse is in the positive or negative sense according as the expression

$$\left(a_{jx}b_{jy} - b_{jx}a_{jy}\right) \lessgtr 0 \tag{A.14}$$

Appendix B

Derivation of Expression for Rotor Co-Ordinates

Let deflection at mid point of a simply supported beam shown in Fig. (B.1) i.e, at $z = l/2$, be given by

$$\delta_c = \frac{Pl^3}{48EI} \tag{B.1}$$

Deflection at any distance z is a partial value of δ_c ie $v\delta_c$. The bending moment at any point for the system is

$$EI\frac{d^2x}{dz^2} = -\frac{P}{2}z \tag{B.2}$$

Integrating

$$EI\frac{dx}{dz} = -\frac{P}{4}z^2 + A \tag{B.3}$$

Constant of integration is evaluated using boundary condition, $EI\frac{dx}{dz} = 0$, which gives

$$\frac{P}{4}\frac{l^2}{4} = A$$

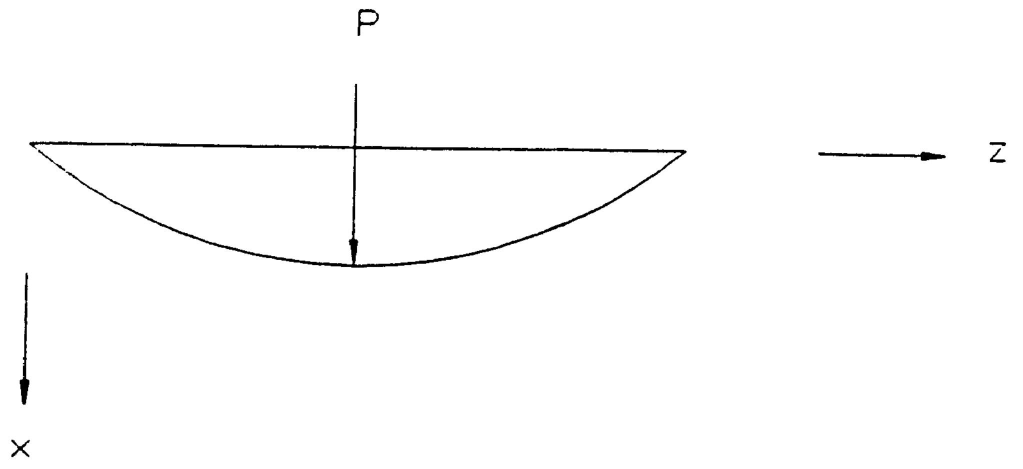

Figure B.1: Simply Supported Beam

Eqn. (B.3) can be further integrated to give

$$EIx = -\frac{P}{12}z^3 + \frac{Pl^2}{16}z + B \qquad \text{(B.4)}$$

Evaluating the constant of integration, using the condition at x = 0 and z = 0, one gets B = 0. Hence,

$$\begin{aligned} x &= \frac{P}{EI}\left(-\frac{1}{12}z^3 + \frac{1}{16}l^2z\right) \\ &= \frac{48\delta_r}{l^3}\left(-\frac{1}{12}z^3 + \frac{1}{16}l^2z\right) \\ &= \delta_r\left(-4(\frac{z}{l})^3 + 3(\frac{z}{l})\right). \\ &= \delta_r\left(3\bar{z} - 4\bar{z}^3\right) \qquad \text{(B.5)} \end{aligned}$$

Hence the partial ν is obtained as

$$\nu = \bar{z}\left(3 - 4\bar{z}^2\right) \qquad 0 \leq \bar{z} \leq \frac{l}{2} \qquad \text{(B.6)}$$

The unbalance response of the rotor at any distance z is given by

$$x = x_j + \nu(x_i - x_j) \tag{B.7}$$

Using non dimensional coefficients

$$\bar{x} = \frac{(x - \nu\delta_s)}{c}$$

$$\bar{y} = \frac{y}{c}$$

Eqn. (B.7)can be written in non-dimensional form as

$$\bar{x} = \bar{x}_j + \nu(\bar{x}_i - \bar{x}_j) \tag{B.8}$$

Similarly

$$\bar{y} = \bar{y}_j + \nu(\bar{y}_i - \bar{y}_j) \tag{B.9}$$

Appendix C

Simply-Supported Beam Carrying a Concentrated Lateral Load

Consider a beam of uniform flexural stiffness EI and length L, which is simply - supported at its ends C and G. The beam carries a concentrated lateral load W at a distance a from C. Then the reactions at C and G are

$$V_C = \frac{W}{L}(L - a), \qquad V_G = \frac{W_a}{L} \tag{C.1}$$

Now consider a section of the beam at a distance x from C; if $x < a$, the bending moment at the section is

$$M = V_C x$$

and if $x > a$

$$M = V_C x - W(x - a) \tag{C.2}$$

The analysis may be simplified by using step-functions during process of integration.

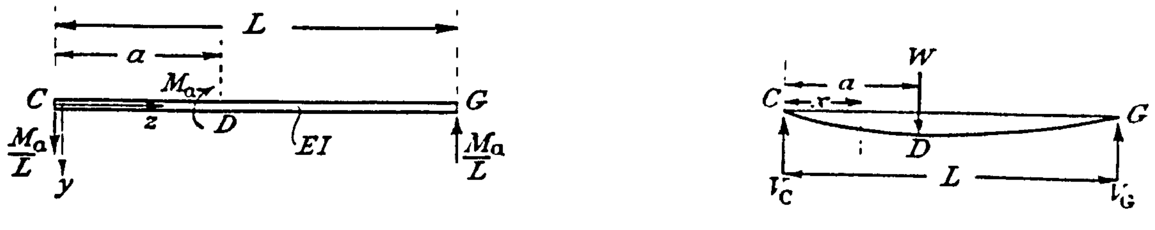

Figure C.1: Simply Supported Beam with a Concentrated Lateral Load

By introducing a function $\phi(x)$, which is zero for the range $0 < x < a$, and equal to unity for the range $0 < x < L$; then ϕ has the 'stepped' form shown in Fig. (C.1), and is called a step-function. Then bending moment for all values of x is in the form

$$M = V_r x - \phi[W(x - a)] \tag{C.3}$$

Since $\phi = 0$ for $x < a$, the second term vanishes and $M = V_r x$. But for $x > a$, $\phi = 1$, and the second term is retained. Here the moment balance for the beam is given by

$$EI\frac{d^2y}{dx^2} = -V_r x + \phi[W(x - a)] \tag{C.4}$$

On integrating once, we have

$$EI\frac{dy}{dx} = -\frac{1}{2}V_r x^2 + \int_0^x \phi[W(x - a)]dx + A \tag{C.5}$$

where A is a constant. Now, if $x < a$,

$$\int_0^x \phi[W(x - a)]dx = 0$$

since $\phi = 0$; and if $x > a$,

$$\int_0^x \phi[W(x - a)]dx = \int_0^a \phi[W(x - a)]dx + \int_a^x \phi[W(x - a)]dx \qquad \text{(C.6)}$$

But

$$\int_0^a \phi[W(x - a)]dx = 0$$

Since $\phi = 0$ for $x < a$, and we may write

$$\int_0^x \phi[W(x - a)]dx = \phi\int_0^{x - a} W(x - a)]d(x - a)$$

So that Eqn. (C.3) becomes

$$\int_0^x \phi[W(x - a)]dx = \phi\int_0^{x - a} W(x - a)]d(x - a) \qquad \text{(C.7)}$$

We may now write Eqn.(C.2) in the form

$$EI\frac{dy}{dx} = -\frac{1}{2}V_c x^2 + \phi\int_0^{x - a} W(x - a)d(x - a) + A \qquad \text{(C.8)}$$

The effect of the step function ϕ on the integration is to introduce a new variable (x - a). So that, on integrating Eqn. (C.1) we take ϕ as unity and integrate the term $W(x - a)$ with respect to (x - a) and not with respect to x. From Eqn. (C.5), we have

$$EI\frac{dy}{dx} = -\frac{1}{2}V_c x^2 + \phi\left[W\frac{(x - a)^2}{2}\right] + A \qquad \text{(C.9)}$$

The presence of ϕ, which is still equal to zero for $x < a$, and to unity for $x > a$, indicates that the term

$$\phi\left[W\frac{(x - a)^2}{2}\right] = 0 \quad for\ x < a$$

is zero for $x < a$, and is equal to

$$W\frac{(x - a)^2}{2} \qquad for\ x > a$$

On repeating the integrating process, we have

$$EIy = -\frac{1}{6}V_c x^3 + \phi\left[\frac{W}{6}(x - a)^3\right] + Ax + B \qquad (C.10)$$

where the second term on the right-hand side of Eqn. (C.6) is integrated with respect to (x - a), and not x. It remains to find the value of the constants A and B in Eqn. (C.7); at $x = 0$ we have $y = 0$, so that $B = 0$, since $\phi = 0$ for $x < a$; at $x = L$, again $y = 0$ giving

$$0 = -\frac{1}{6}V_c L^3 + \frac{W}{6}(L - a)^3 + AL \qquad (C.11)$$

Since $\phi = 1$ for $x > a$ then

$$A = \frac{1}{6}V_c L^2 - \frac{W}{6L}(L - a)^3 \qquad (C.12)$$

So that

$$EIy = -\frac{1}{6}V_c x^3 + \phi\left[\frac{W}{6}(x - a)^3\right] + \left[\frac{1}{6}V_c L^2 - \frac{W}{6L}(L - a)^3\right]x \qquad (C.13)$$

If we put $V_c = \frac{W}{L}(L - a)$, then

$$EIy = -\frac{W}{6L}(L - a)x^3 + \frac{Wa}{6L}(2L^3 - 3aL + a^2)x + \phi\left[\frac{W}{6}(x - a)^3\right] \qquad (C.14)$$

The advantage in using a step-function, such as φ, is that only two constants of integration are introduced. We need not consider continuity of the deflected form of the beam at a point of application of a concentrated load; continuity is ensured automatically by the step function.

Appendix D

Simply-Supported Beam with a Couple Applied at an Intermediate Point

The simply-supported beam of Fig. (D.1) carries a couple M_a applied to the beam at a point a distance a from C. The vertical reactions at each end are (M_a/L). The bending moment at a distance z from C is

$$M = -\frac{M_a z}{L} + \phi[M_a] \tag{D.1}$$

where

$$\phi = 0 \;\; for \;\; 0 < z < a$$
$$\phi = 1 \;\; for \;\; a < z < L$$

Then

$$EI\frac{d^2 v}{dz^2} = \frac{M_a z}{L} - \phi[M_a] \tag{D.2}$$

As before, the step function ϕ introduces a new variable (z - a), and we have

$$EI\frac{dv}{dz} = \frac{M_a z^3}{2L} - \phi[M_a(z - a)] + A$$

Figure D.1: Simply Supported Beam with a Couple

$$EIv = \frac{M_a z^3}{6L} - \phi\left[\frac{M_a}{2}(z - a)^2\right] + Az + B \tag{D.3}$$

The constants A and B are eliminated from the conditions that $v = 0$ and $z = 0$, $z = L$. These give $B = 0$, and

$$A = \frac{1}{6}\left(2L^2 - 6La + 3a^2\right) \tag{D.4}$$

Then

$$EIv = \frac{M_a z^3}{6L} - \phi\left[\frac{M_a}{2}(z - a)^2\right] + \frac{M_a z}{6}\left(2L^2 - 6La + 3a^2\right)z \tag{D.5}$$

The deflection at D, where $z = a$, is

$$v_D = \frac{M_a a}{3EIL}(L - a)(L - 2a) \tag{D.6}$$

Appendix E

The Unbalance Orbit

The orbital behaviour of the rotor supported on identical bearings resulting from unbalance response $S\alpha_0 = 1.385$ and $\mu_s = 0.965$ at the speed ω/ω_s is shown in Fig. (E.1). The whirling is backward over approximately the central two-fifths of the shaft. At the point of transition from backward to forward whirling, the whirl orbit becomes a straight line. The point of transition from forward to backward whirl may be different for another set of system parameters [34].

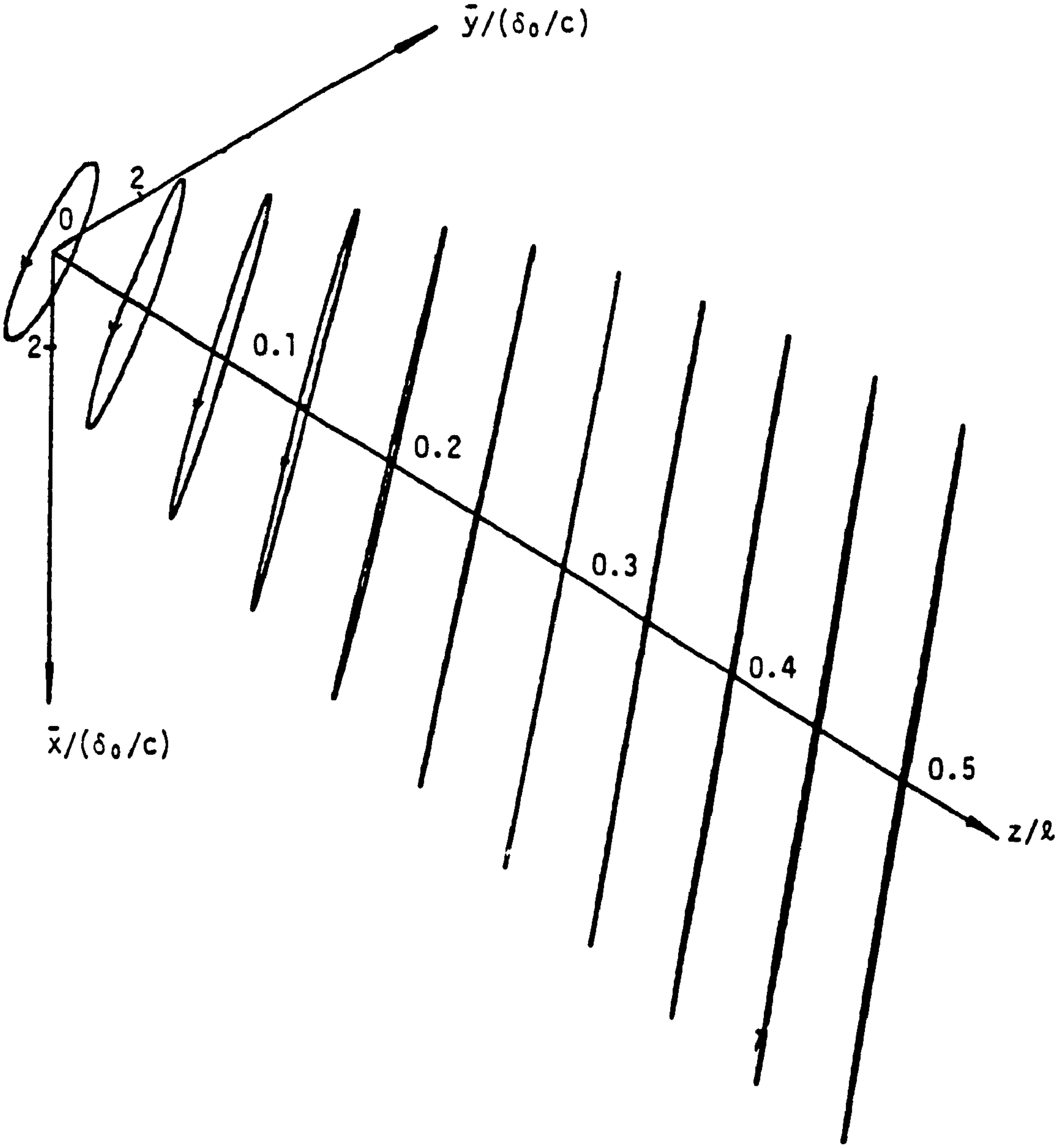

Figure E.1: Unbalance Orbit of Rotor